University of Southampton Research Repository

Copyright © and Moral Rights for this thesis and, where applicable, any accompanying data are retained by the author and/or other copyright owners. A copy can be downloaded for personal non-commercial research or study, without prior permission or charge. This thesis and the accompanying data cannot be reproduced or quoted extensively from without first obtaining permission in writing from the copyright holder/s. The content of the thesis and accompanying research data (where applicable) must not be changed in any way or sold commercially in any format or medium without the formal permission of the copyright holder/s.

When referring to this thesis and any accompanying data, full bibliographic details must be given, e.g.

Thesis: Author (Year of Submission) "Full thesis title", University of Southampton, name of the University Faculty or School or Department, PhD Thesis, pagination.

Data: Author (Year) Title. URI [dataset]

# UNIVERSITY OF SOUTHAMPTON

FACULTY OF ENGINEERING AND PHYSICAL SCIENCES

Chemistry

## SYNTHESIS OF ATOMIC AND MOLECULAR ENDOHEDRAL FULLERENES

**Thesis for the Degree of Doctor of Philosophy (PhD)**

By

**Gabriela Hoffman**

July 2021

**University of Southampton**

# Abstract

Faculty of Engineering and Physical Sciences

Chemistry

Thesis for the degree of Doctor of Philosophy

**Synthesis of atomic and molecular endohedral fullerenes**

By

Gabriela Hoffman

This work presents syntheses of fullerene $C_{60}$ enclosing atoms and molecules inside its cavity. These clusters are very convenient systems to study physical and spectral properties on atomic level.

Endohedral fullerenes can be synthesised by performing a sequence of chemical reactions to open a hole in $C_{60}$, followed by insertion of the guest atom or molecule and chemical closure. This process is known as molecular surgery.

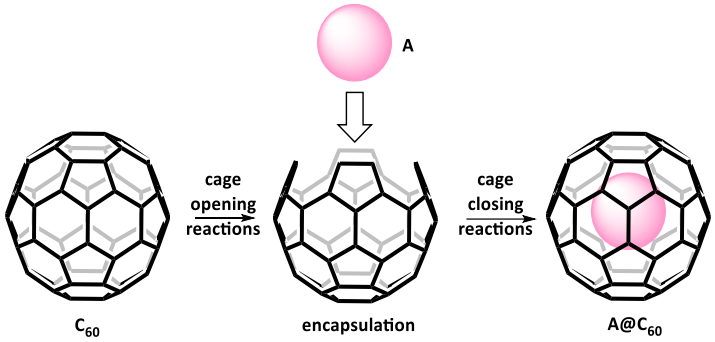


In this work, opening route to key open cage fullerene containing 12-membered ring has been improved. 12-membered ring is a key precursor to open the fullerene cavity in order to insert atoms and molecules. The synthesis has been improved to higher yielding, safer and faster process. Two novel open cage fullerenes have been isolated and crystal structures obtained. These proved to be mechanistically important for the closing steps of the fullerene. Syntheses of $He@C_{60}$, $H_2@C_{60}$ and $Ne@C_{60}$ have been improved and high filling factors between 50-100% achieved. $Kr@C_{60}$ has been prepared for the first time by molecular surgery, isolated with 100% filling factor and a crystal structure was obtained. Finally, $N_2@C_{60}$ was prepared as

a mixture containing empty $C_{60}$ and $H_2O@C_{60}$ and the $^{13}C$ NMR spectra was recorded for the first time.

List of publications:

**A Solid-State Intramolecular Wittig Reaction Enables Efficient Synthesis of Endofullerenes Including Ne@$C_{60}$, $^3$He@$C_{60}$, and HD@$C_{60}$**

Gabriela Hoffman, Dr. Mark C. Walkey, Dr. John Gräsvik,George R. Bacanu,Shamim Alom, Dr. Sally Bloodworth, Dr. Mark E. Light,Prof. Malcolm H. Levitt,Prof. Richard J. Whitby, *Angew.Chem. Int.Ed. 2021, 60, 8960 –8966*

Contributed to:

**First Synthesis and Characterization of $CH_4@C_{60}$**

Dr. Sally Bloodworth, Gabriela Hoffman (*nee* Sitinova), Shamim Alom, Dr. Sara Vidal, George R. Bacanu, Dr. Stuart J. Elliott,Dr. Mark E. Light,Julie M. Herniman,Prof. G. John Langley,Prof. Malcolm H. Levitt,Prof. Richard J. Whitby, *Angew.Chem. Int.Ed. 2019, 58 ,5038 –5043*

**Synthesis of Ar@$C_{60}$ using molecular surgery**

Sally Bloodworth, Gabriela Hoffman, Mark C. Walkey, George R. Bacanu, Julie M. Herniman, Malcolm H. Levitt and Richard J. Whitby *Chem. Commun., 2020, 56, 10521-10524*

**Fine structure in the solution state $^{13}$C-NMR spectrum of $C_{60}$ and its endofullerene derivatives**

George Razvan Bacanu , Gabriela Hoffman , Michael Amponsah , Maria Concistr`e, Richard J. Whitby and Malcolm H. Levitt, *Phys. Chem. Chem. Phys., 2020 ,22, 11850-11860*

**Electronic Spectroscopy of He@$C_{60}^+$ for Astrochemical Consideration**

Ewen K Campbell, Elliott Reedy, Johanna Rademacher, R. J. Whitby, G. Hoffman, *2020 ApJ, 897, 88*

**Rotational Coherence of Encapsulated Ortho and Para Water in Fullerene-$C_{60}$**

Sergey S. Zhukov, Vasileios Balos, Gabriela Hoffman, Shamim Alom, Mikhail Belyanchikov, Mehmet Nebioglu, Seulki Roh, Artem Pronin, George R. Bacanu, Pavel Abramov, Martin Wolf, Martin Dressel, Malcolm H. Levitt, Richard J. Whitby, Boris Gorshunov, Mohsen Sajadi, arXiv:2006.02687v1

**An Internuclear J-Coupling of $^3$He Induced by Molecular Confinement,**

George Razvan Bacanu, Jyrki Rantaharju, Gabriela Hoffman, Mark C. Walkey, Sally Bloodworth, Maria Concistrè, Richard J. Whitby, and Malcolm H. Levitt, *J. Am. Chem. Soc. 2020, 142, 40, 16926–16929*

**Experimental Determination of the Interaction Potential between a Helium Atom and the Interior Surface of a $C_{60}$ Fullerene Molecule** G. R. Bacanu, T. Jafari, M. Aouane, J. Rantaharju, M. Walkey, G. Hoffman, A. Shugai, U. Nagel, M. J. Ruiz, A. J. Horsewill, S. Rols, T. Room, R. J. Whitby, M. H. Levitt *Phys Chem 2021 (Submitted)*

# Contents

**Research Thesis: Declaration of Authorship** ..... **v**

**Acknowledgements** ..... **vi**

**List of Abbreviations** ..... **vii**

**1 Introduction** ..... **1**

1.1 Buckminsterfullerene ..... 1

1.1.1 History ..... 1

1.1.2 Structure ..... 2

1.2 Fullerenes enclosing atoms and molecules ..... 3

1.2.1 Metallofullerenes ..... 4

1.2.2 **N@$C_{60}$** and **P@$C_{60}$** ..... 5

1.2.3 Noble gases in fullerenes ..... 6

1.3 Chemical opening of the fullerene orifice ..... 8

1.3.1 Development ..... 9

1.3.2 OCF *via* fullerene-mixed peroxides ..... 23

1.4 Insertion of atoms and molecules into an open cage fullerene ..... 26

1.4.1 Insertion of $H_2$, He and Ne ..... 26

1.4.2 Insertion of $H_2O$ and HF ..... 29

1.4.3 Insertion of guest molecules into fullerene-mixed peroxides ..... 37

1.4.4 Insertion of atoms and molecules into **58** ..... 40

1.4.5 Insertion of molecules into **60** ..... 42

1.4.6 Insertion of molecules into **47** ..... 42

1.5 Suturing the orifice to **A@$C_{60}$** ..... 46

1.5.1 **$H_2$@$C_{60}$** ..... 46

1.5.2 **$^4$He@$C_{60}$** ..... 47

1.5.3 **$H_2O$@$C_{60}$** ..... 48

1.5.4 **HF@$C_{60}$** ..... 50

1.5.5 **$CH_4$@$C_{60}$** ..... 52

1.5.6 **Ar@$C_{60}$** ..... 53
1.5.7 Summary of **A@$C_{60}$** prepared by molecular surgery ..... 54

**Aims** ..... **55**
**2 Optimised large scale synthesis of precursor 43** ..... **56**
**3 Closure of 42 to $C_{60}$** ..... **61**
**4 Optimised large scale synthesis of He@$C_{60}$ and $H_2$@$C_{60}$ and the first molecular surgery synthesis of Ne@$C_{60}$** ..... **68**

4.1 Intramolecular Wittig reaction of the OCF **88** ..... 68
4.2 Encapsulation of $^4$He and $^3$He ..... 73
4.3 Encapsulation of $H_2$, HD and $D_2$ ..... 79
4.4 Synthesis of **Ne@$C_{60}$** ..... 81
4.4.1 Synthesis of **Ne@$C_{60}$** by molecular surgery for the first time ..... 81
4.4.2 Synthesis of **Ne@$C_{60}$** via intramolecular Wittig reaction ..... 83
4.5 Summary ..... 84

**5 Optimisation of closure of A@89 to A@46** ..... **86**

5.1 Partial closure of empty **89** to **46** ..... 86
5.1.1 Optimisation with empty/naturally $H_2O$ filled OCF **89** ..... 87
5.1.2 Optimisation with **$CH_4$@89** ..... 91
5.1.3 Optimisation of the solvent system of the photoreaction and synthesis of **$CH_4$@43** ..... 95
5.1.4 **Ar@$C_{60}$** ..... 98

**6 Synthesis of Kr@$C_{60}$** ..... **101**

6.1 Filling of **47** cavity with Kr ..... 101
6.2 Loss of Kr atom from **47** ..... 102
6.3 Closure of **Kr@89** to **Kr@$C_{60}$** ..... 104

**7 Synthesis of $N_2$@$C_{60}$** ..... **108**
**Conclusions** ..... **114**
**8 Experimental** ..... **115**

8.1 General methods ..... 115
8.2 Synthesis of precursors ..... 116
8.2.1 Synthesis of 2-bromo-6-(*tert*-butyl)pyridine ..... 116
8.2.2 3,6-bis(6-(*tert*-Butyl)pyridin-2-yl)pyridazine ..... 116
8.3 Optimised procedure for synthesis of **43** ..... 117
8.4 **46** ..... 118
8.5 **45** ..... 119
8.6 **88** ..... 120
8.7 Tetrakis(dimethylamino)ethylene (TDAE) ..... 120
8.8 **47** ..... 121
8.9 Synthesis of dimethyldioxirane ..... 121
8.10 **89** ..... 122
8.11 **92** ..... 122
8.12 **A@47** ..... 123
8.12.1 **$CH_4$@47** ..... 123
8.12.2 **Ar@47** ..... 124
8.12.3 **Kr@47** ..... 124
8.13 **A@89** ..... 125
8.13.1 **$CH_4$@89** ..... 125
8.13.2 **Ar@89** ..... 126
8.13.3 **Kr@89** ..... 127
8.13.4 **$N_2$@89** ..... 128
8.14 **A@43** ..... 129
8.14.1 **$^4$He@43** ..... 129
8.14.2 **$^3$He@43** ..... 130
8.14.3 **$H_2$@43** ..... 131
8.14.4 **$D_2$@43** ..... 132
8.14.5 **HD@43** ..... 133
8.14.6 **Ne@43** ..... 134
8.14.7 **$CH_4$@43** ..... 136

8.14.8 **$CH_4$@99** ..... 136
8.14.9 **Ar@43** ..... 138
8.14.10 **Kr@43** ..... 138
8.15 **A@$C_{60}$** ..... 140
8.15.1 **$^4$He@$C_{60}$** ..... 140
8.15.2 **$^3$He@$C_{60}$** ..... 141
8.15.3 **$H_2$@$C_{60}$** ..... 141
8.15.4 **$D_2$@$C_{60}$** ..... 142
8.15.5 **HD@$C_{60}$** ..... 143
8.15.6 **Ne@$C_{60}$** ..... 144
8.15.7 **$CH_4$@$C_{60}$** ..... 145
8.15.8 **Ar@$C_{60}$** ..... 146
8.15.9 **Kr@$C_{60}$** ..... 147
8.15.10 **$N_2$@$C_{60}$** ..... 148
8.16 Crystallography data ..... 150
8.16.1 X-Ray structure determination of **92** ..... 150
8.16.2 X-Ray structure determination of **88** ..... 151
8.16.3 X-Ray structure determination of **Ne@$C_{60}$** ..... 152
8.16.4 X-Ray structure determination of **$CH_4$@99** ..... 153
8.16.5 X-Ray structure determination of **Kr@$C_{60}$** ..... 154
**9 Literature ..... 155**

# Research Thesis: Declaration of Authorship

Print name: Gabriela Hoffman

Title of thesis: Synthesis of atomic and molecular endohedral fullerenes

I declare that this thesis and the work presented in it are my own and has been generated by me as the result of my own original research.

I confirm that:

1. This work was done wholly or mainly while in candidature for a research degree at this University;
2. Where any part of this thesis has previously been submitted for a degree or any other qualification at this University or any other institution, this has been clearly stated;
3. Where I have consulted the published work of others, this is always clearly attributed;
4. Where I have quoted from the work of others, the source is always given. With the exception of such quotations, this thesis is entirely my own work;
5. I have acknowledged all main sources of help;
6. Where the thesis is based on work done by myself jointly with others, I have made clear exactly what was done by others and what I have contributed myself;
7. Parts of this work have been published as: https://doi.org/10.1002/anie.202100817

Signature: ..... Date: 05.01.2022.....

# Acknowledgements

Firstly, I would like to thank Professor Richard Whitby, Dr Sally Bloodworth and Professor Malcom Levitt for this amazing opportunity, their supervision, knowledge, ideas and their patience. To the past and present members of the Whitby group, thank you for the encouragement and help. A special mention to Mark, Dawid, Andreina, Adan and Sara. Big thank you to Luke for the motivation and help during the extension period during tough covid times, to George for his encouragement, collaboration and amazing work with the materials prepared in this project, and to Dovile for her friendship, advice and support throughout our studies and life.

Additionally, thank you to Ms Julie Herniman, Dr John Langley, Dr Neil Wells and Dr Mark Light for the running of MS, NMR and X-ray and for the help they provided; to the glassblowers and stores staff for their amazing services.

Finally, I would like to express gratitude to my husband David, all my family and friends for continuously supporting, encouraging, and believing in me throughout all my years in education.

# List of Abbreviations

| | |
|---|---|
| 1-Cl-Nap | 1-chloronaphthalene |
| Å | Angstrom |
| Ac | Acetyl |
| APCI | Atmospheric pressure chemical ionisation |
| APPI | Atmospheric pressure photo ionisation |
| Ar | Aryl |
| atm | Atmosphere |
| BOC | Tert-Butyloxycarbonyl |
| $CB_3$ | Benzyloxycarbonyl |
| $^{13}C$ NMR | Carbon Nuclear Magnetic Resonance |
| CN | Nitrile |
| DCM | Dichloromethane |
| DFT | Density Functional Theory |
| DMAPO | 4-(dimethylamino)pyridine 1-oxide |
| DMDO | Dimethyldioxirane |
| DV | Dead volume |
| $E_a$ | Activation energy |
| $E_{esc}$ | Escape energy |
| $E_{in}$ | Insertion energy |
| EMF | Endohedral metallofullerenes |
| Et | Ethyl |
| EtOAc | Ethyl acetate |
| eq | Equivalents |
| $ESI^+$ | Positive electrospray ionisation |
| f.f. | Filling factor |
| FMP | Fullerene mixed peroxides |
| FT-ICR | Fourier-transform ion cyclotron resonance |
| HOMO | Highest occupied molecular orbital |
| HPLC | High performance liquid chromatography |
| HRMS | High resolution mass spectrometry |
| hv | Light |
| INS | Inelastic neutron scattering |
| IR | Infrared spectroscopy |
| LED | Light Emitting Diode |
| LRMS | Low resolution mass spectrometry |
| LUMO | Lowest unoccupied molecular orbital |
| MALDI TOF | Matrix-assisted laser desorption/ionization time of flight spectrometer |
| *m*-CPBA | Meta-Chloroperoxybenzoic acid |
| Me | Methyl |
| MeCN | Acetonitrile |
| MEM | Methoxymethyl |
| mL | Mililiter |
| mM | Milimolar |

| | |
|---|---|
| mmol | Milimole |
| MO | Molecular orbital |
| MS spectra | Mass spectrometry |
| NMMO | *N*-methylmorpholine-*N*-oxide |
| NMR | Nuclear Magnetic Resonance |
| *N*-Ph-mal | *N*-phenylmaleimide |
| OCF | Open cage fullerene |
| *o*-DCB | *Ortho*-dichlorobenzene |
| OH | hydroxyl |
| Ph | Phenyl |
| $PhI(OAc)_2$ | (Diacetoxyiodo)benzene |
| $PMe_3$ | Trimethylphosphine |
| $PPh_3$ | Triphenylphosphine |
| ppm | Parts per million |
| $PR_3$ | Trialkyl phosphine |
| Py | Pyridyl |
| R | Hydrocarbon chain |
| r.t. | Room temperature |
| $R_f$ | Retention factor |
| RRT | Relative retention time |
| RT | Retention time |
| SET | Single electron transfer |
| TBHP | *Tert*-butyl hydroperoxide |
| TCE | Trichloroethane |
| TDAE | Tetrakis(dimethylamino)ethylene |
| TFA | Trifluoroacetic acid |
| THF | Tetrahydrofurane |
| TLC | Thin Layer Chromatography |
| TMS | Trimethylsilane |
| TOF | Time of Flight |
| Tol | Toluene |

# 1 Introduction

## 1.1 Buckminsterfullerene

### 1.1.1 History

In the last century, several theoretical studies were published on the existence of an icosahedral molecule $C_{60}$.[1][2] It was proposed that it consists of 60 $sp^2$ hybridized carbons that are bonded to three other carbons. Therefore, it is an alkene-like molecule, without any hydrogen atoms and comes close to a spherical shell of graphite. The most symmetrical structure possible was truncated icosahedron consisting of 12 pentagonal rings and 20 hexagonal rings and at the time was named ''footballene''.[3]

$C_{60}$ was later called Buckminster fullerene named after an architect Buckminster Fuller who designed geodesic dome structures. Its existence was proven by Kroto in 1985, while attempting to understand the mechanisms of the formation of the long-chain carbon molecules that are produced in circumstellar shells and interstellar space.[4] Kroto, who shared the 1996 Nobel prize in chemistry for this discovery, said: ''This most exciting breakthrough provides convincing evidence that the buckyball has, as I long suspected, existed since time immemorial in the dark recesses of our galaxy.'' A laser pulse was used to vaporise carbon from a graphite target into a stream of helium gas and the vaporised fragments collided and formed clusters. The system was cooled in supersonic beam and analysed by time-of-flight mass spectra to observe a peak counting 60 carbon atoms. Conditions were modified to enhance the $C_{60}$ peak with respect to the others (**Figure 1**).

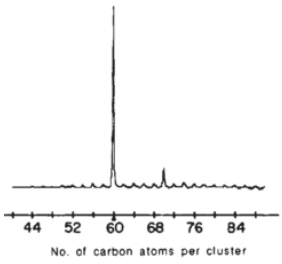


**Figure 1.** Time-of-flight mass spectra – first evidence of $C_{60}$.

In 1986, it was predicted that if a large-scale synthetic route to the $C_{60}$ fullerene could be found, the practical and chemical value of this substance may be extremely high. Derivatives of $C_{60}$ such as halogenated compounds $C_{60}F_{60}$ could be super-lubricants, and also transition metal fullerenes $C_{60}Fe$ or atoms placed in the interior could produce species that will exhibit unusual properties.[4]

In 1990 $C_{60}$ was isolated from soot produced from electrical discharge between carbon rods. It was partially purified to obtain evidence of $C_{60}$ by Infrared spectra and X-ray diffraction studies[5] [6] and the apparatus for large-scale synthesis was described.[7] It was possible to perform solid state $^{13}C$ NMR and confirm two different bond lengths and the calculated predictions were confirmed.[8],[9] Currently, the $C_{60}$ is produced on a large scale by extracting it from soot, purified by column chromatography and sublimed to afford 99.9% pure $C_{60}$. Soot can be prepared by pyrolysis of tetralin or toluene or from graphite by radio frequency or arc plasma.[10]

On Earth, $C_{60}$ occurs naturally in soot, but interestingly in 2010 the presence of $C_{60}$ molecules was also discovered in a nebula[11] and in 2012 in gas orbiting a star[12].

Tenuous gas between the stars is called the interstellar medium and its absorption features are called diffuse interstellar bands. There is approx. 500 interstellar bands measured up to date.[13] In 2015, laboratory evidence was obtained showing that two of the diffuse interstellar bands at 9,632 angstroms and 9,577 angstroms are arising from $C_{60}^+$.[14] In 2019 astronomers confirmed this finding using Hubble telescope and provided further evidence of $C_{60}^+$ floating in the interstellar medium.[15] Some of the fullerenes that have been found in a 65-million-year-old meteorite also contained endohedral noble gases. This suggests that these molecules were formed in the universe.[16] Recently, a method has been developed to detect $He@C_{60}^+$ in space.[17]

### 1.1.2 Structure

In $C_{60}$ (**Figure 2**) every pentagon is surrounded by five hexagons. The pentagons never share an edge (Isolated pentagon rule) and therefore two structural moieties can be observed (**Figure 3**).

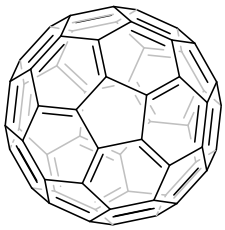

**Figure 2**. **$C_{60}$** molecule.

The bond between two hexagons ([6,6] bond), represented as a double bond is 1.38 Å long. The bond between pentagon and hexagon ([5,6] bond) is 1.45 Å long and is represented as a single bond. Since their discovery, a debate has been going on about the aromaticity of fullerenes. Initially, $C_{60}$ was predicted to be an aromatic, stable and unreactive molecule.[18] The statement about non-reactivity was later proved to be wrong as $C_{60}$ undergoes a wide variety of reactions.[19] It was assumed that poor

delocalisation of electrons causes high reactivity and $C_{60}$ is a massive closed alkene rather than an aromatic molecule.[20] This was then refuted by concluding that the lack of substitution reactions, which are characteristic for planar aromatic molecules, cannot be taken as a reactivity criterion of fullerenes as they do not contain any hydrogen to be substituted. It was proven experimentally and theoretically that fullerenes are aromatic. They sustain ring currents because of the aromaticity, and the difference in bond lengths is directly related to the occupation of its π orbitals. Partial localisation of the π orbital bonds is corresponding to the shortening of the [6,6] bond. [21] The fullerenes are strongly electron-accepting and react readily with nucleophiles.[20] The driving force of these reactions is the strain energy released through a $sp^2$ to $sp^3$ change in the hybridisation of the carbon atoms of the [6,6] bond. When the Smalley group forced hydrogenation of $C_{60}$ with Birch reduction (Li, liquid $NH_3$, $^t$BuOH), they could only prepare $C_{60}H_{36}$ and no more carbon atoms were reduced. The reason for this could be that Birch reduction only attacks conjugated double bonds and after the 36 protons are added, simply no more conjugated bonds are left.[22] The fully reduced $C_{60}H_{60}$ has not been prepared up to date. Calculations suggest that $C_{60}H_{60}$ is energetically less stable than $C_{60}H_{36}$.[23]

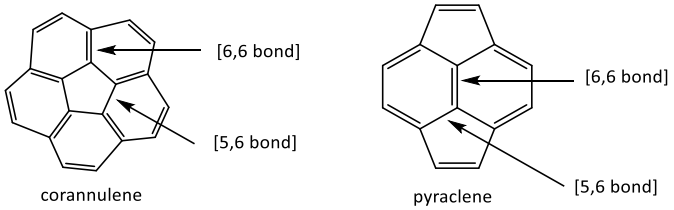


**Figure 3.** Structural moieties in **$C_{60}$**.

Buckminsterfullerene $C_{60}$ is the most common naturally occurring fullerene. It is also one of the largest molecules observed to exhibit wave-particle duality[24] and the smallest fullerene that contains pentagonal and hexagonal rings where no two pentagons share an edge (**Figure 3**). This work is focused on $C_{60}$ because of its icosahedral symmetry and good reactivity however it is only one of the many fullerene balls that exist. Another common fullerene is $C_{70}$ which has $D_{5h}$ symmetry. It is structurally similar to $C_{60}$ but it has a belt of 5 hexagons inserted in the middle.[25]

## 1.2 Fullerenes enclosing atoms and molecules

Fullerene cages have hollow space inside of them which is a unique environment. Since the fullerene discovery, scientists have been eager to explore possibilities of inserting atoms and molecules inside this space. The diameter of the void varies depending on the size of the fullerene and ranges from 0.4 to 1 nm from $C_{60}$ to $C_{240}$.[26]

### 1.2.1 Metallofullerenes

Endohedral metallofullerenes (EMFs) are fullerenes with metallic species encapsulated inside.[27] The electron transfer from the enclosed metal to the fullerene cage hugely alters magnetic and electronic properties of the cage and the EMFs in fact exist in the form of $M^{n+}@C_x^{n-}$.[26]

The first experiment forming lanthanum-fullerene complex was obtained by Smalley only a week after the initial 1985 discovery of the $C_{60}$. Low density graphite disk was exposed to a boiling saturated solution of $LaCl_3$ in water and laser vaporisation was performed. Stable $C_{60}La$ and various $C_nLa$ complexes (where n is an even number) were formed and ionised by ArF excimer radiation to be detected on TOF mass spectrometer. Each complex had one (and only one) La atom which could not be knocked off by the laser blast with dominant ions $C_{60}^+$ and $C_{60}La^+$. This was presented as an evidence that the La atom is inside the carbon cluster.[28] Triggered by Smalley, the Kaldor group tried to provide evidence that the La is not inside the carbon cage but attached on the outside of the fullerene. They demonstrated appearance of fragments of $C_{60}La$ in the MS spectra using higher intensity ArF[29] and attachment of multiple La atoms to a carbon cluster. They also proposed that clusters $C_{70}$ and $C_{60}$ have higher ionisation cross section.[30] Additional proof of metals inside carbon clusters was then shown by Smalley[31] and Freiser, who demonstrated that externally bound metals behave in significantly different way.[32] Modification of preparation of fullerenes enclosing metals was presented in 1991. Graphite rod impregnated with $La_2O_3$ was vaporised using a laser beam in the oven heated to 1200 °C trapping a single lanthanum atom. Vaporised fullerenes were then carried away by the flowing gas. The evidence for $La@C_{60}$ and higher $La@C_n$ was strong, but most of these compounds did not seem to be stable (except $La@C_{82}$) or readily isolable.[33] First isolation of EMFs was achieved in 1993 by recycling HPLC where Shinohara prepared $Sc_2@C_{74}$, $Sc_2@C_{82}$, and $Sc_2@C_{84}$.[34] Since then the HPLC methods allowed to prepare numerous EMFs.[35] In 2006 Stevenson group developed more efficient non-chromatographic separation method called 'stir and filter approach' thanks to the different electrochemical properties of EMFs.[36][37][38] In 2010, Aoyagi prepared and completely isolated $Li@C_{60}$ cation,[39] which later found use in molecular electronics as a 'multi-state molecular switch'.[40] In 2017, Echegoyen group demonstrated that EMFs can be selectively purified by encapsulation into supramolecular nanocapsules,[41] and EMFs like $ScN@C_{80}$[41], $U_2@C_{78,80}$[42][43], $U_2C@_{78,80}$[42][43] and $ScCU@C_{80}$[43] were isolated. EMFs containing one to three metal atoms are called mono-, di-, tri- and numerous examples have been isolated and fully characterized.[44] Moreover, metallic clusters like metal carbides[45], nitrides[46][47], oxide[48][49], sulphides[50][51] and cyanides[52][53] have been trapped inside fullerene cages. Application in advanced magnetic resonance imaging was found for $Gd@C_{82}$[54][55]. The toxic $Gd^{3+}$ ions entrapped in $C_{82}$ functionalised with negatively charged carboxyl or

hydroxyl groups to enhance water solubility, exhibit 10-40 times higher $^{1}H$ relaxivity than most commercial contrast agents.[56] The derivatives of $Gd@C_{82}$ can be also used in cancer treatment as they inhibit tumour cells or damage tumour blood vessels.[57] EMFs have a great potential in other fields such as optoelectronics[58], single molecule magnets[59] and electron spin quantum computer units.[60]

### 1.2.2 $N@C_{60}$ and $P@C_{60}$

Nitrogen and Phosphorus trapped inside $C_{60}$ provide an excellent tool for atomic physics and nanotechnology. N and P inside $C_{60}$ fullerene retain their atomic character because they do not exchange electrons with the $C_{60}$, hence do not form covalent bond. Instead, the electronic charge cloud of N and P contracts and they are in quartet electronic spin state which may be ascribed to a free atomic spin state.[61] The synthesis of atom like nitrogen inside $C_{60}$ was first published in 1996. $C_{60}$ was bombarded with plasma ions from plasma discharge ion source, called ion implantation method. Source of plasma was conveniently a sputter gun used for cleaning. $N@C_{60}$ exhibits paramagnetic centre with hyperfine interaction properties. The presence of single nitrogen was proven experimentally, by confirming the electron spin state to be S = 3/2, which corresponds to three unpaired electrons in the *p* shell in the ground state.[62] This exceptional molecule has found its use in quantum computing as it provides building blocks for the qubits of quantum computers.[63] Several methods for synthesis have been developed in recent years focusing mostly on controlling the energy of the ions by using a different plasma source. Most recent preparation method from 2019 is based on the collision of vaporized fullerenes and dense plasma particles produced by laser ablation from solid boron-nitride. This method achieved purity of $4.52 \times 10^{-3}$% $N@C_{60}$.[64] In 2004 100% filled $N@C_{60}$ was isolated by recycling HPLC using Cosmosil™ columns. Complete UV/Vis spectroscopy was reported, showing that the $N@C_{60}$ lacks the vibrational transitions of $C_{60}$ that occur between 440 nm and 640 nm. (**Figure 4**).[65] It was proposed that this is due to effect of the nitrogen atom on Herzberg–Teller vibronic interactions which enable the vibrational transitions between 440 nm and 640 nm in an empty C60 molecule.[66] UV spectra measured in our laboratory for endohedral fullerenes $A@C_{60}$ (A = He, $H_2$, Ne, Kr, Ar, $CH_4$) do not show this phenomena. $N@C_{60}$ with purity of 0.83% was prepared by the ion implantation method from 2015. Nitrogen ions are generated from nitrogen gas, form a high density plasma and then collide with sublimated $C_{60}$ molecules.[67] Nowadays $N@C_{60}$ and metallofullerenes are produced commercially. Ion implantation method was also used for synthesis of $P@C_{60}$[61] and was enriched by recycling HPLC up to 13% filling factor.[68]

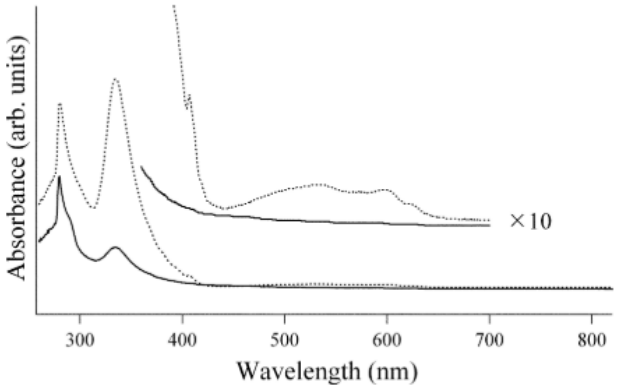


**Figure 4**. Comparison of the UV/Vis absorption of $C_{60}$ (dotted line) and N@$C_{60}$ (solid line).

### 1.2.3 Noble gases in fullerenes

Influence of noble gases on the inside of fullerenes are a great subject for theoretical calculations[69] and various studies[70][71][72][73][74][75][76][77][78][79], such as predicting the heat capacity of Ng@C60 [76] or effects of target polarization in electron elastic scattering[80]. It was presented that the Noble gas inside $C_{60}$ has an impact on the polarization potential [81] and structural and dynamical properties of the $C_{60}$ shell[82] [83] as well as the impact of the unique environment of the shell on the noble gas showing that the noble gas is less 'polarisable' inside $C_{60}$[84] than outside. Mechanical and electronic properties of Ne@$C_{60}$ were predicted via a structure distortions study[85][86] and $^3$He@$C_{60}$ was studied by NMR focusing on magnetic properties of the π-systems showing that it can be used as a tool for following fullerene chemistry using $^3$He NMR. [87][88][89][90][91] Selected articles are for illustrational purposes to stress the variety and high interest in Ng@$C_{60}$.

The development of preparative methods of noble gas inside fullerenes started in early 90s. In 1991 Schwarz group presented that high energy collisions of $C_{60}^{\bullet+}$ with $^4$He and $^3$He produce ions with additional mass that corresponds to $C_{60}$@$^4$He$^{\bullet+}$and $C_{60}$@$^3$He$^{\bullet+}$[92][93] and the endohedral atom was proven in 1992 by neutralisation and then reionisation with a four tandem mass spectrometer.[94] In 1993 Saunders group showed that when $C_{60}$ is prepared from a graphite arc in helium at low pressure, one in a million $C_{60}$ molecules contains a helium atom.[5][95] None of the methods above allowed preparation of noble gases inside $C_{60}$ in macroscopic quantities. In the same publication it was shown that noble gases can be incorporated into $C_{60}$ at high pressure and temperature producing compounds He@$C_{60}$ and Ne@$C_{60}$. It was proposed that the process could take place by the reversible breaking of one or more bonds, opening a 'window' that is big enough for atom entry.[96] Using this method, in 1994 the Saunders group presented incorporation of He, Ne, Ar, Kr and Xenon into fullerenes $C_{60}$ and $C_{70}$ and achieved incorporation factor up to 0.3%. In this process fullerenes are heated in a furnace to

about 600 °C for 5 h in the presence of a noble gas up to a pressure of 2700 atm. This method was done on a substantially larger scale (up to 100 mg) than previous methods.[96] It was later improved by using larger quantities, higher pressure and temperature to achieve better incorporation.[97] In 2003 the filling factor of the heat/high pressure method was improved by using catalyst KCN, that generates the $CN^-$ and helps breaking the bonds in $C_{60}$ to incorporate noble gas. Unfortunately the yield recovery is about 10 times lower than with no catalyst at all.[98]

In 2009, Wang group reported preparation of $He@C_{60}$ and $He_2@C_{60}$ by an explosion method. Fullerenes, together with the explosive and noble gas are in an enclosed space. Using a flying plate, the explosion energy is converted to kinetic energy of the gas molecules and penetrates the wall of the $C_{60}$ encapsulating one or two atoms of helium in yields up to 6% and 0.4% respectively.[99] The endohedral fullerenes can be further enriched by preparative HPLC. The methods and achieved results of noble gas in fullerenes prepared by methods where the gas is forced into the fullerene are summarised in **Table 1**.

| **Fullerene** | **Method** | **Yield**[a] | **Filling factor**[b] | **HPLC enriched** | |
|---|---|---|---|---|---|
| | | | | mass | purity |
| **$^3He@C_{60}$** | High Pressure/Temperature[88] | – | 0.1% | – | – |
| **$^4He@C_{60}$** | High Pressure/Temperature[100] | – | 0.1% | – | – |
| | Explosive[99] | 50% | 6% | – | – |
| | KCN method[98] | 7.5% | 1% | – | – |
| **$^4He_2@C_{60}$** | Explosive[99] | 50% | 0.4% | 0.3 mg | 70%[c] |
| **$Ne@C_{60}$** | High Pressure/Temperature[100] | 66% | 0.2% | – | – |
| **$Ar@C_{60}$** | High Pressure/Temperature[100] | 45% | 0.2% | 1.3 mg[101] | 98% |
| **$Kr@C_{60}$** | High Pressure/Temperature[100] | 25% | 0.2% | 0.14 mg[102] | 90% |
| **$Xe@C_{60}$** | High Pressure/Temperature[100] | 45% | 0.04% | 0.32 mg[103] | 50% |

**Table 1**. Achieved results by original methods of $Ng@C_{60}$ preparations and enrichment. (Ng = Noble gas).

The syntheses of $Ng@C_{60}$ and $Ng@C_{70}$ had improved significantly after the reactivity of fullerenes and the process 'molecular surgery' were discovered and will be discussed in the following sections.

[a] Yield is calculated from recovered $C_{60}$ from the experiment
[b] Filling factor is calculated out of recovered $C_{60}$
[c] Exact purity was not stated, 70% was estimated from the depicted mass spectrum

## 1.3 Chemical opening of the fullerene orifice

Initially endohedral fullerenes were prepared by procedures yielding filling factors of up to 1%.[104] For synthesis of atomic (excluding metallofullerenes) and molecular endohedral fullerenes an efficient pathway has been developed called 'molecular surgery'[105](**Scheme 1**).

This section highlights the most relevant achievements in $C_{60}$ reactivity towards opening holes, large enough to insert atoms and molecules and possibly suture the orifice to prepare A@$C_{60}$.

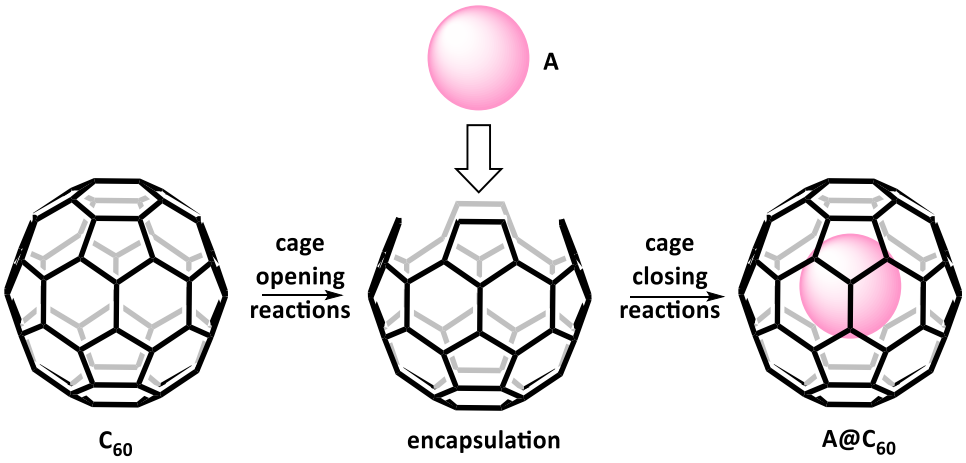


**Scheme 1.** Molecular surgery.

Molecular surgery is a sequence of organic reactions breaking bonds to afford an open cage fullerene (OCF) – a fullerene with a hole in it. If the orifice is an appropriate size a small atom or molecule can be inserted inside. Closure reactions finish the procedure to form endohedral fullerene.[19] This method allows the synthesis of fullerenes containing molecules such as $H_2$[106], $H_2O$[107] and many other that will be mentioned in later paragraphs, which was not possible with explosion and high pressure methods.

Thanks to developed chemical routes, 100% filled endohedral fullerenes can be synthesised allowing methods such as NMR, INS, or IR to study quantum dynamics of the entrapped molecule in detail. It was shown that entrapped molecules behave as if they were in a very low-pressure gas state, exhibiting free rotation at cryogenic temperatures, due to the inert and highly symmetrical environment of the cavity.[108][109][110][111][112]

### 1.3.1 Development

Molecular surgery was developed by exploring reactions on the fullerene cage. The first example of fullerene cage reaction was presented in 1991 by confirming that the $C_{60}$ degrades in the presence of oxygen and light.[113] Important controlled cage reaction was performed in 1992, where the $C_{60}$ derivative was isolated for the first time by reacting with diazomethane and forming thermally unstable $(CH_2N_2)C_{60}$. After reflux, the final molecule $H_2C_{61}$ [5,6]-dihydrofulleroid **1** was formed and isolated (**Figure 5**).[114]

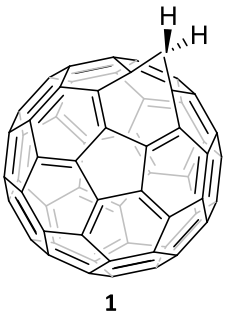


**1**

**Figure 5.** $H_2C_{61}$ [5,6]-dihydrofulleroid.

The adduct on the cage fullerenes can be modified and expanded by a great number of reactions that have been developed since. Fulleroids and azafulleroids could be prepared by addition of diazomethanes[114],[115], diazoacetates[115],[116] and diazoamides[117] to the [6,6] ring junctions of fullerenes in a [3+2] manner (**Scheme 2**).

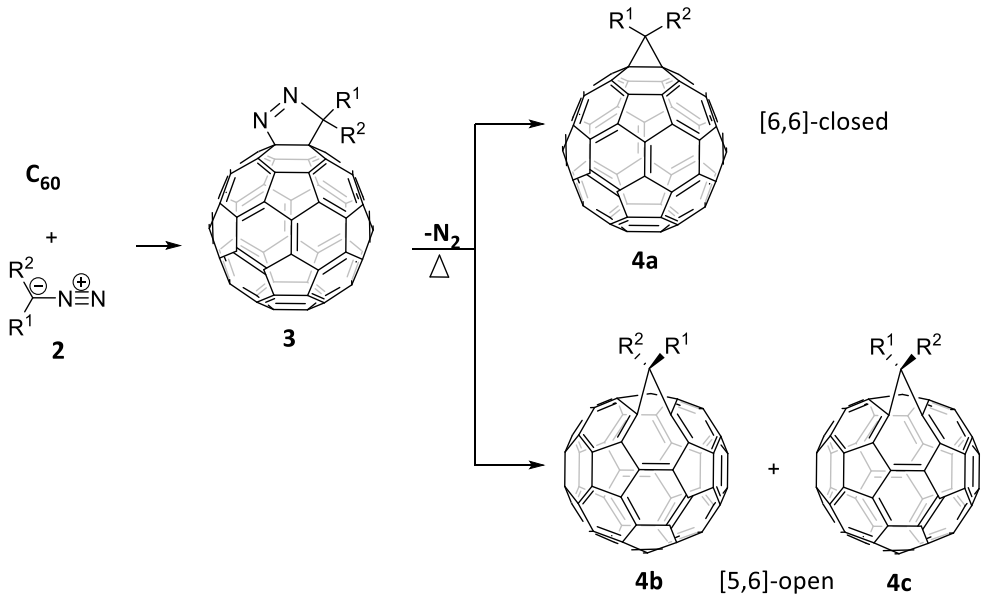


**Scheme 2.** The reaction of diazo compounds with $C_{60}$.

$N_2$ is thermally extruded from [6,6]-bridged closed fullerene, and this leads to the formation of [5,6]-open fullerene or [6,6]-closed fullerene adducts.

Azafulleroids **5** were reported in 1993 for the first time by thermal addition of azides to $C_{60}$.[118] In 1996 [6,6]-bridged fullerotriazoline **6** was characterised by single-crystal X-ray analysis (**Figure 6**).[119]

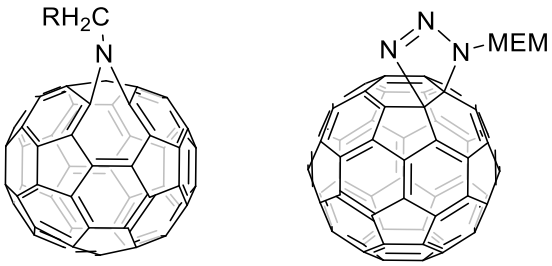


**5** **6**

R:
a) $OCH_2CH_2SiMe_3$
b) $C_6H_5$
c) 4-MeO-$C_6H_4$
d) 4-Br-$C_6H_4$

MEM = $CH_2OCH_2CH_2OCH_3$

**Figure 6.** Azafulleroids and fullerotriazoline.

When self-sensitised photooxygenation[120] was applied to MEM-substituted [5,6]azafulleroid, the first proper controlled opening of the fullerene cage was discovered (**Scheme 3**).[121]

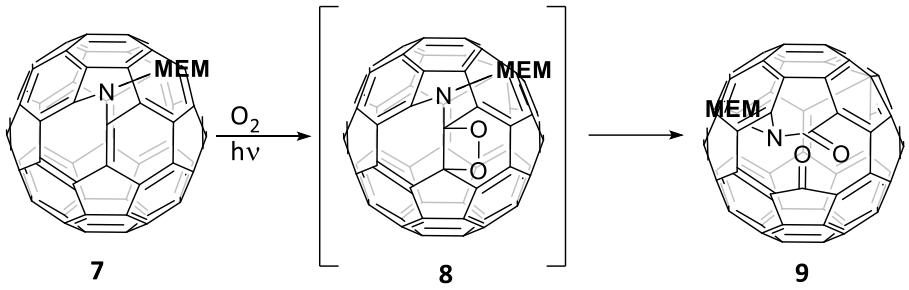


**7** **8** **9**

**Scheme 3.** Self-sensitized photooxygenation of azafulleroid to form **9**.

Another important discovery in open cage fullerene adduct synthesis was made in 1996 when intramolecular [4+4] cycloadditions followed by retro [2+2+2] rearrangement reactions were observed in the synthesis of fullerene cobalt complex (**Scheme 4**).[122],[123]

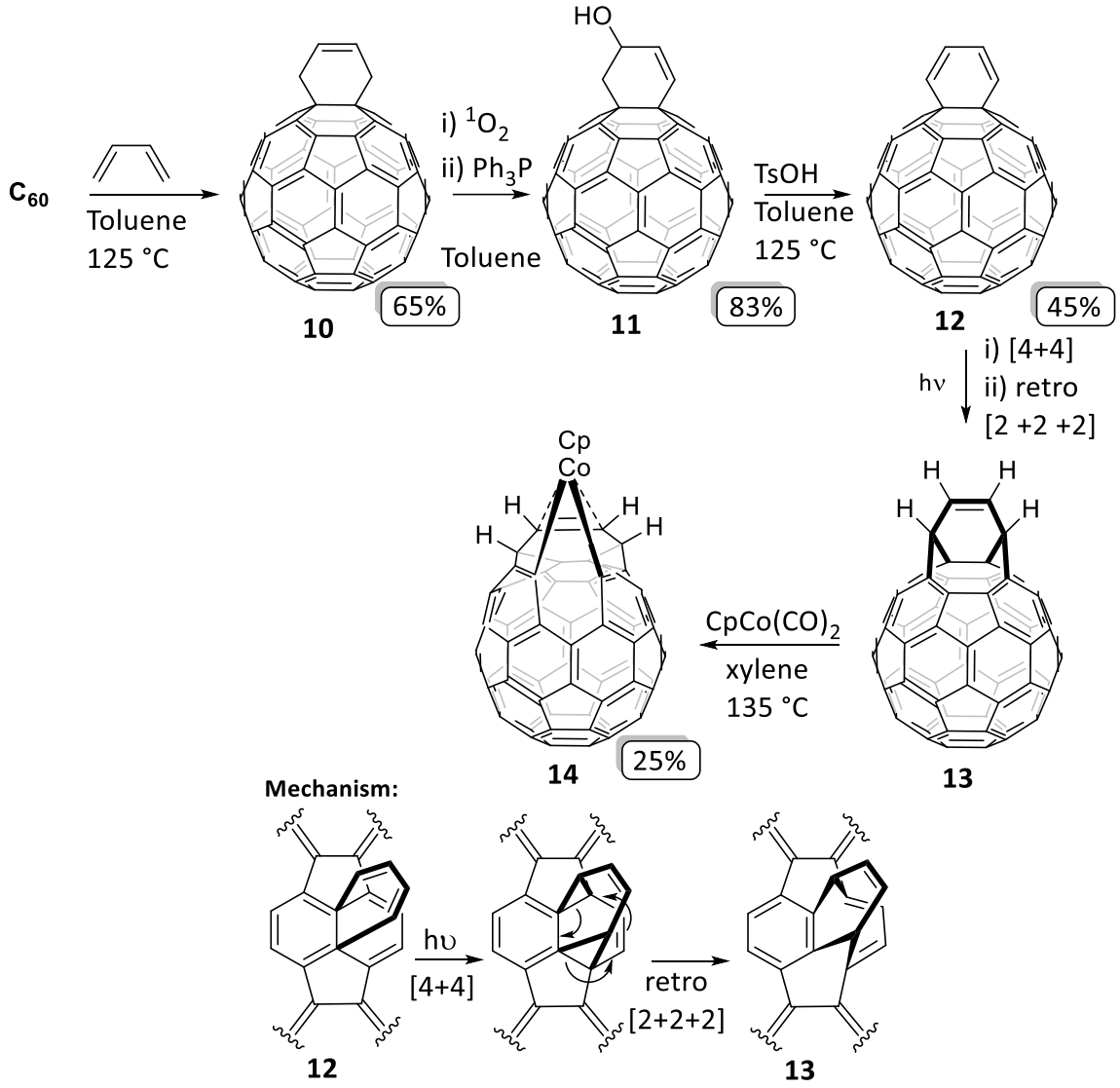


**Scheme 4.** Preparation of fullerene cobalt complex and mechanism of the 8-membered ring formation rearrangement.

A Diels-Alder addition reaction was also demonstrated later by Rubin using a diazidobutadiene system. A hole that was opened was big enough to allow small atoms and molecules such as He or $H_2$ to enter the fullerene cavity.[124] Rubin also coined the term 'molecular surgery'.[105]

Opening $C_{60}$ to give an 8-membered orifice became the first step in 'molecular surgery' in most of the procedures discovered since then (**Scheme 1**). Reaction of 4,6-dimethyl-1,2,3-triazine with $C_{60}$ discovered in 2001 by Murata gives a nice example of formation of the 8-membered ring orifice with a heteroatom on the rim **Scheme 5**.[125]

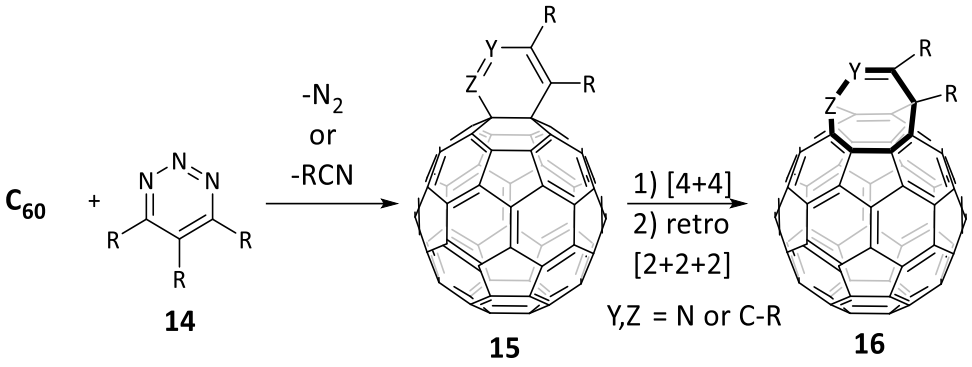


**Scheme 5.** Reaction of **$C_{60}$** with 4,6-dimethyl-1,2,3-triazine **14**.

The mechanism is demonstrated on the example discovered in 2003 by Murata. 1,2,4-triazine derivative **17** reacts smoothly with $C_{60}$, starting with [4+2] addition of triazine to [6,6] bond followed by extrusion of nitrogen giving 2-aza-1,3-cyclohexadiene-fused **$C_{60}$** derivative **18b**. This then undergoes [4+4] cycloaddition, continuing with retro [4+2] rearrangement to form **19** (**Scheme 6**).[126]

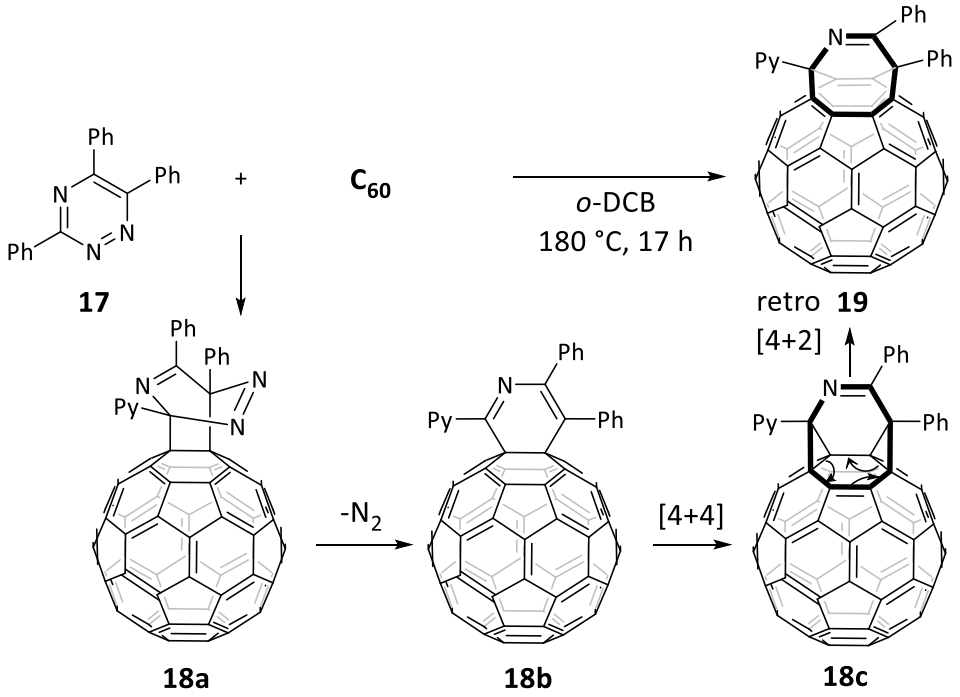


**Scheme 6.** Synthesis of 8-membered ring fullerene derivative **19**.

Another approach to the formation of the 8-membered ring was presented recently by Yamada. One pot cage opening was achieved by reaction of $C_{60}$ with propargylic phosphate **20** in the presence of CuCl. The reaction proceeds via transformation of the phosphate to the 1,3-dienyl phosphate **21** which then reacts with $C_{60}$ via [4+2] cycloaddition to form **22**. *Syn*-elimination of the phosphodiester forms

the intermediate **23**, which then rearranges to 8-membered ring **24** by initiation with *hv* in $CS_2$ (**Scheme 7**).[127] The final step proceeds via similar mechanism as the formation of the 8-membered ring presented in **Scheme 4**.

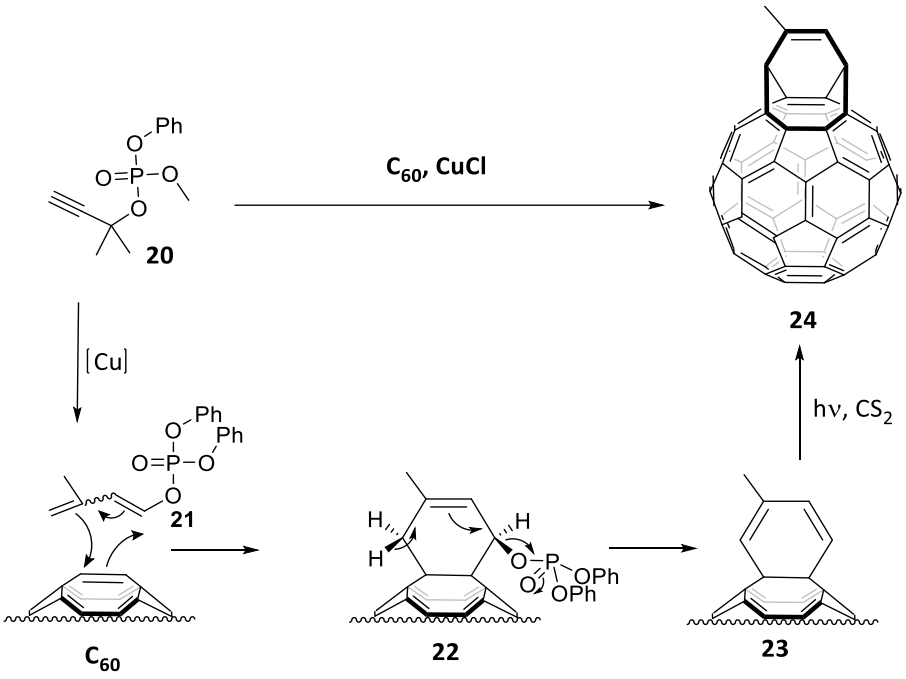


**Scheme 7.** 8-Membered ring formed **24** by copper catalysed cascade reaction.

#### 1.3.1.1 Opening from 12 to 17-membered ring orifices

In 1999 Rubin presented effective opening of $C_{60}$ by 4+2 addition of diazobutadiene followed by immediate loss of two molecules of $N_2$. The intermediate then reacted with oxygen to form a stable 14-membered ring **27** (**Scheme 8**).[124]

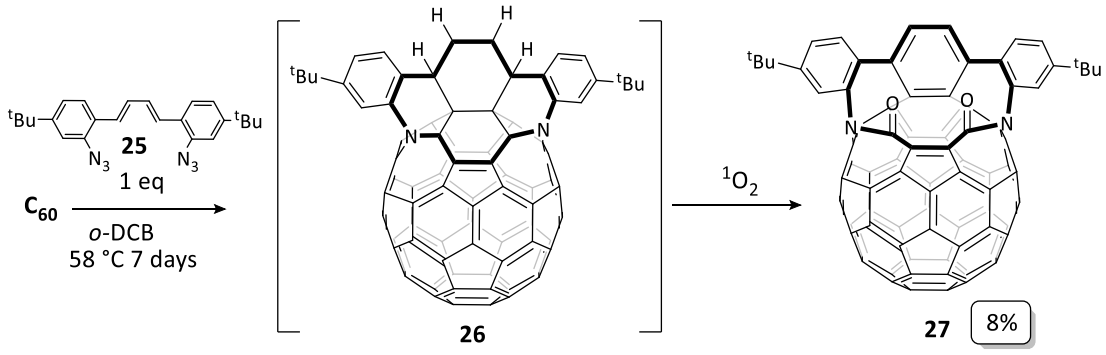


**Scheme 8.** Formation of **27**.

Double bonds in the 8-membered-ring can undergo oxidative cleavage by photochemically generated singlet oxygen[128][129] which allows the orifice to be expanded to a 12-membered ring. Singlet oxygen

adds to the double bond forming dioxetane. The addition of singlet oxygen is kinetically favourable on the double bond closer to the pyridine group probably because of the presence of two bulky phenyl groups (**Scheme 9**).[126] Broken symmetry caused by nitrogen could also explain the selectivity.

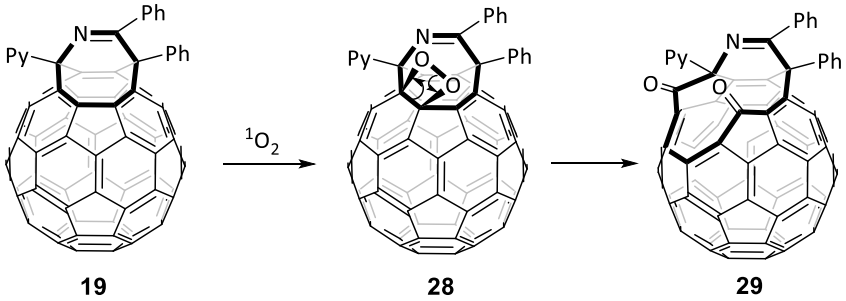


**Scheme 9.** Oxidative cleavage by photochemically induced singlet oxygen.

The important orifice expansion to a 13-membered ring was achieved by inserting sulphur atom into the single C-C bond, achieved by heating with elemental sulphur and the electron donor TDAE (Tetrakis(dimethylamino)ethylene).[126]

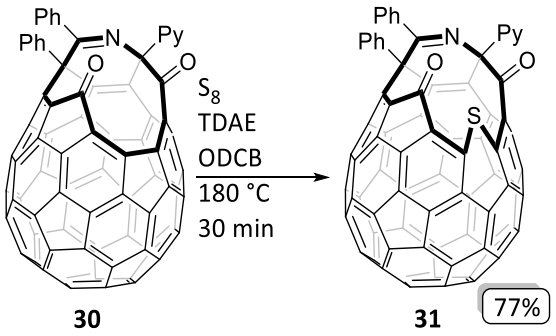


**Scheme 10.** Synthesis of 13-membered ring orifice of $C_{60}$.

The opening to **31** was improved by using alkanethiolate instead of TDAE and this method was also applied to synthesis of a 13-membered ring with selenium **32** instead of sulphur. Using NaSMe for **31** did not require heating but in the case of Se insertion, heating to 180 °C was necessary (**Scheme 11**).[130]

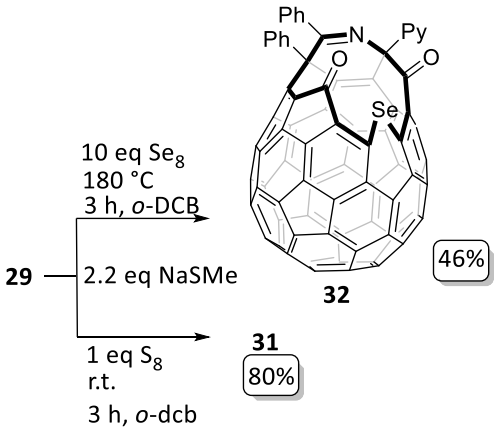


**Scheme 11**. Improved conditions for **31** synthesis and insertion of Se into the **29** orifice.

In 2003 Murata and Iwamatsu presented another approach to OCF when the **9** was expanded by reaction with hydrazines. **9** reacted with phenylhydrazines in a regioselective manner and gave **33.** Two hydrogens from the hydrazine migrate to the OCF rim and form a methylene (**Scheme 12**).[131]

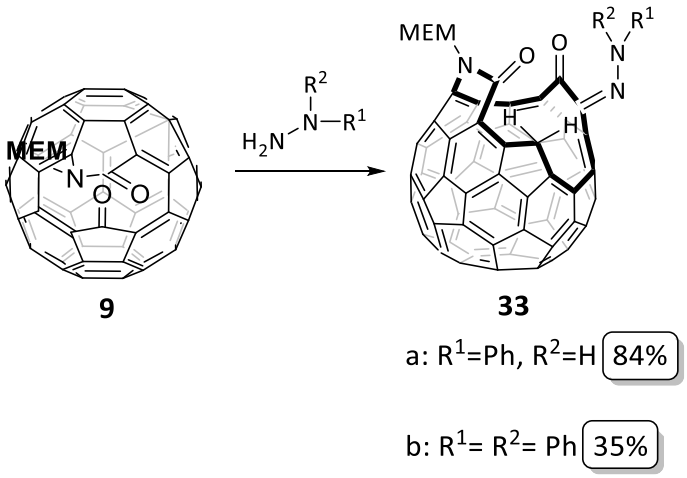


**Scheme 12.** Synthesis of 15-membered ring orifice OCF **33**.

The same reaction conditions were also applied on derivative **34** that formed a 16-membered ring OCF **36**[132] (**Scheme 13**). **34** was prepared by [2+2+2] palladium catalysed cycloaddition of acetylene derivatives[133] followed by singlet oxidation.[129]

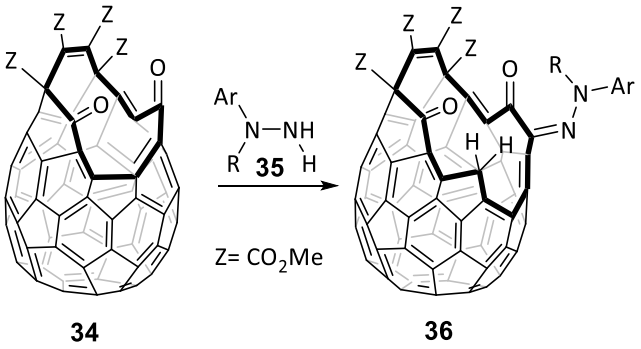


**Scheme 13.** Expansion of the ring orifice of **34** by reaction with hydrazines to form 16-membered ring orifice **36**.

Although this work is focused on $C_{60}$ synthesis, some remarkable advances in molecular surgery must be mentioned on $C_{70}$, because they paved the way for the successful completion of molecular surgery on $C_{60}$. $C_{70}$ has bigger cavity than $C_{60}$ thus the possibility of encapsulation of more than one guest atom or molecule emerges.[134] There are fewer examples for OCF $C_{70}$ than for $C_{60}$ probably because the $D_{5h}$ symmetry causes difficulties in the synthesis, separation and characterisation. In 2008, a similar procedure that was used for $C_{60}$ (**Scheme 6**) was applied on $C_{70}$ by Komatsu. The symmetrical 8-membered ring was formed by Diels Alder reaction with pyridazine derivative followed by singlet oxygen cleavage to form two diketone OCF **39** derivatives with 12-membered ring opening. The sulphur atom was then inserted into the C-C bond on the rim by the same reaction as in **Scheme 10**.[135]

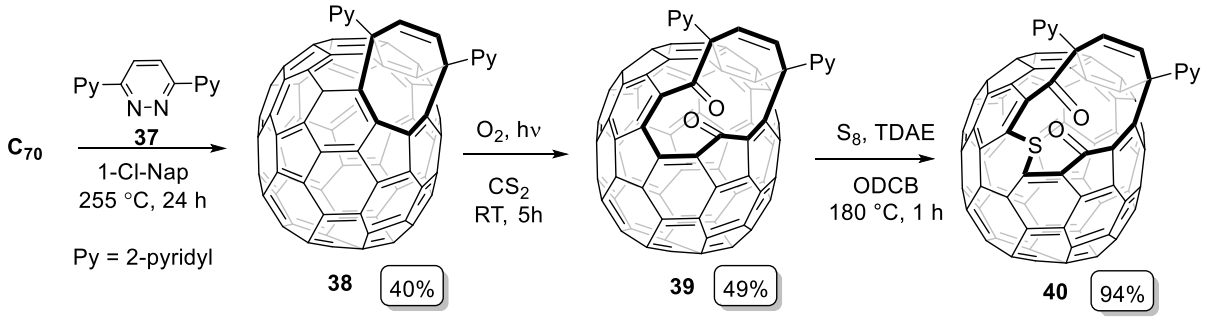


**Scheme 14.** Opening $C_{70}$ into 13-membered ring.

This synthetic method was applied to $C_{60}$ (**Scheme 15**) using different aryl groups in the pyridazine derivative. It was found that the aryl group 2-*tert*-butylpyridyl is contributing to better solubility of the OCF and other OCF derivatives in the subsequent syntheses.[136] The **43** derivative was formed in the same manner as **39** without isolating the **42** 8-membered ring and was taken straight to the single oxygen double bond ring cleavage. To increase the solubility of $O_2$, $CS_2$ was added during the irradiation step which gave 43% yield after 23 h.[136] The $CS_2$ was later substituted for $CCl_4$ which increased the yield to 52% but the reaction time was prolonged to 48 h (**Scheme 15**).[137] Thanks to $C_{60}$

symmetry, the **42** diene molecule is symmetrical unlike the 8-membered ring compound **19** in **Scheme 6**. Diketone **43** was then expanded to 16-membered ring **45** by oxidation with two equivalents *N*-methylmorpholine-*N*-oxide **44** (NMO). **45** is instantly hydrolysed and forms a hemiacetal bridge in the 13-membered ring molecule **46.**

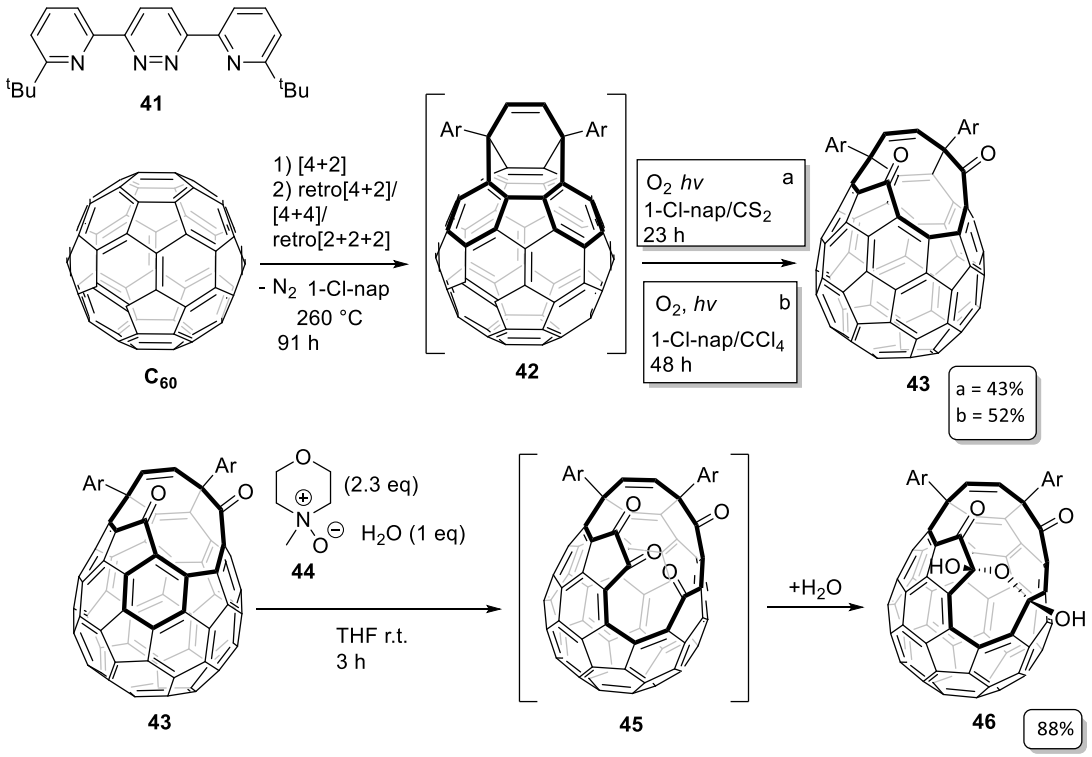


**Scheme 15** Synthesis of open cage fullerenes **42, 43, 45** and **46**.

The 13-membered orifice **46** is in equilibrium with its dehydrated form **45** tetraketone. There are several methods of dehydrating **46.** Possible conditions are reflux in the toluene over molecular sieves or heating the solid **46** in high vacuum (180 °C, ~0.2 mm/Hg). It was discovered to be stable as solid and in dry solution. It gradually hydrates under ambient conditions in solution. Tetraketone **45** can be expanded by inserting sulphur into the C-C bond in the same manner as in the formation of **31** (**Scheme 10**). However, the reactivity of the tetraketone **45** in this reaction is not the same as for the N-diketone **31** or for the N-sulfide **51**. The reaction yields into the desired sulfide **47** when 0.2 eq of TDAE is used. When a higher amount of TDAE is used there are two other unprecedented products formed (**Scheme 16**). When the sulfide **47** was treated with sulphur and TDAE the formation of products **47b** and **47c** occurred showing that these by-products are a result of stepwise insertion of sulphur.[138]

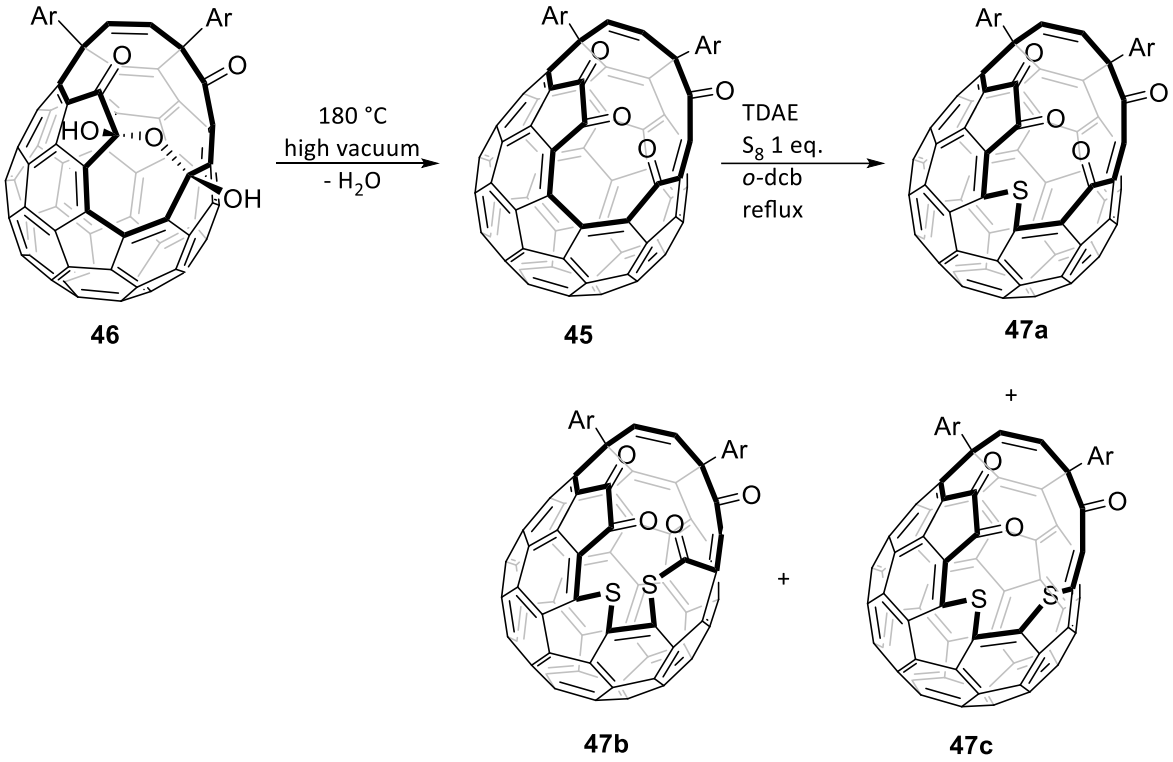


**Scheme 16.** Expansion of the orifice of **45** by inserting sulphur atoms into the rim

| Entry | TDAE/eq | Time/h | Isolated yield of 47 % | | |
|---|---|---|---|---|---|
| | | | a | b | c |
| **1** | 0.2 | 0.25 | 60 | 0 | 0 |
| **2** | 0.5 | 0.25 | 24 | 16 | 31 |
| **3** | 2.0 | 14 | 0 | 0 | 68 |

**Table 2.** Sulphur insertion by-products formed due to electron donor.

A recent study was published by the Murata group about the sulfide **47** forming organophosphorus zwitterions (**Scheme 17**). When **47** was reacted with $PMe_3$ in toluene under inert atmosphere, ylid **48** was rapidly formed. However, upon exposing the reaction mixture to air the compound instantly converted back to sulfide **47**. Despite that, it was possible to form crystal of ylid **48** and analyse by X-ray crystallography to confirm its structure. When sulfide **47** was heated with two equivalents of $PMe_3$, a stable phosphorus compound was formed, and one of the 1,2-diketone oxygens was eliminated by forming $P(O)Me_3$. The reaction was performed with different phosphines and all produced the ylids **49**. It was discovered that during work-up the **48** was hydrolysed to methylene derivative **50** and when the hydrolysis was purposely performed on ylid **48** it was completed after 1 day. The **49b-e** were only hydrolysed up to 13% even after 6 days of reaction providing steric protection of phosphorus centers.[139] Formation of stable ylid by elimination of the 1,2-oxygen of an OCF tetraketone **45** was previously reported in synthesis of **HF@$C_{60}$**[108] and will be discussed in depth later in the discussion (**4.1**).

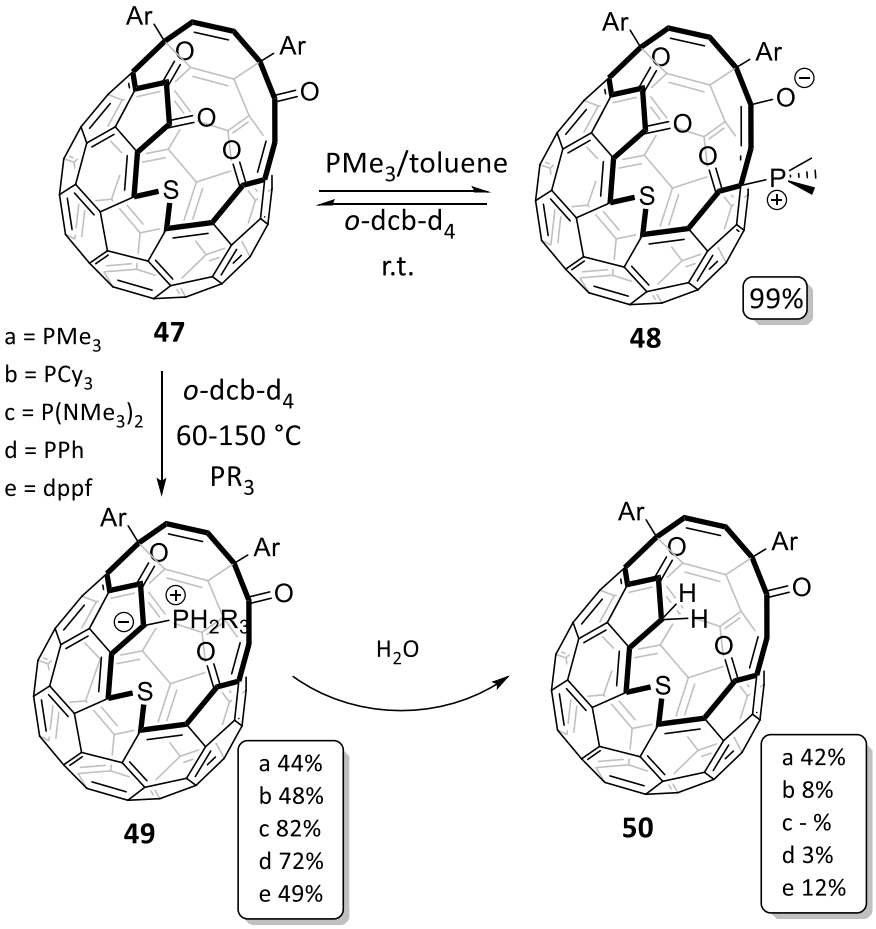


**Scheme 17.** Formation of **48** and **49** zwitterions.

The photophysical properties of $C_{70}$ and $C_{60}$ differ (e.g. stronger absorption of visible light of $C_{70}$ [140]), but their reactivities are somewhat similar leading to the same type of OCF (**Scheme 14**, **Scheme 15**) but there are also cases leading to completely different products. Diketone **51** was oxidised to hemiacetal **52** by one equivalent NMO and the presumed mechanism was confirmed by isolating the epoxide intermediate formed by reaction of one equivalent of NMO at -78 °C (**Scheme 18**). Using more equivalents of NMO leads to a mixture of products indicating a different reactivity pattern between the two fullerenes. Same reaction conditions did not apply to diketone **43** and the intermediate analogue was not isolated. DMAPO (4-(dimethylamino)pyridine 1-oxide) was used to prepare the tetraketone **54** in high yield. Hemiacetal **52** can be dehydrated in the same manner as hemiacetal **46** to tetraketone **54.**

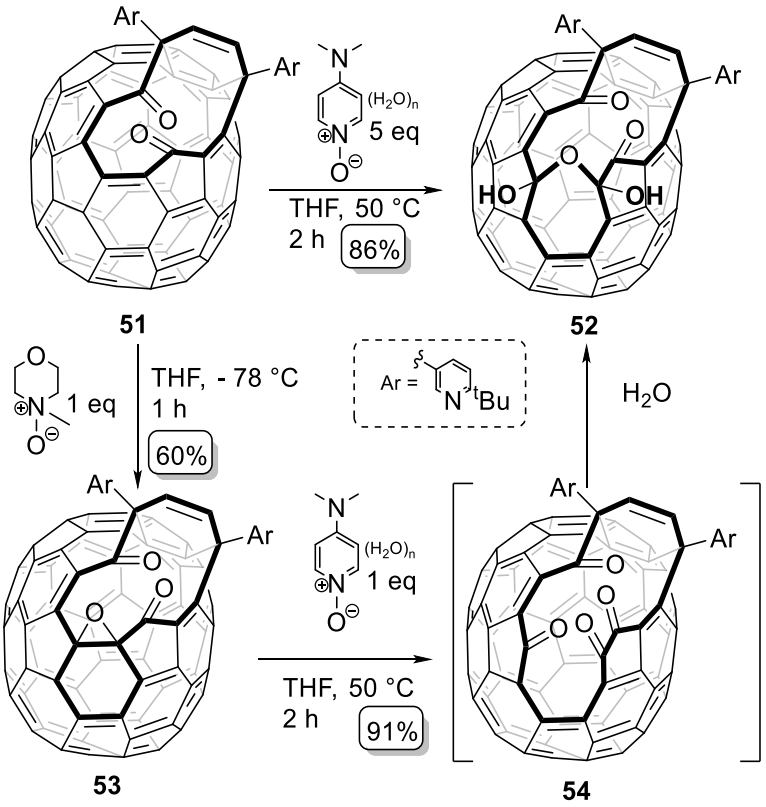


**Scheme 18**. Oxidation of **51** to **54** followed by instant hydration.

Interestingly, when the tetraketone **54** was attempted to be expanded to sulfide **55** by inserting sulphur atom into the C-C bond on the rim by the same procedure as in (**Scheme 16**), an unprecedented by-product thiophene **56** was formed (**Scheme 19**).[141]

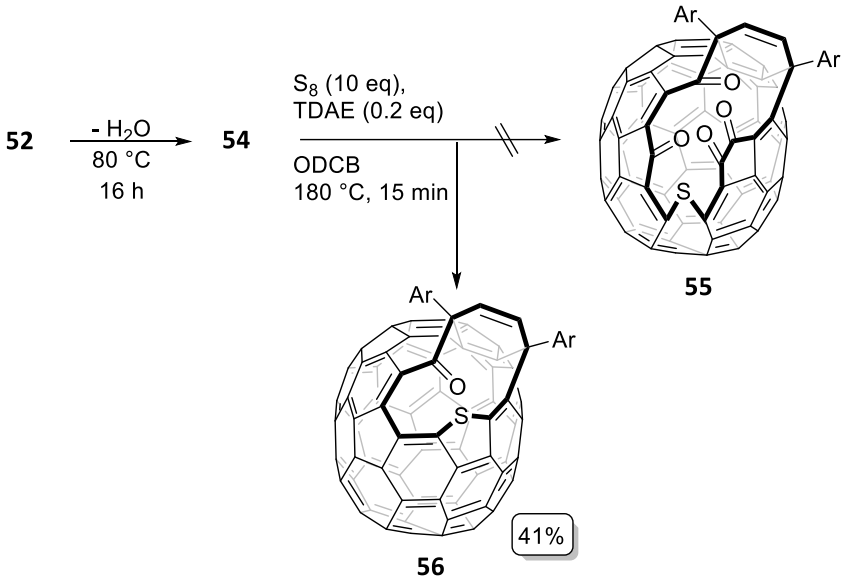


**Scheme 19.** Unprecedented formation of **56** during sulphur insertion attempt.

DFT calculations[d] showed that the opening in $C_{70}$-tetraketone **54** is smaller than $C_{60}$-tetraketone **45** which was also confirmed by lower incorporation of $H_2O$ into hemiacetal **54** than to **45** under 120 °C and 9000 atm (trace and 100% respectively). This could be explained by the degree of strain release from $C_{60}$-tetraketone **45** whereas in $C_{70}$-tetraketone **54** some strain can be defused thanks to the additional 10 carbons. In the case of **54** the sulphur is inserted between 1,2-diketone carbons followed by carbonyl coupling where two oxygen atoms are lost. Finally, the decarbonylation occurs after a single electron transfer to the starting compound **54** affording by-product **56**.

A 17-membered ring orifice OCF was synthesised by Iwamatsu in 2003 (**Scheme 20**). Similar approach as in syntheses of **33** and **36** (**Scheme 12**, **Scheme 13**) was used but this time phenyldiamines instead of phenylhydrazines were used. The initial product was the 16-membered ring **57**, but when an excessive amount of pyridine was used, another skeleton carbon bond was broken forming two methylene carbons and 17-membered ring **58** was formed.[142]

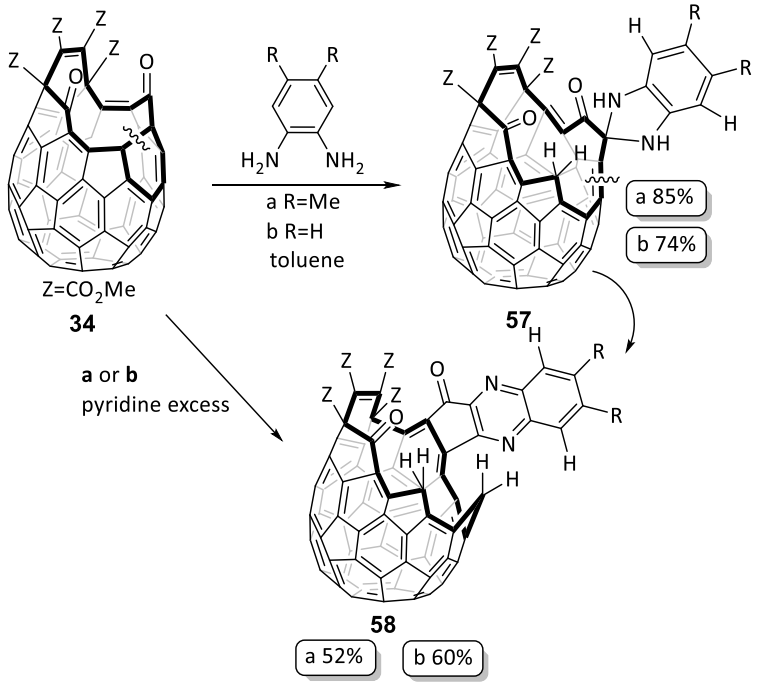


**Scheme 20**. Synthesis of Iwamatsu's 17-membered ring orifice **58**.

In 2016 Chen prepared a 17-membered orifice starting from Komatsu's 12-membered ring (**Scheme 9**) using Iwamatsu's ring-enlargement process (**Scheme 20**). Formation of **60** is shown in **Scheme 21**.[143]

[d] M06-2X/6-31G*

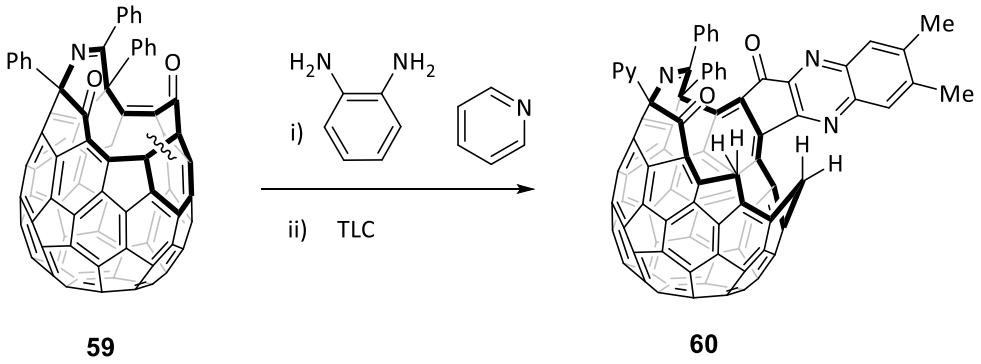


**Scheme 21**. 17-membered ring by Chen.

In 2004 Iwamatsu reported a synthesis of **61** starting from **9** applying the reductive amination used to form **58** shown in **Scheme 20** (**Scheme 22**).[144]

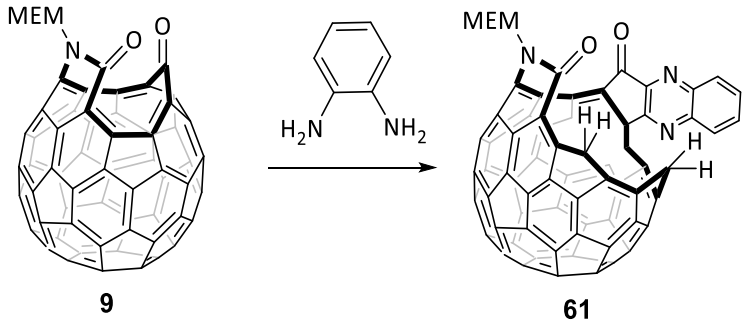


**Scheme 22**. **61** 16-membered ring orifice by Iwamatsu.

The reductive amination on **9** was also investigated by Kabe. In 2018 they reported a regioselective hydroamination that proceeded according to the character of the R group on the rim of **9**. Two hydrogen atoms from the hydrazine migrate to the α,β unsaturated carbonyl carbons. When R was an electron-donating group, the product was a 15-membered ring **62** in regioselectivity ratio 1:1, even when 10 equivalents of the hydrazine were used. When R was an electron-withdrawing group, the product formed was a 19-membered ring **63** with double hydroamination with 1:2 regioselectivity but also a minority of 15 membered ring was formed in 1:1 ratio (**Scheme 23**).[145]

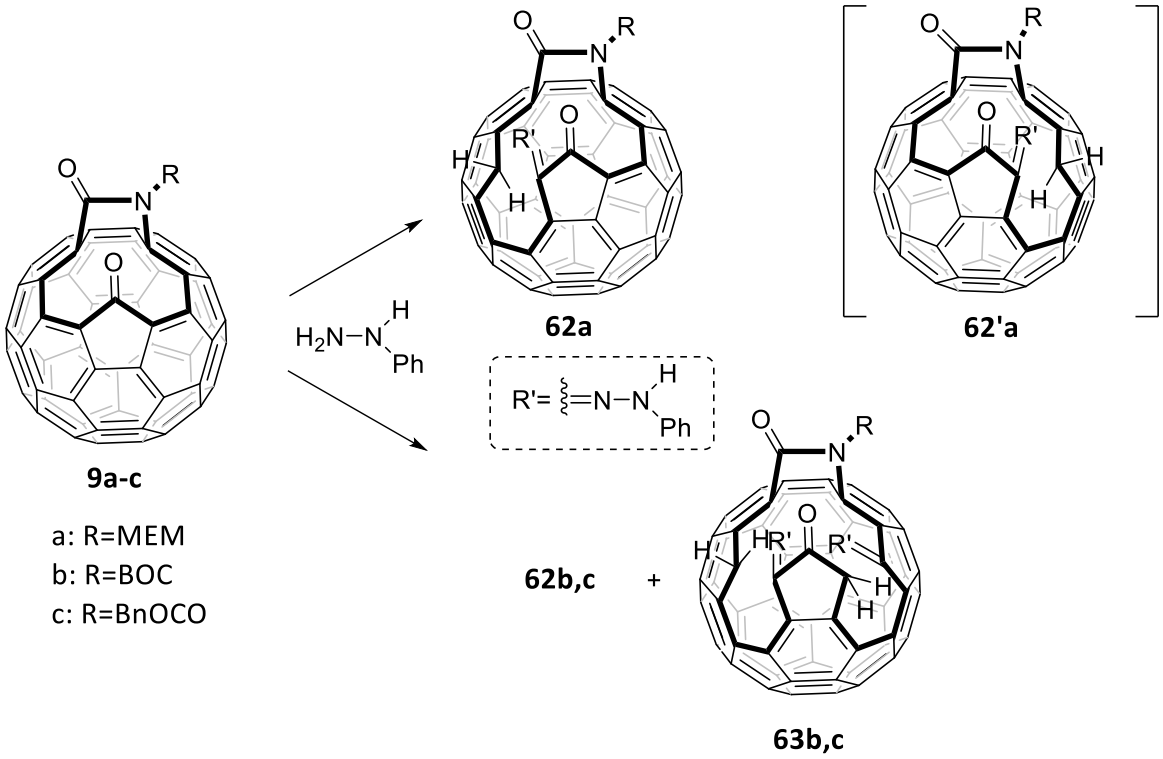


**Scheme 23.** 19-membered ring by Kabe.

## 1.3.2 OCF *via* fullerene-mixed peroxides

Inspired by singlet oxygen cleavage of double bonds on the fullerenes, in 2002 Gan presented results of investigation of reactivity of fullerenes with *tert*-butyl hydroperoxides (TBHP). The reaction catalysed by $FeCl_3$ gave multi-peroxo fullerene derivative **64** (**Scheme 24**).[146]

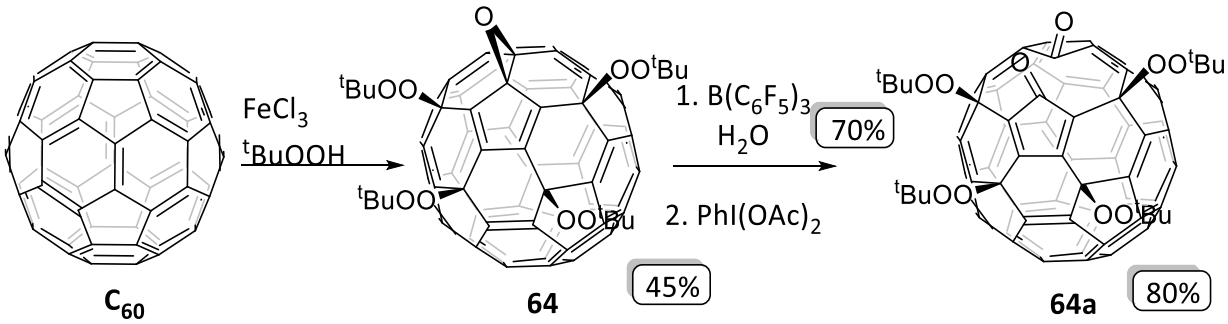


**Scheme 24**. Reaction of $C_{60}$ with *tert*-butyl hydroperoxides to form **64** followed by hydrolysis to vicinal diol and oxidation to diketone FMP **64a**.

Since then, the fullerene-mixed peroxides (FMP) have been deeply investigated and played an important role in encapsulating endohedral species in OCF which will be mentioned in section **1.4.3.**

The preparations of the FMP are complex and consist of large number of steps. Only the syntheses of FMP involved in encapsulating endohedral atoms and molecules will be mentioned in this section.

Various conditions were used to test the reactivity of the peroxo groups which eventually led to cage-opening reactions. For example the oxidation of vicinal hydroxyl groups with $PhI(OAc)_2$, visible light irradiation or thermolysis were successful in synthesis of several FMP open cages. Electrophiles such as anilines or cyclic secondary amines were used to form large orifices. The fullerene skeleton carbons of FMP can also be replaced by oxygen or nitrogen and form oxa- or aza- derivatives. In 2006 the epoxy bridge on **64** was modified by hydrolysis to vicinal diol which was then oxidised to diketone **64a** (**Scheme 24**).[147]

The carbonyl groups on FMPs can be formed either by cleavage of the O-O bonds to form an epoxide or of the O-$^t$Bu bond to form dioxetane. This can be done by domino reactions induced by photolysis, Lewis acid, pyrolysis or aminoacids. One of the first peroxy cleavage reactions was observed in 2004 by forming multiadducts such as **64b.** This was then oxidised in the presence of iodine and visible light to diketone **64c** (**Scheme 25**).[148]

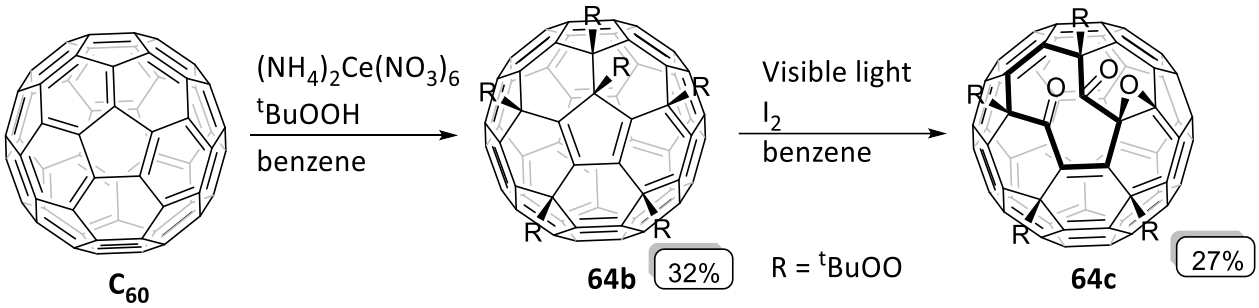


**Scheme 25.** Formation of $C_{60}(^tBuOO)_6$ **64b** followed by oxidation to **64c**.

One of the first molecules where endohedral $H_2O$ was observed was **65.** This was prepared in 2007 by a sequence of reactions starting from **64c (Scheme 26).**[149] The epoxide on **64c** could be opened with various Lewis acids such as $FeCl_3$ or $FeBr_3$ resulting in the corresponding halohydrins. Reaction of **64**c and the $B(C_6F_5)_3$ gave the desired vicinal diol **65a.** The diketone on the **65a** was then protected by forming aminoketal with good regioselectivity thanks to the bulky phenyl group. Orifice of the **65b** was then expanded using $PhI(OAc)_2$ to oxidise the hydroxyl groups to ketone and the amino to imino group. Compound **65c** was then expanded again by hydrazine-initiated domino rearrangement to form **65d** with an 18-membered ring orifice followed by reaction with $Br_2$ in attempt to form acyl bromide that was meant to be hydrolysed. However, the hydrazinocarbonyl moiety was transformed into bromoazocarbonyl which was then removed by $AgClO_4$. This was instantly followed by decarboxylation and removal of the *tert*-butanol to form $C_{59}$ derivative **65e.** Traces of endohedral

water were observed in **65e** therefore the orifice was further expanded with ferrocene in the presence of TFA. This reaction produced **65** by rearrangement of the *tert*-butyl peroxide oxygen -$R^1$ and removal of the group -$R^2$. An aromatic benzene ring fused with isomaleimide moiety was formed.

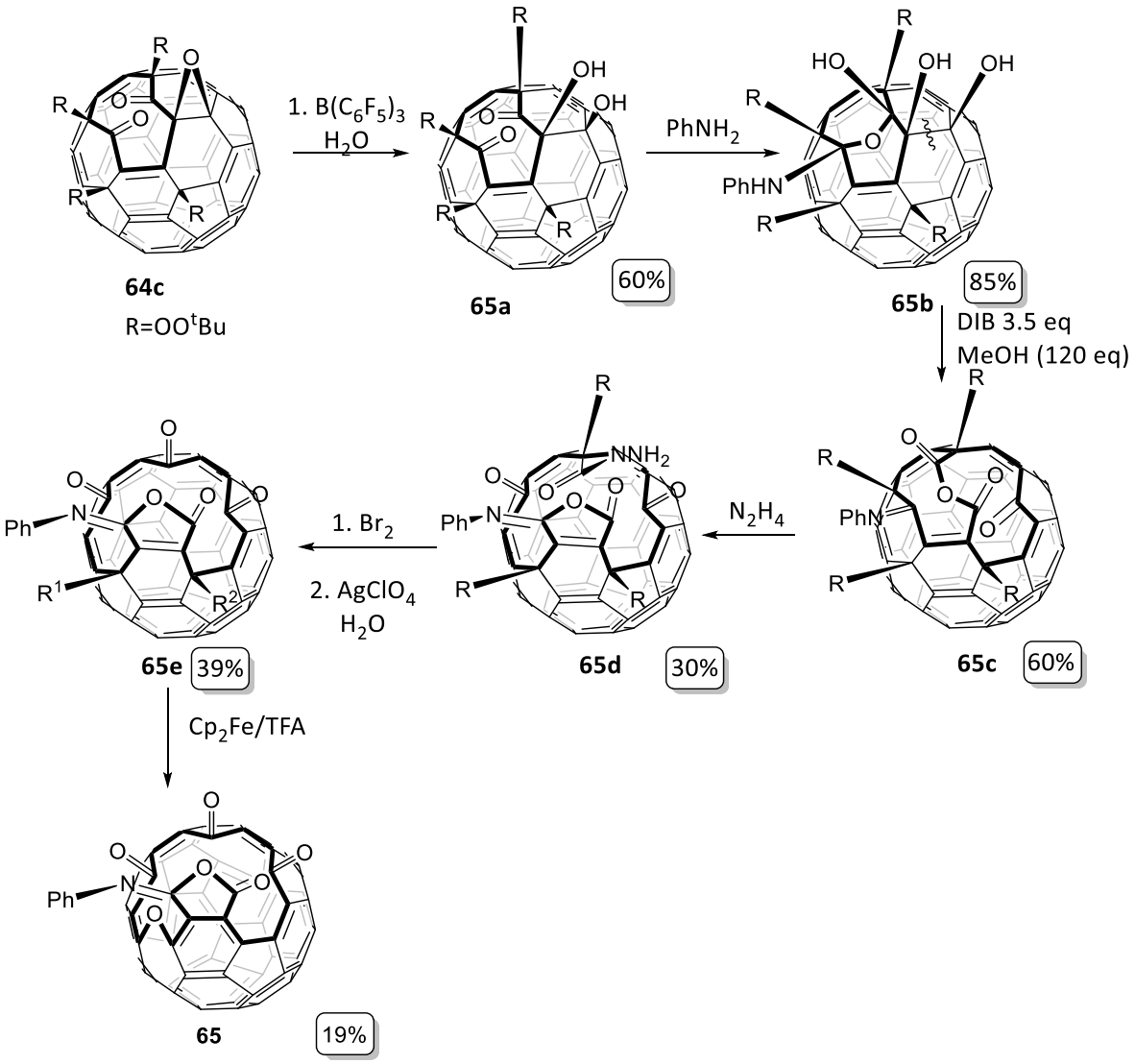


**Scheme 26.** Synthesis of **65**.

## 1.4 Insertion of atoms and molecules into an open cage fullerene

This section will discuss highlights in insertion of guest atoms and molecules in open cage fullerenes. When atoms and molecules are to be inserted into OCF there are several factors that need to be considered:

a) The size of the orifice, implying how many members the ring has and if there is any steric hindrance.
b) The incorporation energy $E_{in}$ that depends on the size and shape of the orifice and is the energy barrier needed for the guest to cross to enter the fullerene cavity.
c) The escape energy $E_{esc}$, needed to leave the cavity of the OCF and usually similar to $E_{in}$. The difference of these energies gives the binding energy $E_{bin}$ which corresponds to the Van der Waals attraction of the guest atom or molecule and the OCF cavity.

### 1.4.1 Insertion of $H_2$, He and Ne

Reactions on the $C_{60}$ that result in an open cage have been successfully developed[150] and one of the key molecules was the 14-membered ring **27** OCF (**Scheme 8**) prepared by Rubin in 1999.[124] The opening on the **27** was large enough to perform the first successful insertion of $H_2$ and He into OCF in 2001 (**Scheme 27**).[105] They predicted by using DFT calculations[e] the energy barrier that needs to be crossed in order to insert $H_2$ and He into fullerene (+41.4 and +24.5 kcal.mol$^{-1}$ respectively) and estimated the temperature needed for the filling with (397 °C and 124 °C respectively). The results achieved are summed up in **Table 3**. The experiments were done with $^3$He as it is a good NMR probe for environment changes.

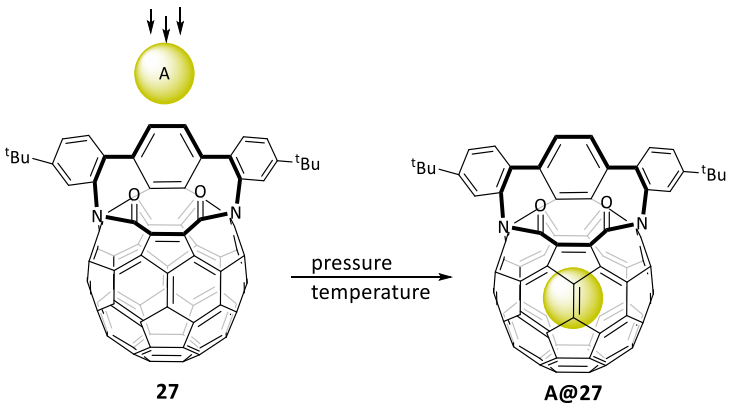


**Scheme 27**. **27** OCF large enough to insert $H_2$ and He.

[e] B3LYP/6-31G**//B3LYP/3-21G

| Guest | Temperature | Pressure | Time | Incorporation |
|---|---|---|---|---|
| **$^3$He** | 100 °C | 3-4 atm | 24 h | 0.05% |
| **$^3$He** | 288-305 °C | 475 atm | 7.5 h | 1.5% |
| **$H_2$** | 400 °C | 100 atm | 48 h | 5% |
| **HD** | 233 °C | 340 atm | 15 h | 5% |

**Table 3**. First insertions of small atoms and molecule into open cage fullerene **27**.

The experiment that yielded in 1.5% incorporation allowed to experimentally measure the escape rate of He from the **27** and the results were in accordance with the calculations that show that the insertion and escape energy are very similar (+ 24.6 kcal.mol$^{-1}$). These experiments have revealed the first experimental NMR of endohedral species and showed that the π-electron shell of a fullerene strongly shifts the peak upfield for $^3$He and $H_2$ (-10.10 ppm and -9.96 ppm respectively) versus free $^3$He and $H_2$.

OCF with heteroatom sulphur and a 13-membered orifice **31** prepared by Komatsu[126] (**Scheme 10**) has a suitable orifice to insert $H_2$ and He. The insertion energy calculated for **31** was lower than that for the **27**, but the low insertion energy barrier also leads to lower escape energy which can result in difficult handling of the filled OCF (**Table 4**). In practice this means that the guest He can freely go in and out of **31** at room temperature. In the case of $H_2$ in **31** the half-life was experimentally shown to be 54.4 h at 160 °C and 4.2 h at 190 °C.[151]

| Guest | **27** | | | **31** | | |
|---|---|---|---|---|---|---|
| | $E_{in}$ | $E_{esc}$ | Experimental $E_{esc}$ | $E_{in}$ | $E_{esc}$ | Experimental $E_{esc}$ |
| **He** | 24.5 | 24.3 | 24.6 | 18.9 | 18.6 | 22.8 |
| **$H_2$** | 41.4 | 40.0 | n | 26.2 | 28.7 | 34.3 |
| **Ne** | 40.6 | 41.7 | n | 30.1 | n | n |
| **Ar** | 136.3 | 130.2 | n | 97.7 | n | n |

**Table 4.** Comparison of energies required for insertion of guest to **27**[105] and **31** [151] in kcal.mol$^{-1}$ by B3LYP/6-31G**//B3LYP/3-21G.

The He insertion into **31** was done on the isotope $^3$He and thanks to its NMR active nucleus the time of escape was measured together with the first measurement of equilibrium constant for the insertion of an atom into an OCF. The insertion of He was initially done at lower pressure achieving incorporation of 0.1%[152] but the conditions were improved later in 2010 to 30% by inserting He into a sulfoxide derivative **66** (preparation shown in **Scheme 28**), in order to suture the orifice right after the filling (**1.5.2**).[153] The achieved results for insertion of He are in **Table 5**.

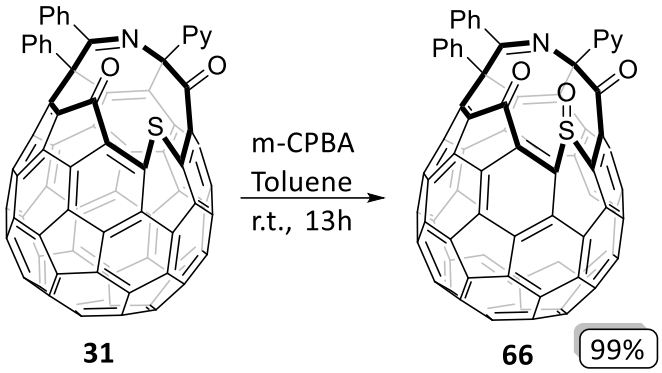


**Scheme 28.** Synthesis of sulfoxide derivate of **31.**

| OCF | Temperature | Pressure | Time | Incorporation | State |
|---|---|---|---|---|---|
| **27** | 288–305 °C | 475 atm | 7.5 h | 1.5% | |
| **31** | 80 °C | 20 atm | 'few hours' | 0.1% | Solution |
| **66** | 115 °C | 1230 atm | 1h | 30% | Solid |

**Table 5.** Achieved insertions of He into OCF.

$H_2$ was also inserted into **31** analogue **32.** Selenium makes the orifice of the **32** larger than **31** which is mirrored in lower activation energy barriers. 100% incorporation of $H_2$ was achieved under milder conditions but also the half-life of $H_2$ in **32** was smaller (18.3 h at 160 °C).[130]

Insertion of $H_2$ was likewise performed with **36** ring orifice shown in **Scheme 13**.[154] Although at the time the synthesis of $H_2@C_{60}$[106] (**1.5**) was already published, the reason for this experiment was to prove that the size of the orifice should allow encapsulation under milder conditions and that the presence of flexible $sp^3$ methylene carbon on the rim will have a positive effect on the $H_2$ entry. Disadvantage of this system is that the $H_2$ leaks from the OCF **36** even at room temperature and is completely gone at 100 °C which is confirmed by the calculated escape energy barrier (**Table 6**). The **31** OCF is suitable for encapsulation of $H_2$ as the hydrogen does not escape at room temperature and only starts leaving when it is heated to 160 °C.[151] The encapsulation through a larger orifice does occur at milder conditions as predicted. The escape rate is equally high, which limits the handling of the filled OCF and makes the retention and possible enclosure to $C_{60}$ very difficult. In 2014 Whitby group reported insertion of $H_2$ into OCF **45** generated *in situ* by molecular sieves, using relatively mild conditions (**Table 6**).[155] This result suggested that if the reaction was done at pressure 800 atm the incorporation would be 100%. The disadvantage of this method was that it was done in solution whereas the insertion into **31** was done in solid state.

| OCF | $E_{in}$ [f]/kcal.mol$^{-1}$ | $E_{esc}$ [g]/kcal.mol$^{-1}$ | Temp. | Pressure | Time | Incorp. | State |
|---|---|---|---|---|---|---|---|
| **27** | 41.4 | 19.8 | 400 °C | 100 atm | 48 h | 5% | |
| **31** | 30.1 | 28.7 | 200 °C | 800 atm | 8 h | 100% | solid |
| **32** | 29.9 | 28.2 | 150 °C | 760 atm | 8 h | 100% | solid |
| **36** | 21.3 | 19.8 | 100 °C | 1350 atm | 4 h | 83% | |
| **45** | – | – | 120 °C | 120 atm | 20 h | 60% | solution |

**Table 6**. Insertion of $H_2$ compared for 5 different types of OCF.

Insertion of Neon into **36** was published in 2009 by Saunders. It was performed in solid state at 190 °C, 825 atm for 9 hours. Incorporation achieved was 42% measured by $ESI^+$. The equilibrium constant and the kinetics of the Ne escape were measured showing that the $E_{esc}$ is 25 ± 1.6 kcal.mol$^{-1}$ which is similar to **$H_2$@36.**[156]

## 1.4.2 Insertion of $H_2O$ and HF

Encapsulation of water started to attract interest mainly because of its behaviour as a confined quantum rotor, displaying a rich energy level structure, which may be studied by various spectral techniques.[157] The inner space of $C_{60}$ molecule has a diameter of approximately 3.7 Å, suitable for $H_2O$ encapsulation as well as for other small molecules. The homogeneity and stability of **$H_2O$@$C_{60}$** allows studying physical phenomena such as nuclear spin interconversion.[110]

In 2004 when Iwamatsu expanded 16-mem ring OCF to **58** ring by cleaving the C-C bond with o-phenyldiamine (**Scheme 20**), it was observed that the molecule of $H_2O$ spontaneously enters the inner space of the fullerene and was the first recorded $H_2O$ in OCF.[142] On the premise that the smaller orifice is better for the encapsulation, it was performed on the 16-mem ring OCF created by taking the singlet oxidation of aza-fulleroid shown in **Scheme 12** and extending the orifice by reaction with o-phenylenediamine, similarly to **Scheme 20**.[144] It was shown that the encapsulation is affected by the substituent on the nitrogen on the orifice rim. The **61a** was treated with TFA to remove the MEM group and leaving the nitrogen with hydroxylmethyl **61b** but was gradually converted to the desired **61c** after stirring with silica.

[f] Calculated energy barrier for encapsulation of $H_2$ by B3LYP/6-31G**//B3LYP/3-21G and by B3LYP/3-21G for **36**
[g] Calculated energy barrier for escape of $H_2$ by B3LYP/6-31G**//B3LYP/3-21G and by B3LYP/3-21G for **36**

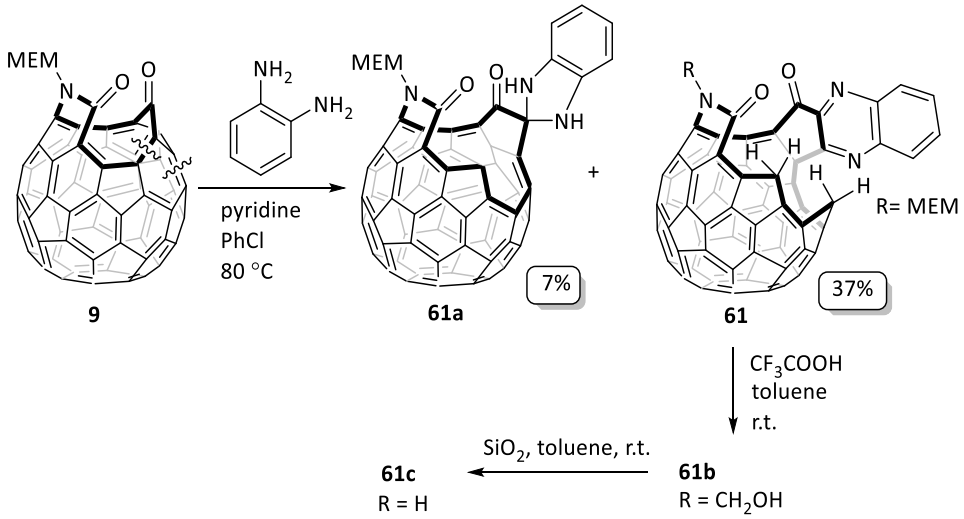


**Scheme 29**. Synthesis of **61** ring orifice and transformation to **61c**.

The spontaneous incorporation of water into **61a** was about 10% and was improved by refluxing it in toluene/water mixture to 85% and unlike from **58** the escape was slow. The same experiment repeated on **61c** resulted in a 35% incorporation showing the effect of the nitrogen substituent. The initial thought was that the escape barrier from **61c** was lower than that from **61a**, but the experiment showed that the escape from **61c** is slower than that from **61a** (**Table 7**). It was thought that the hydrophilic properties of MEM play a more significant role in the insertion of $H_2O$ than the steric hindrance. It would be beneficial to have reliable DFT calculations to confirm this hypothesis.

| Compound | N substituent | Initial filling | After experiment |
|---|---|---|---|
| **61a** | MEM | 48% | 13% |
| **61b** | H | 35% | 26% |

**Table 7.** Change in incorporation of $H_2O$ in compounds **61a** and **61b** after heating for 27 h at 120 °C in a sealed tube in toluene.

Spontaneous incorporation of water was also observed by Gan group in 2007 in the OCF derivative **67** prepared by the fullerene-mixed peroxide methods. After routine purification processes 57% of **67** contained endohedral $H_2O$. Interestingly after keeping the product in the freezer, the filling factor was increased to 88%. $H_2O$ was incorporated into OCF **68** (**Figure 7**) by heating to 80 °C in toluene for 5 h achieving incorporation of 78%.[149]

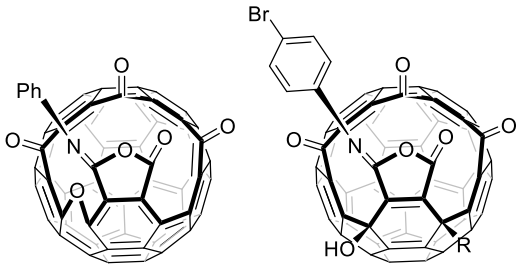


**67** **68**

**Figure 7.** Molecules **67** and **68**.

Quantitative encapsulation of water was achieved by heating compound **69** in homogenous mixture of $H_2O$/EtOH/$CHCl_3$ at 80 °C for 18 hours. It was also demonstrated that groups with different hydrophilicity on the rim change the incorporation ratio of $H_2O$ as observed in Iwamatsu's 20-membered ring derivatives (**Scheme 29**, **Table 7**).

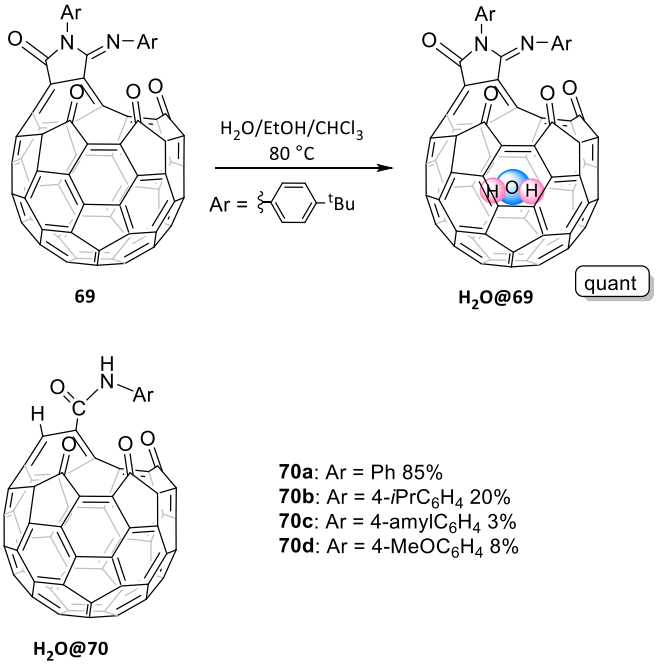


**Scheme 30.** Quantitative encapsulation of $H_2O$ into **69** and achieved incorporations of $H_2O$ in OCF **70** with different functional groups.

Stirring **$H_2O$@67** at room temperature in solution with $D_2O$ led to the exchange of endohedral $H_2O$ to $D_2O$ in 1 hour. This could mean that there is rapid exchange of water molecules from inside the fullerene cavity or the exchange of hydrogen atoms from the endohedral water molecule with hydrogen atoms outside the OCF. During investigation of OCF **$H_2O$@71** which has smaller orifice, slow hydrogen atom exchange was found by observing endohedral HDO after heating with $D_2O$ to 90 °C for 24 hours (**Scheme 31**).[158]

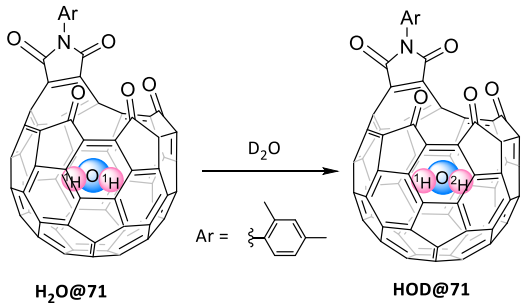


**Scheme 31**. Exchange of hydrogen atoms from endohedral water in OCF **71**.

In 2011 kinetics of the escape of $H_2O$ from anion $[H_2O@\mathbf{72}]^-$ (preparation shown in **Table 8**) were measured and compared with theoretical calculations[h] of electronic energies and determined to be 104 kJ/mol and 110 kJ/mol respectively.[159] Measurements were done using FT-ICR at a pressure of $10^{-9}$ atm heated up to 110 °C. The $H_2O$ removal is important for the synthesis of different endohedral fullerenes when it is desired to avoid contamination of endohedral $H_2O$. This model experiment showed that the endohedral water removal is possible by heating under high vacuum.

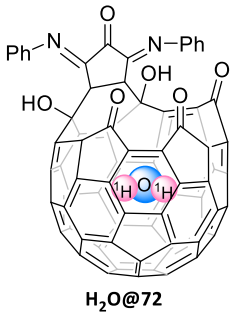


**Figure 8.** Open cage fullerene **72.**

In 2011 Murata reported insertion of $H_2O$ into OCF **46**. The initial experiments were performed following Iwamatsu's procedure, reflux of **46** in wet toluene and the resulting incorporation was 8% and was assumed to be caused by the smaller size of the orifice. This was repeated by Whitby achieving incorporation of 45% after heating for 36 h at 120 °C in a sealed tube. The reason for low filling was that the equilibrium was reached at this temperature.[155] Quantitative insertion was achieved when $H_2O$ was forced into **45** under pressure of 9000 atm at 120 °C. The formation of **$H_2O$@46** can be explained by the dynamic control of elimination of $H_2O$ from **46** to form **45**, in which the insertion takes place, and then another molecule of $H_2O$ regenerates the **46**.[136]

[h] Calculations were done using BP86-D/def2-TZVP

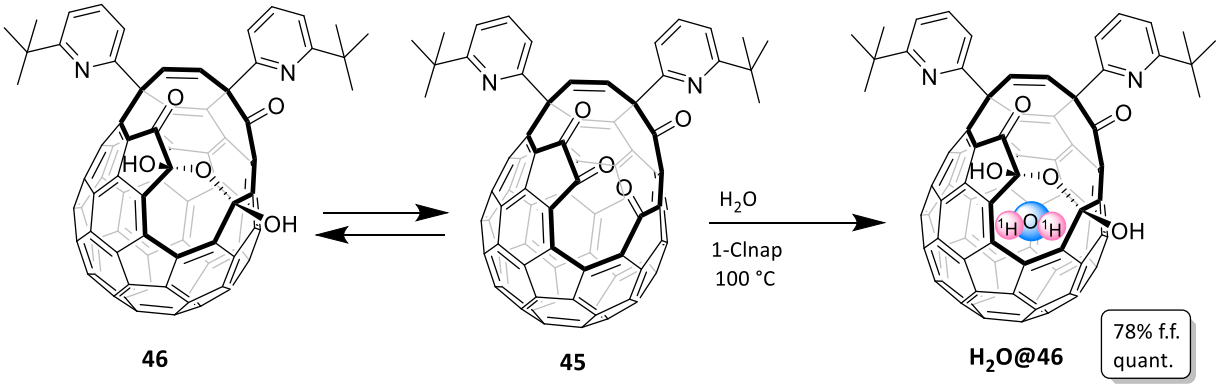


**Scheme 32**. Insertion of water into OCF **46**.

The Whitby group approached the same reaction and improved the filling conditions by using aromatic solvent 1-chloronaphthalene and a lower temperature (to shift the thermodynamic equilibrium) of 100 °C. 78% filling was achieved eliminating the need for high pressure (**Scheme 32**).[155]

In 2018, $H_2O$ was also observed to naturally enter the cavity **61** while investigating hydroamination reactions on the rim of the **9** resulting in an encapsulation ratio of 82%. The exchange with $D_2O$ was investigated and was found to be very slow.[145] In summary it is observed that the water goes spontaneously into the cavity depending on the size and structure of the rim and the environment outside the OCF. Recently a quantitative encapsulation of $H_2O$ into OCF was published by Murata's group, where $H_2O$ was inserted into OCF with 98% encapsulation by coming back to the high-pressure method. The OCF was a modified molecule **29** to 18-membered ring **45n** which was prepared by oxidation with NMMO. These preparations were analogous to the preparation of **46 (Scheme 15**). **46n** was exposed to high pressure at high temperature in the presence of water which forced the dehydration to **45n** and encapsulation of $H_2O$. The advantage of this approach is that the further suturing of the orifice was done in one pot process with shorter reaction times and higher yield (**Scheme 33**).[160] The orifice suturing will be discussed in detail in the section **1.5.**

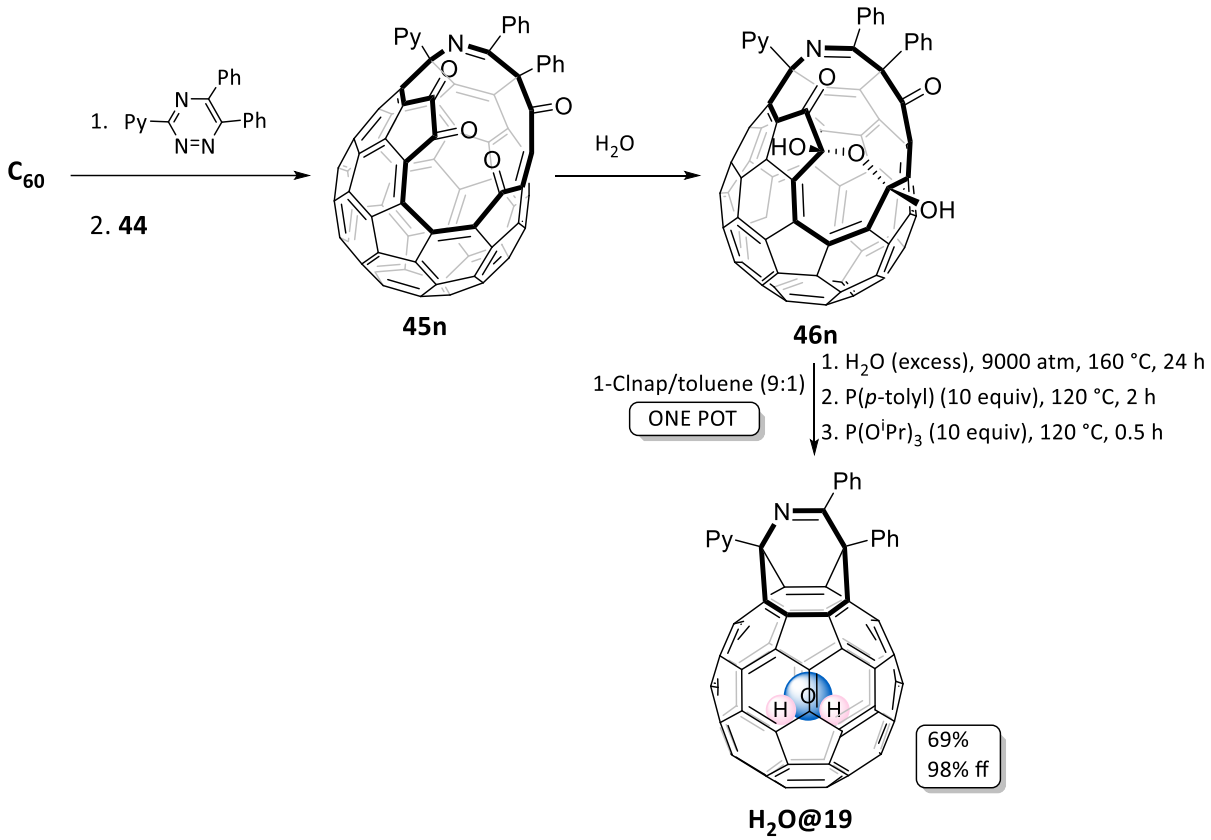


**Scheme 33.** Synthesis of **$H_2O$@19** via one pot filling/suturing reaction.

Achievements of $H_2O$ encapsulations into OCF are summarised in **Table 8**.

| Compound | Solvent | Temperature | Pressure | Time | Filling |
|---|---|---|---|---|---|
| **61a** | toluene | 120 °C | n | | 85% |
| **64** | toluene | 80 °C | n | 5 h | 78% |
| **69** | H2O/EtOH/CHCl3 | 80 °C | n | 18 h | 100% |
| **72** | toluene/water | 80 °C | n | 24 h | 87% |
| **46** | Solid state | 120 °C | 9000 atm | 36 h | 100% |
| **46** | toluene | 120 °C | n | 36 h | 45% |
| **46** | 1-Clnap | 100 °C | n | 48 h | 78% |
| **46n** | 1-Clnap/toluene | 160 °C | 9000 atm | 24 h | 98% |

**Table 8.** Methods of incorporation of $H_2O$ into different types of OCF.

**HF@$C_{60}$** allows the study of the spectroscopic properties of near-isolated and freely rotating HF molecules under a variety of circumstances, free from the difficulties caused by dimerization and hydrogen bonding. DFT calculation for $H_2$, $H_2O$ and HF entry into **45** showed activation energies of 64.3, 52.2 and 29.8 KJ.mol$^{-1}$.[i] The calculated energy difference between $H_2$ and $H_2O$ agreed with the temperature difference needed for the incorporation (120 °C and 100 °C respectively) which made the low energy HF a viable target. The calculated escape energy for HF inside **45** was 55.7 KJ.mol$^{-1}$ which

[i] Calculations were done using m062x/vdz@B3LYP/631d, Pyridine groups in **45** replaced with methyl groups,

suggested that the escape at room temperature would be slow and the formation of the 13 membered **46** allowed trapping of the HF. Successful insertion of HF into compound **46** was achieved by Whitby group by stirring **46** with excess HF.pyridine in DCM (**Scheme 34**) at room temperature.[161] Under these conditions HF was incorporated in 50% filling factor achieving this equilibrium after 24 hours. Larger excess of HF.pyridine or prolonged reaction did not achieve higher incorporation.

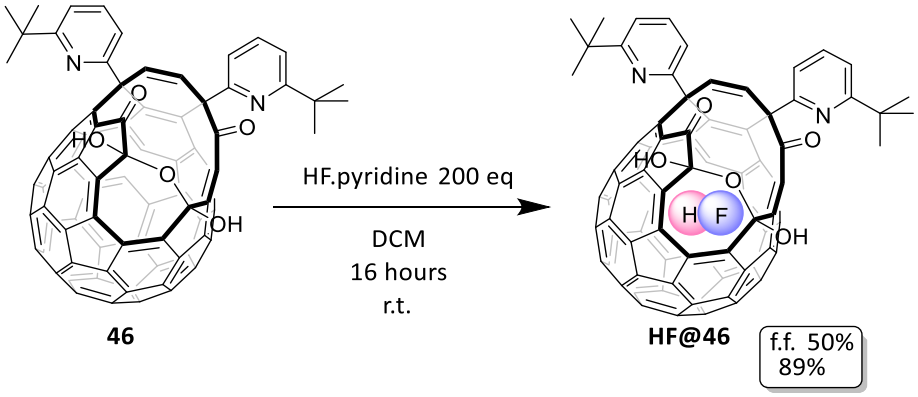


**Scheme 34.** Insertion of HF into the OCF.

In the case of OCF **$H_2O$@69** the water molecule can be pulled out by HF by hydrogen bonding. This was achieved by mixing the empty **69** and **H2O@69** with HF (aq) which produced **74** with no endohedral water**.** This compound was not stable, but after treatment with $B(C_6F_5)_3$ it was converted back to **69**. When the HF (aq) was exchanged for HF.pyridine the **HF@69** was formed with a 5% filling factor. A protonated **HF@69** was present in the ratio of 1:1 (**Scheme 35**).[162]

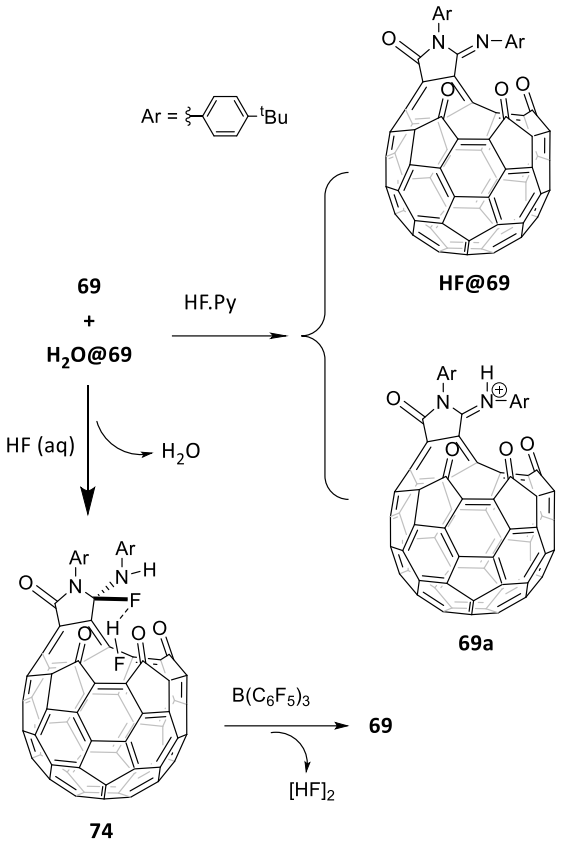


**Scheme 35**. Endohedral $H_2O$ pulled out by HF from the OCF **69**.

The imino group on the rim plays the key role in endohedral $H_2O$ removal from **69**. It is first protonated by the HF and then another equivalent of HF forms the intermediate **$H_2O$@74** and pulls the $H_2O$ out of the cavity via hydrogen bonding (**Scheme 36**).

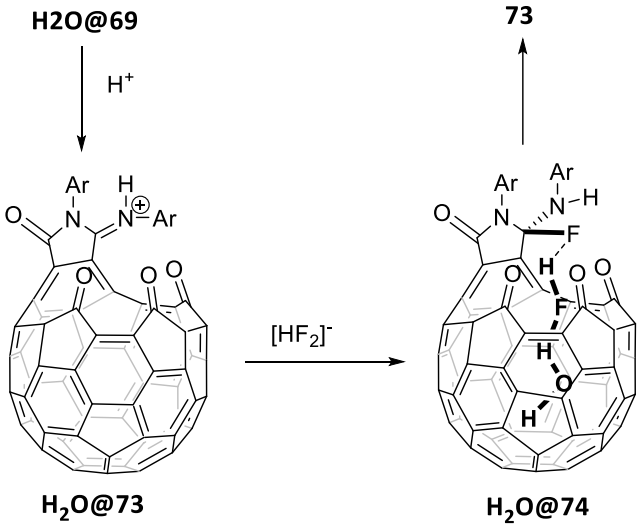


**Scheme 36**. Mechanism proposed for $H_2O$ 'fished out' by HF.

## 1.4.3 Insertion of guest molecules into fullerene-mixed peroxides

Insertion of $H_2O$ into fullerene-mixed peroxides type OCF is shown in the previous section (**1.4.2**).

### 1.4.3.1 Chemical insertion of CO into OCF

In 2013, endohedral fullerenes **CO@77** and **CO@80** were prepared to form $C_{59}$ OCF derivative. One of the fullerene skeleton carbons was used to form the endohedral CO. This synthetic pathway was discovered while optimising the reactions of the OCF derivatives.[163]

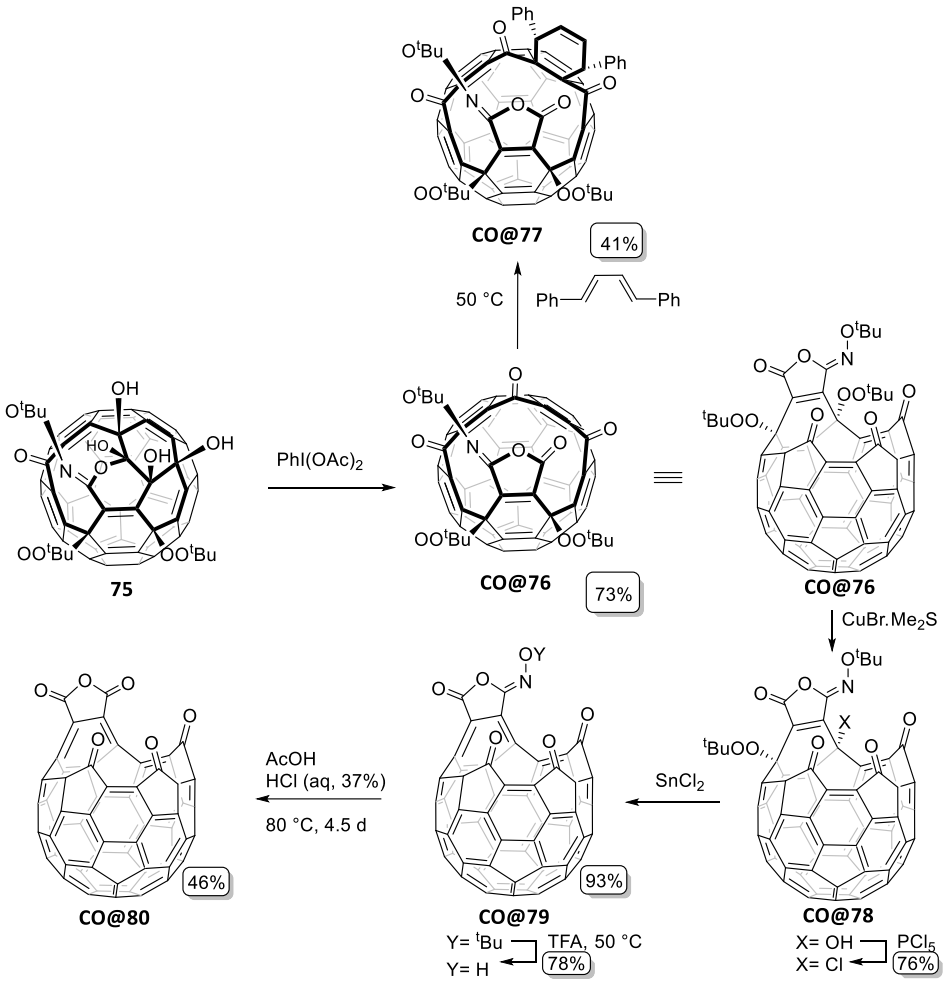


**Scheme 37**. Synthesis of **77** and **80**.

The **CO@80** was prepared with 100% encapsulation but the successful closure methods to **CO@$C_{60}$** have not been discovered yet. Main challenge in the closure to **CO@$C_{60}$** will likely be the reconstruction of the $C_{60}$ skeleton as one of the cage carbon atoms was used to form the encapsulated carbon monoxide.

#### 1.4.3.2 OCF for oxygen delivery

Materials for oxygen delivery are an important research subject in biomedical engineering.[164] They serve as oxygen supplies for metabolically active cells, and are also used in treatment of hypoxia tumours.[165] Hydrogen peroxide can be readily converted to oxygen by a catalyst. Biocompatible polymers such as poly(lactic acid) or poly(methyl-methacrylate), which have microcavities, have been reported to deliver oxygen via this method.[166] In these structures, the exact ratio of $O_2$/$H_2O_2$ cannot be determined due to their complexity. OCF could be suitable materials for oxygen delivery thanks to their well-defined structure which allows the estimation of the number of molecules inside the cavity. In 2018 a 16-step synthesis of OCF **85** filled with $O_2$, $H_2O_2$ and $H_2O$ was reported. This synthesis differs from the 'classical' molecular surgery mainly because the first stage involves replacement of one of the skeleton carbons with nitrogen to form azafullerene derivative **85**. Processes where one or two carbon atoms are cleaved from the $C_{60}$ cage are known and can lead to OCF such as $C_{58}F_{18}$[167] or azafullerenes $C_{59}NR$[168] or $C_{69}NR$[169]. Brief overview of the complex synthesis of **85** and scheme (**Scheme 38**) are described in the next paragraph.

Nitrogen was introduced via addition of $NH_2OH$ followed by rearrangement catalysed by $PCl_5$.[170] By repeating this reaction another two nitrogen atoms were introduced and formed **82**, followed by cleavage of two *tert*-butyl-peroxo groups by 4-methylpiperidine and the two oxygen atoms were introduced into the rim (**83**). The last two **83** *tert*-butyl-peroxo groups were reduced to alcohols and formed **84**. The final step was a double singlet oxidation of amino enol bonds to form stable compound **85.** After the routine workup, 67% of obtained **85** contained endohedral $H_2O$ and the crystal structure revealed ellipse shaped orifice rim. When **85** was treated with $H_2O_2$ extracted into ether solution, 25% of $H_2O_2$ and 15% of $O_2$ were encapsulated. The encapsulation of oxygen was also achieved under pressure of 100 bar obtaining **$O_2$@85** with 80% filling factor showing replacement of endohedral water with oxygen. Encapsulation of oxygen by low pressure (with oxygen filled balloon) was not successful. Therefore, the encapsulation of $O_2$ by the $H_2O_2$ method is not due to oxygen dissolved in solution but possibly thanks to interaction of two $H_2O_2$ molecules with the lactam groups on the rim facilitating its release of oxygen into the cavity. Oxygen slowly escapes $O_2$@**85** at room temperature which was discovered when $O_2$ was completely lost after 3 weeks at room temperature.[171] The slow release of oxygen from **85** has a great potential for **$O_2$@85** to be a good oxygen delivery material. Oxygen-releasing materials could provide supply of oxygen which is needed for the survival of cells and tissues. Delivering hydrogen peroxide could be utilised in photodynamic therapy for hypoxia tumours.

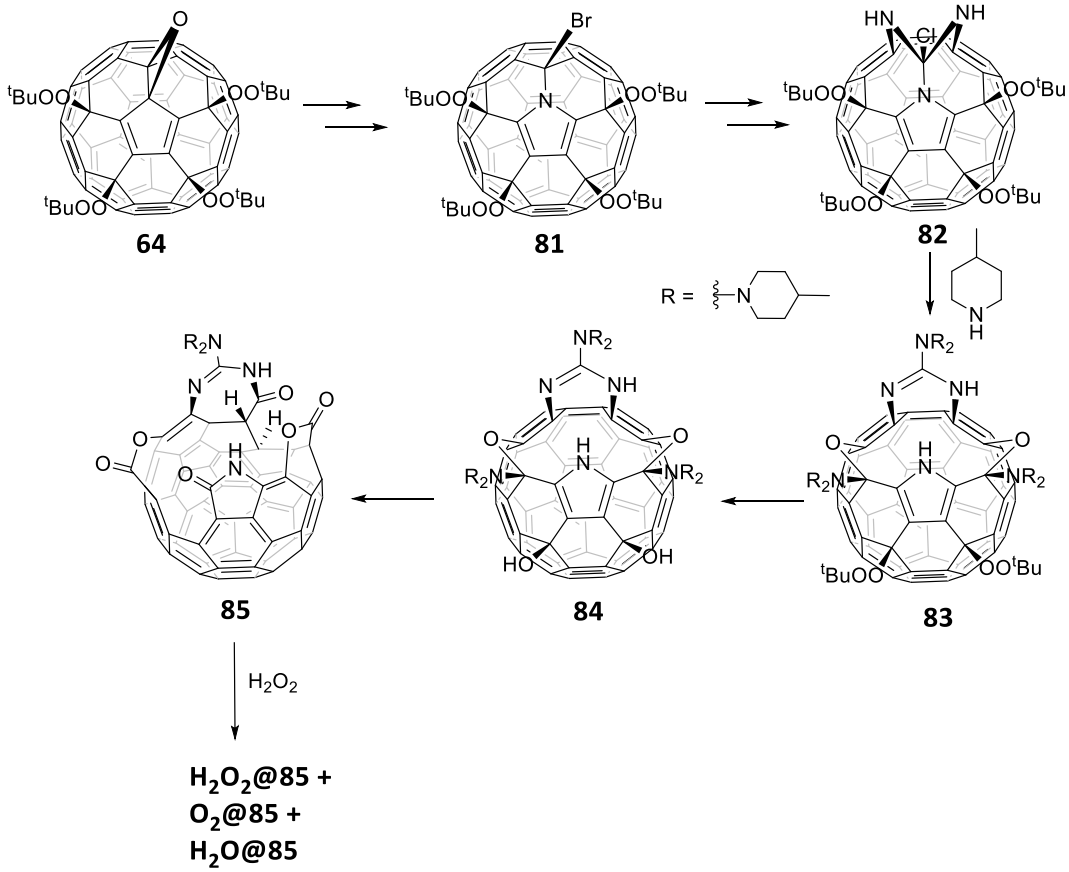


**Scheme 38.** Synthesis of **85** with endohedral $H_2O$, $H_2O_2$ and $O_2$.

Summary of guest molecules encapsulated by **85** molecule is presented in **Table 9**.

| Guest | Temperature | Time | Solvent | Pressure | Filling factor |
|---|---|---|---|---|---|
| **$H_2O$** | r.t. | n | n (routine workup) | 1 atm | 67% |
| **$H_2O$** | r.t. | 5 min | $H_2O_2$/ether/ *o*-DCB | 1 atm | 28% |
| **$H_2O_2$** | | | | | 25% |
| **$O_2$** | | | | | 15% |
| **$O_2$** | r.t. | | *o*-DCB | 99 atm | 80% |

**Table 9.** Conditions of insertion of guest molecules into **85**.

### 1.4.4 Insertion of atoms and molecules into 58

Several atoms and molecules have been inserted into **58 Figure 9.**

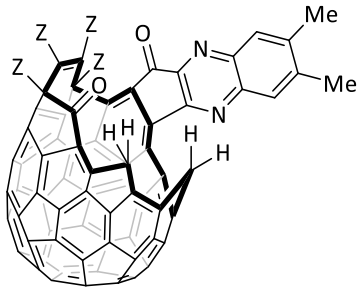


**Figure 9**. **58** 17-membered ring orifice by Iwamatsu.

In 2006 carbon monoxide was incorporated into **58** by Murata. A mixture of **58** and **$H_2O$@58**[142] was heated to 100 °C in TCE under 9 MPa pressure of CO obtaining 84% incorporation. Interestingly when a similar procedure was repeated with $^{13}CO$ in solid state the incorporation factor was only 52% even if temperature was increased to 150 °C. Considering that the reaction starts with mixture of empty **58** and **$H_2O$@58** it is likely that the $H_2O$ is released easier when in solution and that is why the solid state filling is less efficient. The CO inside the **58** is present in three different rotational isomers each having a different relative binding energy to the cavity ranging from calculated energies +2.7 to +8.1 kcal. $mol^{-1}$.[j] As only one resonance is detected by NMR, the interconversion between the isomers is rapid. The IR spectrum of **CO@58** detected two bands (IR (KBr): ν = 2125, 2112 $cm^{-1}$) which could mean the isomers interconversion is not as rapid for the IR timescale. The escape of CO was measured in the presence of $H_2O$ (4.2 equiv.) at 40 °C and after 48 hours the filling factor dropped to 7% and **$H_2O$@58** was formed. Binding energy of water into **58** was calculated to be -2.4 kcal. $mol^{-1}$ [j] meaning that the binding of $H_2O$ into the cavity is stronger and energetically favourable over CO.[172]

In 2008 ammonia was inserted into **58** in solution of TCE by Murata. Liquid ammonia was prepared by refluxing ammonium sulfate and sodium hydroxide and condensed ammonia was collected. Under pressure of 7 atm after 20 hours at room temperature the incorporation was reported to be around 35–50%. The thermodynamics and kinetics for this procedure were not reported. Incorporation of $NH_3$ could be increased by higher temperature, but that caused decomposition of **58**.[173]

[j] Calculated by $E_{bind}$= $E_{CO@58}$-[$E_{58}$+$E_{CO}$] in which the $E_{CO@58}$ is the total energy and $E_{CO}$ and $E_{58}$ are the energies of guest molecule and cage respectively. Energies calculated by B3LYP/6-31G*. Note that the calculations in this publication do not include dispersion and basis-set correction for superposition error. It is assumed that 'Energy' refers to free energy. $E_{bind}$ for **$H_2O$@58** was calculated the same way.

In 2009, a study was published by Saunders where insertion of Ar, Kr, CO and $N_2$ into **58** was performed. All fillings were performed in solution under moderately high pressures and temperatures and the filling factors were measured by $ESI^+$ (**Table 10**). Equilibrium constants were calculated for all the insertions. **58** has two methylene hydrogens on the rim that are affected by the endohedral atom or molecule and are the only protons that show a different shift in the $^1H$ NMR from the empty **58**. This allowed measuring the kinetics of the escape of the endohedral molecules except for Kr (suitable solvent was not found), and the activation energy $E_{esc}$. Half-lives of escape of the endohedral atom or molecule are strongly dependent on temperature (**Table 11**).[156] The results show that the potential closure of the 17-mem would have to be done at lower temperatures in order to retain the endohedral molecule.

$CH_4$ was first inserted into **58** in 2009 by Iwamatsu. Theoretical calculations[k] predicted $E_{in}$ = +37.3 kcal.mol$^{-1}$ suggesting that methane would require high pressure and temperature to enter the fullerene cage. The achieved incorporation was relatively low (**Table 10**) but it was improved by recycling HPLC to 66%. The equilibrium constant or kinetics of escape were not published.[174]

| Guest | Solvent | Pressure | Temperature | Time | Filling factor | Yield |
|---|---|---|---|---|---|---|
| **Ar**[l] | TCE | 100 atm | 140 °C | 18 h | 80% | |
| **Kr**[l] | *o*-DCB | 180 atm | 190 °C | 18 h | 80% | |
| **CO**[l] | TCE | 100 atm | 100 °C | 18 h | 80% | |
| **CO** | TCE | 9 MPa | 100 °C | 20 h | 84% | quant. |
| **$N_2$**[l] | TCE | 100 atm | 140 °C | 18 h | 80% | |
| **$NH_3$** | TCE | 7 atm | r. t. | 20 h | 25–50% | 50% |
| **$CH_4$** | 1-MeNap | 19.2 MPa | 200 °C | | 39% | 20% |

**Table 10.** Insertion of guest atoms and molecules into **58**.

| Guest | Half-life at 60 °C | Half-life 90 °C | $E_{esc}$ measured |
|---|---|---|---|
| **Ar** | 30.1 h | 1.73 h | 23.1 ± 0.7 kcal.mol$^{-1}$ |
| **$N_2$** | 3.8 h | 0.29 h | 19.6 ± 1.6 kcal.mol$^{-1}$ |
| | **Half-life at 40 °C** | **Half-life 70 °C** | |
| **CO** | 8 h | 0.39 h | 21.5 ± 0.3 kcal.mol$^{-1}$ |

**Table 11.** Kinetics of escape of endohedral atom or molecule from **58**.

[k] B3LYP/6-31G(d,p)//B3LYP/3-21G

[l] Exact yields and filling factors are not stated in the paper. Filling factor is estimated from the spectra depicted in supplementary information of the publication.[156]

## 1.4.5 Insertion of molecules into 60

In 2016, Chen published an insertion of $H_2CO$ and HCN into **60.** The neat $H_2CO$ was formed at 150 °C by depolymerisation of paraformaldehyde under nitrogen and then was bubbled through a solution of **60** and **$H_2O@C_{60}$** (**1.4.2**) at 100 °C for 15 min. The incorporation of $H_2CO$ was low and longer exposure did not improve it due to polymerisation of $H_2CO$. No $H_2CO$ was incorporated at room temperature. The HPLC enrichment was unsuccessful and $H_2CO$ content was decreasing after routine workup. For the synthesis of **HCN@60**, neat HCN was prepared *in situ* from $H_2SO_4$ (aq) and NaCN dried over $CaCl_2$ and condensed at -20 °C before adding the solution of **60** and **$H_2O@60$.** The filling factor was very high and also removal of the endohedral water was observed. The reason for this could be similar to the case of HF in **69**. The hydrogen bonding between HCN and $H_2O$ could facilitate the removal of endohedral $H_2O$. No kinetic data for loss of $H_2CO$ and HCN from **60** was published.[143]

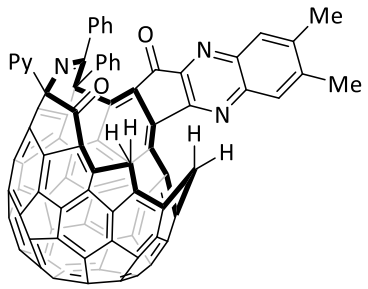


**60**

**Figure 10. 60**.

| Guest | Solvent | Temperature | Time | Filling factor | Yield |
|---|---|---|---|---|---|
| **$H_2CO$** | Ph-Cl | 100 °C | 15 min | 9% (35% $H_2O$) | 90% |
| **HCN** | Ph-Cl | 90 °C | 4 h | 98% | 76% |

**Table 12**. Insertion achievements of $H_2CO$ and HCN to **60**.

## 1.4.6 Insertion of molecules into 47

OCF **47** has a 17-membered ring orifice and is prepared by the method shown in **Scheme 16**. The orifice is large enough to insert atoms or molecules bigger than $H_2O$ or $H_2$.

$N_2$ and $CO_2$ were inserted into **47** by Murata in 2015. $H_2O$ rapidly enters and leaves the cavity of **47** which suggests that **47** behaves as if it was larger than the **58** by Iwamatsu. To prevent the escape of molecules such as $N_2$ or $CO_2$ a 'stopper' on the orifice rim was introduced. The idea of stopper was first presented in 2007 by Komatsu while developing the synthesis of $H_2$ and He[175] and later in 2010 by Gan[176] who proposed a phosphate blocker in order to trap $H_2O$. A selective reduction of **47** using

$NaBH_4$ in a mixture of *o*-DCB formed an OH group on the rim that served as the proposed 'stopper' (**Scheme 39**, Method A). Calculated energies[m] suggested that $N_2$ and $CO_2$ should enter the cavity at room temperature (35.5 and 17.9 kJ.mol$^{-1}$). The encapsulations were performed by heating **47** at 140 °C for 22 h to remove endohedral $H_2O$ and then subjecting it to the desired compressed gas at room temperature. The powdered sample was then dissolved in *o*-DCB at 0 °C (to avoid the escape of $N_2$) and treated with $NaBH_4$ in EtOH to obtain **86** with encapsulated guest molecule. Unfortunately, during the reduction process endohedral water was introduced into the **86**. $CO_2$ could be encapsulated in compound **47** but without the stopper the $CO_2$ filling factor decreased from 72% to 46% after 100 h at room temperature. Neither $N_2$ nor $CO_2$ escaped from **86** using the same conditions. 5% of $CO_2$ was lost from **$CO_2$@86** after heating at 100 °C for 63 hours. Escape energies of $CO_2$ and $N_2$ from **86** were calculated[m] to be (92 .8 and 51.6 kJ.mol$^{-1}$) which corelates with the observed slow escape. The **$CO_2$@86** and **$N_2$@86** can be separated from **$H_2O$@86** by recycling HPLC.[177]

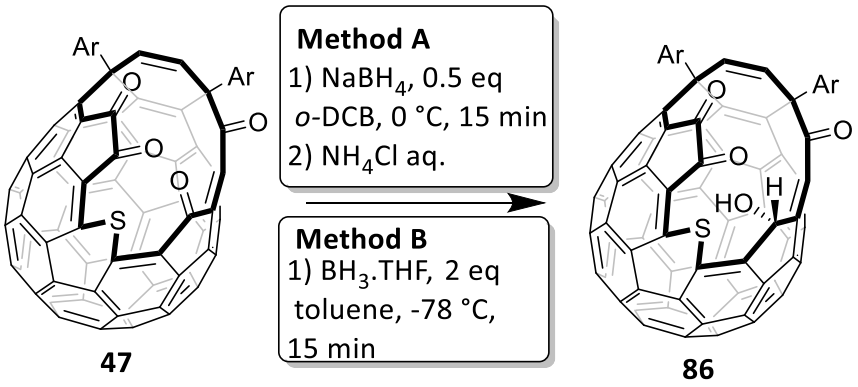


**Scheme 39**. Generating a 'stopper' in order to encapsulate $N_2$, $CO_2$, $CH_2O$, $NH_3$, $O_2$, NO.

In 2017 $CH_3OH$ and $CH_2O$ were encapsulated in **47** and **86** by a similar method as reported above. Both molecules were inserted into **47** at high pressures and temperatures (**Table 14**) resulting in 65% for $CH_3OH$ and 35% for $CH_2O$, however both $N_2$ and $H_2O$ were incorporated into **47** as well. Incorporation of $C_2H_5OH$ and $CH_3CN$ was also attempted in similar conditions but was unsuccessful showing that the orifice of **47** is not large enough for their entry. Escape of $CH_2O$ from **47** was fast, in 30 h at room temperature the filling factor decreased from 12% to 5% therefore **$CH_2O$@47** was converted to **$CH_2O$@86** (**Scheme 39**, Method A) to prevent the loss of $CH_2O$. **$CH_3OH$@47** could be easily separated from **$H_2O$@86** and **$N_2$@86** by recycling HPLC after 1$^{st}$ cycle. **$CH_2O$@86** required many recycling steps to afford reasonable purity. X-ray analysis showed interesting orientations of the encapsulated

[m] DFT calculations performed on models where *tert*-butyl groups were replaced with hydrogen atoms and were calculated at the M06-2X/6-31G* level of theory.

species. While the $CH_2$ group of the formaldehyde is pointing towards the opening of the cage, the $CH_3$ group of methanol sits on the concave inner surface of the carbon cage.[178]

$CH_4$ was inserted into **47** in 2018 by Whitby group at 153 atm at 200 °C achieving filling factor of 65%[179]and was improved a year later by increasing the pressure to 1645 atm to 95%.[180] The rate of loss of $CH_4$ from **47** cavity was measured, showing 1st order kinetics. The entropy of $CH_4$ escape at the transition state was determined to be negative, because of the loss of translational and rotational degrees of freedom when $CH_4$ is leaving the cavity.[179]

Insertion of $NH_3$ was published in the same article as the first insertion of $CH_4$ into **47**. Although the calculated energy[n] for $NH_3$ insertion into **47** is higher than that for $H_2O$ insertion ($E_a$ for entry of $NH_3$ is 62.32 kJ $mol^{-1}$ and for $H_2O$ is 30.72 kJ $mol^{-1}$) it is still low enough to enter the cavity spontaneously. When **47** was treated with 16% aqueous ammonia solution a molar ratio of 85:15 of $H_2O$ and $NH_3$ was observed. To avoid contamination of endohedral $H_2O$, solution of $NH_3$ in dried MeOH was used and rapid formation of **$NH_3$@47** occurred. However, after routine purification all the endohedral $NH_3$ was lost in contrast to **$NH_3$@58 (Table 10)** despite that both are 17-membered ring orifices. $NH_3$ was then trapped by forming compound **86**.[179]

The encapsulation of $^3O_2$ was published in 2017 by Murata. It was achieved at 75 atm at room temperature (**Table 14**), despite the concerns of oxygen reacting with the outside of **47.** The reduction to **$O_2$@86** was immediately performed, to prevent the oxygen from escaping (**Scheme 39**, Method A). During the process 11% of $H_2O$@**86** was also formed but the two molecules were separated by recycling HPLC.[181] Oxygen incorporated in $C_{60}$ is believed to play a very important role in more complex supramolecular systems in the near future.[182]

Radical nitric oxide (**NO**) was encapsulated in **86** in 2018 by Murata. It was achieved under moderate pressure at room temperature (**Table 14**) followed by immediate reduction to **NO@86** (**Scheme 39**, Method B). The attempt to insert NO by purging NO through the solution of **47** in PhCl was unsuccessful due to formation of insoluble NO adducts. Compound **NO@47** showed sharp NMR signals of the cage with different shifts compared to empty **47** thanks to paramagnetic properties of NO. Their decrease could be observed over 40 min at ambient temperature allowing a kinetic analysis of NO loss. The calculated energies were in accordance with the DFT predictions and supported the facile escape of NO. Escape of other species such as $O_2$ or $N_2$ from **47** cannot be determined via this method, because these do not show such sharp signals and shift differences in the $^1H$ NMR. Similar to

[n] Electronic energy calculated in Gaussian 09 using M06-2X with cc-pVTZ basis set at M06-2X/cc-pVDZ geometry

**$CH_3OH$@47** synthesis, $H_2O$ and $N_2$ were incorporated into **47** which later caused difficulties in separation of **NO@86** from **$N_2$@86** by recycling HPLC. The formation of **$N_2$@86** was avoided by bubbling $H_2$ before the reduction to **NO@86.** X-ray crystallography revealed that NO occupies two orientations in the cavity N-up and O-up in a ratio of 0.55:0.35. The DFT calculations UB3LYP-D3/6-31G(d,p) and UM06-2X/6-31G(d) showed that N-up is more stable by 0.17 and 0.18 kcal.mol$^{-1}$ respectively and confirmed the ratio of the two orientations. The transition state between the two orientations was calculated by UB3LYP-D3 to be 1.83 kcal.mol$^{-1}$ which is higher than the most stable conformer of N-up showing that NO rotates freely inside **86** even at 100 K. An NMR study was conducted to show paramagnetic properties of NO by large shifts depending on the temperature. **NO@86** showed dramatic difference in $^1$H NMR in contrast with diamagnetic **$H_2O$@86.**[183]

In 2020, Whitby group inserted Ar atom into the fullerene **47.** Filling conditions were estimated by comparison with the successfully prepared $CH_4$@$C_{60}$ and their entry energies by DFT calculations. It was found that Ar has a lower entry energy and similar binding enthalpy as the $CH_4$ (**Table 13**). Solid state **47** was heated to 180 °C under Ar pressure of ~1400 atm for 17.5 h resulting in >99% filled **Ar@$C_{60}$.**[184]

| Guest | $\Delta H^{\ddagger}_{entry}$/kJ.mol$^{-1}$ | $\Delta H^{bind}$/ kJ.mol$^{-1}$ |
|---|---|---|
| **$CH_4$** | 86 | –50 |
| **Ar** | 55 | –46 |

**Table 13**. Comparison of the entry and binding enthalpies of $CH_4$ and Ar to the cavity of **47**.

Calculations[o] were carried out using Gaussian 09 using the M06-2X/p-ccVDZ1. Aryl groups in **47** were replaced by methyl groups.

| Guest | Solvent | Time | Temperature | Pressure | Filling factor | Yield |
|---|---|---|---|---|---|---|
| **$CH_4$** | solid | 22 h | 190 °C | 1645 atm | 95% | 79% |
| **Ar** | solid | 17.5 h | 180 °C | 1400 atm | >99% | 100% |
| **$NH_3$** | *o*-DCB | 10 min | 0 °C | n | 92% | 45% (of **86**) |
| **$CO_2$** | solid | 24 h | r.t. | 45 atm | 76% (17% $H_2O$) | 50% (of **86**) |
| **$N_2$** | solid | 24 h | r.t. | 100 atm | 43% (37% $H_2O$) | 37% (of **86**) |
| **$CH_3OH$** | PhCl | 50 h | 150 °C | 9000 atm | 60% | 65% |
| **$CH_2O$** | 1,3,5-trioxane | 48 h | 150 °C | 8000 atm | 35% | 31% (of **86**) |
| **NO** | solid | 24 h | r.t. | 28 atm | 75% | 67% (of **86**) |
| **$O_2$** | solid | 24 h | r.t. | 75 atm | 82% (11% $H_2O$) | 35% (of **86**) |

**Table 14**. Conditions for insertions of guest molecules into **47**.

[o] Calculations were carried out using Gaussian 09, 8 using the M06-2X functional9 with cc-pVDZ10 basis set to locate minimum energy and transition state structures and to characterise them through frequency calculations. The cc-pVTZ10 basis set with an ultrafine integration grid was used to calculate electronic energies and to correct for Basis Set Superposition Error using the counterpoise method.11 Thermal corrections to the electronic energy to give the enthalpy at 298 K and 1 atm were derived from frequency calculations at the M06-2X/ccpVDZ level using the Gaussian freqchk utility. The frequencies were not scaled and low frequency modes were not removed.

All the open-cage endohedral fullerenes were successfully isolated in high purity by recycling HPLC. In **Table 14** the best results from literature are summarized.

Except **$CH_4$@47** and **Ar@47** none of the endohedral **47** mentioned above were successfully sutured to **A@$C_{60}$**.

## 1.5 Suturing the orifice to A@$C_{60}$

### 1.5.1 $H_2$@$C_{60}$

After $H_2$ was successfully inserted into OCF **31** the molecular surgery was completed by suturing the orifice in/of $C_{60}$. The first successful closure was done in synthesis of **$H_2$@$C_{60}$** by Komatsu in 2005 (**Scheme 40**)[151][106][185] and later an alternative route was found by the Whitby group.[155] In Komatsu's synthesis of **$H_2$@31** it was found that in strong laser irradiation in the MALDI TOF mass measurement, a weak peak corresponding to **$H_2$@$C_{60}$** (*m/z* 722) is observed which indicated that the orifice could be closed in a gas phase irradiated by powerful laser. In this case 70% loss of $H_2$ was detected and therefore it was necessary to reduce the size of the orifice in order to produce **$H_2$@$C_{60}$** without the loss of $H_2$. The escape rates of $H_2$ from **31** (**Table 4**) showed that reactions at high temperatures had to be avoided. The sulphur atom on the rim of **31** was first oxidised to its corresponding sulfoxide by *m*-chloroperbenzoic acid (m-CPBA) to make the sulphur atom removable. The removal of the SO unit was achieved by irradiation of solution of **$H_2$@66** in benzene with visible light because the attempt of removal by thermal extrusion showed no reaction. Once the orifice was sutured to 12-membered ring **29**, the $H_2$ was encapsulated, and it was assumed that it could not escape. Firstly, the size of the orifice is reduced from 3.89 Å to 3.12 Å and secondly the DFT calculations[p] showed that the $E_{esc}$ would be 50.3 kcal.mol$^{-1}$ which is almost twice the energy $E_{esc}$ from **31** (28.7 kcal.mol$^{-1}$). However, when gas phase laser irradiation was performed on **$H_2$@29** (350 °C, 1 mm/Hg), 20% of $H_2$ had escaped and only a trace amount of **$H_2$@$C_{60}$** was obtained. The 12- membered ring orifice was then further sutured by McMurry reaction with $TiCl_4$ at 80 °C which led to no loss of endohedral $H_2$ and 88% yield in **$H_2$@19** 8-membered ring orifice. This is the same molecule as the product of the first step of molecular surgery in **Scheme 6**. Heating of **$H_2$@19** then proceeded with 61% yield with no loss of $H_2$ achieving the first successful completion of macroscopic molecular surgery (**Scheme 40**) with a 91% filling factor and 118 mg of recovered mass of **$H_2$@$C_{60}$**.[185] The mechanism of the closure consists of an initial [4+2]

[p] B3LYP/6-31G** level with optimized structures at the B3LYP/3-21G level

intramolecular cycloaddition to give a strained intermediate, which rearranges via radical cleavage and then forms the **$C_{60}$** structure by retro [2+2+2].

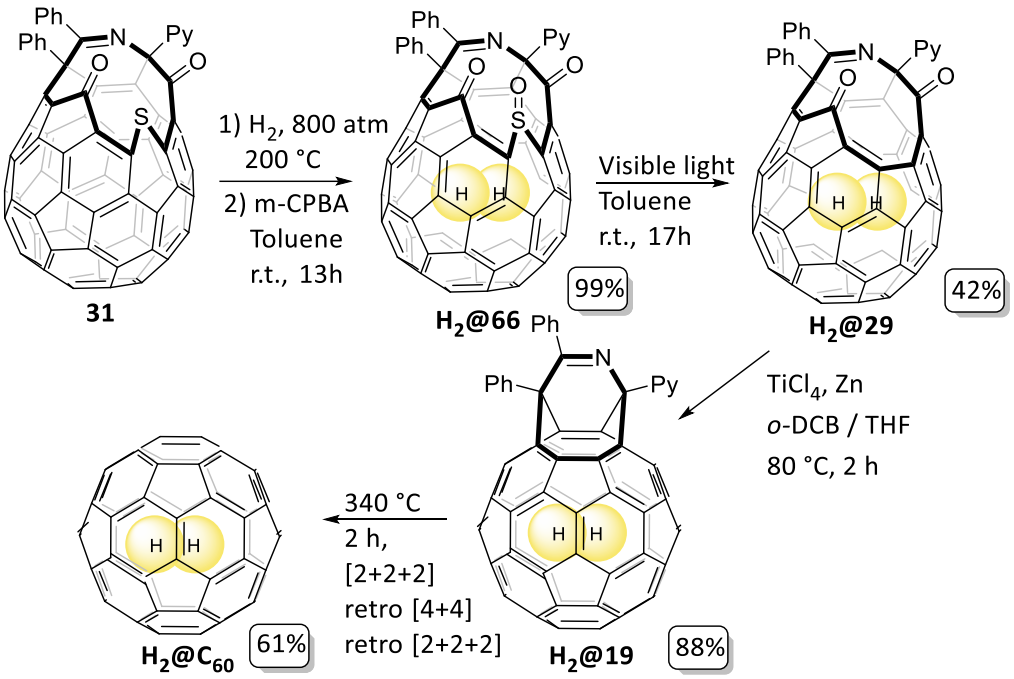


**Scheme 40.** Closure of the $C_{60}$ with trapped $H_2$.

Whitby group filled the OCF **45** with $H_2$ and reported a different route for suturing the orifice that was also employed in synthesis of **$H_2$@$C_{60}$** and other recent **A@$C_{60}$** and is discussed in the section **1.5.3 $H_2O$@$C_{60}$**.

## 1.5.2 $^4$He@$C_{60}$

First synthesis of **$^4$He@$C_{60}$** was carried out by Komatsu group following the procedure established in the synthesis of **$H_2$@$C_{60}$**.[186] Orifice of **31** is big enough for the He atom to freely go in and out of the cavity at room temperature, therefore for the solid state filling step the intermediate **66** was selected (**Table 5**). The irradiation leading to sulfinyl removal was performed immediately after the filling step, followed by the McMurry ring contraction and heating in vacuum. The first **He@$C_{60}$** was obtained with a 30% filling factor corresponding to a mass of 38 mg (**Scheme 41**).

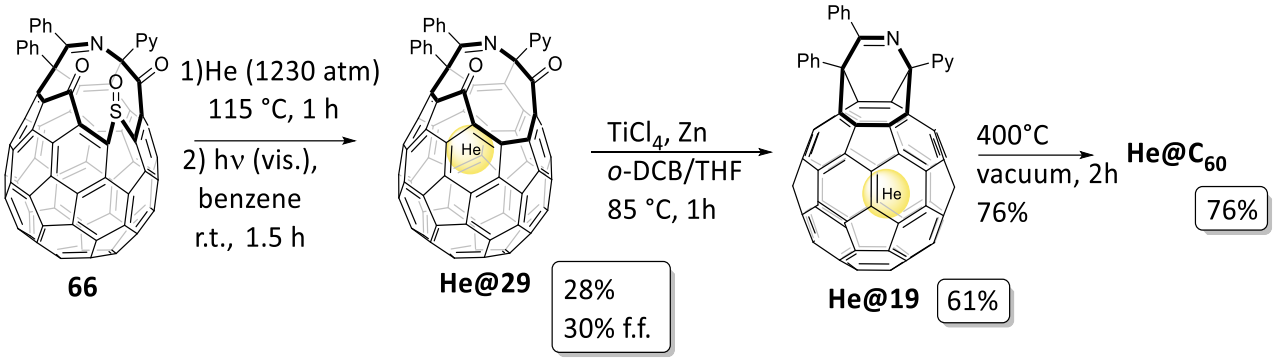


**Scheme 41.** Synthesis of **He@$C_{60}$**.

### 1.5.3 $H_2O@C_{60}$

Encapsulation of water started to attract interest mainly because of its behaviour as a confined quantum rotor, displaying a rich energy level structure, which may be studied by various spectral techniques. The inner space of $C_{60}$ molecule has a diameter of approximately 3.7 Å, suitable for encapsulation of $H_2O$ as well as other small molecules. The homogeneity and stability of **$H_2O@C_{60}$** allows studying physical phenomena such as nuclear spin interconversion.[110]

Successful syntheses of $H_2O@C_{60}$ were achieved by Murata and improved by the Whitby group. Both started from filled OCF discussed in **1.4.2** achieving incorporations shown in (**Table 8**). First suturing of orifice of **45/46** was reported by Murata in 2011 [136] using P($^i$OPr)$_3$ which resulted in a 50% isolated yield of **$H_2O@42$** and formation of the reduced by-product **87**. In 2014 Whitby group reported that using $PPh_3$ leads to clean formation of **$H_2O@43$** with an 84% yield. **$H_2O@43$** then reacts with P($^i$OPr)$_3$ giving **$H_2O@42$** 84% yield improving the overall yield to 70% from **46** to **45** (**Scheme 42**).[155] At the toluene reflux temperature **46** and **45** are in equilibrium and it is possible that the P($^i$OPr)$_3$ reacts with **46** and forms a stable by-product whereas the $PPh_3$ only reacts with the dehydrated form of **45**.

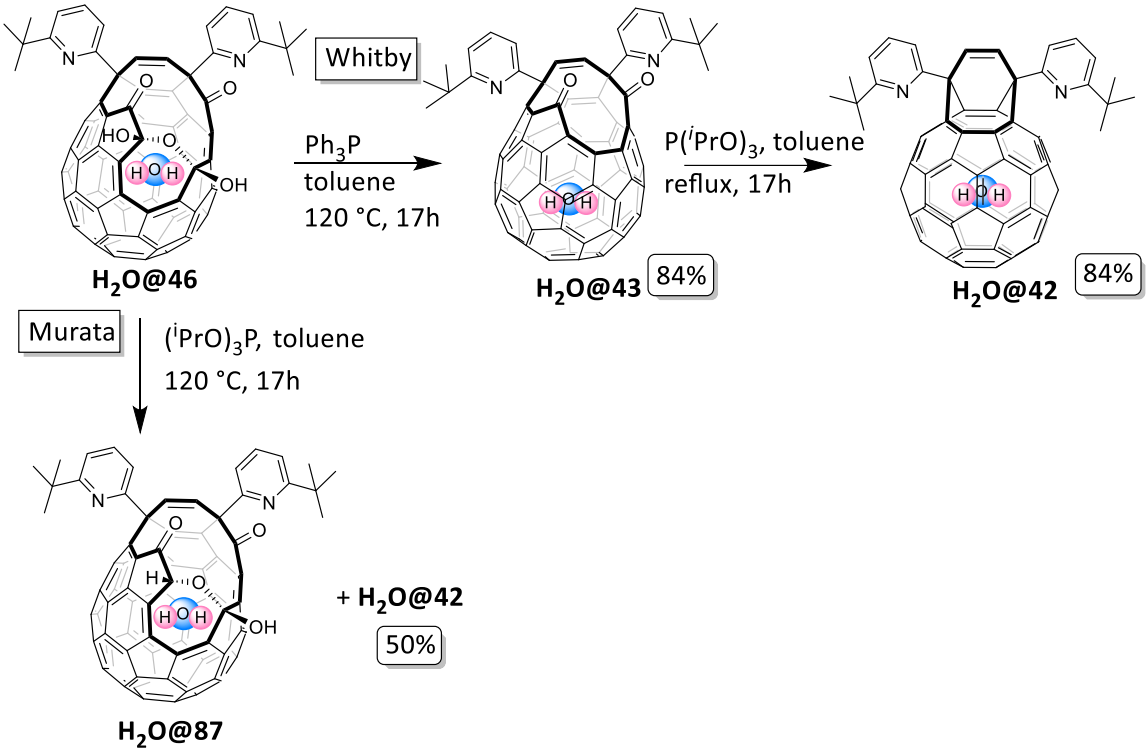


**Scheme 42.** Comparison of ring closure by Murata and Whitby group.

Murata group was the first to report closure of **42** to $C_{60}$, which consisted of heating **42** to 360 °C under high vacuum with $Al_2O_3$.[136] Whitby group discovered that the strong dienophile *N*-phenylmaleimide allowed a lower energy path to $C_{60}$ from **42.** The mechanism starts with [4+2] cycloaddition forming an intermediate that is suitable for another retro [4+2] cycloaddition that regenerates the $C_{60}$ cage. After a 20-hour reaction of **$H_2O$@42** with *N*-phenylmaleimide under reflux in 1-chloronaphthalene and a column chromatography, a 90% yield was obtained. This was then sublimed and resulted in a 72% overall yield from **42** to **$C_{60}$** (**Scheme 43**). [155]

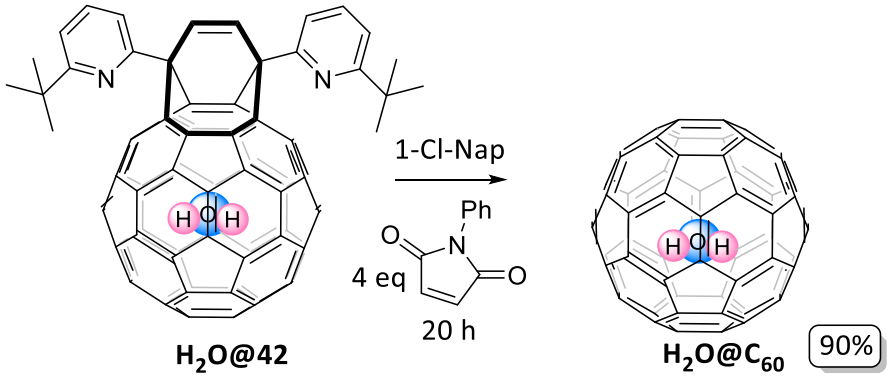

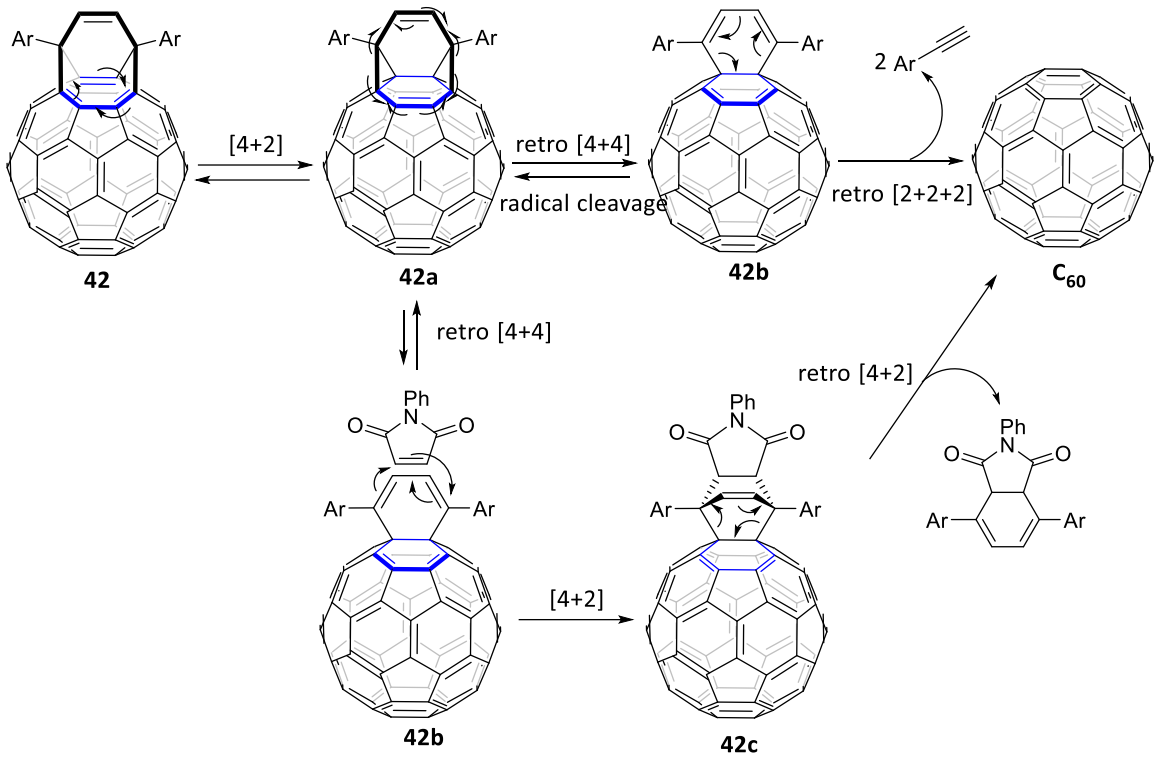


**Scheme 43.** Final closure step of $H_2O@C_{60}$ mechanism.

In 2020 **$H_2O@C_{60}$** was prepared from **$H_2O$@19** by heating under vacuum at 500 °C giving 87% isolated yield of 98% filled **$H_2O@C_{60}$** (**Scheme 44**).

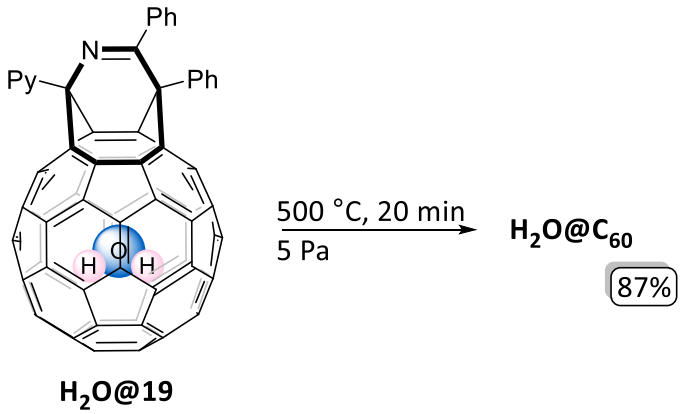


**Scheme 44.** Closure of **$H_2O$@19** by heating under high vacuum

## 1.5.4 HF@$C_{60}$

The most challenging part of the HF@$C_{60}$ was the partial closure step of the **HF@46.** Although a suitable process for the partial closure of **46** had been developed (**Scheme 42**),[155] it was not applicable to the synthesis of **HF@43**. Heating **HF@46** with $PPh_3$ resulted in the complete loss of HF and an empty **43** was obtained. Energy needed for the exit of HF from the **HF@45** was calculated to be 74.9 kJ mol

[1 q] and energy of water leaving **$H_2O$@45** was calculated to be 115.0 kJ $mol^{-1}$ [q]. This explains why water does not escape from the fullerene cage at higher temperature. When **HF@46** was reacted with $PPh_3$ using 3 Å molecular sieves at room temperature, a phosphorus ylid **88** was formed instead of the desired product with retention of HF (**Scheme 45**). Heating ylid **88** to 110 °C led to the formation of **43,** however the complete loss of HF shows that the activation energy for closure of the **88** is higher than the energy needed for the HF to escape.

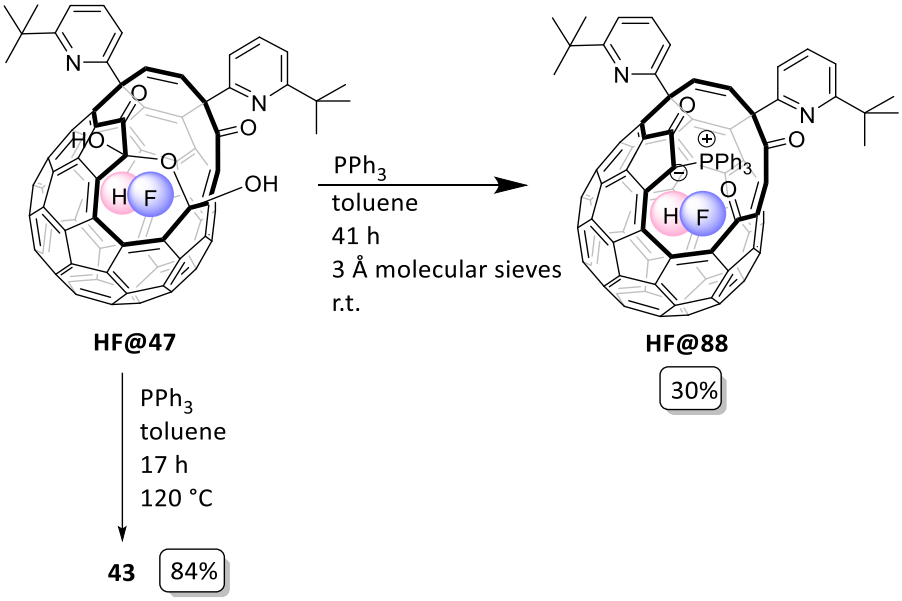


**Scheme 45.** Formation of a phosphorus 88 in room temperature.

To accelerate the rate of closure of the **88** to **HF@43**, the electron deficient tri(2-furyl)phosphine ($P(Fu)_3$) was used. However, the formation of the 88 then required a high temperature (70 °C) and the HF was lost. The most suitable phosphine was found to be $PPh(Fu)_2$, which after 5 days at room temperature gave a 64% yield of **HF@43** with 30% retention of HF (**Scheme 46**).[108] The following closure steps were the same as in the synthesis of **$H_2O$@$C_{60}$** (**Scheme 43**)**.**

[q] B3LYP/6--31G(d)--D3BJ corr

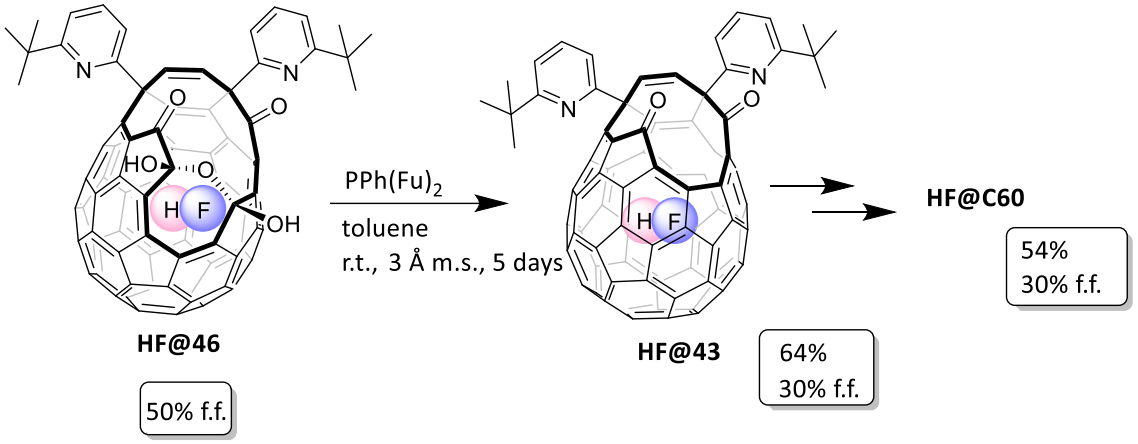


**Scheme 46.** Closure of **HF@46** leading to first **HF@C$_{60}$**.

### 1.5.5 CH$_4$@C$_{60}$

Compound **47** can be further oxidised to **89** (sulfoxide derivate) and sutured to **45** by photochemical removal of the sulfinyl group SO. The sulfone group $SO_2$ is not formed in these conditions, probably because of steric hindrance of the fullerene. In Murata's first synthesis of **H$_2$@C$_{60}$** (**1.4**, **Scheme 40**) and **He@C$_{60}$**[186] sulfoxide derivate **66** is sutured to **29** using visible light irradiation. In the APCI (positive ion source) mass spectrum of **89** the mass corresponding to **45** is present. However, it was also found that exposure to visible light of OCF **89** does not lead to simple removal of sulfinyl group to **45,** but forms number of insoluble compounds together with undesired lactone by-product **90** (**Scheme 47**).[187] The formation of L could be caused by photochemical rearrangement initiated by breaking of C-C bond in the 1,2 diketone five membered ring (green). The protection of the 1,2-diketone moiety could be one of the possible solutions to avoiding unwanted by-products.

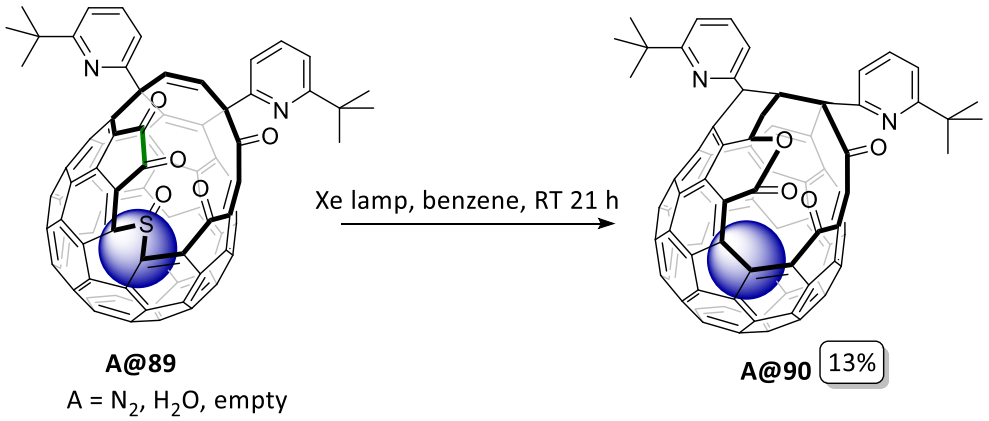


**Scheme 47.** Formation of undesired by-product lactone **90**.

The Whitby group found a suitable irradiation method to obtain **45** using visible light and encapsulated $CH_4$ in $C_{60}$ for the first time (**Scheme 48**). [180]It was achieved by finding suitable ratio of solvents MeCN and toluene, which together with 10% acetic acid in water is thought to have catalysed the immediate formation of **46** from **45**. The discovery of these conditions was prompted by observation of APPI mass spectrum of **89**. Ion m/z = 1102.18 was the dominant species which corresponds to $\mathbf{45}^{+\bullet}$ suggesting that formation of **45** from **89** by photoionization should be feasible. As it was found that **45** decomposes under visible light irradiation, the rationale was that the aqueous acetic acid could catalyse trapping the **45** *in situ* by reaction with $H_2O$ to form its hydrated form **46.**

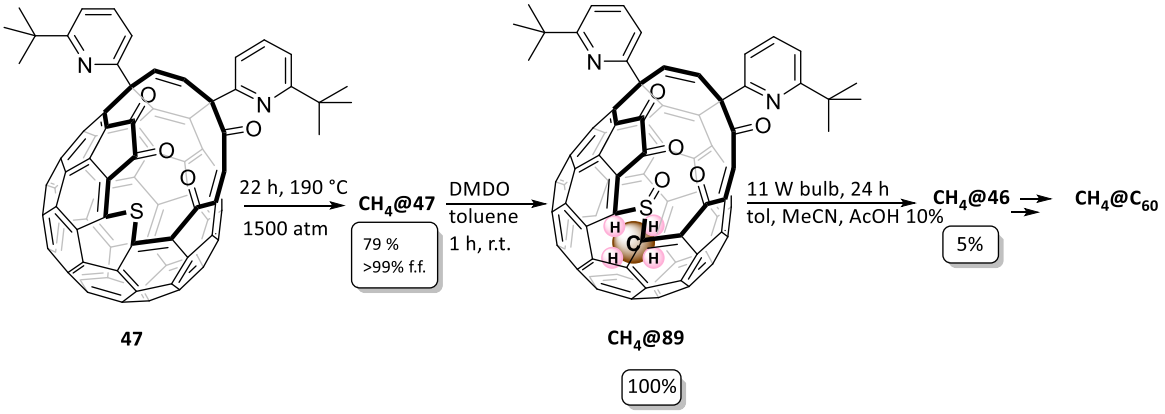


**Scheme 48.** First synthesis of $\mathbf{CH_4@C_{60}}$.

When reaction from **89** to **45** was done on an empty system, which naturally contains endohedral water, the yield of this step was higher (25%) than that with $\mathbf{CH_4@89}$ (5%). It was confirmed that the presence of endohedral methane inhibits the ability of $\mathbf{CH_4@89}$ to convert to **46**. When the reaction was carried out with a lower filling factor of methane, the yield was higher. The filling factor of the obtained $\mathbf{CH_4@46}$ is lower than of the starting $\mathbf{CH_4@89}$ suggesting that the rate of ring contraction of **89** and $\mathbf{H_2O@89}$ is much higher than of $\mathbf{CH_4@89}$. This is one of the rare examples of an endohedral molecule affecting reactivity of OCF.[188] It is either the endohedral methane molecule that inhibits the photoreaction, or it is the presence of endohedral $H_2O$ that catalyses the conversion to **45**.

## 1.5.6 Ar@$C_{60}$

In 2020 Whitby group presented the first synthesis of Ar@$C_{60}$ by molecular surgery. After the smooth preparation of **Ar@47** (**Table 14**), high yielding oxidation with DMDO to **Ar@89** was performed. This was followed by photochemical removal of SO developed for the synthesis of $\mathbf{CH_4@C_{60}}$. Closure to $\mathbf{Ar@C_{60}}$ then followed the same synthetic procedure as for $CH_4@C_{60}$.[184]

### 1.5.7 Summary of A@$C_{60}$ prepared by molecular surgery

| **A@$C_{60}$[ref]** | **Filling conditions** | | | | **Solid/solution** | **Filling factor** | **Scale[a]** | **Yield[b]** |
|---|---|---|---|---|---|---|---|---|
| | OCF | Pressure | Temp. | Time | | | | |
| **$H_2$@$C_{60}$**[106] | **31** | 800 atm | 200 °C | 8 h | Solid | 91% | 118 mg | 22% |
| **$H_2$@$C_{60}$**[155] | **45** | 120 atm | 120 °C | 20 h | toluene | 60% | 68 mg | 50% |
| **$^4$He@$C_{60}$**[186] | **31** | 1230 atm | 115 °C | 1 h | Solid | 30% | 38 mg | 13% |
| **$H_2O$@$C_{60}$**[136] | **45/46** | 9000 atm | 120 °C | 36 h | solid | <99% | 10 mg | 15% |
| **$H_2O$@$C_{60}$**[155] | **45/46** | 1 atm | 100 °C | 48 h | 1-Clnap | 78% | 54 mg | 50% |
| **HF@$C_{60}$**[108] | **45/46** | 1 atm | r.t. | 16 h | DCM | 30% | 153 mg | 34% |
| **$CH_4$@$C_{60}$**[180] | **47** | 1645 atm | 190 °C | 22 h | Solid | 95% | 7 mg | 13% |
| **Ar@$C_{60}$**[184] | **47** | 1400 atm | 180 °C | 17.5 h | Solid | >99% | 20 mg | 9.6% |

**Table 15. Summary of atoms and molecules enclosed in $C_{60}$ prepared up to date.**
a) Mass of recovered A@$C_{60}$. b) Overall yield from the steps after the filling reaction.

Variety of endohedral fullerenes have been prepared by molecular surgery. Not only it allowed to encapsulate atoms such as Helium and Argon in larger quantities and filling factors but also filling $C_{60}$ with molecules like $H_2O$, HF or $CH_4$. There is nevertheless a great room for improvement in the process of molecular surgery and lot of opportunities to learn useful information about the encapsulation and escape of the guest atoms and molecules. Yield of the precursors and closure steps need to be improved to maximise the efficiency of the molecular surgery. Better filling procedures need to be developed to allow synthesis of the A@$C_{60}$ with more expensive gases such as $^3$He or HD. Most importantly, suitable closure steps need to be developed for the bigger atoms such as $O_2$, $N_2$, $CO_2$ to allow preparation of new endohedral fullerenes.

# Aims

The aims of this research were to investigate and optimise molecular surgery route to endohedral fullerenes:

- To optimise synthesis of an important precursor diketone **42**, minimise the safety risks and maximise recovery of unreacted starting material $C_{60}$.
- To investigate closure step from diene **42** to **$C_{60}$,** identify and isolate by-product and improve the yield.
- To prepare endohedral fullerenes He@$C_{60}$, $H_2$@$C_{60}$ and their isotopes in sufficient quantities to provide material for spectroscopy experiments.
- To maximise the scale and filling factor of synthesis of **He@$C_{60}$** and **$H_2$@$C_{60}$** by investigating filling into solid state ylid **88**. Collect kinetic data to better understand the closure of the ylid **88** to diketone **43** encapsulating He or $H_2$.
- To investigate synthesis of **Ne@$C_{60}$** by molecular surgery.
- To optimise closure step of 17-membered ring orifice sulfoxide **89** to hemiacetal **46**. Investigate closure steps at lower temperature to allow encapsulation of molecules with high escape rates such as $O_2$, $N_2$, CO or $CO_2$.
- To investigate insertion of larger atoms and molecules such as Kr or $N_2$ into 17-membered ring sulfide **47** and sulfoxide **89** and the effect on the large endohedral species on the closure reactions.
- To explore isolations on preparative HPLC separating A@$C_{60}$ from the empty $C_{60}$ or undesired $H_2O$@$C_{60}$.

# Results and discussion

## 2 Optimised large scale synthesis of precursor 43

Synthesis of endohedral fullerenes is a challenging process that is performed in series of complicated steps. Sensitive reactions with difficult isolations are often accompanied with degradation and need to be handled carefully. Having a reliable, stable precursor is a key to successful development and preparation of endohedral fullerenes. In this project the main precursor is 12-membered ring compound **43.** This diketone intermediate is a brown powder that can be stored at room temperature in dark container for months without degradation unlike the larger 13-membered ring hemiacetal **46**. During the course of this project, compound **43** was prepared in bulk and was a starting point for series of reactions to synthesise endohedral fullerenes. Having a good yielding, large scale compatible process to prepare compound **43** was crucial for maximising the time available for this research.

Opening of the $C_{60}$ is done in two steps (**Scheme 49**) without isolation of intermediate **42** and was first reported by Murata in 2010.[136] This method requires heating of the $C_{60}$ with 1eq of pyridazine derivative **91** for 26 hours at reflux temperature**.** The following step is a singlet oxygen photo-oxidation with addition of $CS_2$ and irradiation with a 500W xenon lamp for 23-27 hours (1g $C_{60}$, 29% yield). The same group recently reported an improved method in which $CCl_4$ was used instead of $CS_2$ and LED lights (undefined power) were used for irradiation giving a reaction time of 48 h and a 52% yield starting with 3g of $C_{60}$ (**Scheme 15**).[137] In this project, we initially used the original method using $CS_2$ as co-solvent in a custom designed jacketed reactor to avoid overheating. The $O_2$ was passed through the reaction mixture at a flow rate of approximately 20 ml.min$^{-1}$. The initial method involved the use of two 400 W halogen floodlights which allowed a reaction starting with 3.5 g of $C_{60}$ to be complete in 50 hours (53% yield)[189]. The high temperatures generated by the flood lights could cause ignition of the $CS_2$ (auto-ignition temperature is 97-107 °C) if the cooling water supply failed. Switching to two 50W LED lamps at approximately 20 cm distance greatly reduced the heat generation, and still allowed reactions started with 5.2 g of $C_{60}$ to be completed in 35 hours (46% yield) but the synthesis still required unattended overnight reactions.

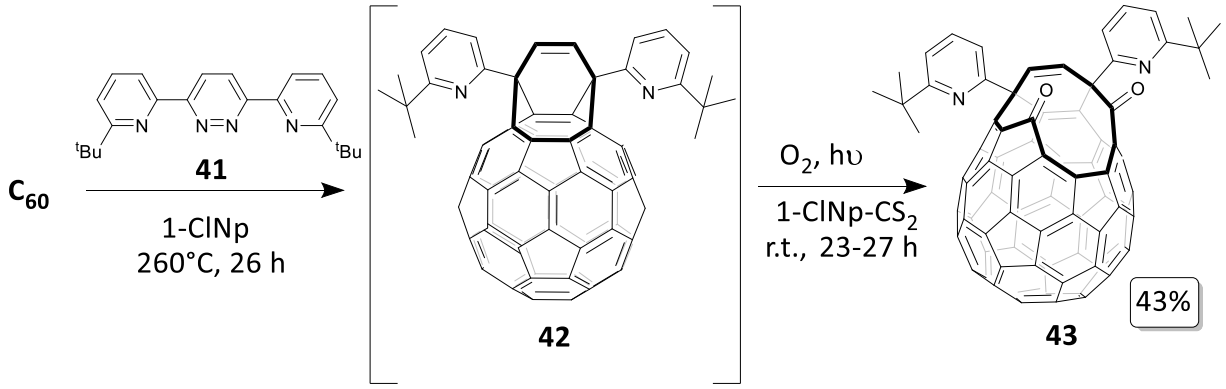


**Scheme 49.** Reported opening of the $C_{60}$ adapted in this project.

The preparation process of compound **43** was further optimised to obtain better yield, shorten the reaction time and avoid the usage of the hazardous $CS_2$ or $CCl_4$. In the formation of **42,** two equivalents of $C_{60}$ instead of one were used, to overcome multiple additions of 4**1**. The excess $C_{60}$ also substantially accelerated the photooxidation step as it is an excellent sensitiser to form singlet oxygen, and was readily recovered during purification of the product **43.**

Multiple additions of **41** can be observed in crude NMR next to the alkenyl peak of intermediate **42 (Figure 11).** The integration shows that at least one third of protons belong to the by-products. Increasing the equivalents of **41** from one to two, reduces the number of by-products by half, which is then reflected on the increase of the yield up to 68%.

2. Optimised large scale synthesis of precursor **43**

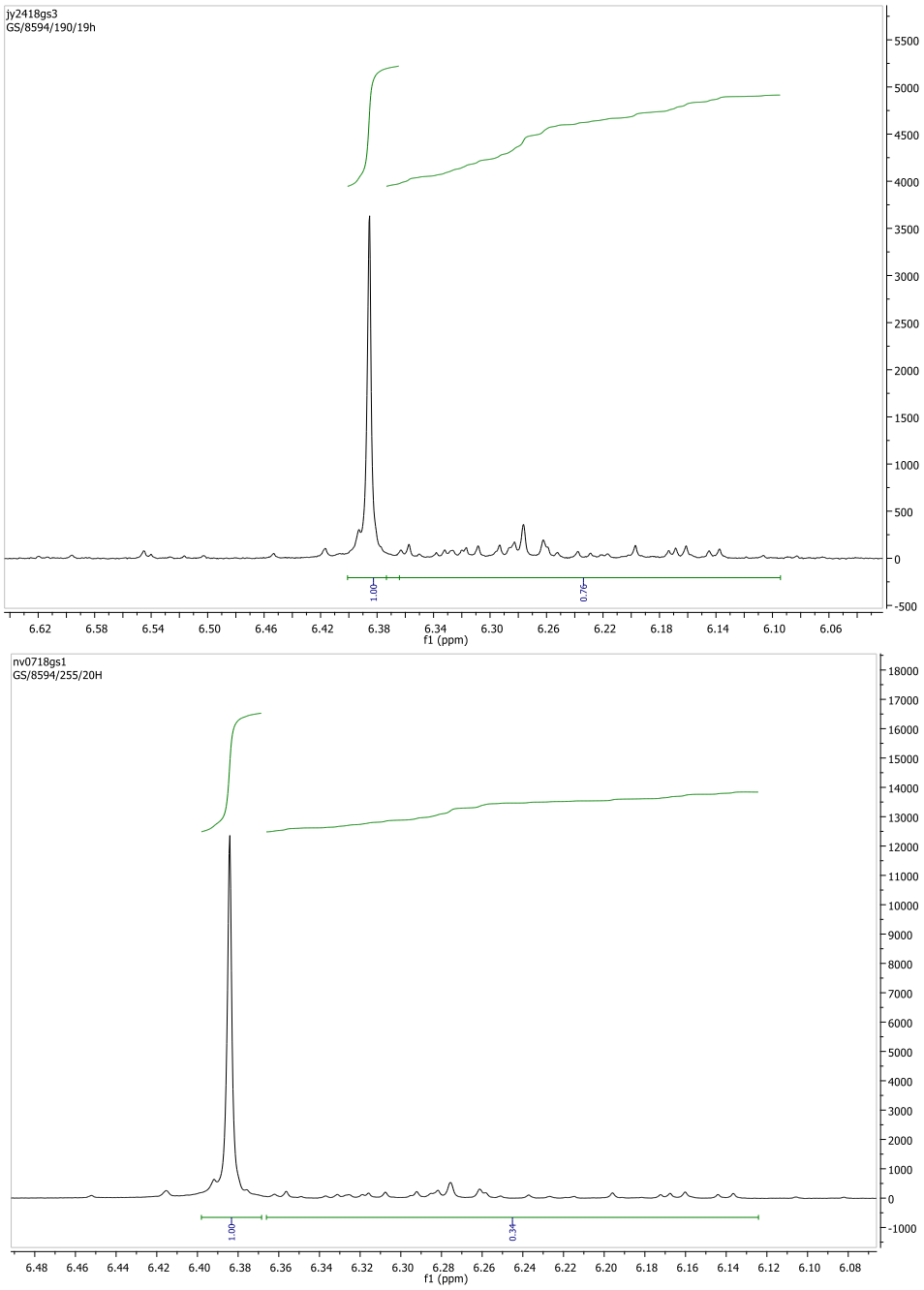


**Figure 11.** Effect on the number of by-products by using 2 eq of $C_{60}$, (Top – 1eq, bottom – 2eq).

Singlet at 6.40 ppm corresponds to the two protons on the orifice alkene bridge of diene **42**. **Figure 11** compares the integration areas between 6.36-6.1 ppm that show the amount if impurities formed.

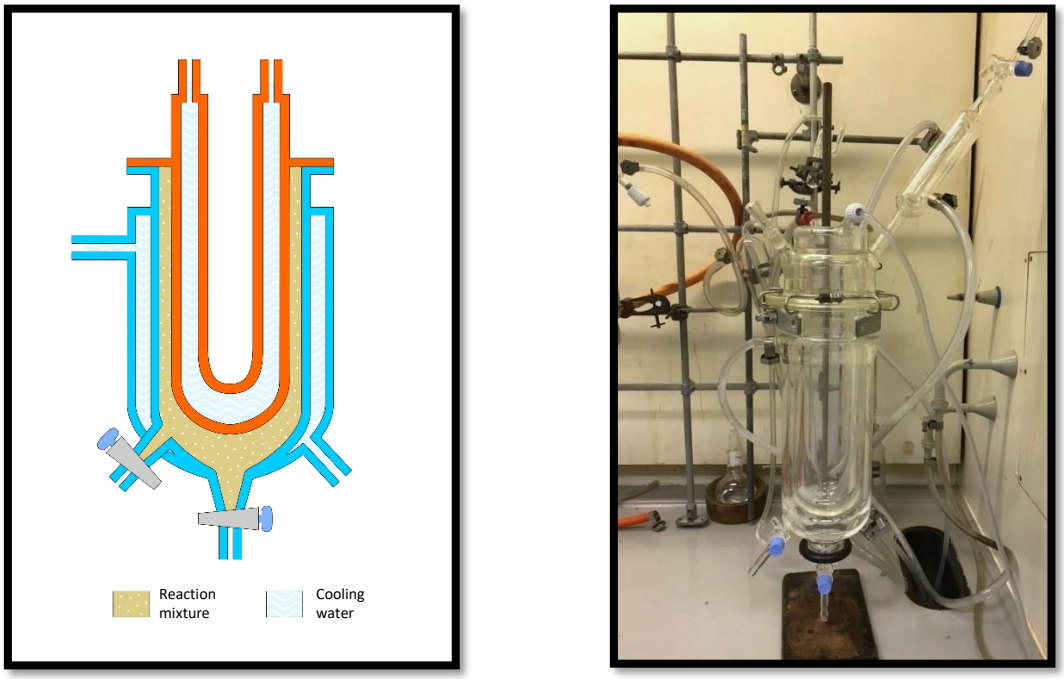


**Figure 12**. Purpose-built photo reactor.

(LEFT: A simplified diagram of the photo reactor. RIGHT: Photo of the reactor.)

A purpose-built photo reactor (**Figure 12**.) was used for the singlet oxygen photooxidation, using a 400W high-pressure sodium lamp in a central well. We found that $CS_2$ could be replaced with toluene without detriment. The reaction time of the photooxidation step was shortened to 1 hour with an isolated yield of up to 68% based on unrecovered $C_{60}$. (Reaction performed on 10g scale). The results are presented in **a)** Yield before column chromatography purification was optimised

**Table 16.** The extra equivalent of the $C_{60}$ can be easily recovered and reused in the synthesis again. The yield in Entry 4 (a) Yield before column chromatography purification was optimised

**Table 16**) was obtained before the purification of the **43** was optimised. The column chromatography purification is done using eluent 1:1 toluene:hexane gradually changed to 100% toluene. In the original procedure using $CS_2$ the reaction mixture was directly poured into $SiO_2$ chromatography column packed with 1:1 toluene:hexane. In the procedure using toluene (Entries 4 and 5) it is necessary to add hexane into the reaction mixture before chromatography to avoid losing product **43** in the initial fractions. The amount of hexane added must be equivalent to the amount of toluene used for dilution in the photoreaction.

| Entry | Eq. of $C_{60}$ | Light | Additive | Time of step 2 | Yield |
|---|---|---|---|---|---|
| **1** | 1 | 50 W LED | $CS_2$ | 16 h | 46% |
| **2** | 2 | 50 W LED | $CS_2$ | 12. 5 h | 63% |
| **3** | 1 | 400 W Na | $CS_2$ | 2 h | 40% |
| **4** | 2 | 400 W Na | toluene | 1 h | 50%[a] |
| **5** | 2 | 400 W Na | toluene | 1 h | 68% |
| **6** | 2 | 400 W Na | toluene | 1 h | 60% |

a) Yield before column chromatography purification was optimised

**Table 16**. Optimisation of synthesis of **43**.

The first fraction during the purification step is $C_{60}$ mixed with 1-chloronaphthalene from which the toluene and hexane are removed on rotary evaporator. The concentration of $C_{60}$ is then assessed by HPLC and this mixture can be reused for the same reaction saving both $C_{60}$ and 1-chloronaphthalene. HPLC calibration curve was plotted for these purposes. In Entry 6**,** the recovered $C_{60}$ was assessed by HPLC and 1-chloronaphthalene was removed by vacuum distillation. The $C_{60}$ was analysed by $^{13}C$ NMR and HPLC to determine the accuracy of the assessment method. The amount of recovered $C_{60}$ calculated from the 1-chloronaphthalene fraction was 4.06 g and the amount obtained in solid after purification assessment was 4.11 g which means the accuracy of this method is 99%.

In conclusion, great advances have been made in the preparation of the diketone **43** precursor:

- Yield of the reaction has been improved by using two equivalents of $C_{60}$ and reliably isolated between 60-70% yield of the product over two steps with the recovery of the unreacted starting material $C_{60}$. The recovery step also introduced saving cost of the $C_{60}$ which is currently in high demand.
- Toxic and low flashpoint solvents ($CS_2$ or $CCl_4$) have been substituted by safer, commonly used solvent toluene which has rapidly decreased the risk of explosion during the oxidation step without having an effect on the yield or rate of the reaction.
- Chromatography step has been improved to isolate high purity material with minimum loss of the yield.
- LED lamps were replaced with high power 400 W sodium lamp which lead to decreasing the reaction time of the oxidation from 27 hours to only one hour which allowed bringing through several batches of the reaction in few hours.
- Batch scale has been increased to up to 10 grams.

# 3 Closure of 42 to $C_{60}$

Whitby group presented successful closure of **42** to $C_{60}$ using dienophile *N*-phenylmaleimide that allows a lower energy path to $C_{60}$ than previously reported.[155] After a 26-hour reaction of **42** with *N*-phenylmaleimide under reflux in 1-chloronaphthalene and a column chromatography, a 90% crude yield was obtained. This was further purified by sublimation and resulted in a 72% yield (**Scheme 50**).[155]

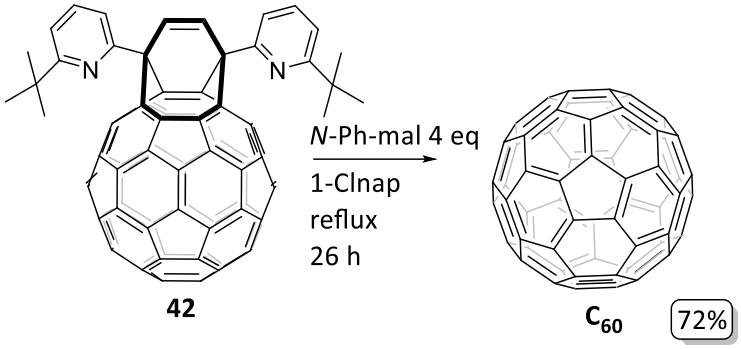


**Scheme 50.** Closure of **42** to obtain $C_{60}$.

While repeating these conditions in closure reactions in this project, a 30% yield of $C_{60}$ was obtained after preparative HPLC purification. It was considered that a minor yield loss could occur during the preparative HPLC and the purity level of the $C_{60}$ is higher than when only purified by sublimation. It is demonstrated in the **Figure 13** taken from the previously published work of HF@$C_{60}$ preparation.[108] In this case the material was first sublimed and then analysed by HPLC (top chromatogram) and therefore showing impurities which weren't accounted for in the yield calculation. The reaction was monitored by HPLC (100% toluene, 1 ml.min$^{-1}$, Cosmosil Buckyprep$^{TM}$) by the disappearance of the starting material diene **42** and formation of the $C_{60}$ peak. Retention time for $C_{60}$ was 7.45 min and for **42** 3.74 min and a small additional peak observed at 6.1 min. In **Figure 13**, the impurity at 6.1 min is observed after the sublimation (top chromatogram) but not after the purification with preparative HPLC (bottom chromatogram). **Figure 13** shows that after purification on the HPLC, in this case also removal of empty **$C_{60}$**, other small unidentified impurities are removed. It is unkown what structures of the impurities are and how much innacuracy in the yield they cause. This section will discuss optimisation of the reaction conditions to minimise yield loss and investigate the formation of by-products.

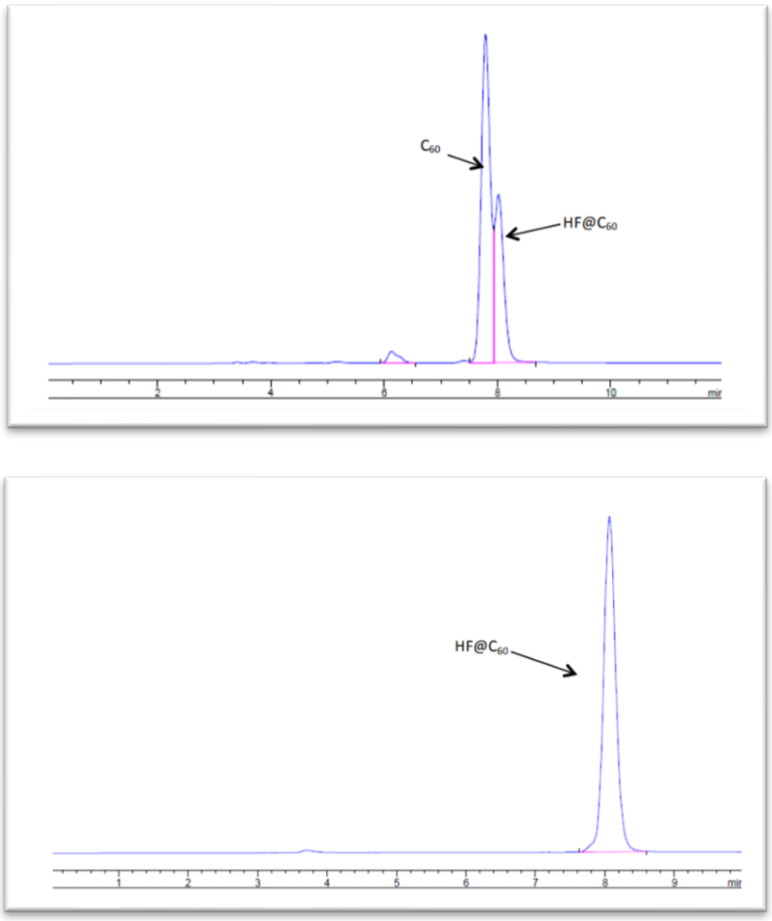


**Figure 13.** HPLC chromatogram of sublimed 30% filled **HF@C$_{60}$** (top) compared with the 100% **HF@C$_{60}$** after preparative HPLC purification (bottom).[108]

To find out why the isolated yield is only 30%, the reaction course was initially monitored by analytical HPLC (100% toluene, 1 ml.min$^{-1}$) observing the disappearance of the starting material at 3.2 minutes and the formation of the $C_{60}$ at 7.6 minutes. The peak at 3.2 minutes did not decrease even after prolonged reaction times or addition of excess dienophile. Previous work in Whitby group[r] implied that in different HPLC conditions (70% toluene 30% hexane, 0.5 ml.min$^{-1}$, Cosmosil Buckyprep$^{TM}$) two main peaks were observed at 9.3 and 10.7 minutes. It was discovered that the 9.3 min peak corresponds to **42** and 10.7 corresponds to an unknown compound **92**. This compound was isolated by the column chromatography and its absolute structure was characterised by NMR and X-ray crystalography (**Figure 14**)**.** The crystal of the **92** was obtained by slow evaporation from mixture of $CS_2$, *o*-DCB and MeOH.

[r] S. Alom

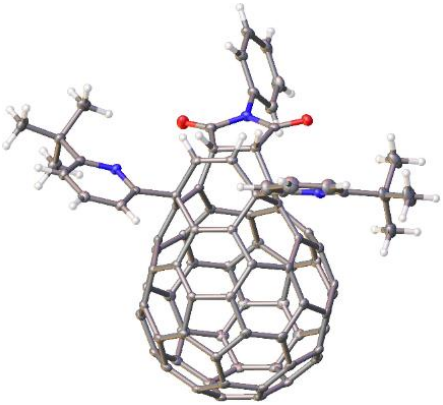

**Figure 14.** Thermal ellipsoid of **92** at 50% probability.

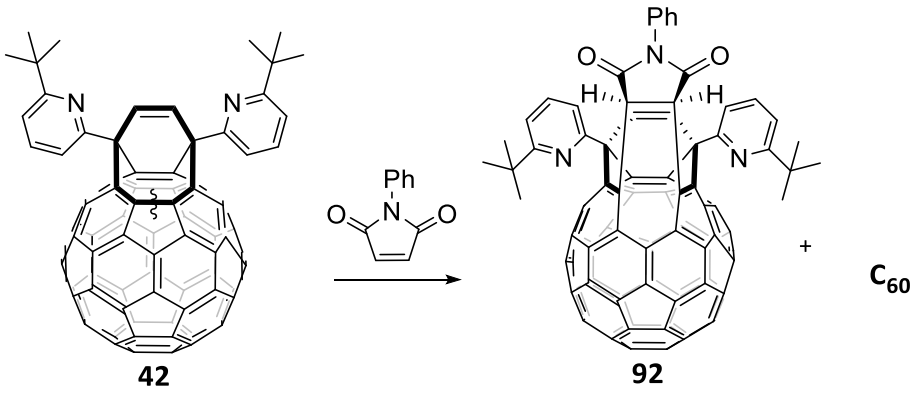


**Scheme 51.** Formation of **92** impurity.

The mechanism of the **42** closure to **$C_{60}$** proceeds via [4+2] cycloaddition of the **42b** intermediate (**Scheme 43** in **1.5.3**). The **42b** is formed by retro [4+4] cycloaddition which is a disallowed reaction unless promoted by external irradiation.[155] The formation of $C_{60}$ proceeds in a sealed tube, completely covered to exclude light. Despite that, the reaction still occurs as the $C_{60}$ is obtained. If the disallowed reactions happen in these conditions, it could be hypothesised that the formation of the unwanted **92** can also proceed via a similar mechanism. When the **42** is heated, it is presumed that it is in an equilibrium with **42a** via [4+2] cycloaddition. **42a** could then react with the *N*-phenylmaleimide via an overall [2+2] cycloaddition persumably via a stepwise mechanism followed by retro [2+2+2] forming the undesired product **92** which could be driven by the strain release of the 4-membered ring. Similar rearrangement is observed in the initial formation of **13** from **$C_{60}$ (Scheme 4).**

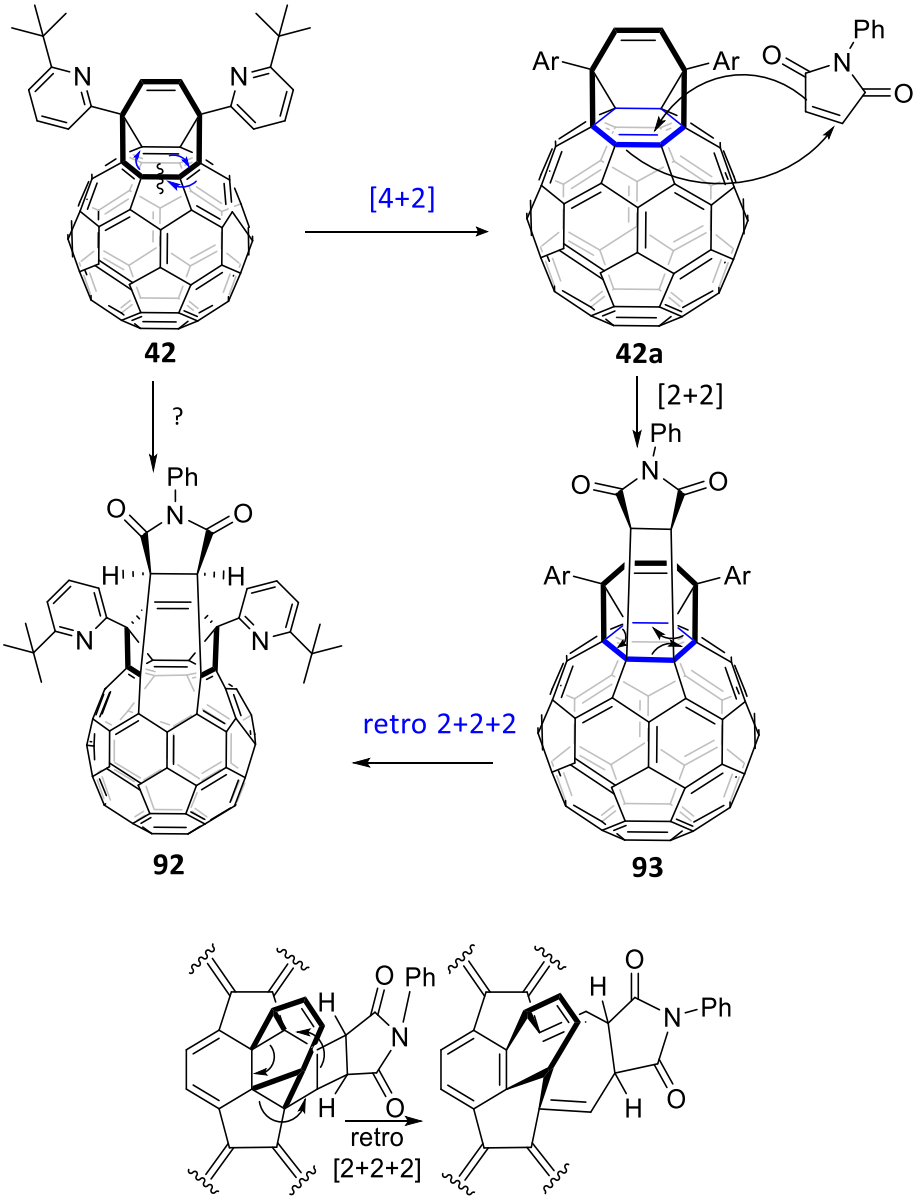


**Scheme 52.** Proposed mechanism of formation of **92** via [2+2] cycloaddition.

As mentioned, the [2+2] cycloaddition is a disallowed process and it is only allowed photochemically. An experiment was done in the group where the reaction was irradiated by visible light and it was anticipated that the major product would be the compound **92**, however this reaction was no different from the experiments without the irradiation.[s] Other potential mechanism explanations could be that it is a stepwise process via a biradical or dipolar intermediate.

By-product observed at 6.1 minutes (100% toluene) was isolated from preparative HPLC as the column chromatography purification was unsuccesful (6.1 minutes in **Figure 13**). After collection of the fraction, precipitation of black powder was observed. Several attempts to redissolve in NMR solvents

[s] Performed by S. Alom

(toluene-$d_8$, *o*-dcb-$d_8$) and 1-chloronaphthalene were unsuccessful and the **93** by-product could not be characterised. It was proposed that this byproduct is a result of a reaction of *N*-phenylmaleimide and $C_{60}$. $C_{60}$ was refluxed with 2 eq of *N*-phenylmaleimide in 1-chloronaphthalene and HPLC monitoring showed formation of the by-product in small amount (1-5%, determined by peak area).

Several reactions (**Table 17**) were performed to find the conditions that would avoid the formation of **92**. The ratio of the HPLC peaks of **92** and **$C_{60}$** was compared. The main variable tested was temperature, however in the sealed tube (Entries 1-4), no difference was observed. Initially it was hypothesised that the side reaction occurs at low temperatures while the heating block reaches temperature needed to form **$C_{60}$**. Experiments performed at lower temperature showed slower formation of **92** than that of **$C_{60}$** (Entries 6, 7 and 14). The best results were obtained at milder temperatures between 240-250 °C and at atmospheric pressure (Entries 15 and 16). In these cases the reaction proceeded slower, but with almost no formation of **92.** All reactions in this study were sampled at 22 hours.

| Entry | N-Ph-Mal eq | Concentration | Temperature/ °C | Flask/Tube | 92:$C_{60}$[t] |
|---|---|---|---|---|---|
| **1** | 4 | 25 mg/ml | 275- gradually | Sealed tube | 0.2:1 |
| **2** | 4 | 25 mg/ml | 275-preheated | Sealed tube | 1:1 |
| **3** | 4 | 24 mg/ml | 260- gradually | Sealed tube | 0.8:1 |
| **4** | 4 | 24 mg/ml | 260-preheated | Sealed tube | 0.7:1 |
| **5** | 4 | 24 mg/ml | Isomantle (300) | Flask, reflux | 0.9:1 |
| **6** | 4 | 25 mg/ml | r.t. | Sealed tube | no reaction |
| **7** | 4 | 10 mg/ml | 200 | Sealed tube | no reaction |
| **8** | 4 | 10 mg/ml | 275 | Sealed tube | 0.5:1 |
| **9** | 4 | 10 mg/ml | 246 | Flask, reflux | 0:1 |
| **10** | 4 | 20 mg/ml | 252 | Sealed tube | 0.8:1 |
| **11** | 2 | 20 mg/ml | 252 | Sealed tube | 0.5:1 |
| **12** | 4 | 20 mg/ml | 240 | Sealed tube | 1:1 |
| **13** | 4 | 20 mg/ml | 260 | Flask, reflux | 0.8:1 |
| **14** | 4 | 20 mg/ml | 225 | Sealed tube | 0.05:1 |
| **15** | 4 | 20 mg/ml | 246 | Flask, reflux | 0.07:1 |
| **16** | 4 | 20 mg/ml | 240 | Tube, atm. pressure | 0.05:1 |

**Table 17.** Optimisation experiments of final closure reaction from **42**.

[t] Normalised peak areas from HPLC spectrum, 70:30 toluene:hexane, 0.5 ml/min

Generally, the maximum safe operating temperature of oil bath is about 160 °C. Therefore, a metal heating block or isomantle must be used. When the reaction was done in a round bottomed or Schlenk flask with condenser, difficulties with stabilising and monitoring the temperature were experienced. The temperature is reliably stabilised when an insulated heating block is used.

Series of experiments in **Table 17** showed that lower temperature and concentration slow down the formation of **92.** It was also hypothesised that the pressure influences the formation of **92.** Series of experiments were performed to compare the reaction in a tube with Youngs tap sealed, and with the Youngs tap loose and the tube outlet connected to a nitrogen bubbler. These conditions were compared at two different concentrations to demonstrate the concentration effect on the reaction **(Figure 15)**.

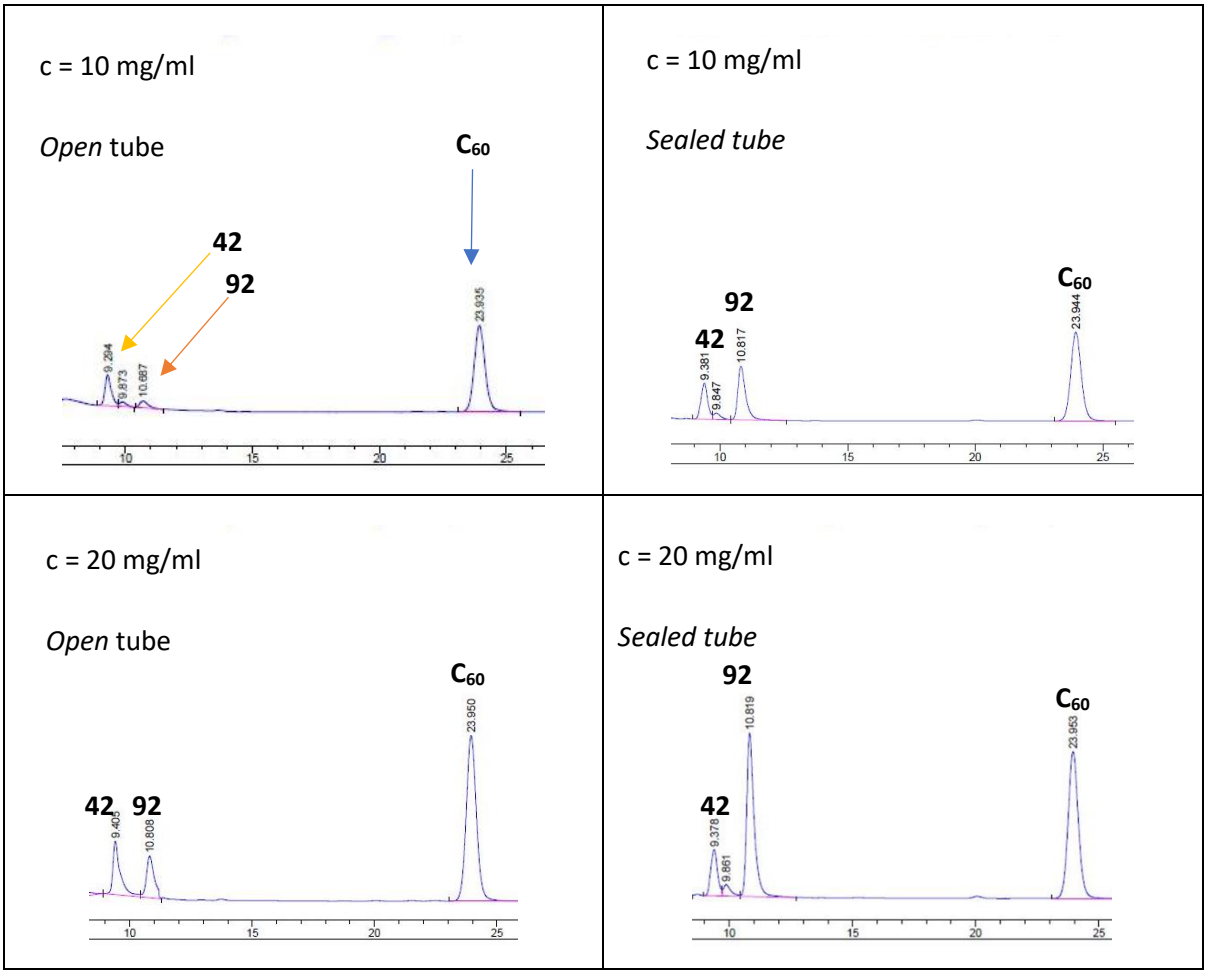


**Figure 15.** HPLC[u] spectra of crude reaction of $C_{60}$ with 4eq of N-Ph-mal (**Scheme 51**) after 20 hours at 245 °C at different concentrations in 1-Cl-Nap.

The results showed a trend that the reaction in the 'open' tube has significantly less **92**. The best achieved crude yield was 70%, corresponding to the reaction at 245 °C for 39 hours and atmospheric

[u] Buckyprep column, 0.5 ml/min, eluent: toluene (70%):hexane (30%)

pressure, using concentration of 10 mg/ml instead of 20 mg/ml. However, the yield after HPLC purification was 40-50% and after sublimation dropped to 30-40%. As the 'open' tube introduces air exchange with the inert atmosphere in the tube, this is an uncontrolled environment and does not increase the yield of the reaction. Air contains oxygen that is well-know to react with fullerenes and cause degradation over time. The low areas of the **92** could be also caused by the instability of **92** in air at high temperatures. It was concluded that the open/closed tube effect does not represent a full solution to the low yielding reaction. The conditions are controlled best in the sealed tube, as there is no exchange with the atmosphere, and the temperature is stabilised by the heating mantle. Further optimisation was performed to determine the effect of the *N*-Ph-maleimide equivalents and concentration. In **Table 17**, entries 10 (4 eq) and 11 (2 eq) show decrease in **92** formation when the number of equivalents of the dienophile was decreased to two. When two equivalents of *N*-Ph-maleimide were used at a concentration of 5 mg/ml, the crude yields obtained from this reaction were between 70% and 90%. After HPLC purification the average yields obtained were between 45% and 55%. (Experimental **8.15**)

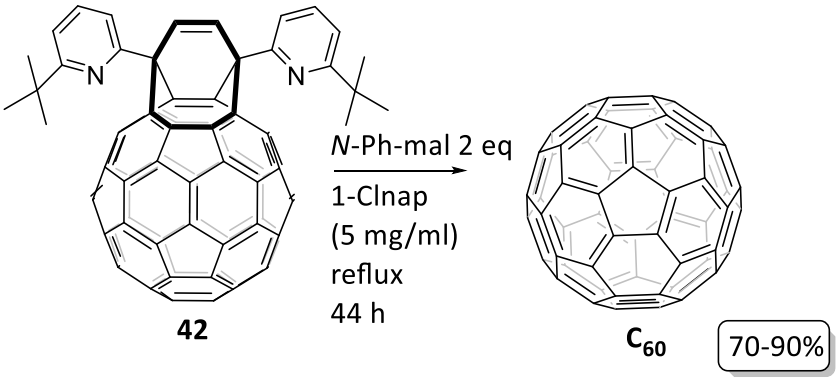


**Scheme 53**. Optimised condition for the closure of **42** to $C_{60}$

In conclusion a modification to reported procedure (**Scheme 53**) has been made to obtain repeatable and reliable yield of $C_{60}$ from compound **42**. The by-product **92** has been identified and characterised and the reaction conditions had been adjusted to supress its formation.

# 4 Optimised large scale synthesis of He@$C_{60}$ and $H_2$@$C_{60}$ and the first molecular surgery synthesis of Ne@$C_{60}$

As discussed in section **1.5**, Murata and Whitby group have pioneered and optimised the synthetic steps for the trapping of small atoms and molecules inside $C_{60}$. This chapter will discuss an approach for closure of He, $H_2$ and Ne in $C_{60}$ which is a strategic combination of known synthetic steps and intermediates utilised in one elegant and concise procedure.

All DFT calculations mentioned in this chapter were done by prof. R.J. Whitby in Gaussian 09 using the M06-2X functional and cc-pVDZ basis set on model systems where the 6-*tert*-butyl-2-pyridyl groups in OCF were replaced by methyl groups.

## 4.1 Intramolecular Wittig reaction of the OCF 88

In the optimised synthesis of **$H_2$@43** compound **$H_2$@45** was refluxed in toluene with $PPh_3$ under $H_2$ pressure to avoid the escape of the $H_2$ molecule due to its relatively low $E_{esc}$ from the **45**.[155] Later in the synthesis of **HF@43** this route was performed at lower temperature as the heating in toluene led to complete loss of HF. During this process, an intermediate compound, **88**, was discovered which is formed by the reaction of **45** with two equivalents of $PPh_3$. The compound **88** is closed via intramolecular Wittig reaction at elevated temperatures. It was proposed[v] that if the $E_{in}$ of **A** (small atom or molecule) is lower than the energy needed for intramolecular Wittig closure, it would be possible to fill the **88** and subsequently induce the closure by raising the temperature to trap the endohedral atom or molecule in **A@43** (**Scheme 54**). This would be a great improvement in the synthesis of **$H_2$@43** which includes venting of $H_2$ followed by addition of $PPh_3$ and re-pressurisation of the solution. The fact that the reaction is done in solution, greatly limits the scale and the pressure as it depends on the size and construction of the vessel. Another benefit of the proposed method is that it would enable the synthesis of the more expensive $H_2$ isotopes HD and $D_2$ as well as the $^4$He and $^3$He.

[v] J. Grasvik,

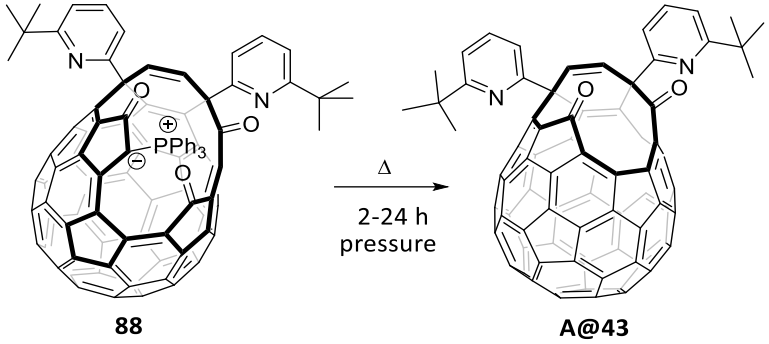


**Scheme 54.** Proposed synthesis of **A@43** by intramolecular Wittig reaction of **88**.

Compound **88** was synthesised and characterised by the spectroscopic methods in **HF@C$_{60}$** work [108] and the position of $PPh_3$ was predicted by DFT calculations of the NMR peaks expected for the possible regioisomers, as well as supported by a coupling observed between the phosphorous and one of the carbonyl carbons.[189] The mechanism of **88** closure was predicted and it was proposed that the closure of **88** to **43** goes via transition state **TS-88** shown in **Scheme 55.** The activation energy was calculated to be 161 kJ.mol$^{-1}$.[189]

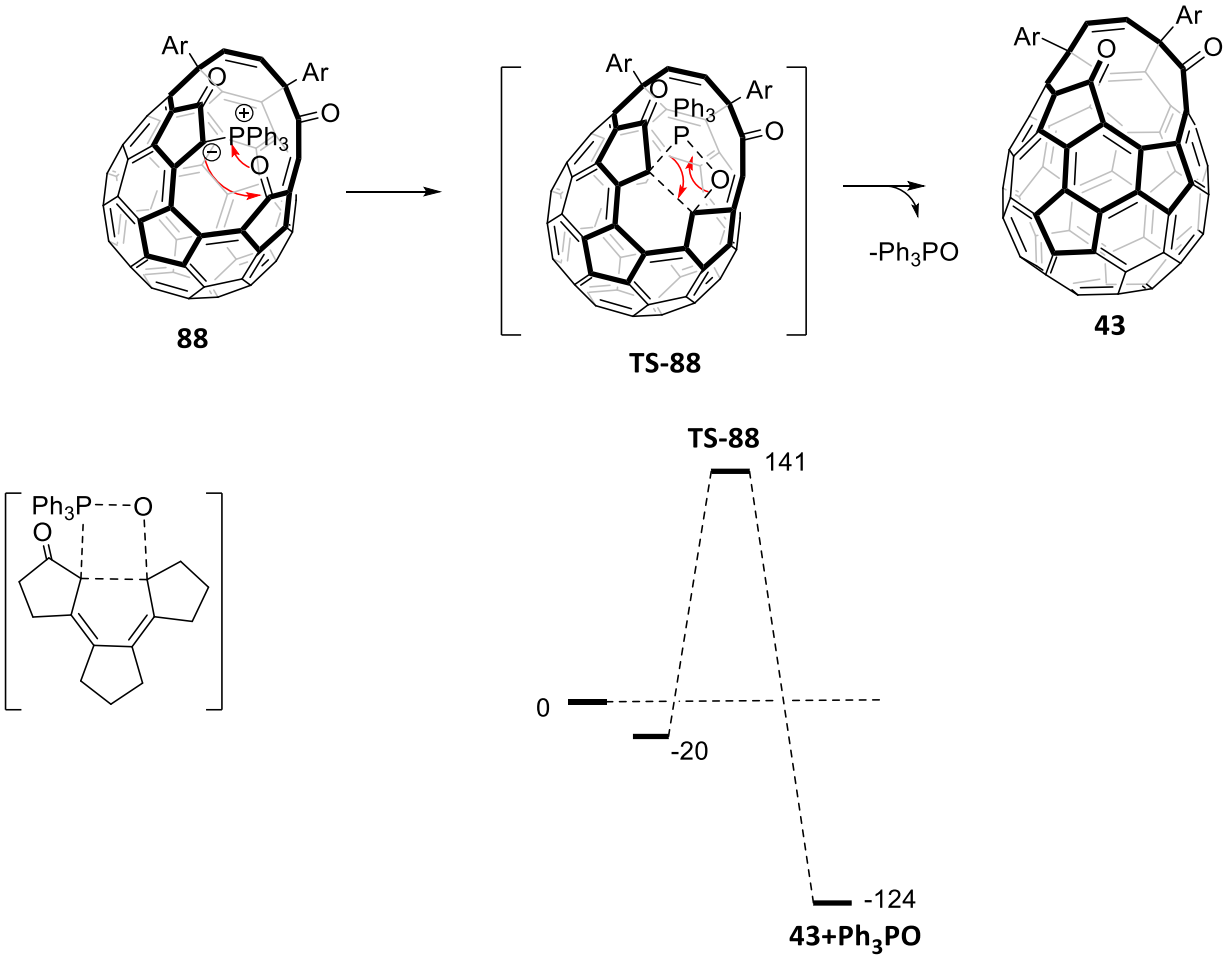


**Scheme 55.** Energy diagram of the conversion from **88** to **43**.

In this work, the compound **88** was characterised by X-ray crystallography and the regioisomer was confirmed (**Figure 16**). It also showed that the C=O bond (1.223 Å) of the carbonyl bonded with the $PPh_3$ group is longer than the other two C=O bonds of the **88** molecule (1.209 Å and 1.202 Å). This suggests that the **88** has an enolate character which can explain its good stability. Similar properties were reported for the **49** mentioned in **1.3.1.1**.[139]

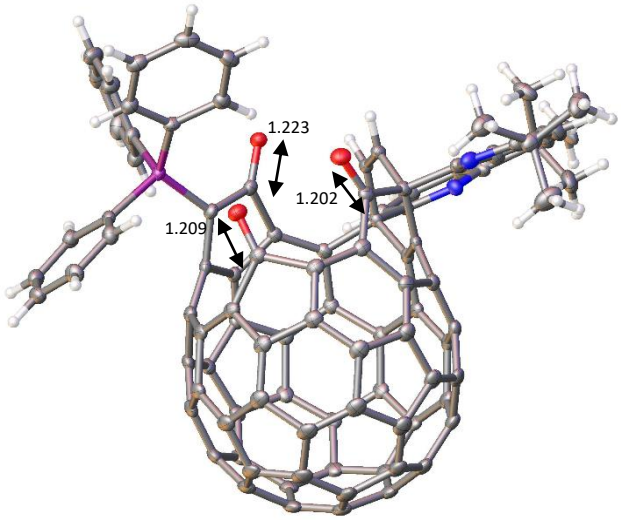


**Figure 16**. Crystal structure of compound **88**.

The reported conditions were used to synthesise the compound **88**. The reaction was scaled up and despite leaving it for longer time the isolated yield was high (between 85-96%) suggesting a good stability of the process. The prolonged conditions were adapted for convenience and compound **88** was prepared on scale up to 5.3 grams (**Table 18**).

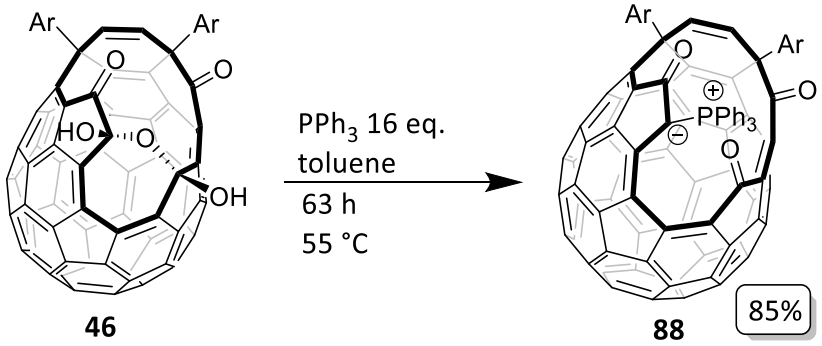


**46** **88**

**Scheme 56.** Synthesis of compound **88**.

| Entry | Scale | Temperature | Time | Yield |
|---|---|---|---|---|
| **Reported**[108] | 0.05 g | 60 °C | 24 h | 86% |
| **1** | 1.5 g | 60 °C | 50 h | 89% |
| **2** | 1.4 g | 50 °C | 62 h | 96% |
| **3** | 5.3 g | 55 °C | 63 h | 85% |

**Table 18.** Synthesis of compound **88**.

Kinetics of the intramolecular Wittig reaction were studied to find the most suitable conditions for the proposed experiment and to better understand the reaction. The measurements were performed in solid state as the filling of **88** with small atom or molecule was planned to be done in solid state as well. OCFs have been filled in the solid state before (**1.4.1**), but this would be the first case where the ring contraction occurs in situ with the filling which comes with advantages such as:

- The volume of the pressure reactor can be small, allowing safer manipulation with high pressures.
- The volume of gas needed to achieve the desired pressure can be smaller – particularly useful when using expensive gas.

Sample of **88** was placed in an NMR tube flushed with $N_2$ gas and immersed into a metal heating block preheated to a desired temperature. After allocated time the sample was cooled to room temperature and dissolved in NMR solvent and analysed by $^1$H NMR. The conversion was calculated by integration of the *tert*-butyl peaks of the **43** and **88**. The results obtained from the kinetic study did not show a first order reaction trend. **Figure 18** shows the first order plot in which the lines would be expected to be linear if the reaction proceeded according to the first order reaction rate law. The temperatures 130 °C and 140 °C show change in conversion rate after about 60% conversion is achieved. It is possible that the present polar by-product triphenylphosphine oxide catalyses the intramolecular reaction.

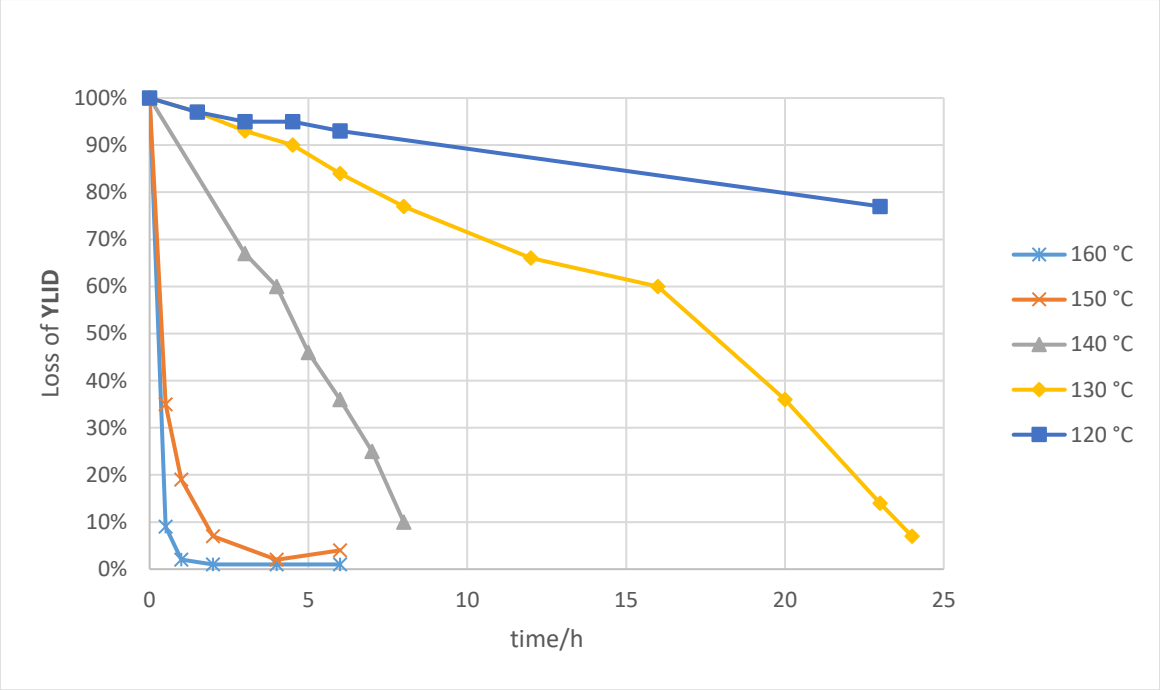


**Figure 17.** Loss of the **88** converting to **43** at different temperatures.

At the end of reaction of 150 °C the collected data suggested that a reversible reaction occurs, but no further evidence to support this was obtained.

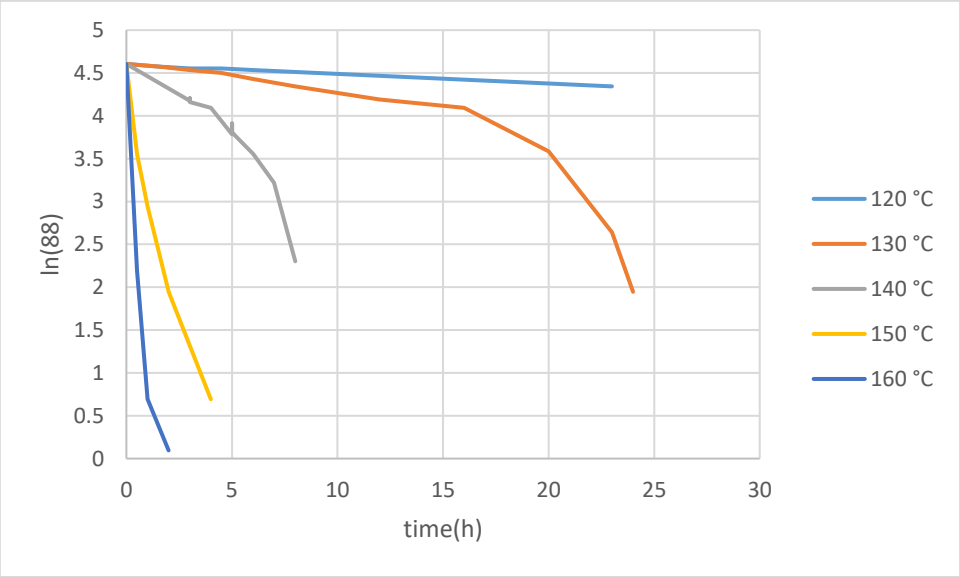


**Figure 18.** Kinetics plot showing natural logarithm of loss of the starting material **88** over time

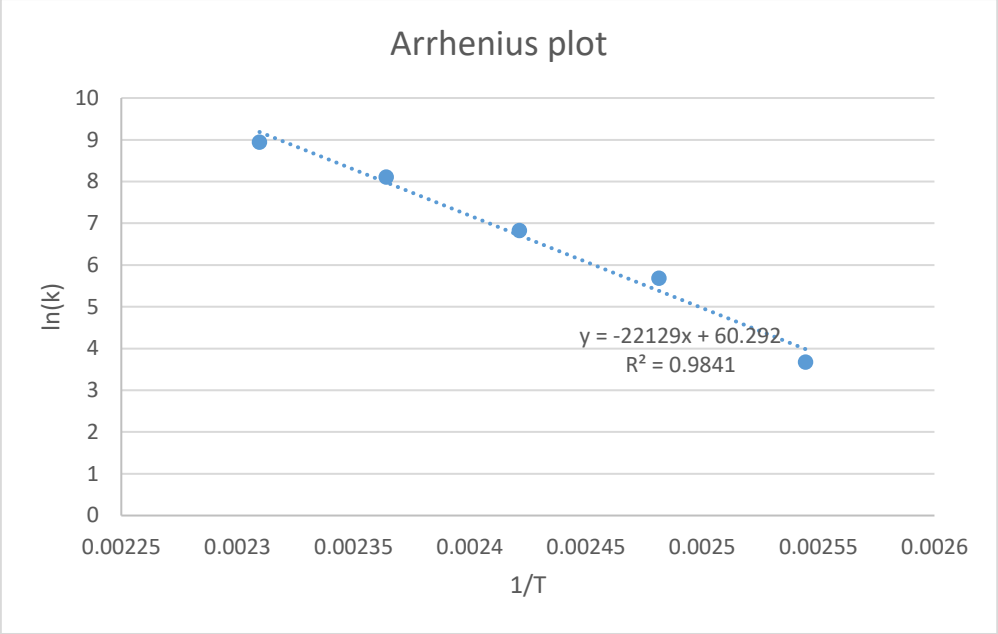


**Figure 19.** Arrhenius plot for the calculation of the activation energy of formation of **43** from **88**.

It was reported that **88** converts to **43** upon heating to 100 °C.[155] **88** was heated in toluene-$d_8$ and in solid state at 110 °C and showed that after 2 hours the conversions to **43** were 23% and 4% respectively showing a significant decrease in the conversion rate in the solid state in comparison with the heating in solution. The most likely explanation is that there are strong interactions in the crystal state of the **88** that inhibit the conversion to **43** as the crystal **88** has to undergo a substantial change. Samples heated to 160 °C were observed to be molten after removed from the heating block. At higher temperature (160 °C) the by-product triphenylphosphine oxide could be molten (b.p. 154-158 °C) and the reaction is more likely to proceed as if it was in solution. From the experimental data the activation energy is 183 kJ.mol$^{-1}$ and the calculated energy was 130 kJ.mol$^{-1}$.

It was concluded that the temperatures needed for the **88** closure in solid state should be between 140–160 °C.

## 4.2 Encapsulation of $^4$He and $^3$He

To perform a solid-state filling of **88**, purpose-built filling apparatus was constructed[w] with reaction volumes between 1.2–5 mL and pressure ratings between 2400–4000 atm (**Figure 20**).

[w] Designed and constructed by prof. R.J.Whitby

4. Optimised large scale synthesis of $He@C_{60}$ and $H_2@C_{60}$ and novel $Ne@C_{60}$

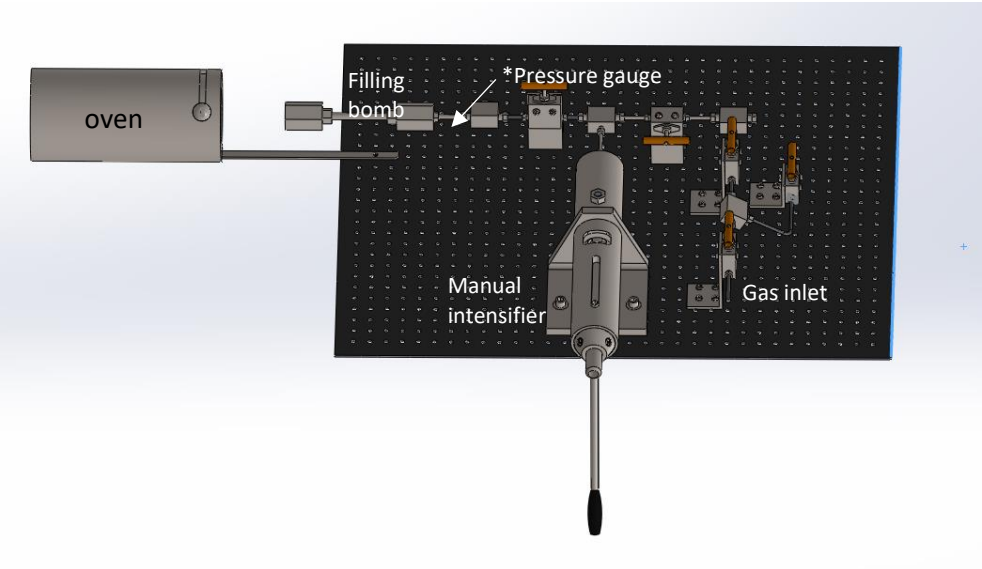


**Figure 20**. Purpose-built high-pressure apparatus.

*Pressure gauge was installed right before the filling bomb (arrow).

The gas is let into the apparatus through the inlet and compressed in the manual intensifier (syringe) into the filling bomb. Initially, due to the dead volumes in the metal tubing and the syringe (around 5 ml) the compression ratio was only around 7:1. First optimisation reactions were performed with $^4He$ and the results are shown in **Table 19**.

| Entry | T/°C | Time | Pressure | Yield | f.f. |
|---|---|---|---|---|---|
| **1** | 140 | 15h | 500 atm | 90% | 16% |
| **2** | 140 | 18h | 783 atm | 77% | 30% |

**Table 19**. First tests of in-situ formation of **$^4He@43$**.

Preliminary achievements of the filling were determined by low resolution mass spectrometry (LRMS ESI+) comparing the intensity of the peaks of the empty and filled compound **43** (**Figure 21**).

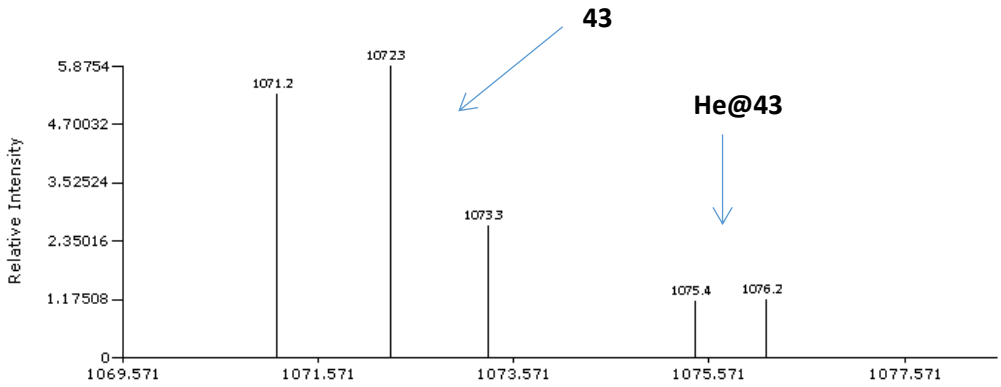


**Figure 21.** MS spectrum (x axis = m/z) of the compound **43** and **He@43**.

Filling factors were then confirmed by high resolution mass spectrometry (HRMS APPI and ESI+) and by $^{13}C$ NMR of the final He@$C_{60}$. The $E_{in}$ of He into **88** and the $E_{esc}$ was calculated to be 39 KJ.mol$^{-1}$ and 49.4 Kj.mol$^{-1}$ respectively[190]. Initially our intensifier had a pressure limit of 1000 atm and the filling factors achieved were ~30%. The filling factor was increased to 40% by cooling the filling bomb to -196 °C by liquid nitrogen bath before compressing to ~1000 atm which upon warming up and heating to 160 °C reached the pressure of 1669 atm. Our pressure apparatus was later equipped with a new intensifier (Sitec) with pressure limit of 4000 atm and a reduced internal dead volume of around 1.7 mL (increasing the theoretical compression ratio to 18:1) as well as inserting 1.5 mm o.d. stainless steel rod into the tubing. We were then able to achieve pressure of 2374 atm and filling factor of 50% for the **He@43**. In synthesis of $^{3}$He@C60 our $^{3}$He cylinder was at initial pressure of 41 atm and due to the dead volumes in the apparatus the pressure reached was only 187 atm resulting in a filling factor of 3%. After improving our equipment and introducing cryogenic filling the apparatus achieved compression from the initial pressure of 107 atm to 1933 atm and **$^{3}$He@43** was prepared in 44% filling factor. (**Table 20**).

| Entry | Gas | Temp. | Time | Pressure | Yield | Filling [a)] |
|---|---|---|---|---|---|---|
| **1** | $^{4}$He | 140 °C | 14 h | 968 atm | 77% | 30% |
| **2** | $^{4}$He | 160 °C | 2,5 h | 981 atm | 80% | 21% |
| **3** | $^{4}$He | 160 °C | 3 h | 978 atm | 89% | 26% |
| **4** | $^{4}$He | 160 °C | 2,5 h | 964 atm | 76% | 33% |
| **5** | $^{4}$He | 160 °C | 2 h | 816 atm | 86% | 20% |
| **6** | $^{3}$He | 160 °C | 3 h | 187 atm | 70% | 3.5% |
| **7** | $^{3}$He | 160 °C | 3 h | 134 atm | 67% | 3.7% |
| **8** | $^{4}$He | 160 °C | 14 h | 1669 atm | 87% | 40% |
| **9** | $^{4}$He | 170 °C | 2 h | 2374 atm | 77% | 50% |
| **10** | $^{3}$He | 178 °C | 1 h | 1933 atm | 80% | 44% |

a) He fillings were determined by LRMS and is not exact. Accurate fillings were determined from final He@$C_{60}$ compounds by 13C NMR and HRMS (APPI).

**Table 20**. Syntheses of **He@43**.

The **He@43** prepared were then sutured to **He@$C_{60}$** using the known closure procedure that consists of ring reduction to **He@42** by refluxing with P$^{i}$(OPr)$_3$[155] in toluene followed by modified procedure of the final closure with *N*-phenylmaleimide in 1-chloronaphthalene (in **Chapter 3. Closure of 42 to C60**). The development of the closure method was ongoing while optimising the synthesis of He@$C_{60}$ therefore the yields for before the reliable procedure was established were lower (25-35%) and after the optimisation the yield was 50% (**Scheme 57**). The usual yields and scales are summarised in **Table 21** and **Table 22**.

4. Optimised large scale synthesis of He@$C_{60}$ and $H_2$@$C_{60}$ and novel Ne@$C_{60}$

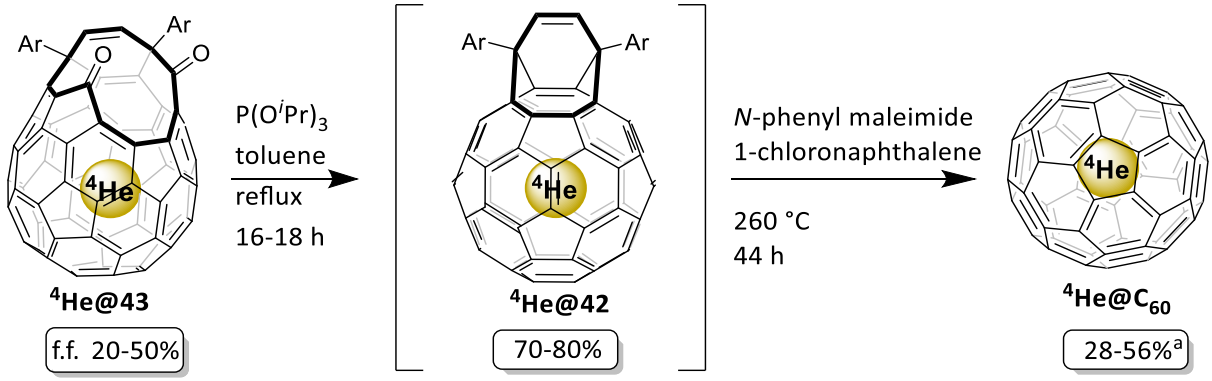


**Scheme 57.** Closure of **He@43** to **He@$C_{60}$**.
a) Yields calculated after purification on HPLC.

| Entry | He | f.f. | He@42 yield |
|---|---|---|---|
| **1** | $^4$He | 21% | 65% |
| **2** | | 32% | 70% |
| **3** | | 30% | 80% |
| **4** | | 40% | 70% |
| **5** | | | 71% |
| **6** | | | 72% |
| **7** | | | 75% |
| **8** | $^3$He | 3.5% | 74% |
| **9** | | 3.5% | 86% |
| **10** | | 44% | 70% |

**Table 21.** Synthesis of **He@42**.

During the course of the development, it was observed that the compound **42** is not stable for storage due to its high sensitivity to oxygen and it is necessary to use it straight after the purification step.

| Entry | He | f.f. | He@$C_{60}$ yield[a] | Scale/g |
|---|---|---|---|---|
| **1** | $^4$He | 21% | 28% | 0.122 |
| **2** | | 32% | 63% | 0.074 |
| **3** | | 30% | 62% | 0.090 |
| **4** | | 40% | 36% | 0.110 |
| **5** | | | 52% | 0.143 |
| **6** | | | 56% | 0.154 |
| **7** | | 50% | 50% | 0.202 |
| **8** | $^3$He | 3.5% | 28% | 0.130 |
| **9** | | 3.5% | 36% | 0.150 |
| **10** | | 44% | 33% | 0.098 |

**Table 22.** Synthesis of **He@$C_{60}$**.
a) Yields of $C_{60}$ were calculated from the **42** except for the entries **7** and **10** which were calculated from the **He@43**.

As the syntheses of the **A@43** from **88** are performed in temperatures higher than 100 °C which is sufficient for activation of $H_2O$ entry, some unwanted $H_2O$ enters the cavity and a very small percentage (estimated 0.01%) of $H_2O$ is encapsulated alongside the He. Despite attempts to eliminate

$H_2O$ by evacuating the filling bomb **88** for at least 30 minutes before the compression the presence of **$H_2O@C_{60}$** was discovered in the **$He@C_{60}$** sample during the first neutron scattering experiments where the **$H_2O@C_{60}$** (f.f. 0.1%) signal was of similar intensity as the **$^4He@C_{60}$** (24%) due to much higher scattering cross-section of the $H_2O$. This has caused even bigger problem in the sample of **$^3He@C_{60}$** (3.5%) where the signals were of almost the same intensity (f.f. **$H_2O@C_{60}$** 0.2%).

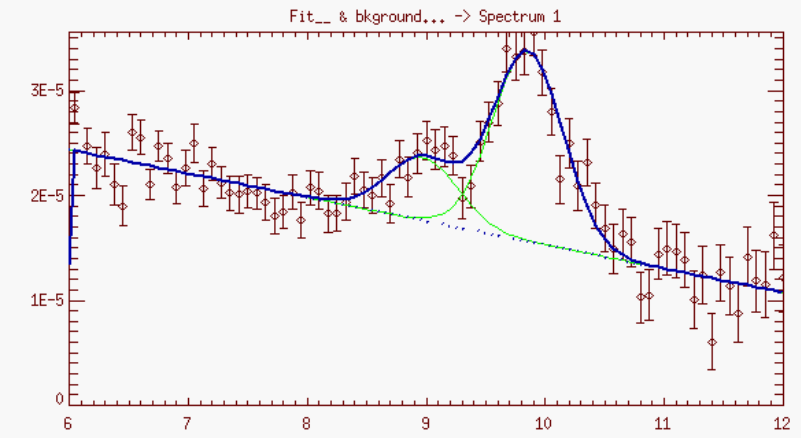


**Figure 22.** Inelastic Neutron Scattering spectra of **$^4He@C_{60}$** (x-axis is meV).

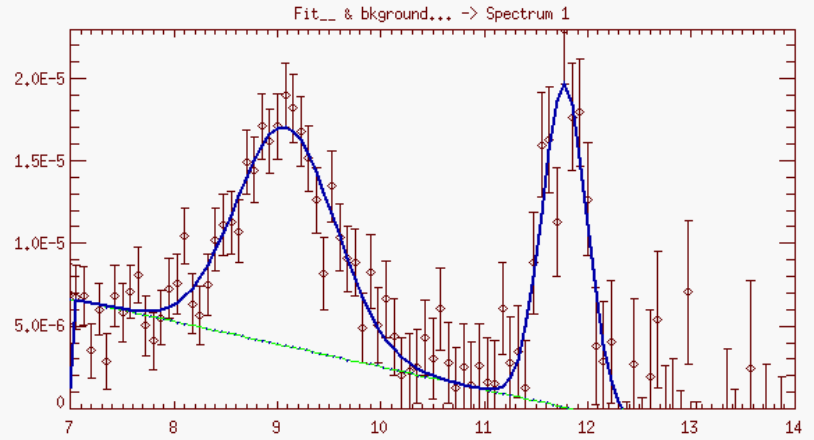


**Figure 23.** Inelastic Neutron Scattering spectra of **$^3He@C_{60}$** (x axis is meV).

Experiments were performed at Institute of Laue Langevin (ILL) at neutron wavelength of 2.2 Å, temperature of 1.6 K and the measuring time was 40 hours. The results (**Figure 22** and **Figure 23**) show the energy difference between transitions to the first translational excited state of $^4He$ (9.85 meV) and $^3He$ (11.77 meV) inside $C_{60}$. Peak at the 9 meV belongs to **$H_2O@C_{60}$**[191].[x] The percentage of **$H_2O@C_{60}$** in

[x] Experiments in ILL were done in collaboration with prof. Anthony Horsewill, George Bacanu and Dr Stephane Rolls

the $He@C_{60}$ samples was then determined by $^{13}C$ NMR on the high resolution 700 MHz spectrometer using >10000 scans.[y]

The **$H_2O@C_{60}$** can be removed from the **$He@C_{60}$** samples by preparative HPLC using the Cosmosil Buckyprep™ column. As the concentration of the **$H_2O@C_{60}$** was very small the peak was only visible after extensive zoom. The usual purification method of **$He@C_{60}$** consisted of 6 cycles (or three cycles of two columns in series). The separation pattern of **$H_2O@C_{60}$** in 100% toluene 1 ml.min$^{-1}$ is well known (**Figure 24**). The 30% filled $H_2O@C_{60}$ was left recycling for 20 cycles (usually collected after 3-5 cycles) to observe the separation pattern.

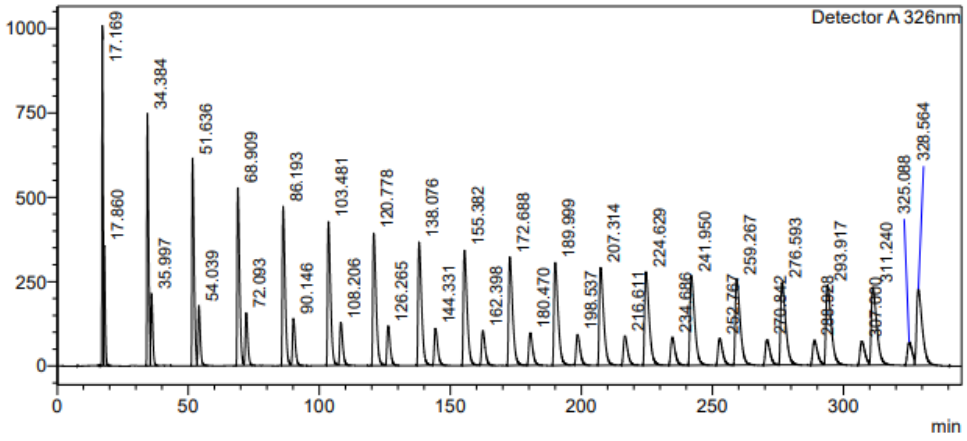


**Figure 24.** Separation of the $H_2O@C_{60}$ from $C_{60}$ on Cosmosil Buckyprep™ column after 1-20 cycles.

[y] Performed by George Bacanu

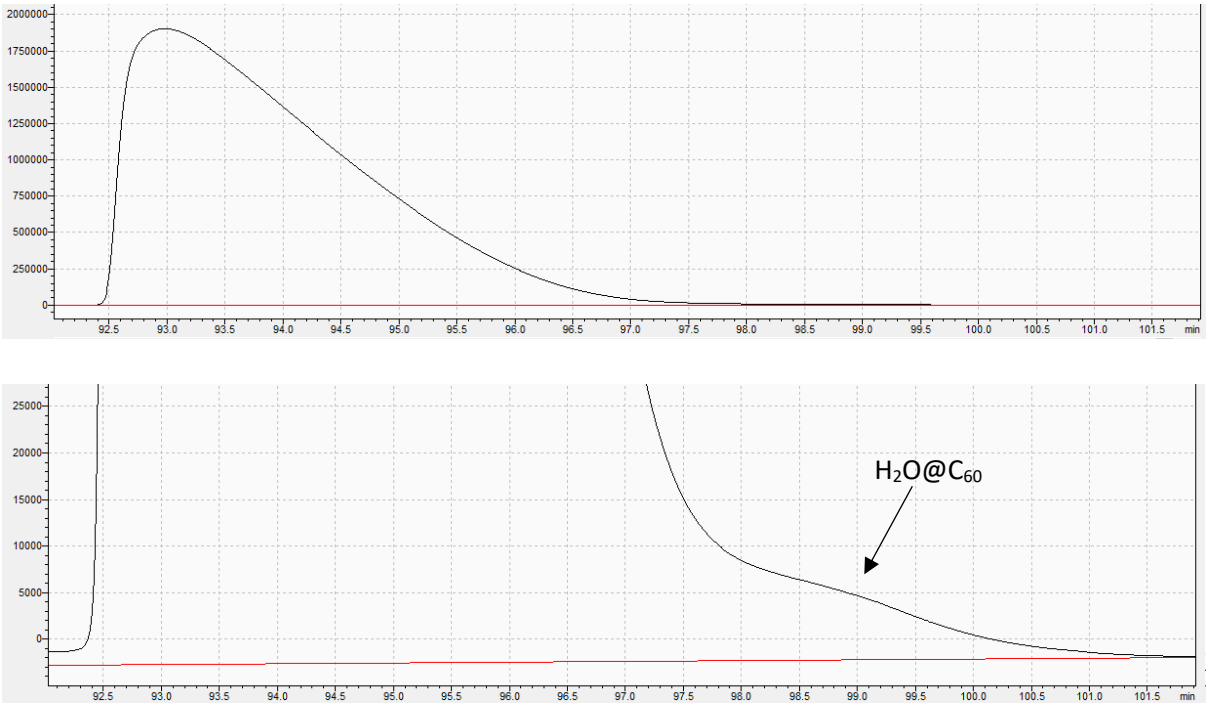


**Figure 25.** Separation of **$H_2O@C_{60}$** from **$He@C_{60}$** (50% f.f.) sample after 3 cycles (two columns in series).

**$He@C_{60}$** shows no visible separation from **$C_{60}$** after 6 cycles in 100%. It was reported that **$He@C_{60}$** starts showing separation from **$C_{60}$** after 20 cycles and good separation is observed after 40 cycles.[153] Disadvantage of the recycling HPLC when great number of cycles is used is the broadening of the peaks because the separation becomes difficult. Six passes of the **$He@C_{60}$** sample through the column is enough for separation from **$H_2O@C_{60}$** before the broadening becomes a serious issue. The sample is collected for up to ~96 minutes and the sample enriched with **$H_2O@C_{60}$** is collected separately and injected into the system again for maximum recovery of **$He@C_{60}$**.

After the **$He@C_{60}$** sample was purified by HPLC, it was then sublimed to achieve maximum purity. The usual sublimation yield was 80-90%. The sublimation was performed on combined batches and done on scale up to ~1 g, at $10^{-6}$ Torr at 550 °C during 12-15 hours.

Samples of **$He@C_{60}$** prepared in this project were used in NMR spectroscopy studies of **$A@C_{60}$** such as an internuclear J-Coupling of $^3$He in **$^3He@C_{60}$**[192], spectroscopy of **$^+He@C_{60}$** for astrochemical detection[17], neutron scattering and cryogenic IR/THz spectroscopy investigations of **$He@C_{60}$**.

## 4.3 Encapsulation of $H_2$, HD and $D_2$

Synthesis of **$H_2@C_{60}$** has been published[185] and optimised[155] and **$H_2@C_{60}$** became of high interest for many spectroscopic studies. A symmetry lacking isotopologue **$HD@C_{60}$** was prepared before as a

mixture with **$H_2@C_{60}$** and **$D_2@C_{60}$** and the INS spectra was acquired.[193] Larger quantities of pure **$HD@C_{60}$** are needed for the INS experiments to confirm detailed predictions of the variable temperature INS spectra.[194] Using the optimised synthesis method of simultaneous ring contraction of **88** and filling is ideal for these purposes overcoming difficulties mentioned in **4.1.** Calculated binding energy of hydrogen molecule is -21 $kJ.mol^{-1}$ which is double that the $E_{bin}$ of the He into the cavity of **88.**[190] This is reflected on higher incorporation levels achieved by significantly lower pressure than for **He@43** synthesis.

| Entry | A | temperature | Time | Pressure | Yield | Filling |
|---|---|---|---|---|---|---|
| **1** | HD | 160 °C | 3 h | 161 atm | 85% | 50% |
| **2** | HD | 160 °C | 3 h | 222 atm | 71% | 57% |
| **3** | HD | 160 °C | 2h | 82 atm | 74% | 44% |
| **4** | $D_2$ | 160 °C | 2h | 95 atm | 75% | 45% |
| **5** | $D_2$ | 176 °C | 1.4 h | 314 atm | 72% | 73% |
| **6** | $H_2$ | 160 °C | 2 h | 398 atm | 88% | 80% |
| **7** | $H_2$ | 160 °C | 2 h | 778 atm | 85% | 88% |
| **8** | $H_2$ | 186 °C | 45 min | 1392 atm | 80% | 95% |

**Table 23.** Syntheses of **$H_2@43$** and isotopes

In our research group[z], higher pressures of HD gas were achieved by using the optimised cryogenic filling method (**4.2**). After heating to 140 °C under 520 atm for 14 hours, the filling factor achieved was 83% and 75% yield. Disproportionation of HD to H2+D2 was a concern as this is known to occur in contact with iron and our apparatus is made of stainless steel.[195] Using the conditions above less than 1% of disproportioned $H_2$ was observed. When this experiment was performed at pressure of 800 atm and 180 °C the observed disproportion was 35%.[190]

Prepared **$H_2@43$** batches were then closed to **$H_2@C_{60}$** by the same procedures as the **$He@C_{60}$** (**Scheme 58**). The yields of the procedures were consistent with the ones for the **$He@C_{60}$** and are summarised in **Table 24**. The **$HD@C_{60}$** yield is lower as it was done before the optimisation of the final closure step.

[z] Experiments performed by Mark Walkey

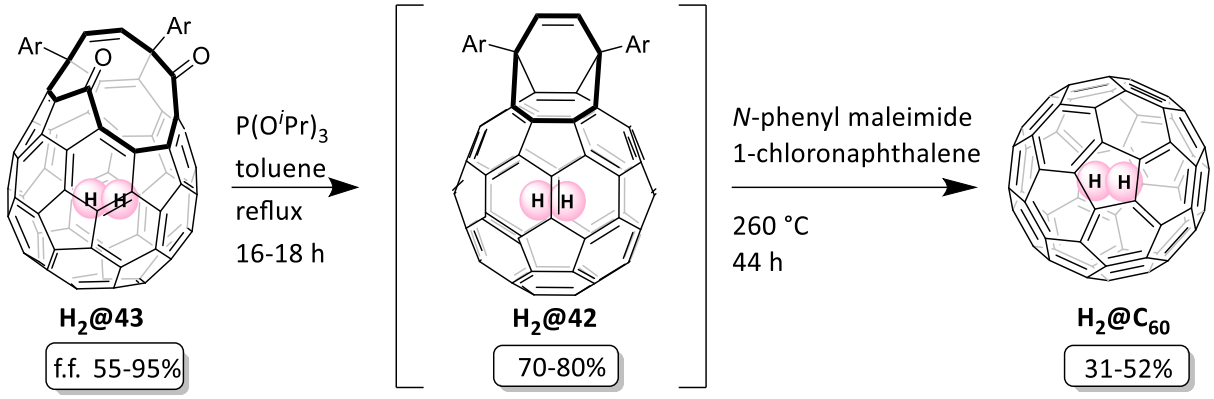


**Scheme 58.** Synthesis of **$H_2$@$C_{60}$**.

| Entry | $H_2$ | f.f. | $H_2$@$C_{60}$ yield[a] | Scale/g |
|---|---|---|---|---|
| **1** | $H_2$ | 93% | 52% | 0.122 |
| **2** | $D_2$ | 73% | 49% | 0.166 |
| **3** | HD | 55% | 31% | 0.120 |

**Table 24.** Synthesis of **$H_2$@$C_{60}$**.
a) All yields calculated from the **$H_2$@43** after purification on HPLC.

Samples of **$H_2$@$C_{60}$** prepared in this project were used for various spectroscopic studies of which to date published in the study of Fine structure in the solution state $^{13}$C-NMR spectrum of $C_{60}$ and its endofullerene derivatives by George Bacanu.[196]

## 4.4 Synthesis of Ne@$C_{60}$

### 4.4.1 Synthesis of Ne@$C_{60}$ by molecular surgery for the first time

Neon and other noble gasses inside $C_{60}$ were previously prepared by methods using extreme conditions. In 1994 the noble gasses were incorporated into $C_{60}$ by putting in high pressure and temperature. **Ne@$C_{60}$** was prepared in 0.1% filling factor, using 2500 atm at 620 °C.[96][197]

The first preparation of **Ne@$C_{60}$** by molecular surgery started by filling into the OCF **45.** DFT calculations predicted that the $E_{in}$ into the **45** is 52.8 kJ.mol$^{-1}$ and $E_{esc}$ 72.9 kJ.mol$^{-1}$ with binding energy -20.1 kJ.mol$^{-1}$. These energies are similar to those of $H_2$ ($E_{in}$ = 50.6 kJ.mol$^{-1}$, $E_{esc}$ = 72.9 kJ.mol$^{-1}$, $E_{bin}$ = -22.3) therefore it was expected that the Ne filling would proceed similarly as the $H_2$ filling of **45**.

4. Optimised large scale synthesis of He@$C_{60}$ and $H_2$@$C_{60}$ and novel Ne@$C_{60}$

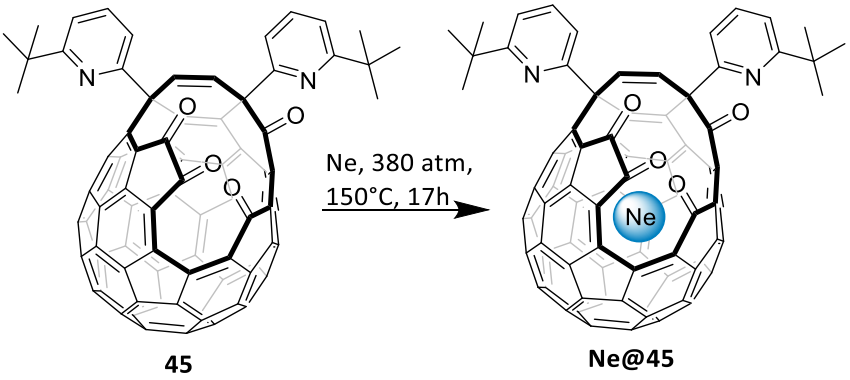


**Scheme 59.** Neon filling into solid compound **45**.

The first filling of **45** with Neon gas was done at 380 atm at 150 °C for 17 hours. The mass spectrometry (ESI+) suggested filling ~16%. NMR also showed presence of endohedral water, ~10%. When **45** was prepared directly in the filling apparatus by leaving under vacuum (0.2 mm/Hg) at 140 °C for 20 hours, and the filling with Neon gas was done by using same the conditions, water incorporation dropped to 3%.

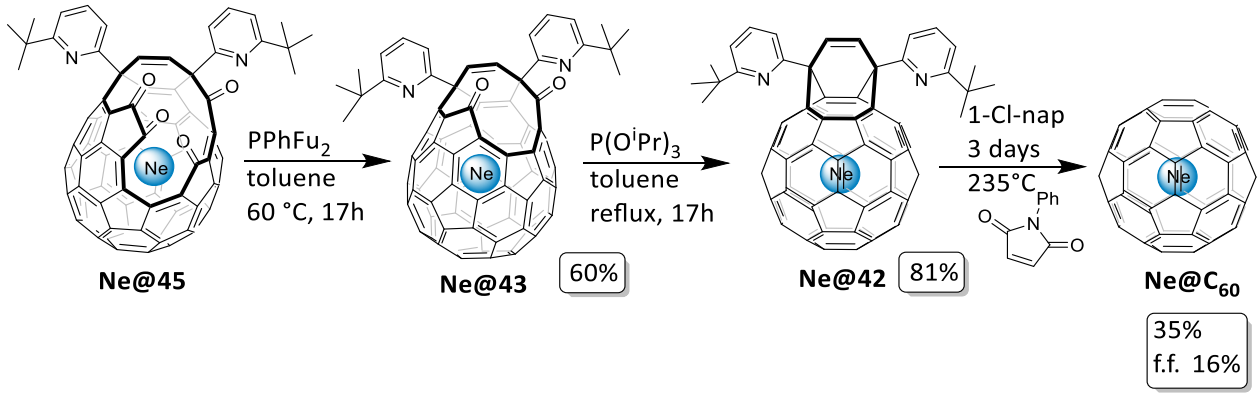


**Scheme 60.** Synthesis of **Ne@$C_{60}$**.

Similarly to $H_2$, when **Ne@45** was closed with $PPh_3$ at 120 °C, complete loss of Neon occurred which is confirmed by the similar activation and binding energies of $H_2$ and Ne. When closure of **45** performed at 60 °C using $PPhFu_2$, product **Ne@43** was prepared with retention of Neon. **Ne@42** was synthesised by the known method using $P(O^iPr)_3$ and refluxing in toluene over 17 hours. **Ne@42** was then converted to **Ne@$C_{60}$** testing conditions with temperature and longer reaction time (235 °C, 72 hours) in order to supress formation of the **Ne@92** (**Scheme 60**). The formation of the **Ne@92** was avoided but the isolated yield was only 35% probably due to decomposition because of the prolonged reaction time. The filling was determined by $^{13}$C NMR and HRMS of the final **Ne@$C_{60}$** and confirmed to be 16% with 3% of **$H_2$O@$C_{60}$**.

### 4.4.2 Synthesis of Ne@$C_{60}$ via intramolecular Wittig reaction

Calculated energies for the Ne $E_{in}$ = 64.6 kJ.mol$^{-1}$ and $E_{esc}$ = 83.8 kJ.mol$^{-1}$ into the **88** were compared with those of $H_2$ (**4.3**) and noted that the Ne $E_{in}$ is only 4 kJ.mol$^{-1}$ higher and only 12 kJ.mol$^{-1}$ higher than Ne entry to **45** (52.8 kJ.mol$^{-1}$). When **88** compressed with Ne to 600 atm at 160 °C, **Ne@43** was obtained in 70% yield with 25% filling factor. When the binding energies of $H_2$ (-21.0 kJ.mol$^{-1}$) and Ne (19.2 kJ.mol$^{-1}$) to the **88** cavity were compared, it was expected to achieve higher filling factor. It is possible that due to the higher $E_{in}$ of Neon a higher temperature is needed which would cause faster contraction of the **88** and therefore the filling factor would not increase. Filling factors up to 70% were achieved using the compression described in **4.2** combined with cryogenic cooling reaching the pressures up to 2176 atm when heated (**Table 25**).

| Entry | temperature | Time | Pressure | Yield | Filling |
|---|---|---|---|---|---|
| **1** | 160 °C | 2h | 600 | 70% | 25% |
| **2** | 160 °C | 17h | 2176 | 70% | 70% |
| **3** | 160 °C | 15h | 2033 | 78% | 68% |
| **4** | 160 °C | 2.5h | 1742 | 84% | 63% |

**Table 25**. Syntheses of **Ne@43**.

**Ne@$C_{60}$** was then prepared by the known methods and the yields were consistent with the yields obtained in syntheses of **$H_2$@$C_{60}$** and **He@$C_{60}$** (**Scheme 61**).

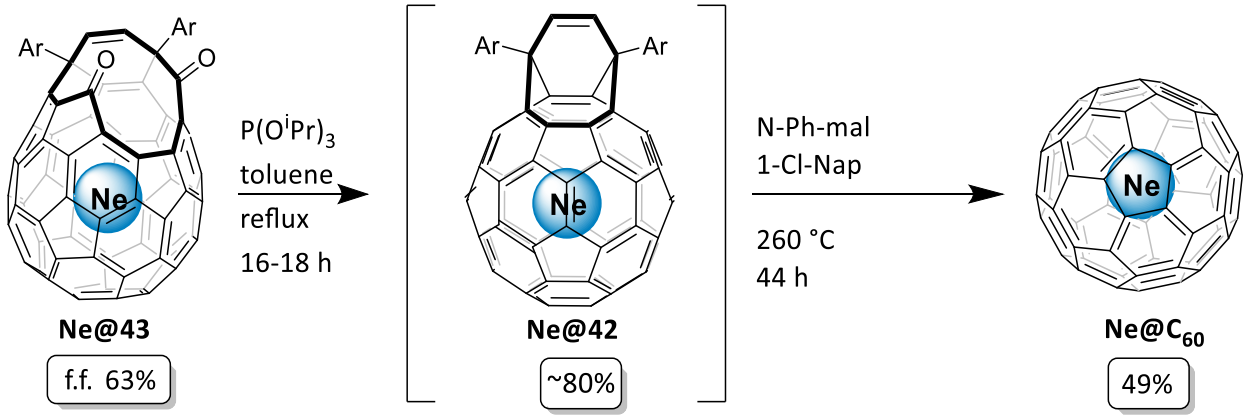


**Scheme 61.** Synthesis of **Ne@$C_{60}$**. Yield for Ne@$C_{60}$ is calculated from **Ne@43** after HPLC purification.

Similar to the **He@$C_{60}$**, the **$H_2$O@$C_{60}$** was separated from the **Ne@$C_{60}$** on the recycling HPLC using the same conditions as for the **He@$C_{60}$**. The 70% **Ne@$C_{60}$** was then enriched to >99% by recycling HPLC (Two Cosmosil Buckyprep™ in series, 100% toluene, 20 cycles, 631 minutes).

4. Optimised large scale synthesis of $He@C_{60}$ and $H_2@C_{60}$ and novel $Ne@C_{60}$

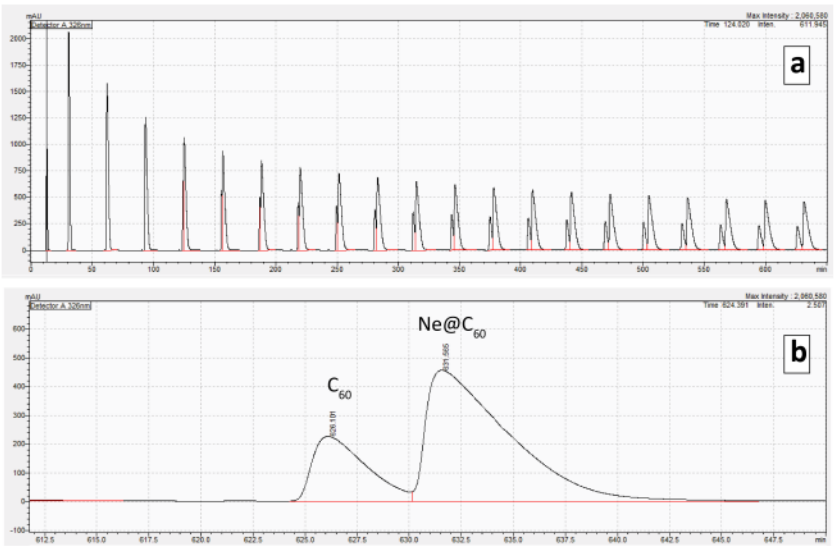


a) Chromatogram of the recycled $Ne@C_{60}$. b) Detailed zoom on the separation of $Ne@C_{60}$ from empty $C_{60}$.

**Figure 26.** Enrichment of the **$Ne@C_{60}$** to >99%.

Crystal structure was obtained of the >99% **$Ne@C_{60}$** nickel(II) porphyrin/benzene solvate (**Figure 27**).[198]

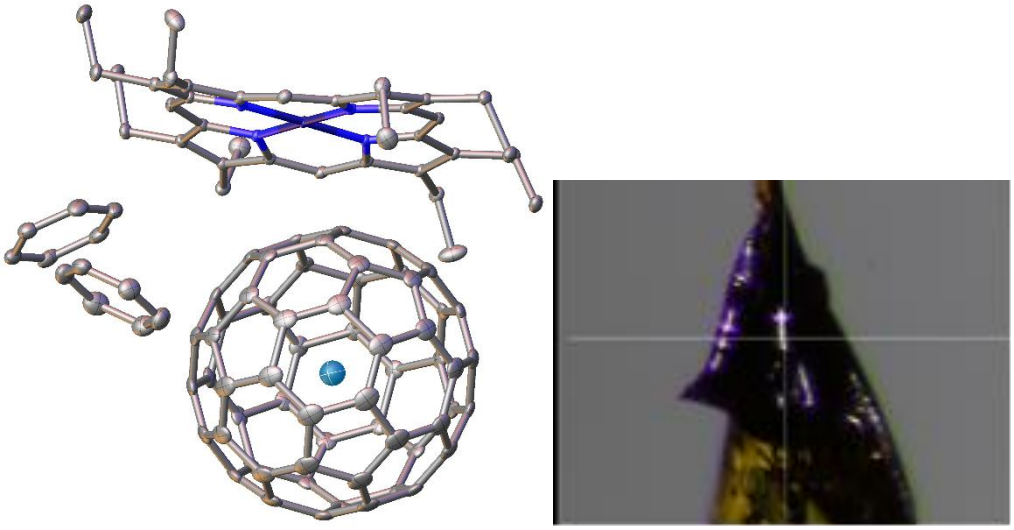

**Figure 27.** Crystal structure of the **$Ne@C_{60}$** (Left). Photo of the crystal on the diffractometer (Right).

## 4.5 Summary

Syntheses of the known **$He@C_{60}$** and **$H_2@C_{60}$** and their isotopomers were optimised and synthesis of the **$Ne@C_{60}$** presented by improving the filling step using intramolecular Wittig reaction to perform *in situ* closure of **88**. This method potentially allows synthesis **$A@C_{60}$** on multigram scale, reduced safety hazards resulting from operations with high pressures, and decreased number of synthetic steps. The

results achieved in this optimisation are compared with the reported results and presented in **Table 26**.

| **A@$C_{60}$[ref]** | **Filling conditions** | | | | **Solid/solution** | **Filling factor** | **Scale[a]** | **Yield[b]** |
|---|---|---|---|---|---|---|---|---|
| | OCF | Pressure | Temp. | Time | | | | |
| **$H_2$@$C_{60}$**[106] | **31** | 800 atm | 200 °C | 8 h | Solid | 91% | 118 mg | 22% |
| **$H_2$@$C_{60}$**[155] | **45** | 120 atm | 120 °C | 20 h | toluene | 60% | 68 mg | 50% |
| **$H_2$@$C_{60}$** | **88** | 1806 atm | 186 °C | 2 h | solid | 93% | 122 mg | 52% |
| **He@$C_{60}$**[186] | **31** | 1230 atm | 115 °C | 1 h | Solid | 30% | 38 mg | 13% |
| **He@$C_{60}$** | **88** | 2374 atm | 160 °C | 2 h | solid | 50% | 142 mg | 50% |
| **Ne@$C_{60}$** | **88** | 1742 atm | 160 °C | 2 h | solid | 70% | 115 mg | 44% |

**Table 26**. Results compared with the reported procedures for syntheses of A@$C_{60}$.
a) Mass of recovered A@$C_{60}$. b) Yield calculated from the steps after the filling reaction.

Results from this chapter are published in: https://doi.org/10.1002/anie.202100817.

# 5 Optimisation of closure of A@89 to A@46

The synthetic route from **A@46** (A = endohedral atom or molecule) has been established[180] (**1.5.3**), therefore the remaining challenge for synthesis of novel fullerenes (such as $O_2@C_{60}$, $NO@C_{60}$, $Kr@C_{60}$, $N_2@C_{60}$ or $CO@C_{60}$) is the partial closure step of **A@89** to **A@46**. No suitable method to encapsulate $O_2$ or NO was found yet, however a deeper insight of this process was gained, and minor improvements achieved. This chapter will discuss experiments and improvement trials to synthesis of **A@46** from **A@89** by testing custom-made experimental set-up and investigating effects of parameters such as reaction time, temperature, solvent system, additives, acid, and irradiation source. A new by-product **99** arising from **45** was discovered, isolated and characterised, which gave an insight into the decomposition mechanism.

## 5.1 Partial closure of empty 89 to 46

In the recently published synthesis of **$CH_4@C_{60}$**, partial closure of compound **89** to **46** was achieved for the first time and allowed the first synthesis of **$CH_4@C_{60}$** discussed in **1.5.5**.[180] The main challenge of the partial closure was trapping the compound **45** which was shown to be unstable to visible light probably due to presence of 1,2-dicarbonyl moiety. The solution to this problem was trapping the **45** *in situ* by introducing 10% v/v aqueous acetic acid together with combination of solvents MeCN and toluene. Using empty **89** and **$H_2O@89$** yielded in 40% of **46/$H_2O$@46** however ~99% filled **$CH_4@89$** yielded in only 10% confirming that the endohedral molecule has an impact on the reactivity of the OCF. When the photochemical ring contraction was performed with 100% filled **Ar@89**, the isolated yield of **Ar@46** was 26% suggesting that the ring contraction process is less inhibited by the smaller endohedral species.[184]

According to the published procedure, the reaction was performed in round bottom flask using 11W or 40W Na lamp in 1 cm proximity from the reaction mixture.[180][184] It was discovered that the energy from the lamp can heat up the reaction up to 50 °C. Due to non-homogenous solvent system, the reaction requires vigorous stirring. To achieve maximum irradiation, the light should be ideally placed in the middle of the stirring solution. For the purposes of inserting atoms and molecules with low binding energy (such as $O_2$ or NO (**Table 14**)), the closure of **89** would have to be done below room temperature. For that reason, a purpose-built jacket reactor flask (**Figure 28**) was used in optimisation reactions. The jacket can be utilised for cooling or heating to desired temperature. The flask has a space in the middle so the irradiation source can be placed at close proximity to the reaction mixture.

Ultimately, usage of this reactor allows better control over the parameters that are temperature, distance of the irradiation source and stirring thanks to the cross shaped magnetic stirrer. The disadvantages of the reactor are that the reaction is limited to volume of ~200 mL and that the Na lamp used in the reported synthesis of **$CH_4$@46** does not fit in the middle compartment.

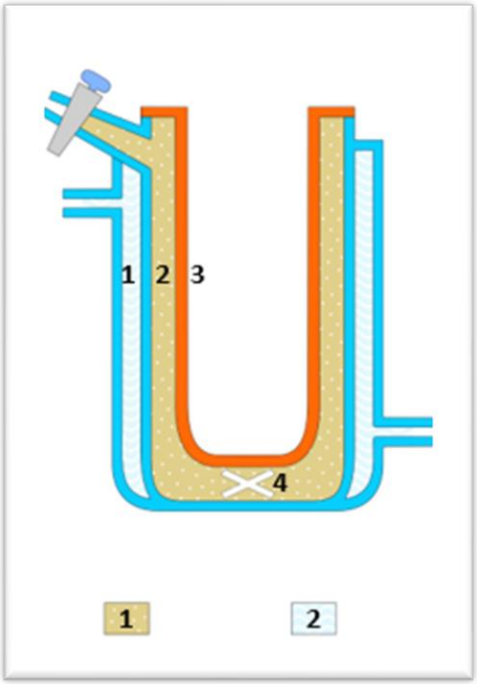


**Figure 28**. The purpose-built photo reactor (**1 –** outer jacker for heating liquid, **2 –** reaction mixture, **3 –** room for the irradiating lamp, **4 –** cross shaped stirrer bar).

### 5.1.1 Optimisation with empty/naturally $H_2O$ filled OCF 89

The purpose of these experiments was to find suitable conditions for the reaction to proceed in the purpose-built reactor (PBR).

The initial screening was done to explore the reaction at different temperatures and wavelengths of the irradiation source. Reactions were done on empty/naturally water-filled compound **89 (Scheme 62).**

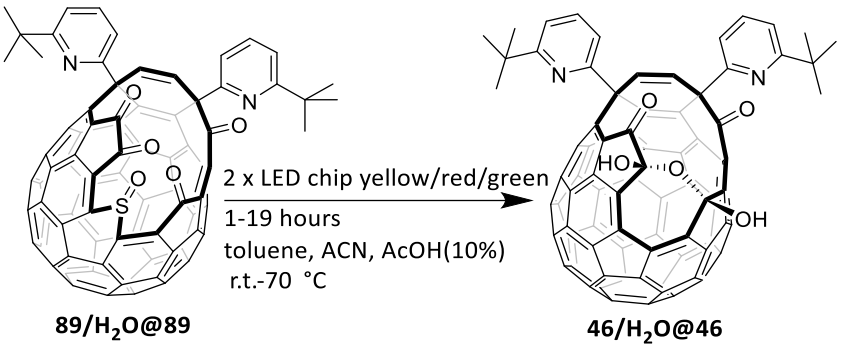


**Scheme 62.** Partial closure of **89** to **46**.

The results of the screening experiments presented in **Table 27** show percentage proportion of the product in the crude mixture calculated by NMR. The best result was observed with the Yellow and Red light at 50 °C and Yellow at 25 °C after 19 hours. When the reaction was done at 70 °C, greater number of by-products was formed after 2 hours, which reflected on significant drop of product **46**. Isolated yield from Entry 1 was 35%.

| Entry | Light (LED 200W) | Time | Temperature | % of 46[a] | % of 89[a] |
|---|---|---|---|---|---|
| **1** | Yellow 590 -595 nm | 4 h | 50 °C | 35% | 21% |
| **2** | Yellow 590 -595 nm | 4 h | 70 °C | 21% | 5% |
| **3** | Yellow 590 -595 nm | 19.5 h | 25 °C | 31% | 35% |
| **4** | Red 620-625 nm | 4 h | 50 °C | 33% | 14% |
| **5** | Green 520-530 nm | 4 h | 50 °C | 25% | 21% |

a) Percentage content is calculated by NMR integrations of the crude mixture

**Table 27.** Initial screening of the closure of **89** to **46** with different light sources and temperatures at concentration of 0.33 mg/ml. Solvent system (vol.%): toluene 33%, MeCN 56%, and AcOH (10% aq.) 11%.

The fact that the consumption of **89** is faster at higher temperature could mean that the sulphur monoxide (SO) removal is supported by the thermal extrusion. The SO removal is not purely thermal process, as upon heating, no reaction is observed. Thermal extrusion of SO was previously reported by Blier from an aromatic compound dibenzo[*b,f*][1,4,6]thiadiazepin 1-oxide (**Scheme 63**).[199]

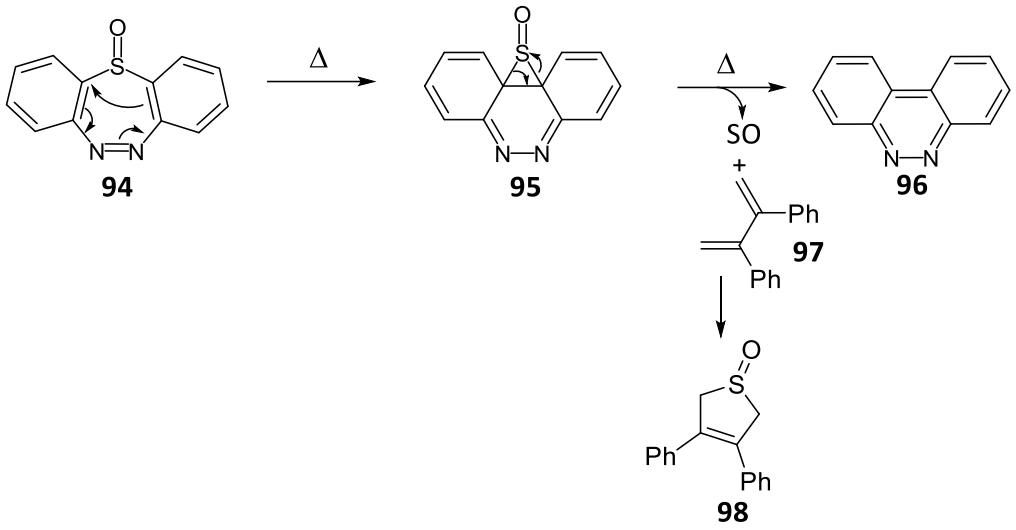


**Scheme 63**. Thermal extrusion of SO from dibenzo[1,4,6]thiadiazepin 1-oxide.

The SO removal could proceed via formation of episulphoxide by electrocyclization. In the study of Blier, the SO was trapped by dienes forming stable dihydrothiophene oxide compounds. It was found that the SO removal is not dependent on the presence of the diene. The removed SO may be in the triplet state or a ground or excited singlet state as both have lifetimes long enough to react with the diene.[199] In the Blier study the SO is probably formed in the singlet state. The singlet state SO is vastly more reactive towards the diene, as the triplet state can only react via stepwise pathway with unstable biradical intermediate. It is likely that in the case of fullerene **89** the removal is a thermal extrusion of a triplet state SO to form a singlet state fullerene and that is why the irradiation source is needed. The energy of the SO in the triplet state is lower than the energy of the singlet or excited singlet state SO (**Figure 29**). This is because the two electrons with parallel spin in different MO are further apart and the Coulombic repulsion is weaker.[200]

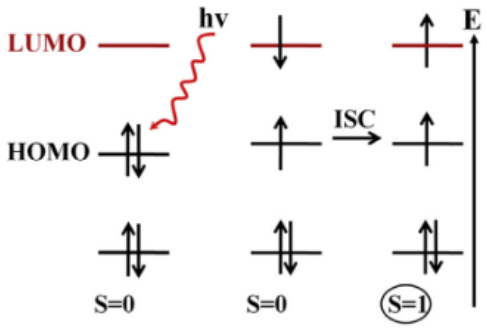


**Figure 29.** When electron in a singlet ground state molecule S=0 is excited from HOMO to LUMO a singlet excited state S=0 occurs. Electron can undergo an intersystem crossing (ICS) and when electrons in separate MO have analogous spins a triplet state S=1 occurs.[200]

Yellow and Red LED lights were chosen for the next set of experiments. **Table 28** shows experiments done with toluene saturated with water and AcOH and no MeCN. In entry 1 an insoluble precipitate was formed containing no trace of starting material. The insoluble precipitate is thought to be polymerisation product that is formed by the decomposition of fullerenes which was reported in literature.[180] This shows that the presence of polar solvent is required for the reaction. When concentration was lowered, the precipitate did not form but only trace of product and starting material was shown in NMR, together with mixture of unknown by-products.

| Entry | LED | Conc. | Temp. | Time | Yield 46 | Recovered 89 | Comments |
|---|---|---|---|---|---|---|---|
| **1** | Red 200 W | 2.35 mg | 50 | 4 | 0 | 0 | Precipitate |
| **2** | Red 200 W | 0.7 mg | 50 | 4 | 0 | 0 | No precipitate |

**Table 28.** Homogenous – toluene saturated with AcOH and $H_2O$.

**Table 29** shows time and concentration effect when using 100 W Yellow LED lights. In entries 1 and 2 the crude NMR analysis showed higher conversion of **89**, however a great part of material was found to precipitate at the top of chromatography column suggesting degradation. It was concluded that the higher concentration and longer irradiation time encourage the decomposition of either starting material or product and lower the yield. The optimum conditions for highest recovery and yield are the Entry 3. The recovery of the starting material **89** was introduced for the purposes of recycling of the **89** and monitoring the losses of **89** and **46** by degradation.

| Entry | LED | Conc. | Temp. | Time | Isolated yield 46 | Isolated unreacted 89 |
|---|---|---|---|---|---|---|
| **1** | Yellow 100 W | 2 $mg.ml^{-1}$ | 50 | 4 | 21% | 30% |
| **2** | Yellow 100 W | 2 $mg.ml^{-1}$ | 50 | 8 | 26% | 20% |
| **3** | Yellow 100 W | 1 $mg.ml^{-1}$ | 50 | 4 | 31% | 66% |

**Table 29.** Concentration effect on isolated yields. Solvent system (vol.%): toluene 33%, MeCN 56%, and AcOH (10% aq.) 11%.

When Lewis acid $CuCl_2$ instead of acetic acid was used, no conversion was observed. $CuCl_2$ initially appeared as a promising reagent to improve the reaction conditions as it is thought to form a complex with the **46**. NMR analysis of crude $CuCl_2$ stirred with HA showed sharp -OH peaks instead of the usual broad -OH hemiacetal signals (**Figure 30**). Rationale for adding $CuCl_2$ was that it could potentially stabilise the **46** and result in higher yield. Wet MeCN was used for this experiment to have enough of the $H_2O$ for the hydrolysis of **45** present. $CuCl_2$ used in addition to AcOH aq., showed no effect on the reaction and the yield and recovered **89** were comparable to the reaction without using $CuCl_2$ (**Table 30**). It is likely that the $CuCl_2$ prefers to coordinate with the $H_2O$ present in the reaction. This also confirms the hypothesis that the AcOH is needed to form the **46** in situ. There is also a possibility that the $CuCl_2$ could be preventing the photolysis due to high recovery of the starting material **89**.

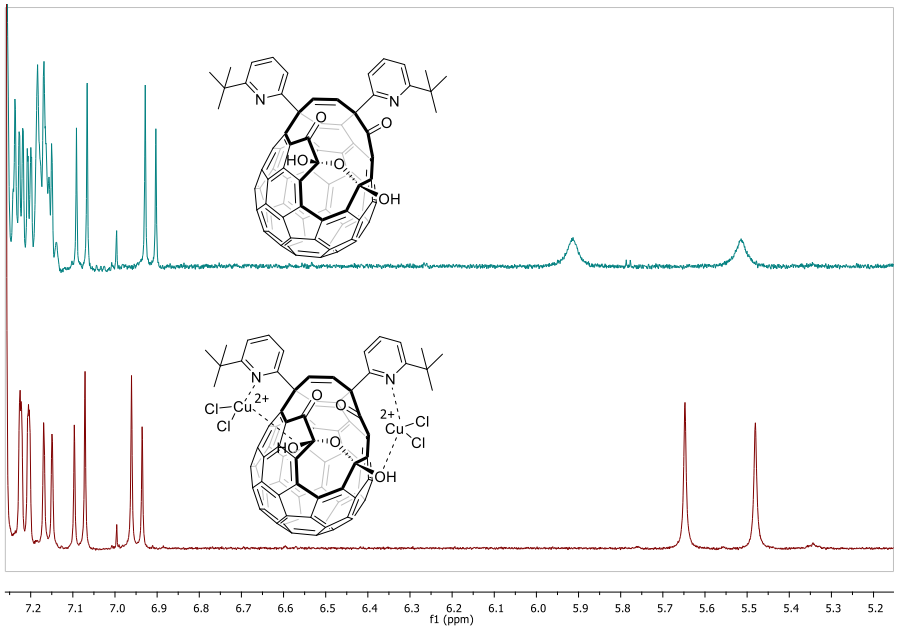


**Figure 30.** Comparison of hydroxyl signals in $^{1}H$ NMR of HA and HA mixed with $CuCl_2$.

| Entry | LED | Conc. | Temp | Acid | Time | Yield 46 | 89 |
|---|---|---|---|---|---|---|---|
| **1**[a)] | Yellow 100 W | 0.3 mg.mL$^{-1}$ | 37 | - | 4 | 0 | 99% |
| **2**[b)] | Yellow 100 W | 0.3 mg.mL$^{-1}$ | 37 | AcOH 10% aq | 4 | 27% | 54% |

**Table 30.** Lewis acid $CuCl_2$ (10 eq) addition effect. Solvent system (vol.%): a) toluene 39%, MeCN 61%, b) toluene 35%, MeCN 55% and AcOH (10% aq.) 10%.

The reported conditions for **89/$H_2O$@89** conversion to **46** with 35 W Na lamp over 24 hours resulted in 40% yield. After optimisation with Yellow LED lamps the reaction time was lowered to 4h and the obtained yield was 30%. Considering that ~55% of the starting material was fully recovered, yield out of unreacted **89** was then 66%. The recovery of the **89** is an important step, as it could be utilised in synthesis of A@$C_{60}$ with an expensive gas such as $^{13}CH_4$ where the filling reaction is a costly step.

## 5.1.2 Optimisation with $CH_4$@89

Best conditions from the initial optimisation were used in the reaction with **$CH_4$@89** which was prepared according to the known procedure (**Scheme 64**).[180]

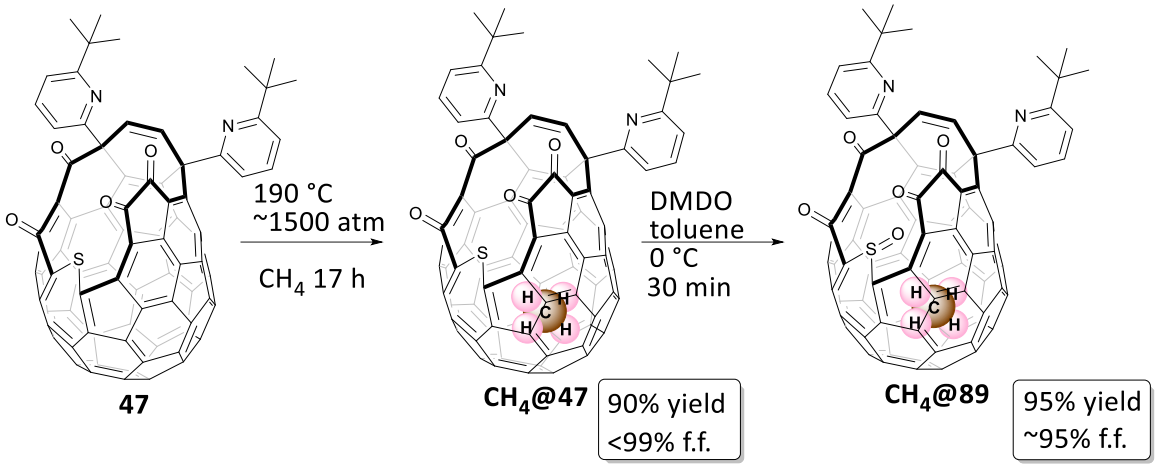


**Scheme 64.** Synthesis of **$CH_4$@89**.

It was expected that **$CH_4$@89** would be less reactive than empty **89** according to reported results.[180] The high filling factor of the **$CH_4$@46** negatively affects the conversion of **$CH_4$@89** to **$CH_4$@46** and allows formation of undesired by-products and decomposition. During the optimisation process important variables were determined: Temperature, concentration time, acid, light power, and solvent system. The initial study concluded that lower concentration avoids decomposition and that the reaction does not proceed without the presence of acid, water and solvent system tol:MeCN.

#### 5.1.2.1 AcOH vs TFA

In the first study, an acid effect of AcOH and $CF_3COOH$ (TFA) was compared in small-scale reactions (**Table 31**). The rationale was that usage of stronger acid may accelerate the conversion of **45** to **46** conversion. 100 eq of TFA and same volume of water as in reaction with AcOH were used as the reaction did not proceed well without water. Results of the reactions were assessed using quantitative NMR using internal standard. Advantage in optimisation of $CH_4$ filled compounds is that each compound has unique signal for the endohedral $CH_4$ in the NMR. A new major peak at -11.37 ppm was observed in the reactions using TFA instead of AcOH and later it was discovered that it belongs to by-product **99. Table 31** shows the percentage composition of the reaction mixture which was determined by quantitative NMR. The set of experiments was done on 20 mg scale with concentration of 0.2 $mg.mL^{-1}$ and using 2x20W yellow LED lamps.

| Entry | Temp. | Acid | Time | 46 | 89 | 99 (-11.37ppm) |
|---|---|---|---|---|---|---|
| **1** | 40 | TFA | 1 | 6% | 63% | 10% |
| **2** | 40 | AcOH (10% aq) | 1 | 8% | 63% | 4% |
| **3** | 40 | TFA | 4 | 14% | 33% | 32% |
| **4** | 40 | AcOH (10% aq) | 4 | 6% | 18% | 9% |
| **5** | 70 | TFA | 1 | 15% | 23% | 45% |

**Table 31**. Results of study to investigate the effect of acid, time and temperature. Solvent system (vol.%): toluene 45%, MeCN 45% and 100 eq TFA and water 10% or AcOH (10% aq.) 10%.

The acid comparison suggested that the presence of TFA not only promotes conversion from **46** to **99**, but also promotes the SO extrusion especially at elevated temperatures. **Figure 31** illustrated the endohedral area of the relevant peaks in the reaction mixture. Each resonance represents a single OCF containing one molecule of $CH_4$ encapsulated inside. It was observed that the peaks are shifted by ~0.1 ppm in the presence of TFA. The experiments executed with AcOH show multiple minor by-product peak. The set of experiments was performed in the solvent system containing higher proportion of toluene than previously. This parameter can also have an effect on the formation of the by-products. The direct comparison shows that the reactivity of **$CH_4$@89** higher in the presence of the TFA.

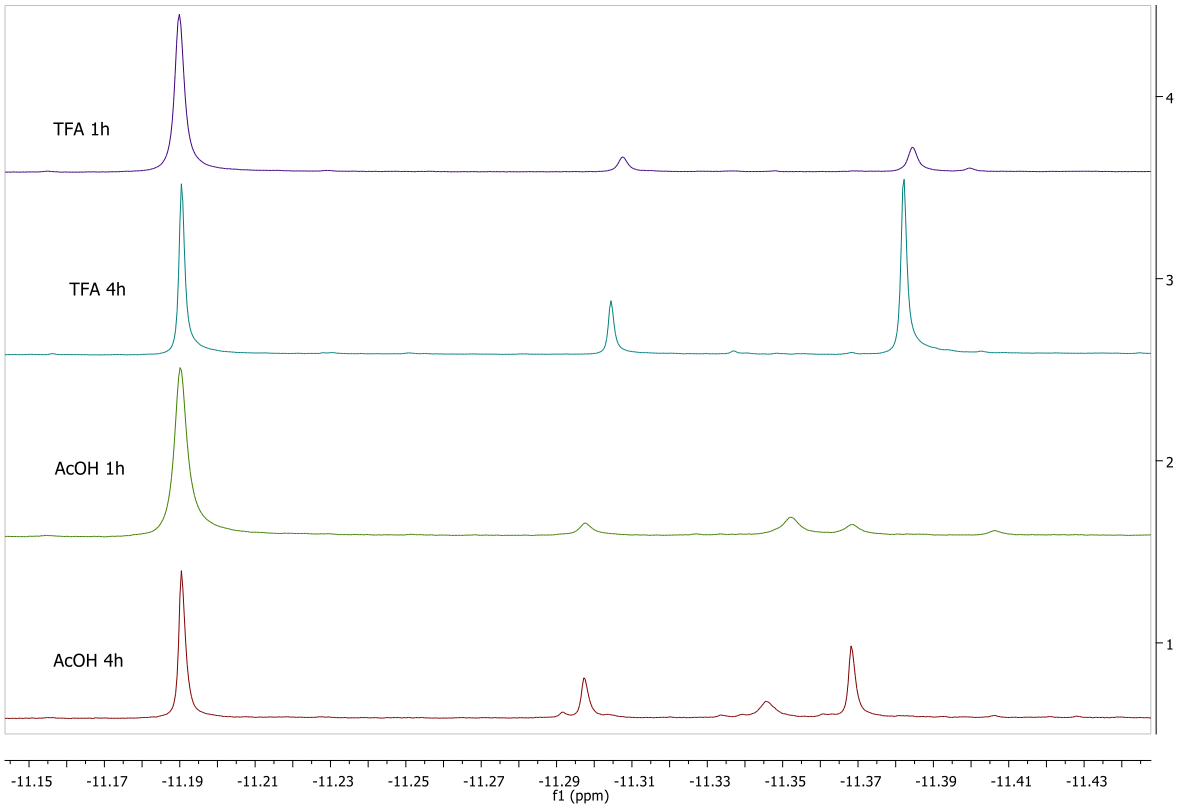


**Figure 31**. Comparison of endohedral peak of $CH_4$ in optimisation reactions at 40 °C listed in **Table 31**. Main area is zoomed in. (-11.19 ppm = **$CH_4$@89,** -11.30 ppm = **$CH_4$4@46**, – 11.37 ppm = **$CH_4$@99**). Note that the resonance changes by ~0.1 in the presence of TFA.

#### 5.1.2.2 By-product 99 characterisation and mechanism of the formation

The by-product **99** was isolated and characterised by X-ray crystallography (**Figure 32**). When compound **46** was irradiated in the solvent system 1:1:0.1 tol:MeCN:$H_2O$ with 100 eq of TFA at 70 °C, 30% conversion to **99** occurred. Formation of **99** could be a secondary radical reaction of the desired product **46.** It was previously established that temperatures above 100 °C the compound **46** is in

equilibrium with its dehydrated form **45**.[155] It possible that reversibility between the hemiacetal **46** and tetraketone **45** exists at lower temperatures as well. This will be shifted towards the **45** when higher exposed to higher temperatures. It is therefore thought that the by-product **99** is arising from the dehydrated **45**. Plausible mechanism for formation of **99** is proposed in **Scheme 65**. Previously reported lactone-like by-product resulting from the attempt of closure of **89** is shown in **Scheme 47**.

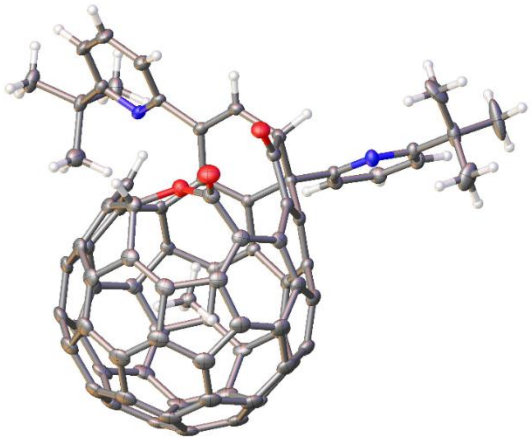

**Figure 32**. Thermal ellipsoid of the by-product 14 -11.37 filled with $CH_4$.

As the reaction is irradiated, a radical may be formed, most likely on the 1,2-diketone similar to the formation of **90** (**Scheme 47**). The radical is then transferred to the carbonyl closest to the alkenyl bridge by forming a new C-C bond and a new five membered ring. The next process could be removal of the CO group and formation of the lactone followed by protonation of the intermediate **99b** assisted by the acid present in the reaction.

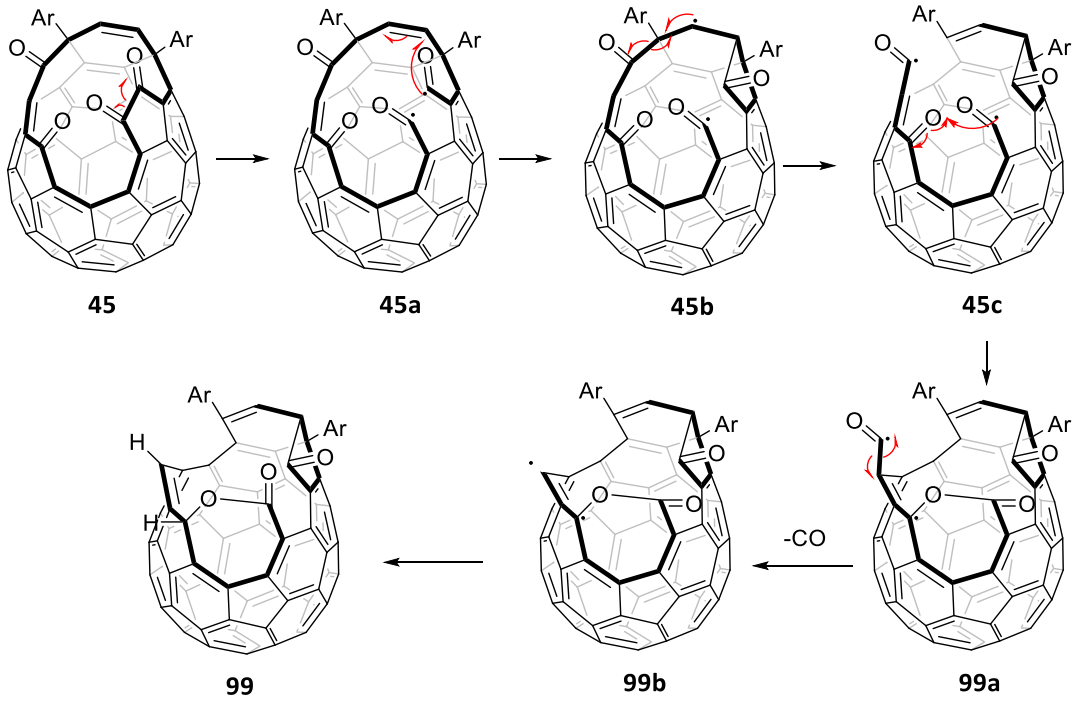


**Scheme 65**. Proposed mechanism for by-product formation.

When **46** was stirred and irradiated with Yellow LED at 50 °C in the solvent system containing 45%vol of toluene, 45%vol of MeCN and 10%vol AcOH (aq 10%) almost no conversion to **99** was observed. Despite the fact that using higher temperatures and TFA seemingly speed up the reaction, it also causes conversion of the **45**/**46** to undesired **99**. It was therefore concluded that the original conditions at 50 °C and AcOH (10% aq) instead of TFA are optimal conditions for the photoreaction.

### 5.1.3 Optimisation of the solvent system of the photoreaction and synthesis of $CH_4$@43

The intermediate **$CH_4$@46** was shown to be unstable if stored for several days and therefore in the following experiments it was used directly in the next step without storage. In the reported procedure the **$CH_4$@46** is dehydrated to **$CH_4$@45** and then sutured to **$CH_4$@43** using $PPh(Fu)_2$ at 50 °C for 118 h.[180] In this study, the **$CH_4$@43** was prepared from **$CH_4$@45** using the $PPh_3$ and refluxed in toluene at 110 °C as reported in the optimised synthesis of $H_2O$@$C_{60}$.[155]

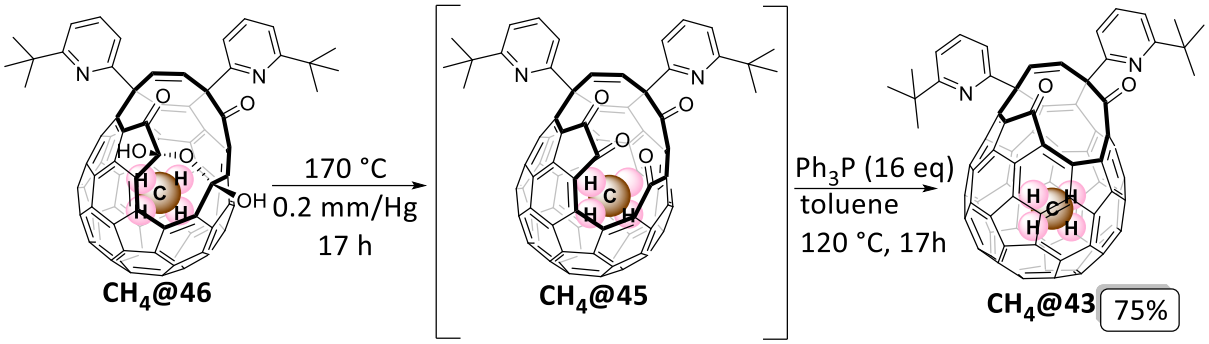


| Entry | Scale /mg | Solvent system (volume %) | | | time | Yellow LED | Yield $CH_4$@46 | Yield $CH_4$@43 | Recovered CH4@89 | Overall yield[b] |
|---|---|---|---|---|---|---|---|---|---|---|
| | | toluene | MeCN | AcOH (10% aq) | | | | | | |
| reported[180] | 84 | 33 | 56 | 11 | 24 h | 11 W[a] | 5% | 5% | – | – |
| reported[180] | 52 | 24 | 63 | 8 | 36 h | 35 W[a] | 13% | 13% | – | – |
| **1** | 100 | 45 | 45 | 10 | 4 h | 40 W | 13% | – | 43% | 23% (**46**) |
| **2** | 100 | 30 | 60 | 10 | 4 h | 40 W | 10% | – | 22% | 13% (**46**) |
| **3** | 100 | 45 | 45 | 10 | 4 h | 100 W | 20% | 13.4% | 50% | 27% (**43**) |
| **4** | 200 | 45 | 45 | 10 | 4 h | 100 W | 8% | – | 30% | 15% (**46**) |
| **5** | 100 | 30 | 60 | 10 | 17h | 20 W | 19% | 15% | 33% | 20% (**43**) |

a) Sodium lamp used. b) Yield based on recovered starting material.

**Table 32.** Experiments to investigate an effect of different solvent ratios and power of irradiation source. Total volume of reactions in entries 1-5 was 210 mL.

The final study was looking at the effect of the solvent system and irradiation source. This study was also supported by experiments with **Kr@89** that are discussed in the following chapter. The consumption of the **89** was faster with more toluene present and higher power LED. In these conditions more by-products were formed, and the chromatography was more difficult. Entries 3 and 5 gave comparable yields however the entry 5 crude mixture contained fewer impurities therefore separation process was easier. Entry 5 was concluded to be the optimal condition for this photoreaction performed in the purpose-built reactor.

**$CH_4$@43** synthetic method could potentially introduce endohedral $H_2O$ into the empty **45** as the activation energy temperature for the water entry is 100 °C. Despite using thoroughly dried equipment and reagents, traces of **$H_2O$@$C_{60}$** were present in the final **$CH_4$@$C_{60}$**. The **$H_2O$@$C_{60}$** can be separated from the **$CH_4$@$C_{60}$** by recycling HPLC using the Cosmosil™ Buckprep column in 100% toluene (**Experimental, Figure 33**).

The **$CH_4$@$C_{60}$** was then prepared via the known route in 52% yield (**Scheme 66**) to study the separation from the undesired **$H_2O$@$C_{60}$**.

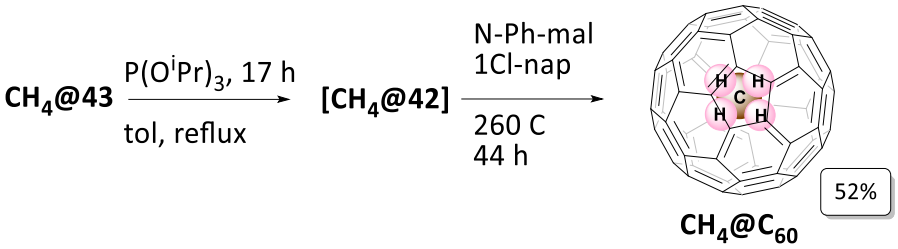


**Scheme 66.** Synthesis of $CH_4@C_{60}$.

The separation of the **$CH_4@C_{60}$** from empty **$C_{60}$** and **$H_2O@C_{60}$** was investigated by running several cycles on the HPLC. The separation of **$C_{60}$** and **$CH_4@C_{60}$** is known to be rapid and was reported in the first synthesis of **$CH_4@C_{60}$**[180]. Sample of **$H_2O@C_{60}$** (30% filled) was recycled on one Cosmosil™ Buckprep column in 100% toluene, 10 mL.min$^{-1}$ to become familiar with its separation pattern. Sample of **$CH_4@C_{60}$** was then recycled using the same conditions and the separation of **$CH_4@C_{60}$** and **$H_2O@C_{60}$** was observed to start after 70 minutes. Optimum separation is observed after 9 cycles which was between 160-170 minutes. Recycling the $C_{60}$ multiple times causes peak broadening. Eventually the peak broadening has contra productive effect on the separation and becomes very insufficient. For 100% separation of **$CH_4@C_{60}$** from **$H_2O@C_{60}$** and minimal material losses, collection of the partially separated product and reinjection on the HPLC would be ideal procedure.

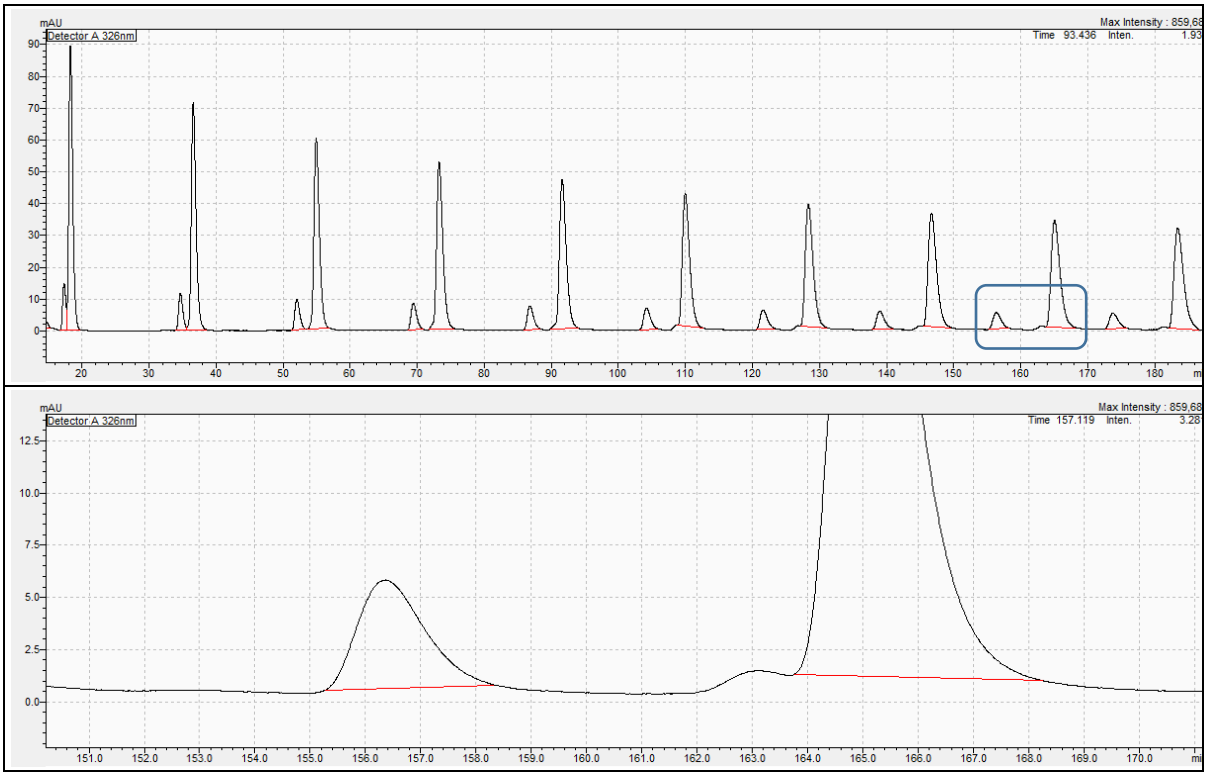


**Figure 33**. HPLC separation of **$CH_4@C_{60}$** (95% ff) from empty **$C_{60}$** and **$H_2O@C_{60}$** (<1% ff).

### 5.1.4 Ar@$C_{60}$

Synthesis of **Ar@$C_{60}$** was published in 2020 by Whitby group[184] and it was observed that the incorporated argon has less of an effect on the ring contraction from **Ar@89** to **Ar@43**. The ring contraction from **Ar@43** to **Ar@42** was performed by using $PPh(Fu)_2$ at 50 °C for 118 h to avoid undesired entry of water. In this project several experiments were performed in order to prepare Ar@$C_{60}$. The closing step from **Ar@43** to **Ar@42** was performed by using $PPh_3$ at 120 °C in toluene over 17 hours and it was anticipated that some endohedral water would incorporate into the **$C_{60}$** as well. Experiments were then performed on recycling HPLC to see if separation of **Ar@$C_{60}$** and **$H_2O$@$C_{60}$** can be performed.

Initially **Ar@47** was prepared according to the reported procedure by filling compound **47**, with estimated filling 99%, based on NMR. **Ar@47** was then oxidised to **Ar@89.** Several experiments were performed with **Ar@89** to investigate the behaviour of the **Ar@89** in the purpose-built flask (**Table 33**).

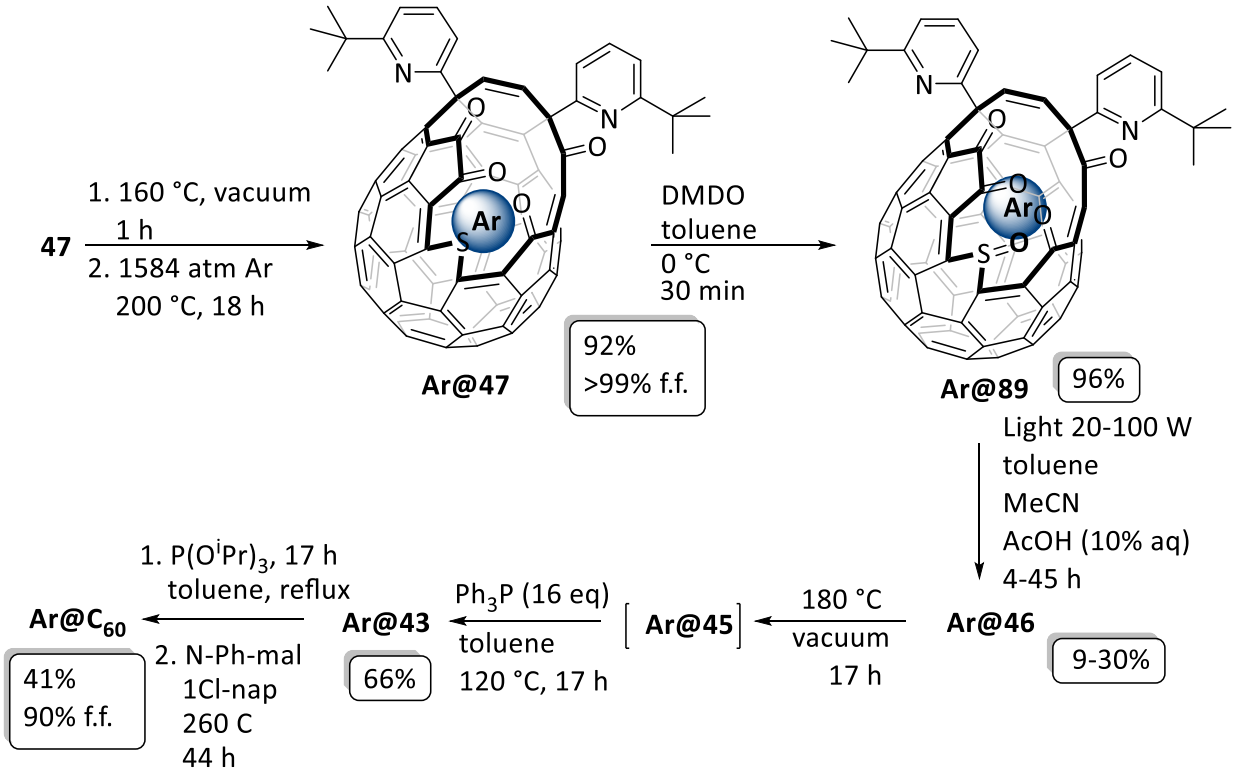


**Scheme 67.** Synthesis of **Ar@$C_{60}$**

The published synthesis of **Ar@46** gave satisfactory result[184], however no recovery of **Ar@89** was reported. It was observed that when lower power light and high reaction time or higher power light and shorter reaction time are used, a decent recovery (26-49%) of **89** is possible. It was also previously

observed that scaling up the reported photoreaction conditions did not lead to good yield recovery of the product.[aa] On these premises it was anticipated that better overall yield would be achieved by using the purpose built reactor. The trialed experiments however did not improve the reaction conditions and despite the recovery being good, the overall yield was still lower than the reported yield and the scale of the photoreactor was limited. The yield of **Ar@46** was consistently around 30% however the isolated yield of **Ar@43** was lower than previously reported[155] (**Table 33**, Entries 1-5).

| Entry | Scale /mg | Solvent system (volume %) | | | T/°C | time | Yellow LED | Yield Ar@46 | Yield Ar@43 | Recovered Ar@89 | Overall yield[c)] |
|---|---|---|---|---|---|---|---|---|---|---|---|
| | | toluene | MeCN | AcOH (10% aq) | | | | | | | |
| d)[184] | 115 | 24 | 63 | 13 | - | 35 h | 35 W | 26% | 19% | – | 19% (**43**) |
| 1 | 100 | 48 | 48 | 5 | 50 | 4 h | 100 W | - | 10% | 37% | 16% (**43**) |
| 2 | 100 | 48 | 48 | 5 | 50 | 4 h | 100 W | 30% | 9% | 49% | 18% (**43**) |
| 3 | 100 | 24 | 71 | 5 | 50 | 4 h | 100 W | 30% | 9% | 37% | 14% (**43**) |
| 4 | 100 | 24 | 71 | 5 | 50 | 17 h | 20 W | 30% | 10% | 35% | 15% (**43**) |
| 5 | 100 | 32 | 63 | 5 | 50 | 4 h | 100 W | 19% | 13% | 26% | 18% (**43**) |
| 6[a)] | 250 | 24 | 63 | 13 | - | 40 h | 35 W[b)] | 28% | 19% | 57% | 43% (**43**) |
| 7[a)] | 250 | 24 | 63 | 13 | - | 45 h | 35 W[b)] | 21% | 15% | 68% | 47% (**43**) |

a) Experiments were performed in round bottom flask with the lamp placed next to it.
b) Performed with Na lamp.
c) Yield based on recovered starting material **Ar@89**.
d) Previously reported

**Table 33.** Synthesis of **Ar@43** from **Ar@89**. Total volume of the entries 1-5 was 200 mL.

The reaction was then trialled using the reported conditions with 35 W Na lamp over prolonged time period and look at potential recovery of **Ar@89** (**Table 33**. Entries 6-7). The reactions were performed in 500 mL flask with the Na sodium lamp in 1 cm distance from the solution. The system was covered with aluminium foil to maximise reflection and minimise light losses. After 40-45 hours, small conversion of around 30 % was achieved however the NMR spectra of the crude mixture did not show formation of any byproducts or impurities. The isolated yields were similar to the reported (21-28%) and the unreacted **Ar@89** was obtained in high amount of 57-68%. It is likely that the very mild exposure to the light is beneficial for the reaction and minimises the decomposition of the starting material and the product. **Ar@46** was then directly transferred to the dehydration reaction followed by ring contraction using $PPh_3$ (**Scheme 67**). Despite the drying step from **Ar@46** to **Ar@45** and using dry $PPh_3$, some incorporation of $H_2O$ was observed (~1%). The **Ar@$C_{60}$** was prepared by the known route with yield of 41% from **Ar@43**. Purification from the undesired water was trialed by recycling HPLC using the same conditions as for the **$CH_4$@$C_{60}$**. Unfortunately it was discovered the retention times of the **$H_2O$@$C_{60}$** and **Ar@$C_{60}$** are too similar to be able to perform the separation. It

[aa] Observed by Dr Sally Bloodworth when using **$CH_4$@89**.

was concluded that the reported procedure for synthesis of **Ar@C$_{60}$**[184] is currently the most suitable method.

# 6 Synthesis of Kr@$C_{60}$

This section will describe synthesis of Kr@$C_{60}$ by molecular surgery, using synthetic method previously optimised for syntheses of **$CH_4$@$C_{60}$** and **Ar@$C_{60}$**.

Note: All DFT Calculations mentioned in this chapter were done by prof. R.J.Whitby in Gaussian 09 using M062x/cc-pVDZ basis set. The Aryl groups were replaced by methyl groups.

## 6.1 Filling of 47 cavity with Kr

The compound **Kr@$C_{60}$** was previously synthesised by the methods discussed in **1.2.3** in microscopic quantities. The first synthesis of **Kr@$C_{60}$** by molecular surgery followed the synthetic approach for synthesis of **$CH_4$@$C_{60}$** and **Ar@$C_{60}$**. The Gibbs free energy for Kr entering the orifice of **47** was calculated by DFT[bb] and compared to the entry energy of $CH_4$. Calculations showed the Gibbs free energy of Kr entry to be 132 kJ.mol$^{-1}$ which is 6 kJ.mol$^{-1}$ lower than $CH_4$ entry into **47** (138 kJ.mol$^{-1}$). This suggested that similar conditions to **$CH_4$@47** could be used to prepare **Kr@47**. Heating solid **47** to 177 °C for 14 hours under approx. 1500 atm of krypton using the high-pressure apparatus (**Figure 20**) gave >99% filled **Kr@47** in full recovery (**Scheme 68**). The **Kr@47** was then oxidised to **Kr@89** using the same known procedure as for the reported **A@89**.[180][184]

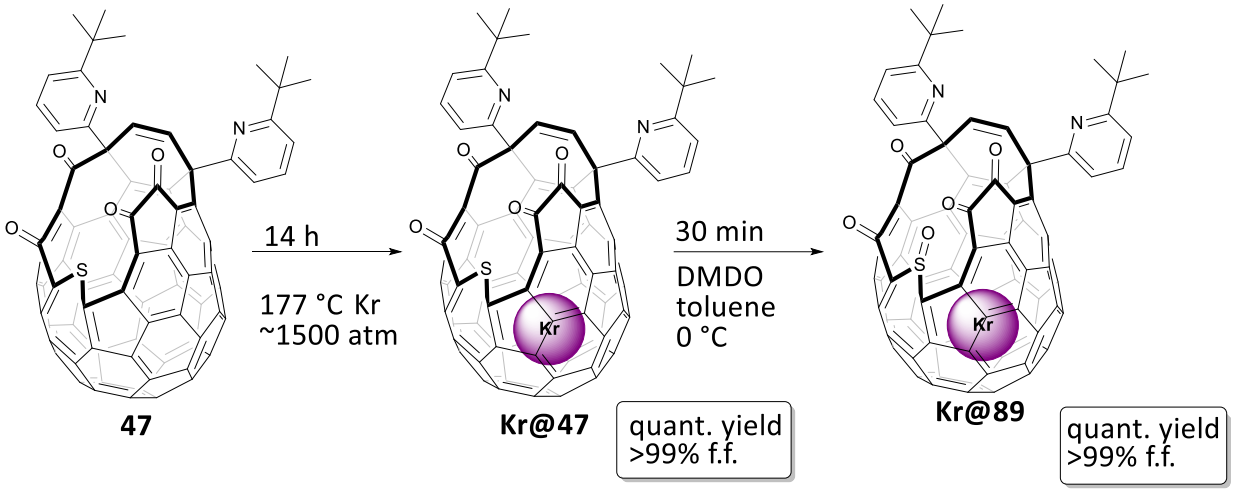


**Scheme 68**. Filling of solid **47** with Kr gas followed by oxidation.

[bb] Calculations performed by R. Whitby in Gaussian 09 using functional M06-2X with basis set cc-pVTZ with ultrafine integration grid using structures and thermodynamic corrections determined using cc-pVDZ.

The filling factor of **Kr@47** was estimated from ESI+ HRMS and by $^1$H NMR. No resonance for endohedral $H_2O$ was observed in $^1$H NMR that is typical for empty **47** at room temperature.[187] The $^1$H NMR spectrum of <99% **Kr@47** and empty **47** were compared and a difference of chemical shift for the alkenyl proton was observed. [$\delta_H$= 6.405 (Kr filled), $\delta_H$= 6.399 ($H_2O$ filled), $\delta_H$= 6.395 (empty), *o*-$DCB_{d4}$, 500 MHz] (**Figure 34**). The shift difference is Δδ= +0.006 ppm for **Kr@47** and **$H_2O$@47** and Δδ= +0.010 ppm for **Kr@47** and empty **47**. This enabled measurements of the kinetics of escape of Kr atom from the cavity of **47** and calculations of the activation energy, enthalpy and entropy.

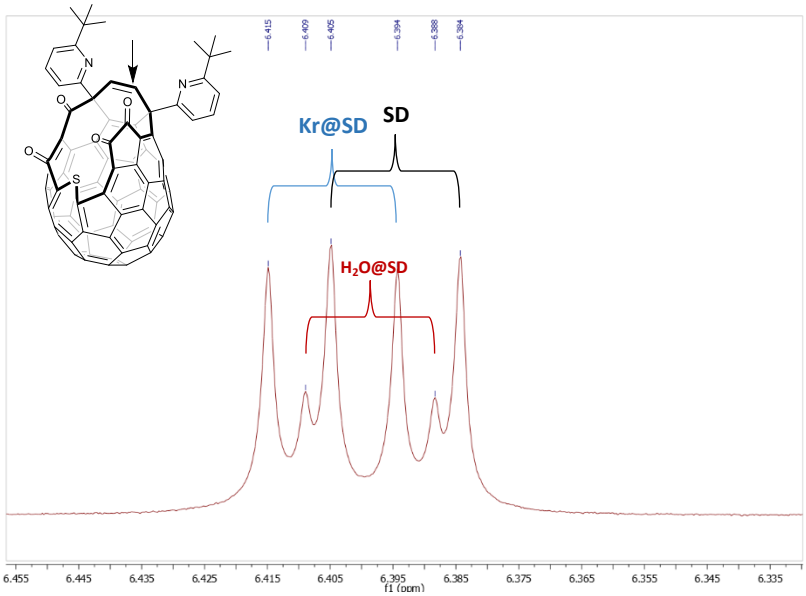


**Figure 34. $^1$H NMR** shift difference for methylene proton of empty **47, $H_2O$@47** and **Kr@47**

## 6.2 Loss of Kr atom from 47

The kinetic measurements were done in *o*-DCB-$d_4$ in the temperature range 433–453 K and the loss of Kr from the **47** was calculated by integration of the methylene doublet shown in **Figure 34** and the rates are shown in **Figure 35**. The dissociation of Kr from **Kr@47** displayed the 1$^{st}$ order kinetics. From the Arrhenius plot (**Figure 36**), the activation energy of Kr escape 133±5 kJ.mol$^{-1}$ and the pre-exponential factor log(A) 10.7 were determined which is comparable to the kinetic measurements of dissociation **$CH_4$@47** ($Ea^{esc}$= 134.6±5 kJ.mol$^{-1}$, log(A) = 10.9).[201] The $Ea^{esc}$ was lower than the calculated value 162.5 kJ.mol$^{-1}$.

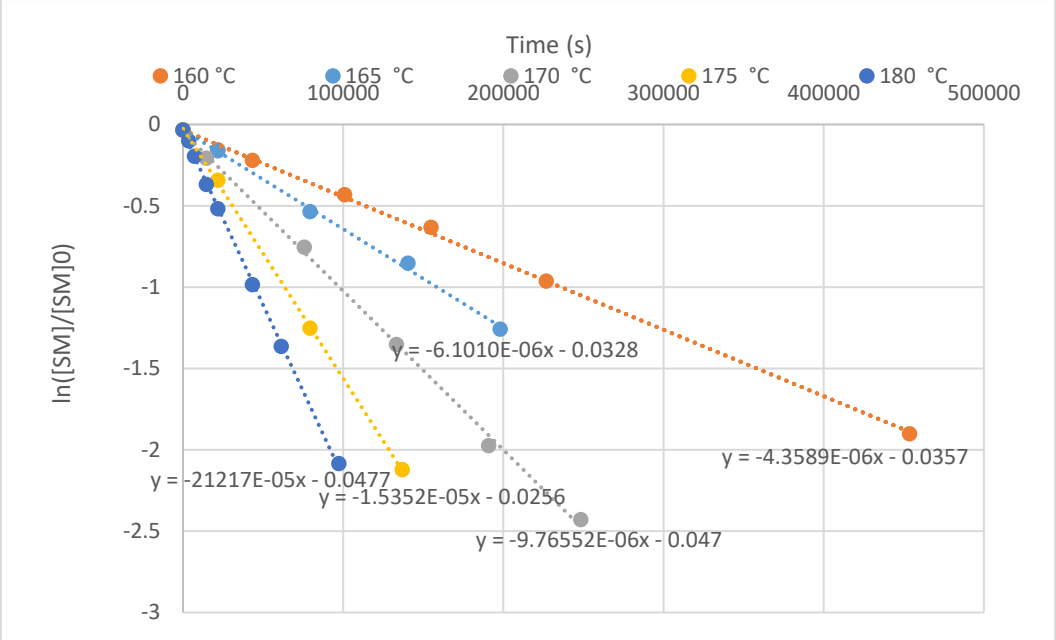


**Figure 35.** Rates of dissociations of Kr from **Kr@47** at between temperatures 433–453 K.

Enthalpy, entropy, and Gibbs free energy were calculated from the Eyring plot (**Figure 36**) and the values obtained were compared with the published data for **$CH_4$@47** loss (**Table 34**). The values obtained were very similar suggesting that the escape profiles of krypton and methane from the **47** cavity are almost identical.

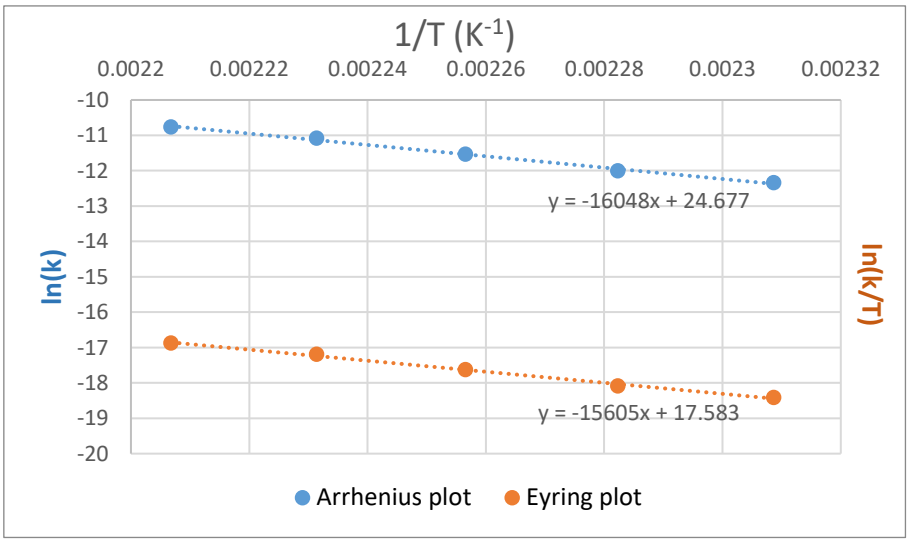


**Figure 36.** Arrhenius and Eyring plot for thermal dissociation of **Kr@47**.

| Energy | Kr@47 loss | $CH_4$@47 loss[201] |
|---|---|---|
| $Ea^{esc}$ | 133.4 ± 4.5 kJ.mol$^{-1}$ | 134.6 ± 5.0 kJ.mol$^{-1}$ |
| $\Delta H^{‡}$ | 129.7 ± 8.2 kJ.mol$^{-1}$ | 131.0 ± 5.0 kJ.mol$^{-1}$ |
| $\Delta S^{‡}$ | -51.6 ± 13.2 J K$^{-1}$ mol$^{-1}$ | -47.0 ± 11.2 J K$^{-1}$ mol$^{-1}$ |
| $\Delta G^{‡}$ at 165 °C | 152.2 ± 2.5 kJ.mol$^{-1}$ | 151.5 ± 0.1 kJ.mol$^{-1}$ |

**Table 34.** Summary of calculated energies of **Kr@47** thermal dissociation and compared with the data obtained for **$CH_4$@47**.

## 6.3 Closure of Kr@89 to Kr@$C_{60}$

The orifice of **Kr@89** was sutured by the photochemical/thermal extrusion of the sulfinyl molecule. The reported procedure[184] was compared with the optimised procedure from (**5.1.2**) and the Kr was found to have similar effect on the orifice as the $CH_4$.

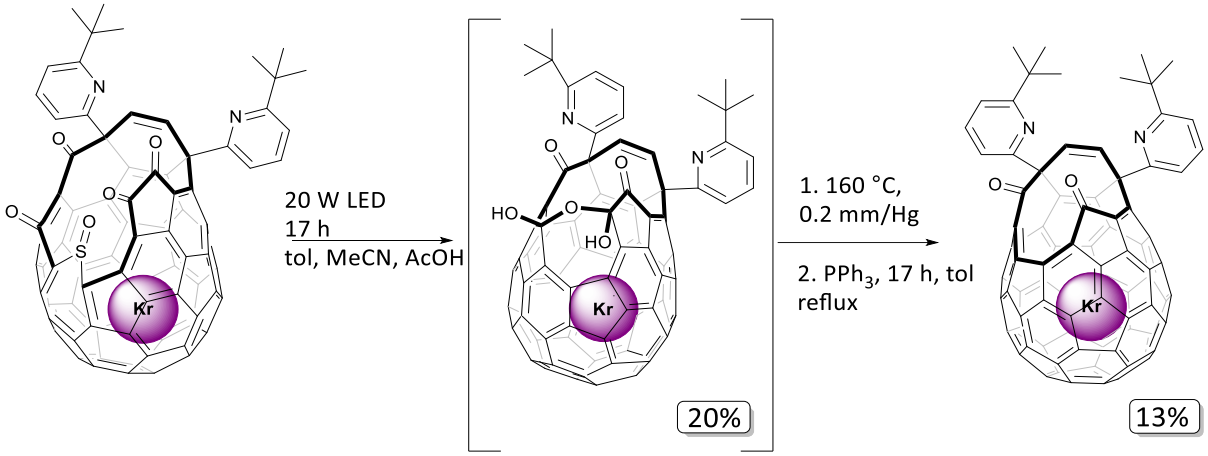


**Scheme 69**. Synthesis of **Kr@43**.

| Entry | Scale /mg | Solvent system (volume %) | | | | time | Yellow LED | T/°C | Yield Kr@46 | Yield Kr@43 | Recovered Kr@89 | Overall yield[c] |
|---|---|---|---|---|---|---|---|---|---|---|---|---|
| | | toluene | MeCN | AcOH 10% aq | TFA 10% aq | | | | | | | |
| **1**[a] | 80 | 22 | 67 | 11 | - | 35 h | 35 W[b] | 50 | 17% | 5% | 25% | 7% |
| **2** | 100 | 24 | 71 | 5 | - | 4 h | 100 W | 50 | 29% | 16% | 35% | 25% |
| **3** | 100 | 24 | 71 | 5 | - | 4 h | 100 W | 50 | 34% | 15% | 40% | 25% |
| **4** | 100 | 47.5 | 47.5 | 5 | - | 4 h | 100 W | 50 | 12% | 6% | 52% | 12% |
| **5** | 100 | 47.5 | 47.5 | - | 5 | 4 h | 20 W | 70 | 35% | 10% | 40% | 15% |
| **6** | 100 | 47.5 | 47.5 | - | 5 | 4 h | 100 W | 50 | 19% | 9% | 31% | 11% |
| **7** | 100 | 47.5 | 47.5 | - | 5 | 17 h | 20 W | 30 | 8% | 6% | 43% | 11% |
| **8** | 50 | 47.5 | 47.5 | - | 5 | 17 h | 100 W | 15 | 10% | 5% | 16% | 6% |
| **9** | 100 | 47.5 | 47.5 | 5 | - | 17 h | 20 W | 50 | 30% | 14% | 23% | 16% |
| **10** | 100 | 24 | 71 | 5 | - | 17 h | 40 W | 50 | 20% | 12% | 10% | 13% |
| **11** | 100 | 47.5 | 47.5 | 5 | - | 17 h | 40 W | 50 | 28% | 9% | - | – |
| **12** | 100 | 24 | 71 | 5 | - | 17h | 20 W | 50 | 20% | 13% | 19% | 16% |

a) Experiment was performed in round bottom flask with the lamp placed next to it.
b) Performed with Na lamp.
c) Yield calculated from the amount of reacted **Kr@89**.

**Table 35.** Optimisation reactions of synthesis of **Kr@43**. Total volume of all experiments was 200 mL.

Reaction was initially performed using the reported conditions from the syntheses of **Ar@43** and **$CH_4$@43** using a 35 W Na lamp in a proximate distance (ca 1 cm) from the reaction flask for 35 h.[184][180] The reaction yield was 17% of the intermediate **Kr@46**. The yield range was expected to be in similar range to the **$CH_4$@43** due to the size of endohedral molecule. The closure of **Kr@89** was then performed in the purpose-built jacketed flask (**Figure 28**) and several reaction conditions were tested (**Table 35**). The reactions using the TFA instead of the Acetic acid confirmed the effect of increasing the reaction rate resulting in the formation of by-product **Kr@99.** Experiments with lower temperature (Entries 7, 8) demonstrated that the closure to **Kr@46** is possible at lower temperatures. Reaction with the empty **89** at 15 °C using the AcOH did not show any conversion to HA. Using TFA at lower temperatures can potentially be utilised in syntheses of A@HA where the guest atom or molecule have low energy barrier of escape and the closure reaction has to be cooled. Comparison reactions of the solvent system ratio and 20W and 40W LED (Entries 9–12) gave similar yields. Entries 10 and 12 proceeded without formation of by-products making the chromatography step more straightforward. The recovery of the **Kr@89** is higher in the entries 2, 3 however overall yield (without considering the recovered s.m.) is comparable to entries 10 and 12. Optimal condition for synthesis of **Kr@46** was concluded to be Entry 12. **Kr@46** was treated as an intermediate due to its instability and immediately converted to **Kr@43** using the conditions reported for synthesis of $H_2O$@**43**.[155] To avoid entry of endohedral water, the **Kr@46** was converted to **Kr@45** by drying under vacuum before the reaction with $PPh_3$. Yields from **Kr@46** to **Kr@43** were lower (30-60%) than previously published[155] (typical 84%), there could be several reasons for the yield drop in the case of **Kr@43.** Drying step could cause some decomposition of the **Kr@45,** the reactions in this series were performed in a sealed tube due convenience using heating block that could have caused overheating of the system and degradation of the **Kr@43.** All these parameters could be investigated in future to maximise the yield of **Kr@43.**

Prepared **Kr@43** samples from this study were combined and the orifice was then closed using the reported procedures and 10 mg of Kr@$C_{60}$ (51% yield) of >99% filling factor was obtained (**Scheme 70**) after purification on HPLC (Specified in **8. Experimental**). $^{13}$C NMR ($\delta_C$=143.192, 500 MHz, *o*-DCB-$d_4$) showed Δδ = +0.39 ppm shift difference from empty $C_{60}$ ($\delta_C$=142.802, 500 MHz, *o*-DCB-$d_4$) which was in accord with reported literature.[102]

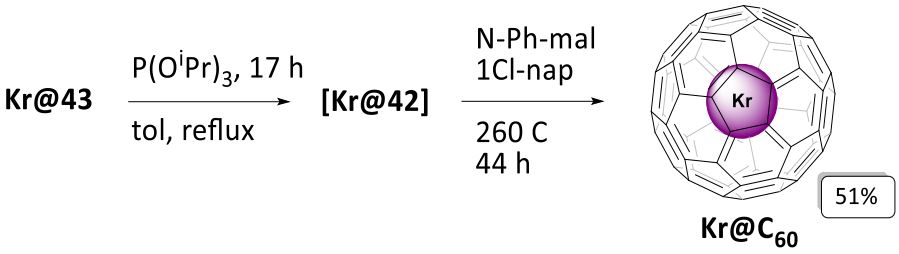


**Scheme 70.** Synthesis of **Kr@C$_{60}$**. Yield calculated from **Kr@43** after HPLC purification.

Traces <1% of **H$_2$O@C$_{60}$** were observed in the sample. The **H$_2$O@C$_{60}$** can be separated from **Kr@C$_{60}$** by recycling HPLC. The experiment was conducted using 98% ff Kr@$C_{60}$ on Cosmosil$^{TM}$ Buckyprep column in 100% toluene solvent and flowrate 10 ml.min$^{-1}$. After 9 cycles on a single column a good separation from **H$_2$O@C$_{60}$** was observed with RRT = 3 min (**Figure 37**).

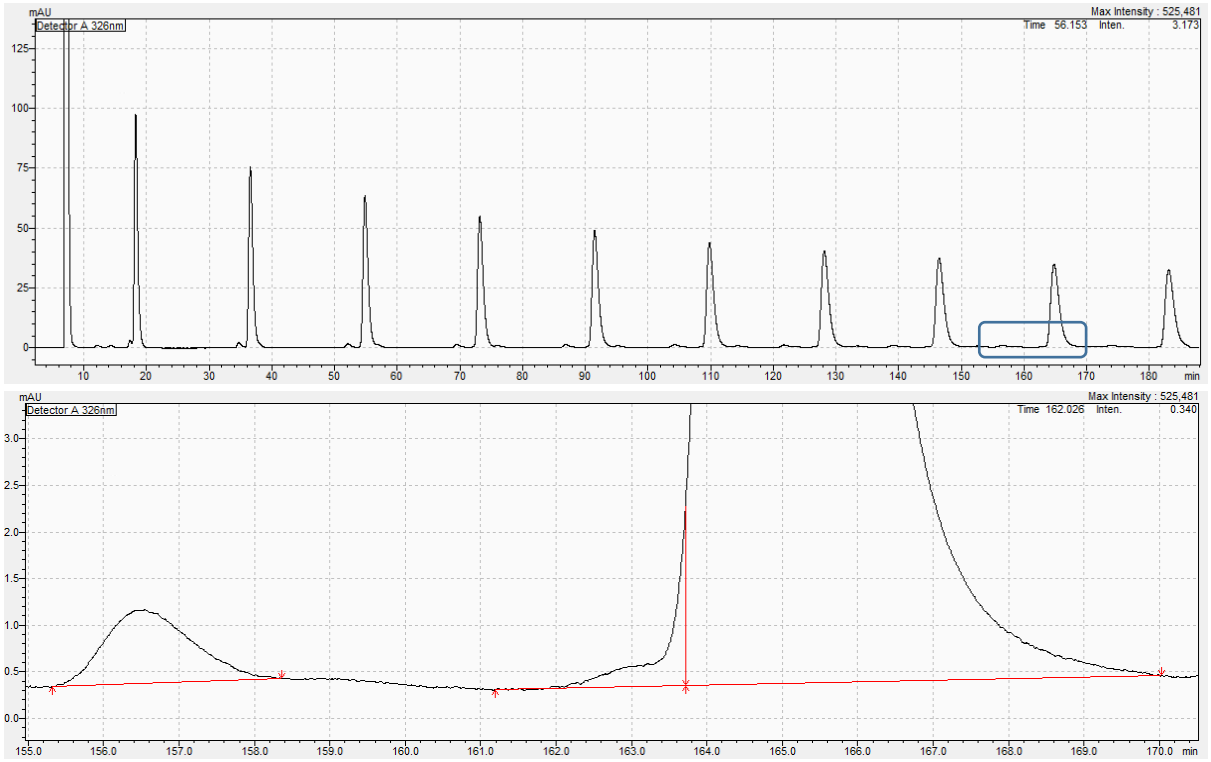


**Figure 37**. HPLC separation of **Kr@C$_{60}$** (98% ff) from empty **C$_{60}$** and **H$_2$O@C$_{60}$** (<1% ff).

The **Kr@C$_{60}$** was crystallised with Ni-porphyrin[198] and the crystal structure was obtained in good quality (**Figure 38**).

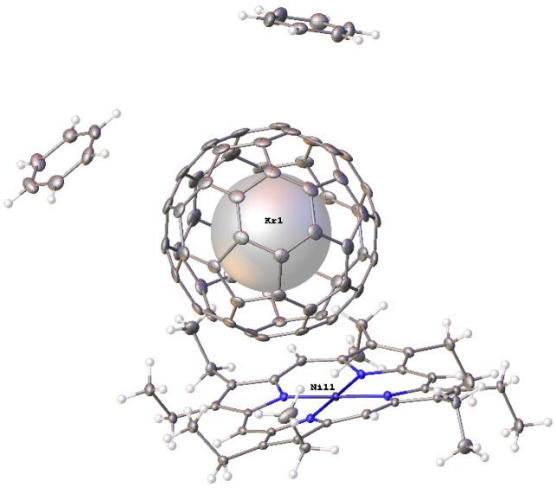


**Figure 38.** Crystal structure of **Kr@$C_{60}$** with Ni-porphyrin and 2 eq of benzene.

In conclusion the Kr@$C_{60}$ was prepared for the first time by molecular surgery and 10 mg of the >99% filled sample was obtained. Kinetic measurements of thermal dissociation of Kr from the **Kr@47** were performed and energy values obtained that were in agreement with previously reported **$CH_4$@47**. Presented synthetic method is more efficient in comparison with the previously reported method (**Table 37**) allowing to study the properties of endohedral Kr by spectroscopic methods. Krypton is the largest noble gas so far enclosed in the $C_{60}$ carbon cage by molecular surgery.

| **Fullerene** | **Method** | **Recovery/Yield** | **Filling factor** | **HPLC enriched** | |
|---|---|---|---|---|---|
| | | | | mass | purity |
| **Kr@$C_{60}$** | High Pressure/Temperature[100] | 25% | 0.2% | 0.14 mg[102] | 90% |
| **Kr@$C_{60}$** | Molecular surgery | 2.5%[a] | 99% | 10 mg | 100% |

a) Yield is calculated from the opening reaction of **$C_{60}$** to closure of **Kr@$C_{60}$**.

**Table 36.** Comparison of the **Kr@$C_{60}$** methods preparations.

# 7 Synthesis of $N_2@C_{60}$

This chapter will discuss the first synthesis of $N_2@C_{60}$ by molecular surgery. $N_2@C_{60}$ was previously isolated by HPLC. It was made by atomic nitrogen ion implantation method[62][202][203] alongside $N@C_{60}$, where 70 µg of sample was obtained containing 0.7% of $N@C_{60}$ and 0.6% $N_2@C_{60}$.[204] In 2008 synthesis of $N@C_{60}$ accompanied by $N_2@C_{60}$ formation was performed by the optimised glow discharge method[202] and the products were isolated by preparative HPLC. The fullerene $N_2@C_{70}$ was observed by mass spectrometry for the first time. Calculations[cc] were performed to determine possible conformations of the dinitrogen inside the $C_{60}$. The results showed that the dinitrogen conformation changes (relative energies between 0.2080-0.2265 Kj.mol$^{-1}$) cause very small changes in the overall energy and suggest that the $N_2$ rotates freely inside the $C_{60}$.[205]

Nitrogen molecule was previously inserted into OCF **58** in 2009 by Saunders[156] **(1.4.4**, **Table 10.)** and into OCF **47** in 2015 by Murata, entrapping the $N_2$ by forming a 'stopper' **$N_2@86$**[177] **(Table 14)**. During the optimisation process of the **$Kr@C_{60}$** synthesis, several reactions were performed at temperatures below 50 °C (**Table 35**). This prompted the idea that if the closure is possible below room temperature, it would be possible to prepare **$N_2@C_{60}$** by molecular surgery. Reported data from the literature suggested that escape from the **47** will occur rapidly. It was proposed that if the insertion was performed on the fullerene **89**, the escape energy of the $N_2$ will be higher and it would be possible to perform the ring contraction to **$N_2@45$** without significant loss of $N_2$. It was also considered that if the insertion of the $N_2$ into the fullerene **45** was possible, it would omit the low yielding closure step of **89** to **46**.

| DFT level of theory | Ar group replacement | OCF | $E_{in}$/kJ.mol$^{-1}$ | $E_{esc}$/kJ.mol$^{-1}$ |
|---|---|---|---|---|
| **M06-2X/6-31G*** [177] | Hydrogen | **47** | 35.5 | – |
| **M06-2X/6-31G*** [177] | Hydrogen | **86** | – | 69.9 |
| **M062x/vdz@631d_d3**[dd] | Methyl | **47** | 51.7 | 107.2 |
| **M062x/vdz@631d_d3**[dd] | Methyl | **89** | 63.9 | 117.6 |
| **M062x/vdz@631d**[dd] | Methyl | **45** | 156.6 | 211.8 |

**Table 37.** Comparison of the theoretical calculations of $N_2$ entry and escape from OCF.

Calculations reported in literature were performed with different levels of theory and **Table 37** shows comparison with the values obtained from literature and in this project[dd], performed on models of OCF where Aryl groups were replaced with methyl. $E_{in}$ of the $N_2$ insertion into **89** was calculated to be only 12 kJ.mol$^{-1}$ higher than insertion to **47**, similarly for the escape. Experiments presented in **Table**

[cc] Performed at HF/3-21G level of theory
[dd] Performed by prof. Richard Whitby

**38** were performed to optimise the insertion of the $N_2$ into the **89**. Powdered **89** was initially heated under vacuum at 160 °C for 90 min in order to remove endohedral water from the compound **89.** It was then exposed to high pressure of $N_2$ and heated. Relatively mild conditions in Entry 1 (**Table 38**) only gave 50% filling factor therefore the pressure and the temperature were increased. Entry 2 gave higher filling factor, however, the formation of compound **$N_2$@47** was observed. Formation of compound **47** from **89** was previously observed by a member of our group when **47** was exposed to higher pressure.[ee] Satisfying result was obtained from **Entry 3** when milder pressure and higher temperature was used.

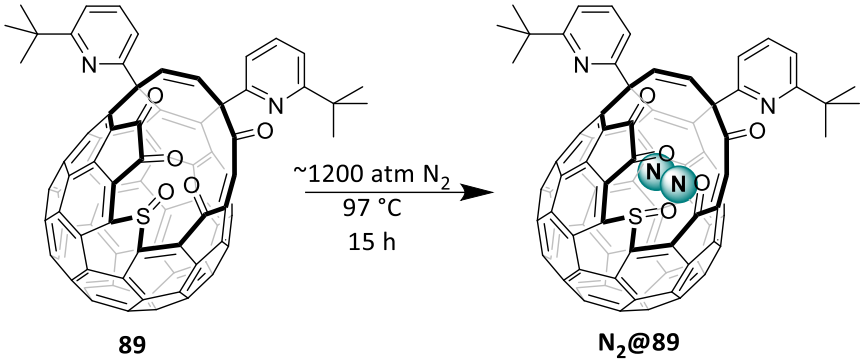


**Scheme 71**. Filling of $N_2$ into **89**.

| Entry | Pressure | Time | Temperature | Filling factor | Yield | 47 |
|---|---|---|---|---|---|---|
| **1** | 1105 | 15 h | 50 °C | 50% | 90% | – |
| **2** | 2531 | 17 h | 77 °C | 70% | 50% | 50% |
| **3** | 1224 | 15 h | 97 °C | 75% | 90% | – |

**Table 38.** Optimisation of filling of **89** with **$N_2$@89**.

The filling factor was determined by integration of the $^1$H NMR shift of **$N_2$@89** of the alkene bridge. NMR shift of the **$N_2$@OCF** was previously observed in the literature[177] even for the *tert*-butyl peaks despite being located far away from the guest $N_2$ molecule. In $CDCl_3$ δ = ~0.01 ppm was observed among the empty **89** and **$N_2$@89**. The sample of **$N_2$@89** was kept at room temperature and monitored over the course of 3 months, and no escape of $N_2$ was observed.

[ee] Observed by Sally Bloodworth

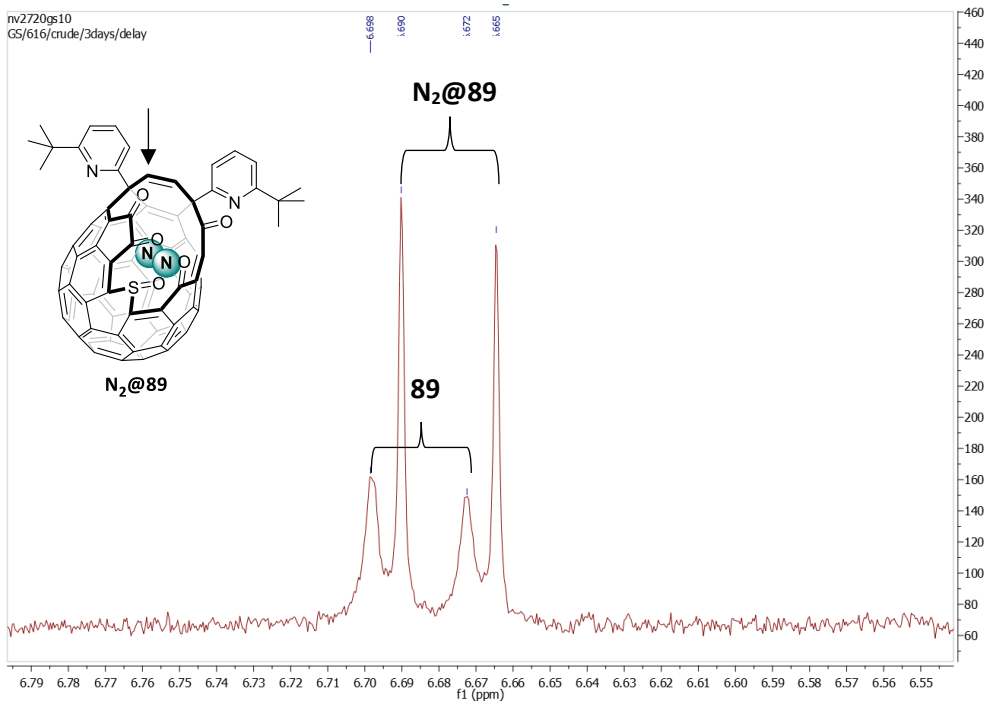


**Figure 39**. $^1$H NMR shift difference between empty **89** and **$N_2$@89**

Following the synthesis of **$N_2$@89** fullerenes obtained in the Entries 1–3 from **Table 38**, the orifice was then contracted to obtain the **$N_2$@43.** First, the **$N_2$@89** was irradiated by Yellow LED to obtain **$N_2$@46.** This was then directly reacted with $PPh_3$ to form **$N_2$@43** as per previously optimised process.

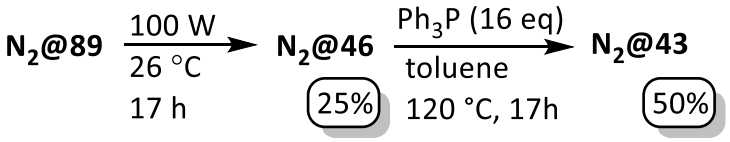


**Scheme 72**. Suturing the orifice of **$N_2$@89** to **$N_2$@43**

| Reaction Entry | Starting filling factor | Yellow LED | Temp. | Time | Yield[a] A@46 | Yield A@43 | Recovered A@89 | Filling factor $N_2$@43 | Filling factor $H_2O$@43 |
|---|---|---|---|---|---|---|---|---|---|
| **1**[a)] | 50% | 100 W | 15 °C | 22 h | 10% | 50% | 25% | 10% | 50% |
| **2**[b)] | 70% | 100 W | 26 °C | 17 h | 25% | 50% | – | 58% | 25% |

a) Mixture of empty **43, $N_2$@43** and **$H_2O$@43**

**Table 39.** Synthesis of **$N_2$@43**. Solvent system (vol.%): a) toluene 40%, MeCN 53%, $H_2O$ 5% and TFA 1%. b) toluene 37%, MeCN 53%, AcOH (10 % aq) 10%.

Entry 1 (a) Mixture of empty **43, $N_2$@43** and **$H_2O$@43**

**Table 39**) was performed before the stability data of the $N_2$ inside the **89** were obtained, therefore the reaction was performed at lower temperature to avoid potential $N_2$ loss. The filling factor of the product **$N_2$@46** dropped due to the fact that lower temperature slows down the conversion of the **89**

to **46**. The conversion of **$N_2$@89** is even slower due to the presence of the endohedral $N_2$. In this case 25% of the **$N_2$@89** was recovered. During the formation of **43,** the water entered the cavity of the empty **46,** therefore 50% of the obtained **43** was filled with $H_2O$. In the entry 2, the closure was performed at room temperature and higher yield of the product was obtained, however still some drop of the filling factor was observed. It is unlikely that the $N_2$ escaped during the closure of **$N_2$@46/45** to **$N_2$@43** due to the predicted high activation energy of the $N_2$ escape from **45** (**Table 37**).

Despite the high activation energy of $N_2$ entry into the **45** cavity, experiments were performed to investigate this possibility at high pressures and temperatures. Powdered sample of **46** was placed into the reactor and heated under vacuum to remove endohedral water. It was then exposed to high pressure of $N_2$ gas and high temperature for 15 hours (**Table 40**). Sample of **$N_2$@45** was then immediately reacted with $PPh_3$ to perform the well-known ring contraction to **$N_2$@43**. During these experiments it was discovered that the compound TK is unstable under these conditions and very low yields were obtained. Filling factors were detected by the HRMS. Entry 1 was only able to achieve 1% filling factor. Increasing the pressure and temperature in Entry 2 achieved higher filling 5%, however, even greater decomposition of the **45** was observed which resulted in yield of **$N_2$@43** to only be 10%.

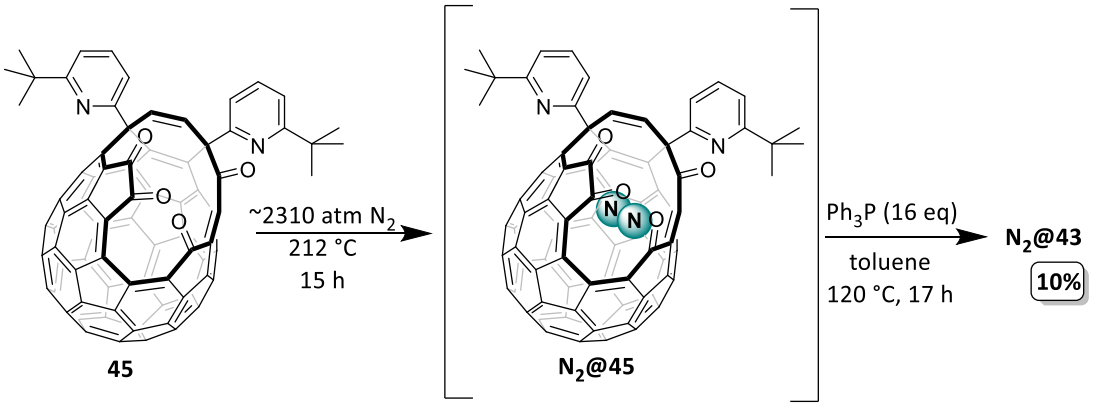


**Scheme 73.** Insertion of $N_2$ molecule into tetraketone **45** followed by instant closure to **$N_2$@43**.

| Entry | Pressure/atm | Time | Temperature | Filling factor | Yield of A@43 |
|---|---|---|---|---|---|
| **1** | 2100 | 15 h | 187 °C | 1% | 25% |
| **2** | 2310 | 15 h | 212 °C | 5% | 10% |

**Table 40.** Filling of $N_2$ into **89**.

**$N_2$@43** was then sutured to **$N_2$@$C_{60}$** using the known preparation methods. The prepared samples and filling factors are summarised in **Table 41**.

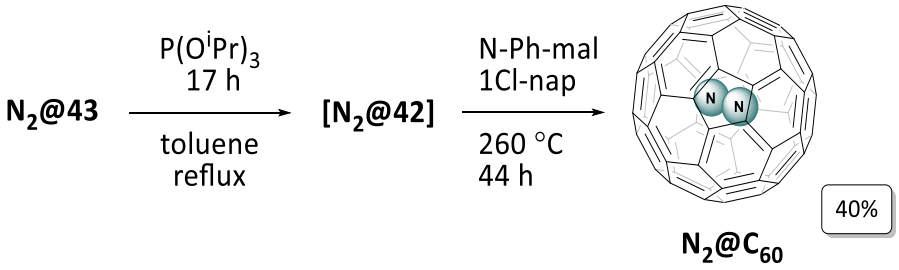


**Scheme 74.** Synthesis of $N_2@C_{60}$ from $N_2@43$

| Entry | Filling factor | Yield | mass |
|---|---|---|---|
| **1** | 1% | 53% | 35 mg |
| **2** | 58% | 40% | 2.1 mg |
| **3** | 5% | 50% | 11 mg |

**Table 41.** Synthesis of $N_2@C_{60}$.

$^{13}C$ NMR of the $N_2@C_{60}$ (mixed with $H_2O@C_{60}$ and empty $C_{60}$) was obtained for the first time and the presence of the $N_2@C_{60}$ and the filling factor were further confirmed by HRMS.

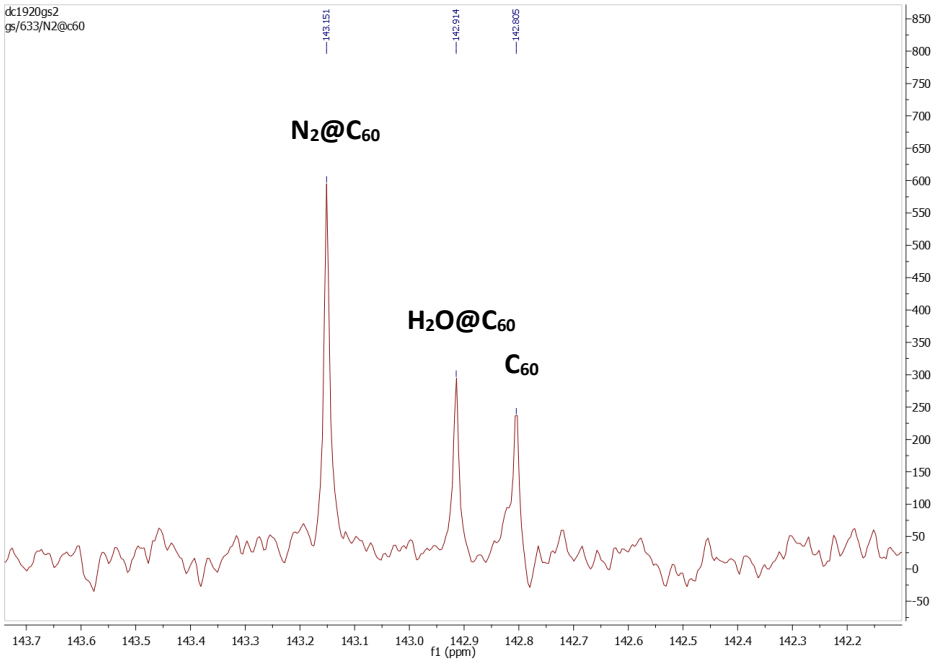


**Figure 40**. First $^{13}C$ NMR of the $N_2@C_{60}$.

In conclusion, the $N_2@C_{60}$ was prepared by the molecular surgery for the first time. The isolation of the $N_2@C_{60}$ from $H_2O@C_{60}$ was unsuccessful. The aim of this synthesis was to obtain molecule $N_2@43$ as this can be converted to $N_2@C_{60}$ by the known routes. Two options of inserting the $N_2$ into OCF were investigated: **89** and **45.** High losses of the material and low filling factors were observed when the **45** was used. **89** is currently considered as the best OCF derivate for the insertion of $N_2$.

Demonstrating that $N_2@C_{60}$ can be made a good indicator that this method will allow preparation of **$CO@C_{60}$**, **$CO_2@C_{60}$** and potentially **$O_2@C_{60}$**.

The study of the **$N_2@C_{60}$** synthesis was in the early stage and there is still a great room for investigation. Future work could cover several potential investigations:

- Thanks to the $^1$H NMR shift of the OCF containing $N_2$ molecules it would be straightforward to obtain good kinetic data of the $N_2$ escape from the **47** and the **89** and obtain experimental activation energies, enthalpies and entropies to compare them with the theoretical calculations.
- There is a great opportunity to prepare 100% **$N_2@C_{60}$**. Possible ways to achieve this could be via performing the filling of the **89** with $N_2$ at higher temperatures. Another option to remove endohedral water would be to introduce drying step (heating under vacuum) when performing ring contraction from **46** to **43,** followed by suturing the orifice with $PPh(Fu)_2$[180][108] at room temperature rather than $PPh_3$ at 120 °C.
- From the HPLC recycling chromatogram it is understood that the **$N_2@C_{60}$** and **$H_2O@C_{60}$** have very similar retention times, however, the **$N_2@C_{60}$** can be separated from the empty **$C_{60}$**. Suitable HPLC method development investigating solvent systems of toluene, and hexane could lead to successful separations of **$N_2@C_{60}$** and **$H_2O@C_{60}$**.
- $^{15}$N NMR of **$N_2@C_{60}$** could be obtained when sufficient amount of **$N_2@C_{60}$**is prepared.

# Conclusions

- Synthesis of an important precursor diketone **42** was optimised, the safety risks were mitigated, and yield of the reaction was increased to 60-70% with good recovery method of unreacted starting material.
- Closure of the **42** to **$C_{60}$** was investigated and a reliable, repetitive yield 50% was obtained to over two steps (from diketone **43**).
- A new by-product **92** was identified and fully characterised.
- The encapsulations of He atom, $H_2$ molecule and their isotopes into diketone **43** were improved (50% for He@$C_{60}$ 93% for $H_2$@$C_{60}$) by performing the filling step into solid ylid **88** with simultaneous closure allowing preparation of suitable quantities for further experiments. Investigation of closure of **88** to **43** by intramolecular Wittig reaction was conducted by collecting kinetic data.
- **Ne@$C_{60}$** was prepared for the first time by molecular surgery. Two paths were investigated and in-situ closure method by filling to ylid **88** was successful. **Ne@$C_{60}$** was enriched to >99% on preparative HPLC and the crystal structure was obtained.
- Closure step of 17-membered ring orifice sulfoxide **89** to hemiacetal **46** was investigated, a new by-product **99** was discovered and fully characterised. It was discovered that the closure step is viable at lower temperature however with very low yield.
- Kr atom was inserted in the sulfide **47** in >99% filing factor for the first time. Kinetics of the escape rate of the Kr from the **47** were measured. **Kr@$C_{60}$** was isolated in >99% filling factor and the crystal structure was obtained. It was discovered that Kr atom has a similar effect on the closure of the **89** to **46** as $CH_4$ most likely due to its large size.
- $N_2$ was inserted into the sulfoxide **89** for the first time in up to 75% filling factor. **$N_2$@$C_{60}$** was then prepared in 58% filling factor as a mixture with **$H_2O$@$C_{60}$** and empty **$C_{60}$** and $^{13}C$ NMR of **$N_2$@$C_{60}$** was measured for the first time.

# 8 Experimental

## 8.1 General methods

Reactions were performed under $N_2$ atmosphere using standard Schlenk and syringe techniques (unless stated otherwise), except high-pressure filling reactions which were conducted under an atmosphere of Ne, $^3$He, $^4$He, $H_2$, $D_2$, HD, Ar, $CH_4$ and Kr at the pressure stated in the filling reaction procedure, using the compression apparatus in **Figure 20**. All glassware was dried overnight in an oven (160 °C) and cooled in a desiccator over silica granules or assembled while still warm. Monitoring of the reactions was done by TLC (Merck silica gel 60 F254 plates) and/or by analytical HPLC (Cosmosil™ Buckyprep, 326 nm detection). Separations were performed using flash column chromatography, with silica gel (Merck Geduran Si60, 40–63 μm) as the stationary phase. Toluene and THF were distilled from sodium benzophenone ketal, acetonitrile (HPLC grade) from $CaH_2$, 1-chloronaphthalene (≥85%, technical grade) over molecular sieves under reduced pressure. Other solvents were used directly from the contained bottles from the suppliers. Solutions of 1-chloronaphthalene were degassed under dynamic vacuum (0.2–0.4 mm Hg) until evolution of gas stopped. $P(O^iPr)_3$ was distilled under reduced pressure from $CaH_2$ and stored in a sealed flask over $CaH_2$ under $N_2$. All other solvents and reagents were used directly from the supplier without further purification. Kr, Ar, $^4$He, Ne, $H_2$, and $D_2$ were CP quality gases from BOC. $^3$He was >99.9 atom%, 99.999% pure gas from BOC. HD was >97% D from Cambridge Isotopes Ltd.

NMR spectra were recorded on following spectrometers: Bruker AVII400 FT-NMR, AVIIIHD500 FT-NMR spectrometer, Bruker Ascend 700 NB magnet with Bruker AVANCE NEO console in the indicated solvent at 298 K. $^{13}$C and $^1$H chemical shifts in NMR are reported in ppm. $^{13}$C NMR spectra were $^1$H decoupled and are referenced to $CDCl_3$ at $\delta_C$ = 77.160 ppm (centre of the 1:1:1 triplet) and 1,2-dichlorobenzene-$d_4$ at $\delta_C$ = 127.19 ppm (centre of the 1:1:1 of the lower shifted triplet). The solvent chemical shift is referenced to TMS ($\delta_C$ = 0.00 ppm). $^1$H NMR spectra collected in 1,2-dichlorobenzene-$d_4$ are referenced to residual solvent at $\delta_H$ = 6.93 ppm (the lower shift peak); and this solvent chemical shift is referenced to TMS ($\delta_H$ = 0.00 ppm). The following abbreviations are used to assign multiplicity and may be compounded: s = singlet, d = doublet, t = triplet, q = quartet and m = multiplet. Coupling constants, *J*, are measured in Hertz (Hz). The confidence limits of the absolute chemical shift are dominated by the chemical shift of reference solvents, reported to 2 d.p. for $^1$H NMR and $^{13}$C NMR. Dimethyldioxirane (DMDO) was prepared according to the literature procedure.[206] High resolution positive ion atmospheric pressure photoionisation mass spectra were recorded using a solariX (Bruker Daltonics, Bremen, Germany) mass spectrometer equipped with a 4.7 T magnet

and FT-ICR cell. Samples were introduced to the mass spectrometer using a syringe driver at a flow rate of 5 µL/min. High resolution positive ion electrospray ionisation mass spectra were recorded using a MaXis time of flight (TOF) mass spectrometer (Bruker Daltonics, Bremen, Germany). Samples were introduced to the mass spectrometer using a syringe driver at a flow rate of 5 µL/min.

## 8.2 Synthesis of precursors

### 8.2.1 Synthesis of 2-bromo-6-(*tert*-butyl)pyridine

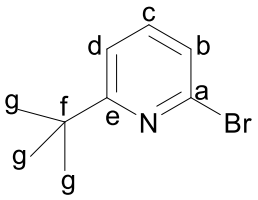


$C_9H_{12}BrN$ (214.11)

2,6-Dibromopyridine (30.0 g, 127 mmol) and copper(I) iodide (7.28 g, 38.2 mmol) were suspended in distilled THF (140 ml) under $N_2$ atmosphere. The suspension was cooled inside a liquid $N_2$/acetone bath to –40 °C and *t*-butylmagnesium chloride (1.7 M in THF, 111 mL, 190 mmol) was slowly added during 1 h. The reaction mixture was stirred for 19 hours at room temperature. The reaction mixture was filtered over celite® and concentrated to remove the bulk of the THF. Aqueous ammonia solution (35% $NH_3$, 100 mL) was added, and after stirring in air for 10 min the organic phase was extracted with $Et_2O$ (2 × 250 mL). The combined organic phases were dried over $MgSO_4$ and concentrated to obtain a dark brown oil which was purified by Kugelrohr distillation (100 °C, vacuum unknown) to obtain colourless oil (21.2 g, 99.0 mmol, 78% yield).

**$^1$H NMR**: (400 MHz, $CDCl_3$), δ): 7.43 (t, *J* = 7.9 Hz, 1H, Hc), 7.26-7.22 (m, 2H, Hb and Hd), 1.33 (s, 9H, *t*-butyl, Hg).

Followed reported procedure. Spectral data was consistent with the reported literature. [136]

### 8.2.2 3,6-bis(6-(*tert*-Butyl)pyridin-2-yl)pyridazine

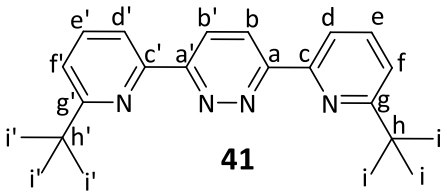


$C_{22}H_{26}N_4$ (346.48)

2-bromo-6-(*tert*-butyl)pyridine (20.0 g, 93.4 mmol) was dissolved in distilled THF (68 mL) under $N_2$ atmosphere. The reaction mixture was cooled in a liquid $N_2$/acetone bath to -80 °C, then *n*-butyllithium (2.5 M in hexanes, 41.0 mL, 102 mmol) was slowly added (35 min) keeping the reaction in -80 °C. A 1.0 M solution of anhydrous $ZnCl_2$ in distilled THF (140 mL, 140 mmol) was added in 10 min in –80 °C. The solution was allowed to warm up to room temperature and then stirred for 30 min. 3,6-Dichloropyridazine (4.70 g, 30.8 mmol) and $Pd(PPh_3)_4$ (1.8 g, 1.2 mmol) were added and the reaction mixture was refluxed for 15 h. The reaction mixture

was quenched with saturated $NaHCO_3$ (300 mL) and the two layers were separated. The aqueous layer was extracted with dichloromethane (500 mL) and MeOH (100 mL) was added to help with the separation of the layers. The combined organic extracts were dried over $MgSO_4$, filtered, and evaporated to dryness to obtain brown oil. The crude product was purified by flash column chromatography over silica gel (eluent 10% EtOAc in hexanes). The fractions containing the spot located at $R_f$ 0.27 (eluent: 10% EtOAc in hexanes) were collected and evaporated to yield 3,6-bis(6-(*tert*-butyl)pyridin-2-yl)pyridazine **91** as an off white solid (7.88 g, 22.7 mmol, 74%).

**$^1$H NMR:** (400 MHz, $CDCl_3$, δ): 8.77 (s, 2H, Hb), 8.56 (dd, *J* = 7.8, 0.8 Hz, 2H, Hd), 7.81 (t, *J* = 7.9 Hz, 2H, He), 7.44 (d, *J* = 7.8, 0.8 Hz, Hf), 1.45 (s, 18H, t-butyl, Hi).

Minor modification of reported procedure. Spectral data was consistent with the reported literature.[189]

## 8.3 Optimised procedure for synthesis of 43

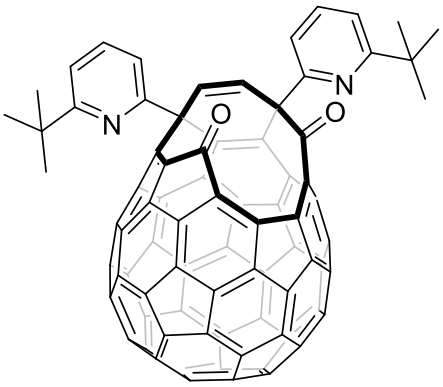


**43**

$C_{82}H_{26}N_2O_2$ (1071.12)

A solution of $C_{60}$ (6.82 g, 9.47 mmol) and 3,6-bis(6-(*tert*-butyl)pyridin-2-yl)pyridazine (1.62 g, 4.68 mmol) in 1-chloronaphthalene (200 mL) was degassed under dynamic vacuum (approx. 0.2 mm Hg) and sonication in 1 L r.b.f. The solution was then warmed to reflux in an iso-mantle for 42 h under $N_2$, connected to an oil-bubbler to ensure pressure release. It was then cooled to room temperature and diluted with toluene (150 mL). This mixture was transferred to a jacketed photo reactor (**Figure 41**) and the water-cooled solution was irradiated with a high-pressure Na lamp (400 W), placed in the middle of the reactor at an approximate distance of 2 cm from the solution, bubbling oxygen at a continuous flow rate of approx. 20 mL $min^{-1}$ for 1 h. The reaction mixture was then diluted with hexane (200 mL) and poured directly over a silica column (7 cm diameter column, 600 mL of $SiO_2$) packed with hexane:toluene (1:1). Using an eluent gradient of hexane:toluene (1:1) → 100% toluene, a purple band containing unreacted $C_{60}$ and 1-chloronaphthalene was first collected. From quantitative HPLC assay, the amount of recovered $C_{60}$ was calculated to be

**Figure 41.** Purpose-built Jacketed photoreactor.

4.06 g (60%), and the quantity of $C_{60}$ not recovered was 2.76 g (3.83 mmol). Solvents were removed by vacuum distillation and residual $C_{60}$ was washed with $Et_2O$ (3 × 30 mL) before drying *in vacuo* to give 4.566 g. Recovered $C_{60}$ was of sufficient purity (~90% by HPLC) to be used in a repeat reaction. A second band containing material with $R_f$ = 0.5 in toluene was collected, and removal of solvents *in vacuo* gave open-fullerene **43** as a brown powder (2.85 g, 2.66 mmol, 69% based on $C_{60}$ consumption).

**$^1$H NMR** (400 MHz, $CDCl_3$) δ 7.68 (t, *J* = 7.9 Hz, 1H, pyridyl), 7.65 (t, *J* = 7.8 Hz, 1H, pyridyl), 7.51 (dd, *J* = 7.8, 0.7 Hz, 1H, pyridyl), 7.38 (dd, *J* = 7.8, 0.8 Hz, 1H, pyridyl), 7.23 (d, *J* = 7.9 Hz, 1H, pyridyl), 7.23 (d, *J* = 7.9 Hz, 1H, pyridyl), 7.19 (d, *J* = 10.0 Hz, 1H, alkenyl), 7.17 (d, *J* = 10.0 Hz, 1H), 1.26 (s, 9H, *t*-butyl), 1.18 (s, 9H, *t*-butyl).

**$^{13}$C NMR** (125 MHz, $CDCl_3$) δ 200.406, 192.311, 169.199, 168.850, 165.408, 162.206, 154.753, 150.084, 148.835, 147.948, 147.916, 147.752, 147.433, 146.976, 146.642, 146.624, 146.528, 146.355, 146.171, 146.161, 146.137, 145.984, 145.928, 145.897, 145.775, 145.638, 145.444, 145.172, 145.145, 144.746, 144.737, 144.385, 144.312, 144.041, 143.042, 142.709, 142.541, 142.254, 142.063, 141.939, 141.761, 141.116, 140.758, 140.725, 140.568, 140.203, 140.148, 139.987, 139.695, 139.572, 139.487, 138.794, 138.528, 138.477, 137.477, 137.446, 137.208, 136.432, 136.215, 135.862, 134.968, 133.826, 132.922, 132.875, 132.661, 132.510, 131.701, 129.836, 120.094, 119.690, 117.698, 116.913, 61.099, 54.915, 37.929, 37.835, 30.085, 30.068.

**HRMS (ESI+)** (*m/z*): Calculated for $[C_{82}H_{27}N_2O_2]^+$ 1071. 2107, found 1071.2060.

Spectral data was consistent with the reported literature.[136]

## 8.4 46

Compound **43** (1.90 g, 1.77 mmol) was dissolved in distilled THF (140 ml) under $N_2$ atmosphere. *N*-methylmorpholine-*N*-oxide (624 mg, 4.08 mmol) was added followed by degassed $H_2O$ (0.31 mL, 1.21 mmol). The reaction mixture was stirred at room temperature for 15 h. Silica gel (40 mL) was added and the mixture was evaporated to dryness to afford a black powder compound absorbed onto silica. This material was dry loaded on a chromatography column (300 mL of silica gel, 7 cm diameter column) packed with 100% toluene and gradually eluted to 90:8:2 toluene:EtOAc:AcOH). The fractions containing the spot located at $R_f$ 0.21 (90:8:2

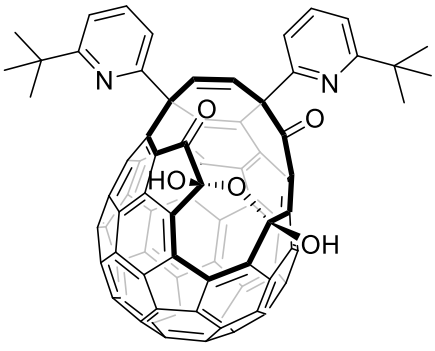


**46**
$C_{82}H_{28}N_2O_5$ (1121.14)

toluene:EtOAc:AcOH) were collected and evaporated to afford compound **46** as a black solid (1.69 g, 1.51 mmol, 85%).

**$^1$H NMR**: (400 MHz, $CDCl_3$, δ): 7.64 (t, *J* = 7.9 Hz, 1H, pyridyl), 7.57 (t, *J* = 7.8 Hz, 1H), 7.44 (d, *J* = 7.8 Hz, 1H, pyridyl), 7.26 – 7.15 (m, 3H, pyridyl) (overlapping with toluene), 7.09 (d, *J* = 10.2 Hz, 1H, alkenyl), 6.94 (d, *J* = 10.1 Hz, 1H, alkenyl), 5.42 (s, 1H, hydroxyl), 5.34 (s, 1H, hydroxyl), 1.24 (s, 9H, *t*-butyl), 1.18 (s, 9H, *t*-butyl).

**HRMS (ESI+)** (*m/z*): Calculated for $[C_{82}H_{29}N_2O_5]^+$ 1121.2076, found 1121.2037.

Modification of reported procedure. Spectral data was consistent with the reported literature.[136]

## 8.5 45

Procedure 1

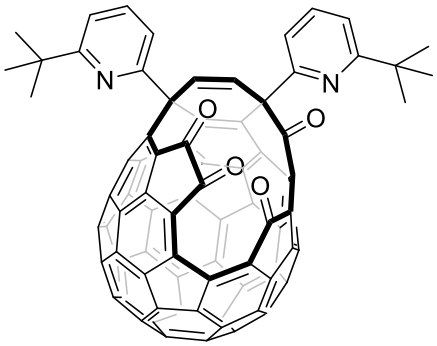


**45**
$C_{82}H_{26}N_2O_4$ (1103.12)

Compound **46** (0.66 g, 0.05 mmol) was placed inside Schlenk flask. The flask was connected to a 5 mL dropping funnel with a pressure regulating arm. The funnel was completely filled with 3 Å activated molecular sieves. The top of the dropping funnel was connected to a straight condenser linked to a vacuum/ $N_2$ inlet. The system was put under $N_2$ atmosphere and then toluene (20 mL) was added. The apparatus was placed inside an oil bath heated to 120 °C, and the tap of the dropping funnel was closed so that the solvent vapours could start refluxing through the pressure regulating arm and then condense and accumulate inside the dropping funnel. The tap was turned on and the system was refluxed for 2 h. The reaction mixture was allowed to cool down to room temperature. The solution was transferred to a distillation apparatus under $N_2$ atmosphere. The solvent was distilled off under $N_2$ to afford compound **45** as a black solid (66 mg, 0.05 mmol, quant. yield).

Procedure 2

Compound **46** (1.22 g, 1.09 mmol) was placed into Schlenk flask. The flask was put under high vacuum (0.2 mm/Hg) and heated to 130 °C for 16 h. (1.21 g, 1.09 mmol, quant. yield).

**$^1$H NMR** (400 MHz, $CDCl_3$) δ 7.64 (t, *J* = 7.9 Hz, 1H, pyridyl), 7.58 (t, *J* = 7.8 Hz, 1H, pyridyl), 7.41 (d, *J* = 7.8, 1H, pyridyl), 7.25 (d, *J* = 10.2 Hz, 1H, alkenyl), 7.22 (d, *J* = 7.8 Hz, 2H, pyridyl), 7.18 (d, *J* = 7.9 Hz, 1H, pyridyl), 6.99 (d, *J* = 10.2 Hz, 1H, alkenyl), 1.19 (s, 9H, *t*-butyl), 1.15 (s, 9H, *t*-butyl).

**HRMS (ESI+)**(*m/z*): Calculated for $[C_{82}H_{27}N_2O_4]^+$ 1103.1965., found 1103.1978.

Followed reported procedure.[180] Spectral data was consistent with the reported literature.[136]

## 8.6 88

Compound **46** (5.30 g, 4.72 mmol) and triphenylphosphine (19.8 g, 75.6 mmol) were placed inside Schlenk flask under $N_2$ atmosphere. Distilled toluene (300 mL) was added, and the solution was heated to 55 °C for 63 h. The solution was concentrated under reduced pressure and then purified by flash column chromatography over silica gel (eluent gradient: toluene to 20% EtOAc in toluene). The fractions containing the spot running at $R_f$ 0.16 (eluent: toluene) were collected and evaporated to afford compound **88** as a dark green solid (5.40 g, 3.99 mmol, 85%).

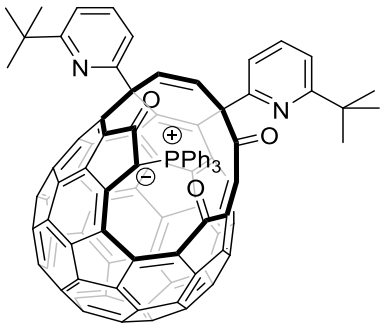


**88**
$C_{100}H_{42}N_2O_3P$ (1350.42)

**$^1$H NMR** (400 MHz, $CDCl_3$, δ): 8.60 – 8.35 (m, 2 H, phenyl), 8.25 – 8.10 (m, 2 H, phenyl), 8.05 – 7.95 (m, 2 H, phenyl), 7.95 – 7.85 (m, 1 H, phenyl), 7.85 – 7.70 (m, 2 H, phenyl), 7.70 – 7.48 (m, 4 H, phenyl), 7.57 – 7.50 (m, 2H, pyridyl), 7.47 – 7.34 (m, 3 H, phenyl and pyridyl), 7.37 – 7.33 (m, 1H, pyridyl), 7.29 – 7.27 (m, 1H alkenyl (overlapping with $CDCl_3$)), 7.17 (d, *J* = 7.7 Hz, 1H, pyridyl), 7.12 (d, *J* = 7.8 Hz, 1H, pyridyl), 6.93 (d, *J* = 10.2 Hz, 1H alkenyl), 1.21(s, 9H, *t*-butyl), 1.15 (s, 9H, *t*-butyl).

Modification of reported procedure. Spectral data was consistent with the reported literature.[42]

## 8.7 Tetrakis(dimethylamino)ethylene (TDAE)

Tris(dimethylamino)methane (5.96 mL, 3.44 mmol) was refluxed at 190 °C under mild $N_2$ pressure for 60 h. After this time the product was obtained by short path vacuum distillation (0.4 mm/Hg) at 50 °C as light yellow oil (3.90 mL, 49%).

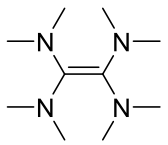


$C_{10}H_{24}N_4$ (200.33)

**$^1$H NMR** (400 MHz, $CDCl_3$, δ): 2.69 (s, 24H).

Followed reported procedure. Spectral data was consistent with the reported literature.[207]

## 8.8 47

Stirring solution of compound **45** (1.22 g, 1.10 mmol) and elemental sulphur ($S_8$) (284 mg, 1.10 mmol) in freshly distilled *o*-DCB (70 mL) was heated to 180 °C under $N_2$ atmosphere for 30 min. TDAE (50 µl, 0.21 mmol) was added quickly at this temperature and reaction was stirred for 15 min before cooling in ice bath. *o*-DCB was distilled at reduced pressure (0.4 mm/Hg, 50 °C). Product was purified by column chromatography. $SiO_2$ eluted with 2% EtOAc in toluene then gradually increased to 5% EtOAc in toluene. Fractions at $R_f$ 0.2 (5% EtOAc in toluene) were collected and concentrated to obtain dark red powder (850 mg, 0.75 mmol, 68% yield).

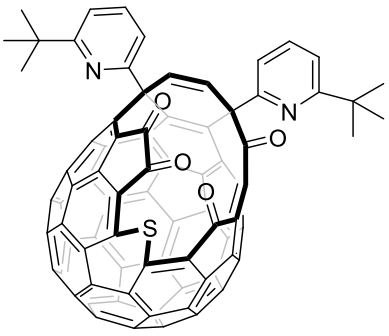


**47**
$C_{82}H_{26}N_2O_4S$ (1135.18)

**$^1$H NMR** (400 MHz, $CDCl_3$) δ: 7.60 (t, *J* = 7.8 Hz, 1H, pyridyl), 7.50 (t, *J* = 7.9 Hz, 1H, pyridyl), 7.22 (d, *J* = 7.8 Hz, 1H, pyridyl) 7.22 (d, *J* = 7.8 Hz, 1H, pyridyl), 7.12 (d, *J* = 7.9 Hz, 1H, pyridyl), 7.09 (d, *J* = 7.9, 1H, pyridyl), 7.04 (d, *J* = 10.3 Hz, 1H, alkenyl), 6.50 (d, *J* = 10.3 Hz, 1H, alkenyl), 1.21 (s, 9H, *t*-butyl), 1.08 (s, 9H, *t*-butyl).

**HRMS (ESI+)** (*m/z*): Calculated for $[C_{82}H_{27}N_2O_4S]^+$ 1135.1686, found 1135.1673.

Followed reported procedure. Spectral data was consistent with the reported literature.[138]

## 8.9 Synthesis of dimethyldioxirane

To a stirring solution of distilled $H_2O$ (46.5 mL) and $NaHCO_3$ (10 g) at 0 °C, Oxone (22 g) was added in two portions in 5 min interval. After stirring for 5 min, system was put under mild vacuum (10 Torr) and DMDO was distilled into a flask cooled to –78 °C. 7 mL of transparent liquid was obtained and after titration with methyl-p-tolyl sulphide the concentration was determined to be 102.4 mM (3% yield).


Dimethyldioxirane
$C_3H_6O_2$ (74.08)

Consistent with reported literature.[206]

## 8.10 89

To a stirring solution of **47** (1.70 g, 1.49 mmol) in toluene (150 mL) at 0 °C, was added dimethyldioxirane (20.1 mL of a 95.7 mM solution in acetone, 2.01 mmol) rapidly using an ice-chilled syringe. The resulting mixture was stirred at 0 °C for 5 min before removal of the cooling bath and stirring for 1.75 h, during which time the mixture warmed to room temperature. Solvents were removed *in vacuo* to give the title compound as a crude brown powder (1.71 g, 1.47 mmol, 99%) that was used directly in the next step without purification.

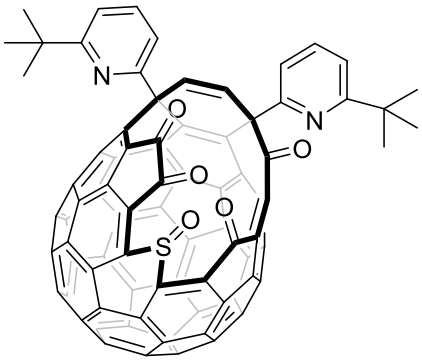

**89**
$C_{82}H_{26}N_2O_5S$ (1151.18)

**$^1$H NMR** (400 MHz, $CDCl_3$) δ: 7.61 (t, *J* = 7.6 Hz, 1H, pyridyl), 7.60 (t, *J* = 7.9 Hz, 1H, pyridyl), 7.26 (d, *J* = 7.8 Hz pyridyl, 1H), 7.26 (d, *J* = 7.8 Hz pyridyl, 1H), 7.22 (d, *J* = 7.8 Hz, 1H, pyridyl), 7.18 (d, *J* = 7.2 Hz, 1H, pyridyl), 6.75 (d, *J* = 10.3 Hz, 1H, alkenyl), 1.18 (s, 9H, *t*-butyl), 1.14 (s, 9H, *t*-butyl).

**HRMS (ESI+)** (*m/z*): Calculated for $[C_{82}H_{27}N_2O_5S]^+$ 1151.1635, found 1151.1618.

Spectral data was consistent with the reported literature.[187]

## 8.11 92

Compound **42** (50 mg, 0.048 mmol) and N-phenyl maleimide (33 mg, 0.19 mmol) were placed inside a Schlenk flask under $N_2$ atmosphere. Distilled 1-chloronaphthalene (5 mL) was added. The solution was degassed, the system was put under $N_2$ atmosphere and sealed. The reaction mixture was heated to 300 °C for 18 h. The reaction mixture was allowed to cool down to room temperature and poured over a silica column packed with toluene. The column was eluted with toluene to collect a red band ($R_f$: 0.38, 4:1 Hex:EtOAc). This solution was concentrated under reduced pressure and evaporated to dryness to afford **92** as a red solid (10 mg, 17% yield).

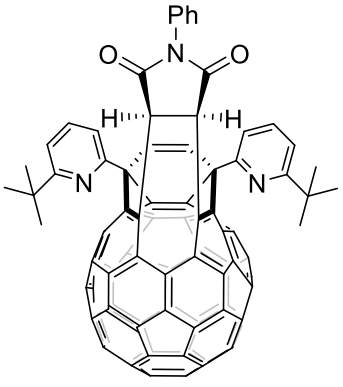

**92**
$C_{92}H_{33}N_3O_2$ (1212.30)

**$^1$H NMR** (400 MHz, $CDCl_3$) δ 7.75 (t, *J* = 7.8 Hz, 2H, pyridyl), 7.63 (dd, *J* = 7.7, 0.7 Hz, 2H, pyridyl), 7.51 – 7.36 (m, 3H, phenyl), 7.31 (dd, *J* = 7.8, 0.6 Hz, 2H pyridyl), 7.29 – 7.27 (m, 2H, phenyl), 6.98 (s, 2H alkenyl), 5.57 (s, 2H, alkanyl), 1.33 (s, 18H, *t*-butyl).

**$^{13}$C NMR** (126 MHz, $CDCl_3$) δ 174.66, 168.00, 163.39, 146.28, 146.14, 146.09, 145.60, 145.00, 144.75, 144.19, 144.13, 144.00, 143.92, 143.80, 143.69, 141.33, 141.00, 139.93, 139.75, 138.74, 138.65, 137.50, 137.09, 136.44, 136.31, 136.08, 134.21, 133.57, 133.20, 131.17, 130.76, 130.54, 129.93, 128.46, 128.25, 128.14, 127.98, 125.48, 125.06, 119.04, 116.18, 56.85, 52.79, 36.77, 28.95.

**HRMS (APPI)** (*m/z*): Calculated for $[C_{92}H_{33}N_3O_2]^{+\bullet}$ 1211.2567, found 1211.2529.

**IR:** $V_{max}$ / $cm^{-1}$ : 2955, 1718, 1571, 1372, 747, 532.

## 8.12 A@47

### 8.12.1 $CH_4$@47

A steel filling bomb was charged with powdered open-fullerene **47** (967 mg, 0.851 mmol) and loose plugged with glass wool. The bomb was connected to the purpose-built filling apparatus and heated under a dynamic vacuum (0.4 mm Hg) at 170 °C for 30 min in order to remove endohedral water from the compound **47**. After cooling to room temperature during 30 min, the reactor was charged with $CH_4$ gas to 1005 atm. using Sitec 750.01 hand-operated pressure intensifying syringe (1000 bar working pressure, 30 mL capacity). The reactor was then heated to 190 °C and maintained at this temperature for 18 h, with a stable internal pressure of ~1645 atm during this time, before cooling to room temperature and slow release of the pressure. The title compound was obtained as a dark red/brown solid (967 mg, 0.839 mmol, 99%). >90% $CH_4$ filling was estimated from the $^1$H NMR.

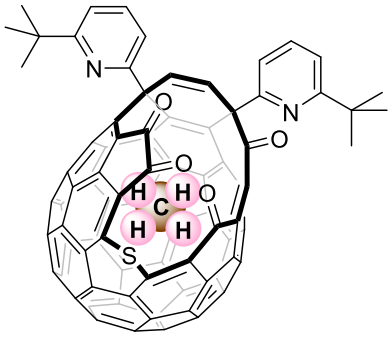


**$CH_4$@47**
$C_{83}H_{30}N_2O_4S$ (1151.22)

**$^1$H NMR** (400 MHz, $CDCl_3$) δ 7.60 (t, *J* = 7.8 Hz, 1H, pyridyl), 7.51 (t, *J* = 7.9 Hz, 1H, pyridyl), 7.22 (dd, *J* = 7.8, 1.1 Hz, 2H, pyridyl), 7.11 (dd, *J* = 7.9, 0.7 Hz, 1H, pyridyl), 7.09 (dd, *J* = 7.9, 0.8 Hz, 1H, pyridyl), 7.03 (d, *J* = 10.3 Hz, 1H, alkenyl), 6.50 (d, *J* = 10.3 Hz, 1H, alkenyl), 1.21 (s, 9H, *t*-butyl), 1.09 (s, 9H, *t*-butyl), -12.40 (s, 4H, $CH_4$).

**HRMS (ESI+)** (*m/z*): Calculated for $[C_{83}H_{31}N_2O_4S]^+$ 1151.1999, found 1151.1992.

Spectral was data consistent with the reported literature.[180]

## 8.12.2 Ar@47

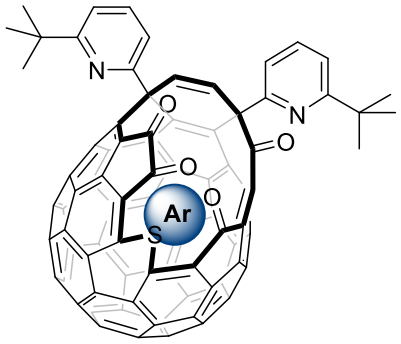


**Ar@47**
$C_{82}H_{26}N_2O_4SAr$ (1175.13)

A steel filling bomb was charged with powdered open-fullerene **47** (400 mg, 0.352 mmol) and loose plugged with glass wool. The bomb was connected to the purpose-built filling apparatus and heated under a dynamic vacuum (0.4 mm Hg) at 160 °C for 1 h in order to remove endohedral water from the compound **47**. After cooling to room temperature, the reactor was charged with Ar gas to 1000 atm using Sitec 750.01 hand-operated pressure intensifying syringe (1000 bar working pressure, 30 mL capacity). The reactor was then heated to 200 °C and maintained at this temperature for 18 h, with a stable internal pressure of 1584 atm during this time, before cooling to room temperature and slow release of the pressure. The powder was dissolved in toluene and purified by column chromatography in 5% AcOH in toluene. The fractions collected at $R_f$ 0.17 (eluent 5% AcOH in toluene) were concentrated. The title compound was obtained as a dark red/brown solid (380 mg, 0.323 mmol, 92%). >99% Ar filling was estimated from the $^1$H NMR by no presence of endohedral water peak.

**$^1$H NMR** (400 MHz, $CDCl_3$) δ 7.60 (t, *J* = 7.8 Hz, 1H, pyridyl), 7.50 (t, *J* = 7.9 Hz, 1H, pyridyl), 7.22 (dd, *J* = 7.8, 0.6 Hz, 2H, pyridyl), 7.12 (dd, *J* = 7.9, 0.8 Hz, 1H, pyridyl), 7.09 (dd, *J* = 7.9, 0.8 Hz, 1H, pyridyl), 7.04 (d, *J* = 10.3 Hz, 1H, alkenyl), 6.50 (d, *J* = 10.3 Hz, 1H, alkenyl), 1.21 (s, 9H, *t*-butyl), 1.09 (s, 9H, *t*-butyl).

**HRMS (ESI+)** (*m/z*): Calculated for $[C_{82}H_{27}N_2O_4SAr]^+$ 1175.1310, found 1175.1306.

Followed reported procedure. Spectral data was consistent with the reported literature.[184]

## 8.12.3 Kr@47

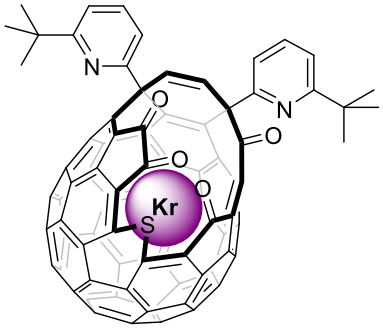


**Kr@47**
$C_{82}H_{26}N_2O_4SKr$ (1219.08)

A steel filling bomb was charged with powdered open-fullerene **47** (721 mg, 0.591 mmol) and loose plugged with glass wool. The bomb was connected to the purpose-built filling apparatus and heated under a dynamic vacuum (0.2 mm Hg) at 170 °C for 50 min in order to remove endohedral water from the compound **47**. After cooling to room temperature, the reactor was charged with krypton gas to 45 atm before compressing to 961 atm using two Sitec 750.01 hand-operated pressure intensifying syringes (1000

bar working pressure, 30 mL capacity). The reactor was then heated to 177 °C and maintained at this temperature for 14 h, with a stable internal pressure of 1496 atm during this time, before cooling to room temperature and slow release of the pressure. The title compound was obtained as a dark red/brown solid (721 mg, quant). >99% Krypton filling was estimated from the $^{1}$H NMR, ESI+ high resolution mass spectrum and from the $^{13}$C NMR of the final compound Kr@$C_{60}$ (**8.15.9**).

**$^{1}$H NMR** (400 MHz, $CDCl_3$) δ δ 7.60 (t, *J* = 7.8 Hz, 1H, pyridyl), 7.51 (t, *J* = 7.9 Hz, 1H, pyridyl), 7.22 (d, *J* = 8.3 Hz, 2H, pyridyl), 7.12 (dd, *J* = 7.9, 0.7 Hz, 1H, pyridyl), 7.10 (dd, *J*= 7.9, 0.7 Hz, 1H, pyridyl), 7.04 (d, *J* = 10.3 Hz, 1H, alkenyl), 6.50 (d, *J* = 10.3 Hz, 1H, alkenyl), 1.21 (s, 10H, *t*-butyl), 1.09 (s, 10H, *t*-butyl).

**$^{13}$C NMR** (126 MHz, *o*-DCB-$d_4$) δ 190.65, 185.54, 182.41, 180.50, 168.41, 168.37, 163.94, 162.52, 155.95, 152.09, 150.92, 150.49, 150.00, 149.82, 149.61, 149.41, 149.40, 149.37, 149.16, 149.06, 148.85, 148.75, 148.65, 147.12, 146.06, 145.80, 145.38, 145.01, 144.86, 144.78, 144.67, 144.28, 144.26, 143.18, 143.08, 142.31, 141.99, 141.52, 141.10, 141.01, 140.57, 139.37, 139.20, 138.39, 138.00, 137.91, 137.78, 137.56, 137.51, 137.48, 137.48, 137.22, 136.67, 136.55, 136.39, 136.33, 136.22, 134.58, 133.25, 132.95, 132.69, 131.58, 131.34, 131.11, 129.09, 128.45, 128.28, 126.39, 125.83, 125.40, 120.05, 119.81, 117.25, 117.20, 59.75, 54.68, 37.59, 37.48, 29.91, 29.75. Two overlapping resonances are not reported.

**HRMS (ESI+)** (*m/z*): Calculated for $[C_{82}H_{27}N_2O_4SKr]^+$ 1219.0815, found 1219.0788.

**IR:** $V_{max}$ / $cm^{-1}$ 2951, 1734, 1568, 1436, 747, 561.

## 8.13 A@89

### 8.13.1 $CH_4$@89

To a stirring solution of **$CH_4$@47** (403 mg, 0.349 mmol) in toluene (40 mL) at 0 °C was added dimethyldioxirane (9.6 mL, 0.52 mmol of a 54 mM solution in acetone) rapidly using an ice-chilled syringe. The resulting mixture was stirred at 0 °C for 5 min before removal of the cooling bath and stirring for 2 h, during which time the mixture warmed to room temperature. Solvents were removed *in vacuo* to give the title compound as a crude brown powder (402 mg, 0.345 mmol, 99%) that was used directly in the next step without purification.

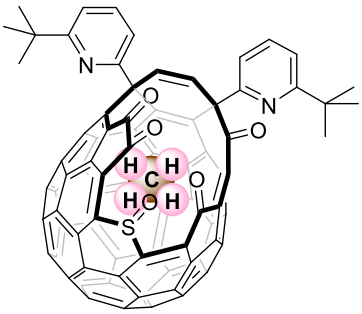


**$CH_4$@89**
$C_{83}H_{30}N_2O_5S$ (1167.23)

**$^1$H NMR** (400 MHz, $CDCl_3$): δ 7.62 (t, *J* = 7.9 Hz, 1H, pyridyl), 7.60 (s, *J* = 7.9 Hz, 1H, pyridyl), 7.29 – 7.15 (m, 5H 4 × pyridyl and 1 × alkenyl overlapping with residual toluene), 6.75 (d, *J* = 10.2 Hz, 1H, alkenyl), 1.19 (s, 9H, *t*-butyl), 1.15 (s, 9H, *t*-butyl), -11.20 (s, 4H, $CH_4$).

**HRMS (ESI+)** (*m/z*): Calculated for $[C_{83}H_{31}N_2O_5S]^+$ 1167.1948, found 1167.1946.

Spectral data was consistent with the reported literature.[180]

## 8.13.2 Ar@89

To a stirring solution of **Ar@47** (0.30 g, 0.26 mmol) in toluene (30 mL) at 0 °C was added dimethyldioxirane (10 mL, 0.61 mmol of a 61 mM solution in acetone) rapidly using an ice-chilled syringe. The resulting mixture was stirred at 0 °C for 30 min before removal of the cooling bath and stirring for 2.5 h, during which time the mixture warmed to room temperature. Solvents were removed *in vacuo* to give the title compound as a crude brown powder (0.30 g, 0.25, 96%*) that was used directly in the next step without purification.

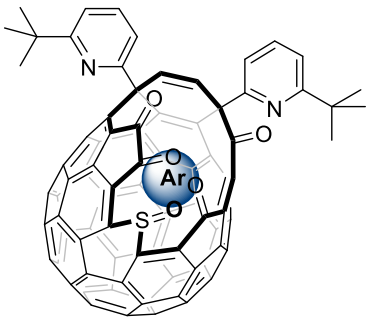


**Ar@89**
$C_{82}H_{26}N_2O_5SAr$ (1191.13)

*4% yield lost due to sampling.

**$^1$H NMR** (400 MHz, $CDCl_3$) δ 7.61 (t, *J* = 7.9, 1H, pyridyl), 7.60 (t, *J* = 7.9 Hz, 1H, pyridyl), 7.28 – 7.15 (m, 5H, 4 × pyridyl and 1× alkenyl overlapping with residual toluene), 6.75 (d, *J* = 10.2 Hz, 1H, alkenyl), 1.18 (s, 9H, *t*-butyl), 1.15 (s, 9H, *t*-butyl).

**HRMS (ESI+)** (*m/z*): Calculated for $[C_{82}H_{27}N_2O_5SAr]^+$ 1191.1259, found 1191.1255.

Followed reported procedure except larger excess of DMDO added (2.4 eq instead of 1.5 eq). It did not have a negative effect on the reaction. Spectral data was consistent with the reported literature.[184]

## 8.13.3 Kr@89

To a stirring solution of **Kr@47** (710 mg, 0.582 mmol) in toluene (70 mL) at 0 °C was added dimethyldioxirane (16 mL, 0.98 mmol of a 61 mM solution in acetone) rapidly using an ice-chilled syringe. The resulting mixture was stirred at 0 °C for 30 min before removal of the cooling bath and stirring for 2 h, during which time the mixture warmed to room temperature. Solvents were removed *in vacuo* to give the title compound as a crude brown powder (718 mg, 0.582 mmol, quant.) that was used directly in the next step without purification.

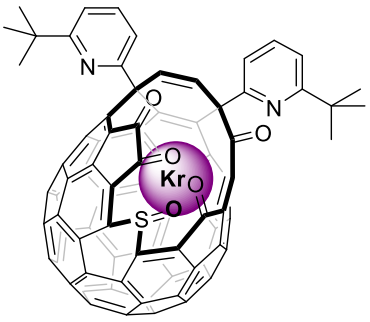


**Kr@89**
$C_{82}H_{26}N_2O_5SKr$ (1234.98)

**$^1$H NMR** (500 MHz, *o*-DCB-$d_4$) δ 7.47 (t, *J* = 7.9 Hz, 1H, pyridyl), 7.42 (t, *J* = 7.9 Hz, 1H, pyridyl), 7.23 (dd, *J* = 7.9, 0.8 Hz, 1H, pyridyl), 7.22 (dd, *J* = 7.9, 0.8 Hz, 1H, pyridyl), 7.17 (d, *J* = 10.3 Hz, 1H, alkenyl), 7.08 (dd, *J* = 7.9, 0.8 Hz, 1H, pyridyl), 6.98 (dd, *J* = 7.9, 0.8 Hz, 1H, pyridyl), 6.66 (d, *J* = 10.3 Hz, 1H, alkenyl), 1.21 (s, 9H, *t*-butyl), 1.12 (s, 9H, *t*-butyl).

**$^{13}$C NMR** (126 MHz, *o*-DCB-$d_4$) δ 190.74, 185.31, 183.76, 181.15, 168.60, 168.49, 163.72, 162.43, 156.90, 156.14, 151.14, 150.40, 150.18, 149.87, 149.73, 149.64, 149.41, 149.32, 149.20, 149.09, 148.93, 148.63, 148.24, 147.38, 147.27, 146.94, 146.86, 145.31, 145.20, 144.48, 143.74, 143.72, 143.70, 143.20, 143.17, 143.14, 142.79, 141.63, 141.16, 140.57, 139.78, 139.47, 138.73, 138.28, 137.80, 137.66, 137.60, 137.58, 137.53, 137.44, 137.35, 137.23, 137.18, 136.93, 136.87, 136.59, 134.87, 134.64, 133.63, 133.47, 132.88, 131.56, 131.37, 129.09, 128.49, 128.28, 127.67, 126.73, 126.02, 125.40, 120.14, 119.83, 117.52, 117.35, 59.75, 54.92, 37.59, 37.58, 29.88, 29.82. Two overlapping resonances are not reported.

**HRMS (ESI+)** (*m/z*): Calculated for $[C_{82}H_{27}N_2O_5SKr]^+$ 1235.0764, found 1235.0758.

**IR:** $V_{max}$ / $cm^{-1}$ 2961, 1738, 1568, 1441, 791.

## 8.13.4 $N_2$@89

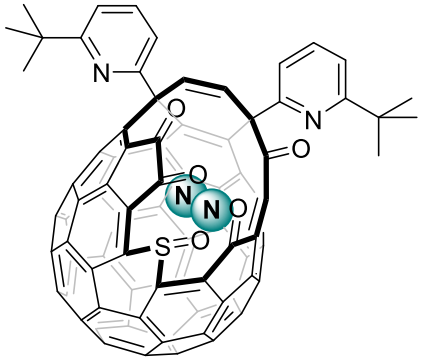


**$N_2$@89**
$C_{82}H_{26}N_4O_5S$ (1179.20)

A steel filling bomb was charged with powdered open-fullerene **89** (83 mg, 0.072 mmol) and loose plugged with glass wool. The bomb was connected to the purpose-built filling apparatus and heated under a dynamic vacuum (0.4 mm Hg) at 160 °C for 90 min in order to remove endohedral water from the compound **89**. After cooling to room temperature, the reactor was charged with $N_2$ gas to 1028 atm using Sitec 750.01 hand-operated pressure intensifying syringe (30 mL capacity). The reactor was then heated to 97 °C and maintained at this temperature for 15 h, with a stable internal pressure of 1224 atm during this time, before cooling to room temperature and slow release of the pressure. The title compound was obtained as a dark red/brown solid (83 mg, 0.070 mmol, 98%). 75% $N_2$ filling was estimated from the $^1$H NMR and the HRMS ESI+ spectra.

**$^1$H NMR** (400 MHz, $CDCl_3$) δ 7.62 (t, *J* = 7.8 Hz, 1H, pyridyl), 7.60 (t, *J* = 7.9 Hz, 1H, pyridyl), 7.27 (dd, *J* = 7.8, 0.8 Hz, 1H, pyridyl), 7.22 (dd, *J* = 7.8, 0.5 Hz, 2H pyridyl (two overlapping doublets)), 7.19 (d, *J* = 10.3 Hz, 1H, alkenyl), 7.18 (dd, *J*= 7.8, 0.8 Hz, 1H pyridyl), 6.75 (d, *J* = 10.2 Hz, 1H, alkenyl), 1.18 (s, 9H, *t*-butyl), 1.14 (s, 9H, *t*-butyl).

**$^{13}$C NMR** (126 MHz, $CDCl_3$) δ 190.87, 185.44, 184.01, 181.17, 168.97, 168.61, 163.37, 162.04, 156.45, 156.16, 151.12, 150.92, 150.87, 150.56, 150.52, 150.23, 150.05, 150.05, 149.97, 149.84, 149.63, 149.32, 149.01, 148.01, 147.65, 147.58, 147.15, 145.57, 145.39, 144.93, 144.28, 144.22, 144.14, 143.97, 143.59, 143.57, 143.54, 143.46, 143.42, 143.09, 142.08, 141.45, 140.70, 140.23, 139.56, 138.93, 138.80, 138.27, 138.00, 137.91, 137.80, 137.73, 137.40, 137.38, 137.33, 137.15, 137.08, 137.07, 136.68, 135.38, 134.90, 133.67, 133.15, 133.09, 131.34, 131.04, 129.17, 128.62, 128.36, 127.11, 126.71, 126.22, 125.43, 120.27, 119.72, 117.77, 117.54, 59.82, 54.94, 37.88, 37.83, 30.02.

**HRMS (ESI+)** (*m/z*): Calculated for $[C_{82}H_{27}N_4O_5S]^+$ 1179.1697, found 1179.1676.

**IR:** $V_{max}$ / $cm^{-1}$ 2952, 1738, 1568, 1441, 747, 563.

## 8.14 A@43

### 8.14.1 $^{4}$He@43

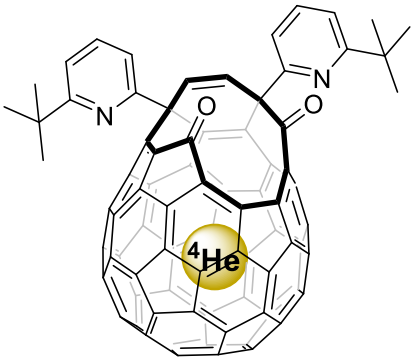


**$^{4}$He@43**

$C_{82}H_{26}N_2O_2He$ (1075.12)

Fullerene **88** (494 mg, 0.366 mmol) was placed into a glass tube which was then inserted into a steel high-pressure reactor. The apparatus was placed under dynamic vacuum (approx. 0.2 mm Hg) for 15 min before charging with $^{4}$He gas to 72 atm and compressed in the reactor using a Sitec 750.01 hand-operated pressure-intensifying syringe (30 mL capacity) to 439 atm. The reactor was cooled to around –196 °C using liquid $N_2$. The He gas was then compressed to 762 atm, before allowing the reactor to warm to room temperature, at which point the pressure reached 1828 atm. The system was then heated to 180 °C and maintained at this temperature for 2 h, with a stable internal pressure of 2374 atm during this time. After cooling to room temperature and slow release of the pressure, the solid residue was purified by flash column chromatography ($SiO_2$ eluted with toluene). Material with $R_f$ = 0.5 in toluene was collected, and removal of solvents *in vacuo* gave **$^{4}$He@43** as a brown powder (331 mg, 0.307 mmol, 84%, 50% f.f.).

50% filling factor was confirmed by $^{13}$C NMR of the final compound **$^{4}$He@C$_{60}$** (**8.15.1**).

**$^{1}$H NMR** (500 MHz, $CDCl_3$) δ 7.68 (t, *J* = 7.8 Hz, 1H, pyridyl), 7.65 (t, *J* = 7.8 Hz, 1H, pyridyl), 7.51 (dd, *J* = 7.7, 0.6 Hz, 1H, pyridyl), 7.39 (dd, *J* = 7.7, 0.7 Hz, 1H, pyridyl), 7.23 (d, *J* = 7.8, Hz, 2H, pyridyl), 7.21 (d, *J* = 10.0 Hz, 1H, alkenyl), 7.17 (d, *J* = 10.0 Hz, 1H, alkenyl) 1.26 (s, 9H, *t*-butyl), 1.18 (s, 9H, *t*-butyl).

**$^{13}$C NMR** (126 MHz, $CDCl_3$) δ 200.41, 192.32, 169.20, 168.84, 165.42, 162.20, 154.82, 150.12, 148.86, 147.96, 147.94, 147.79, 147.46, 146.99, 146.67, 146.63, 146.57, 146.38, 146.18, 146.17, 146.14, 146.02, 145.95, 145.91, 145.80, 145.66, 145.47, 145.18, 145.15, 144.78, 144.74, 144.38, 144.34, 144.06, 143.05, 142.75, 142.58, 142.29, 142.08, 141.98, 141.78, 141.10, 140.74, 140.75, 140.59, 140.27, 140.18, 139.96, 139.68, 139.60, 139.50, 138.79, 138.54, 138.49, 137.49, 137.45, 137.21, 136.50, 136.31, 135.93, 134.97, 133.89, 132.98, 132.91, 132.66, 132.51, 131.68, 129.84, 120.09, 119.69, 117.70, 116.91, 61.10, 54.92, 37.93, 37.84, 30.09, 30.07. The peaks arising from empty open-fullerene **43** are present but not reported.

**HRMS (APPI)** (*m/z*)**:** Calculated for $[^{12}C_{82}\,^{1}H_{26}{}^{14}N_2{}^{16}O_2{}^{4}He]^{+\bullet}$ 1074.2015 found 1074.1997, Calculated for $[^{12}C_{81}\,^{13}C\,^{1}H_{26}{}^{14}N_2{}^{16}O_2{}^{4}He]^{+\bullet}$ 1075.2048 found 1075.2074.

**HRMS (ESI+)** (*m/z*)**:** Calculated for $[^{12}C_{82}\,^{1}H_{27}{}^{14}N_2{}^{16}O_2{}^{4}He]^+$ 1075.2093 found 1075.2089.

**IR:** $V_{max}$ / $cm^{-1}$ 2956, 1740, 1567, 1442, 743, 541.

## 8.14.2 $^3$He@43

Solid open-fullerene **88** (705 mg, 0.523 mmol) was packed directly into a steel high-pressure reactor equipped with pressure intensifier. The reactor was degassed under dynamic vacuum (approx. 0.2 mm Hg) before cooling to −196 °C using liquid $N_2$ and charging with $^3$He gas to 35 atm. The gas was then compressed in the reactor using a Sitec 750.01 hand-operated pressure-intensifying syringe (30 mL capacity) to 653 atm, before allowing the reactor to warm to room temperature, at which point the pressure reached 1532 atm. The reactor was then heated to 178 °C and maintained at this temperature for 1 h, with a stable internal pressure of 1933 atm during this time. After cooling to room temperature, the pressure was slowly released back into the source cylinders. The Sitec syringe was used to transfer as much $^3$He as possible from the reactor and back into the source cylinders and the main part of the pressure system. The residual $^3$He in the reactor was then recovered sequentially into two 1 L evacuated cylinders. The solid residue from the reactor was purified by flash column chromatography ($SiO_2$ eluted with toluene). Material with $R_f$ = 0.5 in toluene was collected, and removal of solvents *in vacuo* gave **$^3$He@43** as a brown powder (502 mg, 0.468 mmol, 89%, 44% f.f.).

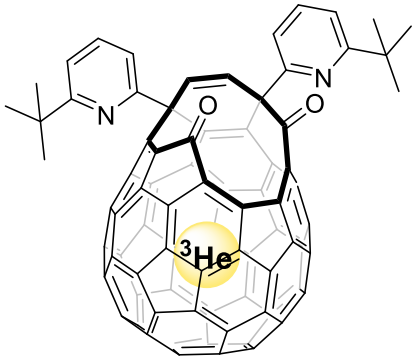


**$^3$He@43**

$C_{82}H_{26}N_2O_2{}^3He$ (1074.12)

50% filling factor was confirmed by $^{13}$C NMR of the final compound **$^3$He@$C_{60}$** (**8.15.2**).

**$^1$H NMR** (500 MHz, $CDCl_3$) δ = 7.68 (t, *J* = 7.8 Hz, 1H, pyridyl), 7.65 (t, *J* = 7.8 Hz, 1H, pyridyl), 7.51 (dd, *J* = 7.8, 0.8 Hz, 1H, pyridyl), 7.39 (dd, *J* = 7.8, 0.8 Hz, 1H, pyridyl), 7.24 (dd, *J* = 7.9, 0.9 Hz, 2 × 1H separated by 0.002 ppm), 7.21 (d, *J* = 10.0 Hz, 1H, alkenyl), 7.17 (d, *J* = 10.0 Hz, 1H, alkenyl) 1.26 (s, 9H, *t*-butyl), 1.18 (s, 9H, *t*-butyl).

**$^{13}$C NMR** (126 MHz, $CDCl_3$) δ 200.41, 192.32, 169.20, 168.85, 165.42, 162.21, 154.82, 150.12, 148.86, 147.96, 147.94, 147.78, 147.46, 146.99, 146.66, 146.64, 146.57, 146.38, 146.18, 146.17, 146.14, 146.01, 145.94, 145.91, 145.80, 145.65, 145.47, 145.17, 145.15, 144.77, 144.75, 144.38, 144.33, 144.06, 143.05, 142.74, 142.58, 142.29, 142.08, 141.97, 141.78, 141.10, 140.74, 140.74, 140.59, 140.26, 140.17, 139.96, 139.70, 139.60, 139.50, 138.82, 138.54, 138.48, 137.49, 137.45, 137.21, 136.49, 136.31, 135.93, 134.97, 133.89, 132.98, 132.91, 132.66, 132.58, 131.67, 129.84, 120.09,

119.69, 117.70, 116.91, 61.10, 54.92, 37.93, 37.84, 30.09, 30.07. The peaks arising from empty open-fullerene **43** are present but not reported.

**HRMS (APPI)** (*m/z*): Calculated for $[^{12}C_{82}\,^{1}H_{26}{}^{14}N_2{}^{16}O_2{}^{3}He]^{+\bullet}$ 1073.2149 found 1073.2159.

**HRMS (ESI+)** (*m/z*): Calculated for $[^{12}C_{82}\,^{1}H_{27}{}^{14}N_2{}^{16}O_2{}^{3}He]^{+}$ 1074.2227 found 1074.2214.

**IR:** $V_{max}$ / $cm^{-1}$ 2955, 1740, 1696, 1567, 1442.

## 8.14.3 $H_2$@43

Fullerene **88** (556 mg, 0.411 mmol) was placed into a glass tube which was then inserted into a steel high-pressure reactor. The apparatus was placed under dynamic vacuum (approx. 0.2 mm Hg) for 5 min before charging with $H_2$ gas to 121 atm and compressed reactor using a Sitec 750.01 hand-operated pressure-intensifying syringe (30 mL capacity) to 500 atm. The reactor was cooled to around –196 °C using liquid $N_2$. The $H_2$ gas was then compressed to 700 atm, before allowing the reactor to warm to room temperature, at which point the pressure reached 1384 atm. The system was then heated to 186 °C and maintained at this temperature for 2 h, with a stable internal pressure of 1806 atm during this time. After cooling to room temperature and slow release of the pressure, the solid residue was purified by flash column chromatography ($SiO_2$ eluted with toluene). Material with $R_f$ = 0.5 in toluene was collected, and removal of solvents *in vacuo* gave **$H_2$@43** as a brown powder (521 mg, 0.327 mmol, 80%, 95% f.f.).

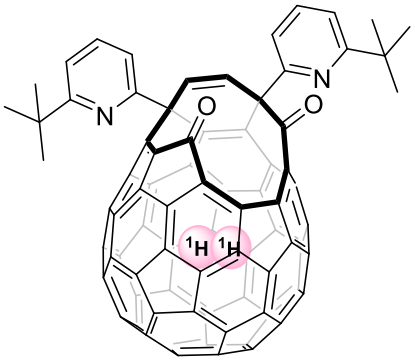


**$H_2$@43**

$C_{82}H_{28}N_2O_2$ (1073.14)

95% filling factor was determined by $^1$H NMR.

**$^1$H NMR** (400 MHz, $CDCl_3$) δ 7.68 (t, *J* = 7.8 Hz, 1H, pyridyl), 7.65 (t, *J* = 7.8 Hz, 1H, pyridyl), 7.51 (dd, *J* = 7.7, 0.6 Hz, 1H, pyridyl), 7.39 (dd, *J* = 7.7, 0.7 Hz, 1H, pyridyl), 7.23 (d, *J* = 7.8, Hz, 2H, pyridyl), 7.21 (d, *J* = 10.0 Hz, 1H, alkenyl), 7.17 (d, *J* = 10.0 Hz, 1H, alkenyl), 1.26 (s, 9H, *t*-butyl), 1.18 (s, 9H, *t*-butyl), 1.18 (s, 9H), -5.71 (s, 2H endohedral $H_2$ 95% filled).

**HRMS (APPI)** (*m/z*): Calculated for $[^{12}C_{82}\,^{1}H_{28}{}^{14}N_2{}^{16}O_2]^{+}$ 1072.2150 found 1072.1990.

Spectral data was consistent with the reported literature.[155]

## 8.14.4 $D_2$@43

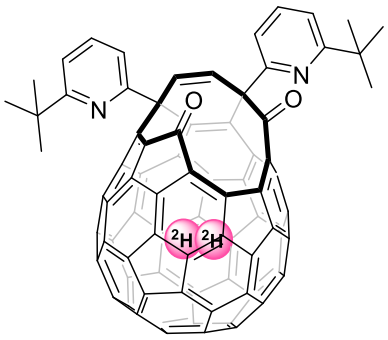


**$^2H_2$@43**

$C_{82}{}^1H_{26}{}^2H_2N_2O_2$ (1075.14)

Fullerene **88** (616 mg, 0.456 mmol) was placed into a glass tube which was then inserted into a steel high-pressure reactor. The apparatus was placed under dynamic vacuum (approx. 0.2 mm Hg) for 30 min before cooling to around –196 °C using liquid $N_2$. Reactor was charged with $D_2$ gas to 17 atm and compressed reactor using a Sitec 750.01 hand-operated pressure-intensifying syringe (30 mL capacity) to 83.2 atm, before allowing the reactor to warm to room temperature, at which point the pressure reached 1384 atm. The system was then heated to 176 °C and maintained at this temperature for 1.5 h, with a stable internal pressure of 423 atm during this time. After cooling to room temperature and slow release of the pressure, the solid residue was purified by flash column chromatography ($SiO_2$ eluted with toluene). Material with $R_f$ = 0.5 in toluene was collected, and removal of solvents *in vacuo* gave **$D_2$@43** as a brown powder (352 mg, 0.329 mmol, 73%, 73% f.f.).

73% filling factor was confirmed by $^{13}C$ NMR of the final compound **$D_2$@$C_{60}$** (**8.15.4**).

**$^1H$ NMR** (500 MHz, $CDCl_3$) δ 7.68 (t, *J* = 7.8 Hz, 1H, pyridyl), 7.65 (t, *J* = 7.8 Hz, 1H, pyridyl), 7.51 (dd, *J* = 7.7, 0.6 Hz, 1H, pyridyl), 7.39 (dd, *J* = 7.7, 0.7 Hz, 1H, pyridyl), 7.23 (d, *J* = 7.8, Hz, 2H, pyridyl), 7.22 (d, *J* = 10.0, 1H, alkenyl), 7.17 (d, *J* = 10.0 Hz, 1H, alkenyl), 1.26 (s, 9H, *t*-butyl), 1.18 (s, 9H, *t*-butyl).

**$^{13}C$ NMR** (126 MHz, CDCl3) δ 200.43, 192.34, 169.20, 168.85, 165.42, 162.21, 154.90, 150.19, 148.92, 148.02, 148.02, 147.85, 147.51, 147.04, 146.73, 146.72, 146.62, 146.44, 146.24, 146.17, 146.14, 146.08, 145.99, 145.96, 145.87, 145.70, 145.53, 145.23, 145.17, 144.83, 144.82, 144.40, 144.39, 144.10, 143.07, 142.82, 142.65, 142.36, 142.18, 142.04, 141.82, 141.13, 140.81, 140.76, 140.63, 140.33, 140.20, 139.96, 139.75, 139.64, 139.55, 138.90, 138.58, 138.52, 137.52, 137.45, 137.21, 136.57, 136.47, 136.05, 134.99, 133.95, 133.04, 132.95, 132.67, 132.64, 131.68, 129.85, 120.11, 119.69, 117.70, 116.92, 61.11, 54.92, 37.93, 37.84, 30.09, 30.07. The peaks arising from empty open-fullerene **43** are present but not reported.

**HRMS (APPI)** (*m/z*): Calculated for $[^{12}C_{82}{}^1H_{26}{}^{14}N_2{}^{16}O_2{}^2H_2]^{+\bullet}$ 1074.2271 found 1074.2285.

**HRMS (ESI+)** (*m/z*): Calculated for $[^{12}C_{82}{}^1H_{27}{}^{14}N_2{}^{16}O_2{}^2H_2]^+$ 1075.2351 found 1075.2336.

**IR:** $V_{max}$ / $cm^{-1}$ : 2957, 1738, 1567, 1441, 791, 540.

## 8.14.5 HD@43

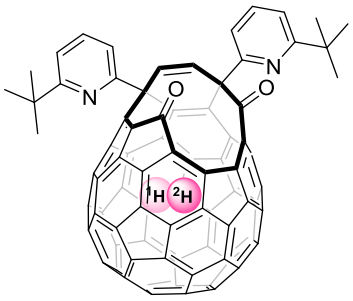


**$^1$H$^2$H@43**

$C_{82}{}^1H_{27}{}^1H_2N_2O_2$ (1073.14)

Fullerene **88** (380 mg, 0.281 mmol) was placed into a glass tube which was then inserted into a steel high-pressure reactor. The apparatus was placed under dynamic vacuum (approx. 0.2 mm Hg) for 15 min before charging with HD gas to 8.5 atm and compressed in the reactor using a Sitec 750.01 hand-operated pressure-intensifying syringe (30 mL capacity) to 123 atm. The system was then heated to 160 °C and maintained at this temperature for 3 h, with a stable internal pressure of 160 atm during this time. After cooling to room temperature and slow release of the pressure, the solid residue was purified by flash column chromatography ($SiO_2$ eluted with toluene). Material with $R_f$ = 0.5 in toluene was collected and removal of solvents *in vacuo* gave **HD@43** as a brown powder (255 mg, 0.237 mmol, 84%, 50% f.f.).

**$^1$H NMR** (500 MHz, $CDCl_3$) $\delta$ 7.68 (t, *J* = 7.8 Hz, 1H, pyridyl), 7.64 (t, *J* = 7.8 Hz, 1H, pyridyl), 7.51 (dd, *J* = 7.8, 0.8 Hz, 1H, pyridyl), 7.38 (dd, *J* = 7.8, 0.8 Hz, 1H, pyridyl), 7.24 (dd, *J* = 7.9, 0.9 Hz, 2H pyridyl) 7.22 (d, *J* = 7.9 Hz, 1H pyridyl), 7.22 (d, *J* = 7.9 Hz, 1H, pyridyl), 7.17 (d, *J* = 9.9 Hz, 1H, alkenyl), 7.17 (d, *J* = 9.9 Hz, 1H, alkenyl) 1.26 (s, 9H, *t*-butyl), 1.18 (s, 9H, *t*-butyl), −5.74 (t, *J* = 41.8 Hz, 1H endohedral HD).

**$^{13}$C NMR** (126 MHz, $CDCl_3$) $\delta$ = 200.43, 192.35, 169.20, 168.85, 165.41, 162.20, 154.91, 150.19, 148.92, 148.02, 148.02, 147.85, 147.51, 147.04, 146.73, 146.72, 146.62, 146.44, 146.24, 146.17, 146.14, 146.08, 145.99, 145.95, 145.87, 145.70, 145.53, 145.23, 145.17, 144.83, 144.82, 144.40, 144.39, 144.10, 143.07, 142.82, 142.65, 142.36, 142.18, 142.04, 141.82, 141.13, 140.81, 140.76, 140.62, 140.33, 140.21, 139.96, 139.74, 139.64, 139.55, 138.91, 138.58, 138.52, 137.52, 137.47, 137.21, 136.57, 136.47, 136.05, 134.99, 133.95, 133.04, 132.95, 132.67, 132.64, 131.68, 129.84, 120.11, 119.69, 117.70, 116.91, 61.10, 54.92, 37.93, 37.84, 30.09, 30.07. The peaks arising from empty open-fullerene **43** are present but not reported.

**HRMS (APPI)** (*m/z*): Calculated for $[^{12}C_{82}{}^1H_{27}{}^2HN_2O_2]^{+\bullet}$, 1073.2208; found 1073.2179. This peak overlaps with the $[^{12}C_{79}{}^{13}C_3H_{26}N_2O_2]^{+\bullet}$ isotope peak of empty open-fullerene **43**.

**HRMS (ESI+)** (*m/z*): Calculated for $[^{12}C_{82}{}^1H_{28}{}^2HN_2O_2]^+$ 1074.2286; found 1074.2261.

**IR:** $V_{max}$ / $cm^{-1}$ 2950, 1740, 1567, 1442 $cm^{-1}$.

## 8.14.6 Ne@43

### 8.14.6.1 First synthesis via Ne@45

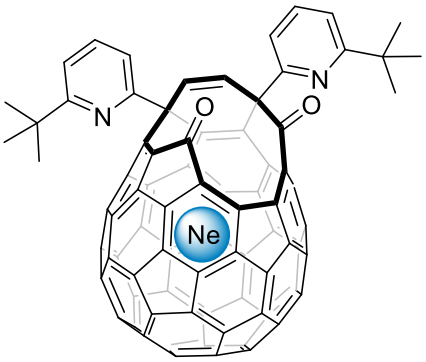


**Ne@43**

$C_{82}H_{26}N_2O_2Ne$ (1091.30)

Fullerene **46** (182 mg, 0.162 mmol) was placed in an oven-dried glass tube stoppered with glass wool. The tube was inserted into a purpose-built steel high-pressure reactor and heated to 140 °C for 20 h under dynamic vacuum (approx. 0.2 mm Hg). The reactor was then cooled to room temperature before pressurising with neon gas to 280 atm, using a Sitec 750.01 hand-operated pressure-intensifying syringe. The system was then heated to 150 °C and maintained at this temperature for 17 h, with a stable internal pressure of 380 atm during this time. After cooling to room temperature and slow release of the pressure, the title compound **Ne@45** was obtained as a brown solid (179 mg, 0.156 mmol, 97%). 16% Ne filling, and 2% $H_2O$ filling, were estimated from the ESI+ mass spectrum and $^1$H NMR spectrum, respectively.

Due to the facile hydration of **Ne@45** to form **Ne@46,** this compound was treated as an intermediate and was not further purified or fully characterised.

A solution of crude 15% filled **Ne@45** (170 mg, 0.154 mmol) and $PPhFu_2$ (0.298 g 1.230 mmol) in toluene (10 mL) was heated at 60 °C for 18 h. The mixture was then cooled to room temperature and poured over a silica column, eluting with a slow gradient of toluene:hexane (1:1) → 100% toluene. Material eluted in a brown band, with $R_f$ = 0.5 in toluene, was collected, and removal of solvents *in vacuo* gave the title compound **Ne@43** as a brown powder (90 mg, 0.083 mmol, 55%). 15% Ne filling and the presence of 1% endohedral water was confirmed from the ESI+ mass and $^1$H NMR spectrum.

**LRMS (ESI+)** *m/z* 1071.39 (90%, $[M+H]^+$, **43**), 1091.48 (15%, $[M+H]^+$, **Ne@43**), 1089 (1% **$H_2O$@43**).

Fullerene **Ne@43** is fully characterised in the following section.

### 8.14.6.2 Optimised synthesis: Cryogenic filling into 88

Fullerene **88** (588 mg, 0.438 mmol) was placed into a glass tube which was then inserted into a steel high-pressure reactor. The apparatus was placed under dynamic vacuum (approx. 0.2 mm Hg) for 15 min before charging with Ne gas to 37 atm and compressed in the reactor using a Sitec 750.01 hand-operated pressure-intensifying syringe (30 mL capacity) to 346 atm. The reactor was cooled to around –196 °C using liquid $N_2$. The Ne gas was then compressed to 338 atm, before allowing the reactor to

warm to room temperature, at which point the pressure reached 1301 atm. The system was then heated to 180 °C and maintained at this temperature for 1.5 h, with a stable internal pressure of 1742 atm during this time. After cooling to room temperature and slow release of the pressure, the solid residue was purified by flash column chromatography ($SiO_2$ eluted with toluene). Material with $R_f$ = 0.5 in toluene was collected and removal of solvents *in vacuo* gave **Ne@43** as a brown powder (391 mg, 0.365 mmol, 84%, 63% f.f.).

63% filling factor was confirmed by $^{13}C$ NMR of the final compound **Ne@$C_{60}$** (**8.15.6**).

**$^{1}$H NMR** (500 MHz, $CDCl_3$) *δ* 7.68 (t, *J* = 7.8 Hz, 1H, pyridyl), 7.65 (t, *J* = 7.8 Hz, 1H, pyridyl), 7.51 (dd, *J* = 7.8, 0.8 Hz, 1H, pyridyl), 7.39 (dd, *J* = 7.8, 0.8 Hz, 1H, pyridyl), 7.24 (d, *J* = 7.9, 0.9 Hz, 2H, pyridyl), 7.21 (d, *J* = 10.0 Hz, 1H, alkenyl), 7.17 (d, *J* = 10.0 Hz, 1H, alkenyl) 1.26 (s, 9H, *t*-butyl), 1.18 (s, 9H, *t*-butyl).

**$^{13}$C NMR** (126 MHz, $CDCl_3$) *δ* 200.41, 192.32, 169.20, 168.85, 165.42, 162.21, 154.85, 150.14, 148.88, 147.96, 147.95, 147.78, 147.47, 146.97, 146.69, 146.65, 146.59, 146.36, 146.18, 146.16, 146.13, 146.00, 145.93, 145.90, 145.78, 145.64, 145.49, 145.15, 145.11, 144.76, 144.75, 144.35, 144.34, 144.08, 143.00, 142.76, 142.60, 142.33, 142.08, 142.01, 141.83, 141.07, 140.74, 140.71, 140.63, 140.33, 140.24, 139.93, 139.67, 139.62, 139.51, 138.84, 138.51, 138.45, 137.50, 137.45, 137.21, 136.56, 136.36, 135.94, 134.95, 133.90, 133.03, 132.92, 132.67, 132.62, 131.64, 129.84, 120.10, 119.69, 117.70, 116.91, 61.10, 54.91, 37.93, 37.84, 30.09, 30.07. The peaks arising from empty open-fullerene 5 are present but not reported.

**HRMS (APPI)** *(m/z)*: Calculated for $[^{12}C_{82}\,^{1}H_{26}{}^{14}N_2{}^{16}O_2{}^{20}Ne]^{+\bullet}$ 1090.1913 found 1090.1917.

**HRMS (ESI+)** (*m/z*): Calculated for $[^{12}C_{82}\,^{1}H_{27}{}^{14}N_2{}^{16}O_2{}^{20}Ne]^{+}$ 1091.1991 found 1091.1985.

**IR:** $V_{max}$ / $cm^{-1}$ 2955, 1737, 1696, 1566, 1442.

## 8.14.7 $CH_4$@43

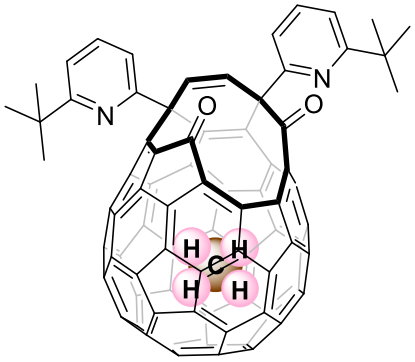


**$CH_4$@43**
$C_{83}H_{30}N_2O_2$ (1087.17)

A purpose-built Jacketed Schlenk flask (**Figure 28**) was charged with >95% **$CH_4$@89** (103 mg, 0.088 mmol) and the apparatus placed under a $N_2$ atmosphere. Distilled MeCN (100 mL), AcOH (10 mL of a degassed 10% v/v aqueous solution) and distilled toluene (50 mL) were added, and the resulting mixture was vigorously stirred under irradiation with a yellow LED lamp (20 W) for 17 h at 50 °C heated by water in the Jacket. Solvents were then removed *in vacuo*. Purification by rapid, repeat column chromatography ($SiO_2$ eluted with a 90:8:2 mixture of toluene:EtOAc:AcOH; then $SiO_2$ eluted with toluene → 5% AcOH in toluene) gave **$CH_4$@46** as a black solid (19 mg, 19%) which was used directly in the next step. **$CH_4$@46** obtained above (19 mg, 0.016 mmol) was heated at 170 °C under vacuum (0.2 mm/Hg) for 17 h before cooling to room temperature under vacuum, and dissolution in toluene (6 mL). Dry triphenylphosphine (0.035 g, 0.133 mmol) was added and the resulting mixture stirred at reflux for 24 h with exclusion of light. After cooling to room temperature, solvents were removed *in vacuo*. Purification by column chromatography ($SiO_2$ eluted with a gradient of 1:1 hexane:toluene → toluene) gave the title compound, **$CH_4$@43**, as a brown/black solid (14 mg, 0.013 mmol, 15% yield from **$CH_4$@89**). >95% filling was determined by comparison of integrals in the experimental $^1$H NMR spectrum.

**$^1$H NMR** (400 MHz, $CDCl_3$) δ 7.68 (t, *J* = 7.9 Hz, 1H, pyridyl), 7.66 (t, *J* = 7.8 Hz, 1H, pyridyl), 7.51 (dd, *J* = 7.8, 0.8 Hz, 1H pyridyl), 7.39 (dd, *J* = 7.8, 0.8 Hz, 1H, pyridyl), 7.24 (dd, *J* = 7.8, 0.8 Hz, 1H, pyridyl), 7.22 (dd, *J* = 7.8, 0.8 Hz, 1H, pyridyl), 7.22 (d, *J* = 10.0 Hz, 1H, alkenyl), 7.17 (d, *J* = 10.0 Hz, 1H, alkenyl), 1.27 (s, 9H, *t*-butyl), 1.18 (s, 9H, *t*-butyl), -9.84 (s, 4H, endohedral $CH_4$).

**HRMS (ESI+)** (*m/z*): Calculated for $[^{12}C_{83}{}^{1}H_{31}{}^{14}N_2{}^{16}O_2]^+$ 1087.2380 found 1087.2385.

Modification of the reported procedure. Spectral data was consistent with the reported literature.[180]

## 8.14.8 $CH_4$@99

A purpose-built Jacketed Schlenk flask (**Figure 28**) was charged with **$CH_4$@89** (40 mg, 0.034 mmol) and the apparatus placed under a $N_2$ atmosphere. MeCN (90 mL, degassed), $CF_3COOH$ (0.26 mL), $H_2O$ (10 mL) and toluene (120 mL) were added, and the resulting mixture was vigorously stirred under irradiation with a yellow LED lamp (100 W) for 4 h at 50 °C heated by water in the Jacket. Solvents

were then removed *in vacuo*. Purification by rapid column chromatography ($SiO_2$ eluted with toluene → 5% AcOH in toluene) gave fraction coming at $R_f$ = 0.61 (5% AcOH in toluene) compound **$CH_4$@99** as a black solid (10 mg, 26%). Traces of **$CH_4$@46** and starting material **$CH_4$@89** were present in the analysis of the crude product, but not isolated.

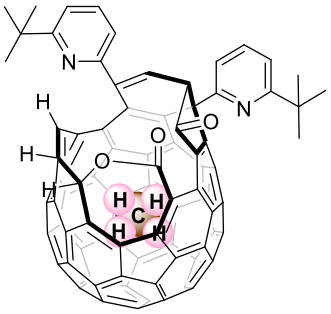


**$CH_4$@99**
$C_{82}H_{32}N_2O_3$ (1093.17)

The absolute structure was determined by X-ray crystallography (**8.16.4**).

**$^1$H NMR** (400 MHz, $CDCl_3$) δ 8.5 (d, *J* = 1.2 Hz, 1H, alkenyl), 7.95 (dd, *J* = 7.9, 0.8 Hz, 1H, pyridyl), 7.77 (t, *J* = 7.9 Hz, 1H, pyridyl), 7.76 (d, *J* = 1.2 Hz, 1H, alkenyl), 7.58 (t, *J* = 7.8 Hz, 1H, pyridyl), 7.35 (d, *J* = 8.0 Hz, 1H, alkenyl), 7.28 (dd, *J* = 7.7, 0.8 Hz, 1H, pyridyl), 7.26 (dd, *J* = 7.9, 0.7 Hz, 1H, pyridyl), 7.22 (dd, *J* = 8.0, 0.8 Hz, 1H, pyridyl), 4.70 (d, *J* = 8.0 Hz, 1H, alkanyl), 1.23 (s, 9H, *t*-butyl), 1.21 (s, *J* = 9H, *t*-butyl), -11.29 (s, 4H, $CH_4$).

**$^{13}$C NMR** (126 MHz, $CDCl_3$) δ 203.70, 176.95, 169.85, 169.57, 168.72, 161.59, 155.03, 150.18, 150.04, 149.94, 149.68, 149.05, 148.99, 148.93, 148.90, 148.71, 148.66, 148.48, 148.36, 148.32, 147.93, 147.76, 147.55, 147.16, 146.77, 146.69, 146.46, 146.31, 145.98, 145.86, 145.42, 145.07, 144.98, 144.87, 144.54, 143.61, 142.63, 142.55, 142.35, 142.17, 142.16, 141.90, 141.83, 141.58, 140.28, 140.03, 139.86, 138.67, 137.90, 137.45, 137.38, 137.32, 137.29, 136.99, 136.78, 136.30, 135.92, 133.54, 132.25, 132.02, 131.73, 131.67, 129.79, 127.76, 125.15, 122.08, 119.96, 119.84, 118.22, 117.93, 86.96, 56.55, 54.95, 37.91, 37.80, 31.74, 30.09, 30.03. (Endohedral $CH_4$ peak was not measured)

**HRMS (APPI)** (*m/z*): Calculated for $[^{12}C_{82}{}^{1}H_{32}{}^{14}N_2{}^{16}O_3]^{+\bullet}$ 1092.2407, found 1092.2386.

**IR:** $V_{max}$ / $cm^{-1}$ 2960, 1773, 1707, 1569, 1445, 797, 747, 696, 527.

## 8.14.9 Ar@43

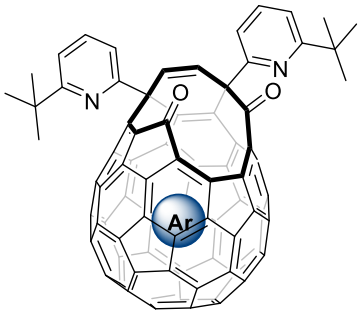


**Ar@43**
$C_{82}H_{26}N_2O_2Ar$ (1111.07)

A round bottom flask (500 mL) was charged with **Ar@89** (0.250 g, 0.209 mmol) and the apparatus placed under a $N_2$ atmosphere. Distilled MeCN (160 mL), AcOH (32 mL of a degassed 10% v/v aqueous solution) and toluene (60 mL) were added, and the resulting mixture was vigorously stirred under irradiation with a low-pressure Na lamp (35 W) for 40 h. Solvents were then removed *in vacuo*. Purification by rapid, repeat column chromatography ($SiO_2$ eluted with a 90:8:2 mixture of toluene:EtOAc:AcOH; then $SiO_2$ eluted with toluene → 5% AcOH in toluene) gave **Ar@46** as a black solid (69 mg, 28%) which was used directly in the next step. **Ar@46** obtained above (69 mg, 0.059 mmol) was heated at 180 °C under vacuum (0.2 mm/Hg) for 17 h before cooling to room temperature under vacuum, and dissolution in toluene (15 mL). Dry triphenylphosphine (129 mg, 0.491 mmol) was added and the resulting mixture stirred at reflux for 17 h with exclusion of light. After cooling to room temperature, solvents were removed *in vacuo*. Purification by column chromatography ($SiO_2$ eluted with a gradient of 1:1 hexane:toluene → toluene) gave the title compound, **Ar@43**, as a brown/black solid (43 mg, 0.038 mmol, 15% yield from **Ar@89**). >95% filling was determined by comparison of integrals in the experimental HRMS spectrum.

**$^1$H NMR** (400 MHz, $CDCl_3$) δ 7.68 (t, *J* = 7.8 Hz, 1H, pyridyl), 7.66 (t, *J* = 7.8 Hz, 1H, pyridyl), 7.51 (dd, *J* = 7.8, 0.9 Hz, 1H, pyridyl), 7.39 (dd, *J* = 7.8, 0.8 Hz, 1H, pyridyl), 7.24 (dd, *J* = 7.8, 0.9 Hz, 1H, pyridyl), 7.22 (dd, *J* = 7.8 Hz, 0.9 Hz, 1H, pyridyl), 7.22 (d, *J* = 10.0 Hz, 1H, alkenyl), 7.17 (d, *J* = 10.0 Hz, 1H, alkenyl), 1.27 (s, 9H, *t*-butyl), 1.18 (s, 9H, *t*-butyl).

**HRMS (ESI+)** (*m/z*): Calculated for $[^{12}C_{82}\,^{1}H_{28}{}^{14}N_2{}^{16}O_2Ar]^+$ 1111.1691 found 1111.1688.

Followed reported procedure. Spectral data was consistent with the reported literature.[184]

## 8.14.10 Kr@43

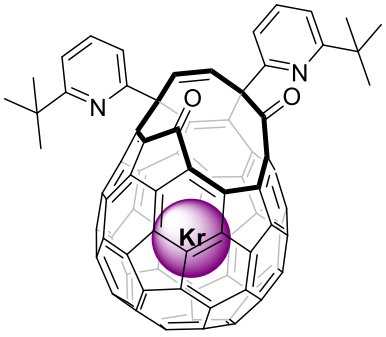


**Kr@43**
$C_{82}H_{26}N_2O_2Kr$ (1154.92)

A purpose-built Jacketed Schlenk flask (**Figure 28**) was charged with >99% filled **Kr@89** (102 mg, 0.081 mmol) and the apparatus placed under a $N_2$ atmosphere. Distilled MeCN (150 mL), AcOH (10 mL of a degassed 10% v/v aqueous solution) and toluene (50 mL) were added, and the resulting mixture was vigorously stirred under

irradiation with a yellow LED lamp (20 W) for 17 h at 50 °C heated by water in the Jacket. Solvents were then removed *in vacuo*. Purification by rapid, repeat column chromatography ($SiO_2$ eluted with a 90:8:2 mixture of toluene:EtOAc:AcOH; then $SiO_2$ eluted with toluene → 5% AcOH in toluene) gave **Kr@46** as a black solid (22 mg, 23%) which was used directly in the next step. **Kr@46** obtained above (22 mg, mmol) was heated at 180 °C under vacuum (0.2 mm/Hg) for 18 h before cooling to room temperature under vacuum, and dissolution in toluene (7 mL). Dry triphenylphosphine (35 mg, 0.133 mmol) was added and the resulting mixture stirred at reflux for 17 h with exclusion of light. After cooling to room temperature, solvents were removed *in vacuo*. Purification by column chromatography ($SiO_2$ eluted with a gradient of 1:1 hexane:toluene → toluene) gave the title compound, **Kr@43**, as a brown/black solid (11 mg, 0.010 mmol, 13% yield from **Kr@89**). >99% filling was determined by comparison of integrals in the experimental HRMS spectrum.

**$^1$H NMR** (500 MHz, $CDCl_3$) δ 7.68 (t, *J* = 7.9 Hz, 1H, pyridyl), 7.66 (t, *J* = 7.8 Hz, 1H, pyridyl), 7.51 (dd, *J* = 7.8, 0.8 Hz, 1H, pyridyl), 7.39 (dd, *J* = 7.8, 0.8 Hz, 1H, pyridyl), 7.24 (dd, *J* = 7.9, 0.8 Hz, 1H, pyridyl), 7.23 (dd, *J* = 7.9, 0.8 Hz, 1H, pyridyl), 7.22 (d, *J* = 10.0 Hz, 1H, alkenyl), 7.17 (d, *J* = 10.0 Hz, 1H, alkenyl), 1.27 (s, 9H, *t*-butyl), 1.17 (s, 9H, *t*-butyl).

**$^{13}$C NMR** (126 MHz, $CDCl_3$) δ 200.41, 192.41, 169.20, 168.88, 165.48, 162.24, 155.46, 150.58, 149.35, 148.29, 148.27, 148.10, 147.87, 147.40, 147.17, 146.99, 146.96, 146.59, 146.35, 146.29, 146.22, 146.13, 146.12, 145.97, 145.89, 145.84, 145.36, 145.21, 145.02, 145.00, 144.73, 144.49, 144.27, 143.39, 143.23, 143.04, 142.90, 142.69, 142.48, 141.34, 141.25, 141.09, 141.04, 140.99, 140.64, 140.14, 139.92, 139.86, 139.81, 139.43, 138.63, 138.49, 137.84, 137.61, 137.60, 137.45, 137.22, 136.71, 134.96, 134.41, 133.90, 133.47, 133.38, 132.70, 131.49, 129.90, 129.19, 128.38, 120.17, 119.71, 117.70, 116.91, 61.14, 54.94, 37.94, 37.85, 30.09, 30.09.

**HRMS (ESI+)** (*m/z*): Calculated for $[^{12}C_{82}\,^{1}H_{31}{}^{14}N_2{}^{16}O_2Kr]^+$ 1155.1196 found 1155.1157.

**IR:** $V_{max}$ / $cm^{-1}$ 2960, 1739, 1566, 1441, 791, 542.

## 8.15 A@$C_{60}$

### 8.15.1 $^{4}$He@$C_{60}$

Dry triisopropyl phosphite (2.00 mL, 8.11 mmol) was added to a solution of 50% filled **$^{4}$He@43** (419 mg, 0.391 mmol) in toluene (42 mL) and the resulting mixture was stirred at reflux for 17 hours under $N_2$ atmosphere. After cooling to room temperature, the mixture was concentrated *in vacuo* and purified by column chromatography ($SiO_2$ eluted with toluene). The fractions containing material with $R_f$ = 0.95 were collected and evaporated to dryness to afford **$^{4}$He@42** (365 mg). The compound was not completely dried due to its sensitivity to air.

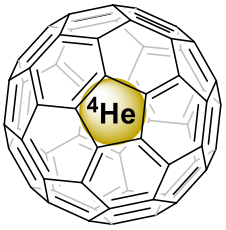


**$^{4}$He@$C_{60}$**
$C_{60}{}^{4}$He (724.66)

The residue was dissolved in dry 1-chloronaphthalene (72 mL) and transferred to a Schlenk tube containing N-phenyl maleimide (121 mg, 0.698 mmol). The solution was degassed under dynamic vacuum for 15 min, put under $N_2$ atmosphere and sealed. The flask was immersed into a preheated metal heating block at 260 °C and stirred for 44 h. After cooling to room temperature, the solution was flushed through a $SiO_2$ column packed with toluene, collecting a purple band. The bulk of the 1-chloronaphthalene was distilled off under high vacuum (110 °C, 0.2 mm/Hg). The residue was washed three times with $Et_2O$ to give a black powder (202 mg, 72% crude yield). The compound was purified by preparative HPLC on a Cosmosil™ Buckyprep column (eluted with 100% toluene) and evaporated to dryness to give **$^{4}$He@$C_{60}$** (142 mg, 0.195 mmol, 50%, f.f. 50%) as a black powder.

**$^{13}$C NMR** (175 MHz, *o*-dcb-$d_4$) δ 142.827 ($^{4}$He@$C_{60}$) 142.803 ($C_{60}$).

**HRMS (APPI)** (*m/z*)**:** Calculated for $[^{12}C_{60}{}^{4}He]^{+\bullet}$ 724.0021 found 724.0027.

**IR:** $V_{max}$ / $cm^{-1}$ 1427, 1180, 574.

**UV (toluene):** $\lambda_{max}$ 335.7 nm, ε 37000 $M^{-1}cm^{-1}$.

Characterisation data was consistent with the reported literature.[186]

## 8.15.2 $^{3}He@C_{60}$

Dry triisopropyl phosphite (1.50 mL, 6.70 mmol) was added to a solution of 44% filled **$^{3}He@43$** (450 mg, 0.419 mmol) in toluene (45 mL) and the resulting mixture was stirred at reflux for 17 hours under $N_2$ atmosphere. After cooling to room temperature, the mixture was concentrated *in vacuo* and purified by column chromatography ($SiO_2$ eluted with toluene). The fractions containing material with $R_f$ = 0.95 were collected and evaporated to dryness to afford **$^{3}He@42$** (0.334 g). The compound was not completely dried due to its sensitivity to air.

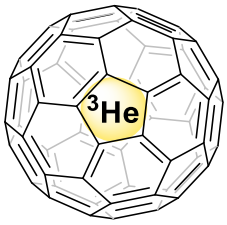


**$^{3}He@C_{60}$**
$C_{60}{}^{3}He$ (723.68)

**$^{3}He@42$** (270 mg, 0.259 mmol) was dissolved in dry 1-chloronaphthalene (55 mL) and transferred to a Schlenk tube containing N-phenyl maleimide (179 mg, 1.036 mmol). The solution was degassed under dynamic vacuum for 15 min, put under $N_2$ atmosphere and sealed. The flask was immersed into a preheated metal heating block at 260 °C and stirred for 44 h. After cooling to room temperature, the solution was flushed through a $SiO_2$ column packed with toluene, collecting a purple band. The bulk of the 1-chloronaphthalene was distilled off under high vacuum (110 °C, 0.2 mm/Hg). The compound was purified by preparative HPLC on a Cosmosil™ Buckyprep column (eluted with 100% toluene) and evaporated to dryness to give **$^{3}He@C_{60}$** (98 mg, 33%, 0.14 mmol, f.f. 44%) as a black powder.

**$^{13}C$ NMR** (176 MHz, odcb-$d_4$) δ 142.828 ($^{3}He@C_{60}$) 142.803 ($C_{60}$).

**HRMS (APPI)** (*m/z*)**:** Calculated for $[^{12}C_{60}{}^{3}He]^{+\bullet}$ 723.0155 found 723.0151.

**IR:** $V_{max}$ / $cm^{-1}$ 1427, 1180, 574.

**UV (toluene):** $\lambda_{max}$ 335.7 nm, ε 39000 $M^{-1}cm^{-1}$.

## 8.15.3 $H_2@C_{60}$

Dry triisopropyl phosphite (1.25 mL, 5.24 mmol) was added to a solution of 95% filled **$H_2@43$** (351 mg, 0.327 mmol) in toluene (35 mL) and the resulting mixture was stirred at reflux for 16 h under $N_2$ atmosphere. After cooling to room temperature, the mixture was concentrated *in vacuo* and purified by column chromatography (SiO2 eluted with toluene). The fractions containing material with $R_f$ = 0.95 were collected and evaporated to dryness to afford

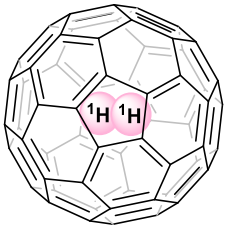


**$H_2@C_{60}$**
$C_{60}{}^{1}H_2$ (722.68)

**$H_2$@42** (0.321 g). The compound was not completely dried due to its sensitivity to air.

The residue was dissolved in dry 1-chloronaphthalene (65 mL) and transferred to a Schlenk tube containing N-phenyl maleimide (107 mg, 0.614 mmol). The solution was degassed under dynamic vacuum for 15 min, put under $N_2$ atmosphere and sealed. The flask was immersed into a preheated metal heating block at 260 °C and stirred for 44 h. After cooling to room temperature, the solution was flushed through a $SiO_2$ column packed with toluene, collecting a purple band. The bulk of the 1-chloronaphthalene was distilled off under high vacuum. The residue was washed three times with ether to give a black powder (194 mg, 84% crude yield). The compound was purified by preparative HPLC on a Cosmosil™ Buckyprep column (eluted with 100% toluene) and evaporated to dryness to give 93% filled **$H_2$@$C_{60}$** (122 mg, 0.168 mmol, 52%, 95% f.f.) as a black powder.

**$^1$H NMR** (500 MHz, *o*-dcb-$d_4$,) δ -1.46.

**$^{13}$C NMR** (126 MHz, odcb-$d_4$) δ 142.880 ($H_2$@$C_{60}$) 142.803 ($C_{60}$).

Spectral data was consistent with the reported literature.[155]

## 8.15.4 $D_2$@$C_{60}$

Dry triisopropyl phosphite (1.25 mL, 5.22 mmol) was added to a solution of 73% filled **$D_2$@43** (352 mg, 0.328 mmol) in toluene (35mL) and the resulting mixture was stirred at reflux for 17 h under $N_2$ atmosphere. After cooling to room temperature, the mixture was concentrated *in vacuo* and purified by column chromatography ($SiO_2$ eluted with toluene). The fractions containing material with $R_f$ = 0.95 were collected and evaporated to dryness to afford **$D_2$@42** (307 mg). The compound was not completely dried due to its sensitivity to air.

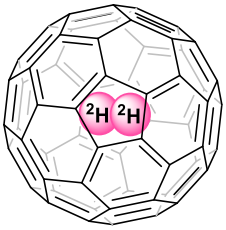


**$^2H_2$@$C_{60}$**
$C_{60}{}^2H_2$ (724.68)

The residue was dissolved in dry 1-chloronaphthalene (62 mL) and transferred to a Schlenk tube containing N-phenyl maleimide (102 mg, 0.588 mmol). The solution was degassed under dynamic vacuum for 20 min, put under $N_2$ atmosphere and sealed. The flask was immersed into a preheated metal heating block at 260 °C and stirred for 44 h. After cooling to room temperature, the solution was flushed through a $SiO_2$ column packed with toluene, collecting a purple band. The bulk of the 1-chloronaphthalene was distilled off under high vacuum. The residue was washed three times with ether to give a black powder (184 mg, 78% crude yield). The compound was purified by preparative HPLC on a Cosmosil™ Buckyprep column (eluted with 100% toluene) and evaporated to dryness to give **$D_2$@$C_{60}$** (116 mg, 0.160 mmol, 49%, 73% f.f.) as a black powder.

**$^{13}$C NMR** (126 MHz, odcb-$d_4$, δ) 142.877 ($D_2$@$C_{60}$) 142.803 ($C_{60}$).

**HRMS (APPI)** (*m/z*)**:** Calculated for $[^{12}C_{60}{}^{2}H_2]^{+\bullet}$ 724.0277; found 724.0276.

**IR:** $V_{max}$ / $cm^{-1}$ 1426, 1180, 573.

**UV (toluene):** $\lambda_{max}$ 335.3 nm, ε 42000 $M^{-1}cm^{-1}$.

## 8.15.5 HD@$C_{60}$

Dry triisopropyl phosphite (1.84 mL, 7.31 mmol) was added to a solution of 50% filled **HD@43** (490 mg, 0.457 mmol) in toluene (50 mL) and the resulting mixture was stirred at reflux for 17 h under $N_2$ atmosphere. After cooling to room temperature, the mixture was concentrated *in vacuo* and purified by column chromatography ($SiO_2$ eluted with toluene). The fractions containing material with $R_f$ = 0.95 were collected and solvent was evaporated to afford **HD@42** (447 mg, 0.428 mmol, 93%).

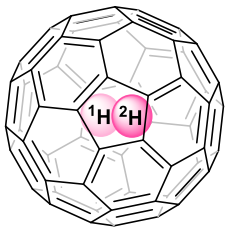


**$^{1}$H$^{2}$H@$C_{60}$**
$C_{60}{}^{1}H^{2}H$(723.68)

Compound **HD@42** (55%, combined fractions) (550 mg, 0.53 mmol) was dissolved in dry 1-chloronaphthalene (25 mL) and transferred to a Schlenk tube containing N-phenyl maleimide (180 mg, 1.06 mmol). The solution was degassed under dynamic vacuum for 20 min, put under $N_2$ atmosphere and sealed. The flask was immersed into a preheated metal heating block at 256 °C and stirred for 22 h. After cooling to room temperature, the solution was flushed through a $SiO_2$ column packed with toluene, collecting a purple band. The bulk of the 1-chloronaphthalene was distilled off under high vacuum. The compound was then purified by preparative HPLC on a Cosmosil™ Buckyprep column (eluted with 100% toluene) and evaporated to dryness to give **HD@$C_{60}$** (120 mg, 0.165 mmol, 31%, 55% f.f.) as a black powder.

The yield is calculated from the **HD@42**.

**$^{1}$H NMR** (500 MHz, *o*-dcb-$d_4$) δ −1.49 (1:1:1 t, *J* = 41.6 Hz, 1H, endohedral HD).

**$^{13}$C NMR** (126 MHz, odcb-$d_4$) δ 142.879 ($^{1}H^{2}H$@$C_{60}$) 142.803 ($C_{60}$).

**HRMS (APPI)** (*m/z*)**:** Calculated for $[^{12}C_{60}{}^{1}H^{2}H]^{+\bullet}$ 723.0214; found 723.0218.

**IR:** $V_{max}$ / $cm^{-1}$ 1427, 1180, 574.

**UV (toluene):** $\lambda_{max}$ 335.7 nm, ε 35000 $M^{-1}cm^{-1}$.

## 8.15.6 Ne@$C_{60}$

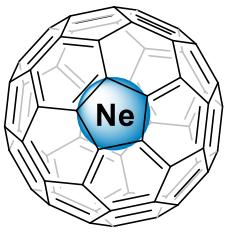


**Ne@$C_{60}$**
$C_{60}Ne$ (740.84)

Dry triisopropyl phosphite (1.63 mL, 6.61 mmol) was added to a solution of 63% filled **Ne@43** (391 mg, 0.365 mmol) in toluene (39 mL) and the resulting mixture was stirred at reflux for 17 h under $N_2$ atmosphere. After cooling to room temperature, the mixture was concentrated *in vacuo* and purified by column chromatography ($SiO_2$ eluted with toluene). The fractions containing material with $R_f$ = 0.95 were collected and evaporated to dryness to afford **Ne@42** (341 mg). The compound was not completely dried due to its sensitivity to air.

The intermediate was dissolved in dry 1-chloronaphthalene (68 mL) and transferred to a Schlenk tube containing N-phenyl maleimide (113 mg, 0.652 mmol). The solution was degassed under dynamic vacuum for 15 min, put under $N_2$ atmosphere and sealed. The flask was immersed into a preheated metal heating block at 260 °C and stirred for 44 h. After cooling to room temperature, the solution was flushed through a $SiO_2$ column packed with toluene, collecting a purple band. The bulk of the 1-chloronapthalene was distilled off under high vacuum (110 °C, 0.2 mm/Hg). The residue was washed three times with $Et_2O$ to give a black powder (176 mg, 67% crude yield). The compound was purified by preparative HPLC on a Cosmosil™ Buckyprep column (eluted with 100% toluene) and evaporated to dryness to give **Ne@$C_{60}$** (115 mg, 0.155 mmol, 44%, 63% f.f.) as a black powder.

**$^{13}$C NMR** (125 MHz, odcb-$d_4$) δ 142.827 (Ne@$C_{60}$) 142.803 ($C_{60}$).

**HRMS (APPI)** (*m/z*): Calculated for $[^{12}C_{60}Ne]^{+\bullet}$ 739.9919 found 739.9928.

**IR:** $V_{max}$ / $cm^{-1}$ = 1427, 1180, 574.

**UV (toluene):** $\lambda_{max}$ 335.3 nm, ε 40000 $M^{-1}cm^{-1}$.

Compound Ne@$C_{60}$ was enriched to f.f. <99% by preparative recycling HPLC in 100% toluene (2 × Cosmosil™ Buckyprep 20 mm i.d. × 250 mm columns in series), 10 mL/min, 20 cycles, r.t. 626 min (empty $C_{60}$), 631 min (Ne@$C_{60}$) **Figure 42**.

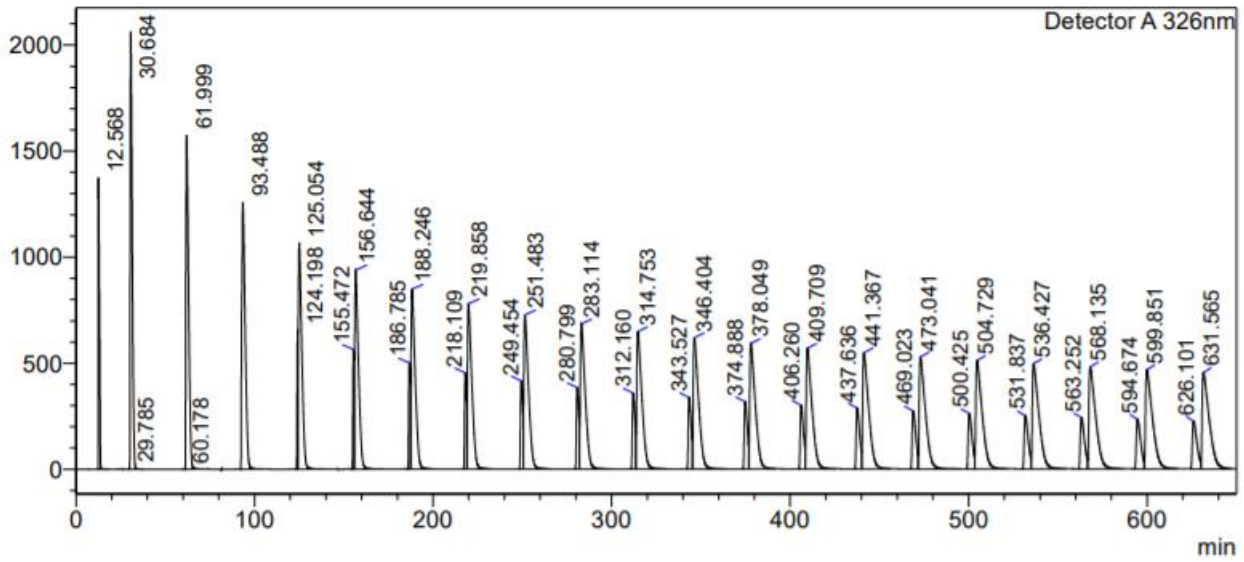


**Figure 42**. Recycling HPLC chromatogram of enrichment of **Ne@C$_{60}$**.

## 8.15.7 CH$_4$@C$_{60}$

Dry triisopropyl phosphite (0.11 mL, 0.51 mmol) was added to a solution of ~95% filled **CH$_4$@43** (38 mg, 0.032 mmol) in toluene (3 mL) and the resulting mixture was stirred at reflux for 17 h under $N_2$ atmosphere. After cooling to room temperature, the mixture was concentrated *in vacuo* and purified by column chromatography ($SiO_2$ eluted with toluene). The fractions containing material with $R_f$ = 0.95 were collected and evaporated to dryness to afford **CH$_4$@42** (28 mg). The compound was not completely dried due to its sensitivity to air.

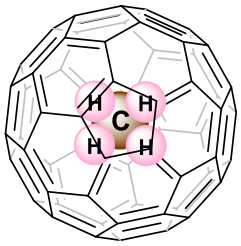


**CH$_4$@C$_{60}$**
$C_{61}{}^1H_4$ (736.71)

The intermediate was dissolved in dry 1-chloronaphthalene (4 mL) and transferred to a Schlenk tube containing N-phenyl maleimide (6 mg, 0.03 mmol). The solution was degassed under dynamic vacuum for 10 min, put under $N_2$ atmosphere and sealed. The flask was immersed into a preheated metal heating block at 260 °C and stirred for 44 h. After cooling to room temperature, the solution was flushed through a $SiO_2$ column packed with toluene, collecting a purple band. The crude was directly injected into preparative HPLC where final compound was purified on a Cosmosil™ Buckyprep column (eluted with 100% toluene) and evaporated to dryness to give **CH$_4$@C$_{60}$** (13 mg, 0.018 mmol, 52%, 95% f.f.) as a black powder.

**$^1$H NMR** (500 MHz, odcb-$d_4$) δ -5.71.

**$^{13}$C NMR** (125 MHz, odcb-$d_4$) δ 143.324 (CH$_4$@C$_{60}$), -13.157 (endohedral CH$_4$).

**HRMS (APPI)** (*m/z*): Calculated for $[^{12}C_{61}{}^{1}H_4]^{+\bullet}$ 736.0308 found 736.0294.

Spectral data was consistent with the reported literature.[180]

## 8.15.8 Ar@$C_{60}$

Dry triisopropyl phosphite (0.29 mL, 1.19 mmol) was added to a solution of ~90% filled **Ar@43** (83 mg, 0.074 mmol) in distilled toluene (8 mL) and the resulting mixture was stirred at reflux for 17 h under $N_2$ atmosphere. After cooling to room temperature, the mixture was concentrated *in vacuo* and purified by column chromatography ($SiO_2$ eluted with toluene). The fractions containing material with $R_f$ = 0.95 were collected and evaporated to dryness to afford **Ar@42** (83 mg). The compound was not completely dried due to its sensitivity to air.

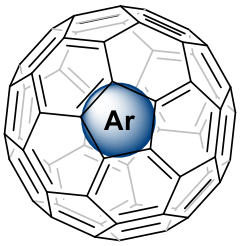


**Ar@$C_{60}$**
$C_{60}$Ar(760.61)

The intermediate was dissolved in dry 1-chloronaphthalene (16 mL) and transferred to a Schlenk tube containing N-phenyl maleimide (27.6 mg, 0.159 mmol). The solution was degassed under dynamic vacuum for 10 min, put under $N_2$ atmosphere and sealed. The flask was immersed into a preheated metal heating block at 260 °C and stirred for 44 h. After cooling to room temperature, the solution was flushed through a $SiO_2$ column packed with toluene, collecting a purple band. The crude was directly injected into preparative HPLC where final compound was purified on a Cosmosil™ Buckyprep column (eluted with 100% toluene) and evaporated to dryness to give **Ar@$C_{60}$** (23 mg, 0.030 mmol, 41%, 90% f.f.) as a black powder.

**$^{13}$C NMR** (125 MHz, odcb-$d_4$) 142.986 (Ar@$C_{60}$), 142.805 ($C_{60}$).

**HRMS (APPI)** (*m/z*): Calculated for $[^{12}C_{60}Ar]^{+\bullet}$ 759.9618 found 759.9618.

Spectral data was consistent with the reported literature.[184]

## 8.15.9 Kr@$C_{60}$

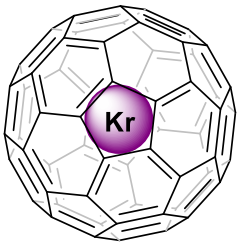


**Kr@$C_{60}$**
$C_{60}Kr$ (804.46)

Dry triisopropyl phosphite (0.186 mL, 0.755 mol) was added to a solution of >99% filled **Kr@43** (38 mg, 0.033 mmol) in toluene (5 mL) and the resulting mixture was stirred at reflux for 17 h under $N_2$ atmosphere. After cooling to room temperature, the mixture was concentrated *in vacuo* and purified by column chromatography ($SiO_2$ eluted with toluene). The fractions containing material with $R_f$ = 0.95 were collected and evaporated to dryness to afford **Kr@42** (23 mg). The compound was not completely dried due to its sensitivity to air.

The intermediate was dissolved in dry 1-chloronaphthalene (4 mL) and transferred to a Schlenk tube containing N-phenyl maleimide (16.3 mg, 0.0941 mmol). The solution was degassed under dynamic vacuum for 10 min, put under $N_2$ atmosphere and sealed. The flask was immersed into a preheated metal heating block at 260 °C and stirred for 44 h. After cooling to room temperature, the solution was flushed through a $SiO_2$ column packed with toluene, collecting a purple band. The crude was directly injected into preparative HPLC where final compound was purified on a Cosmosil™ Buckyprep column (eluted with 100% toluene) and evaporated to dryness to give **Kr@$C_{60}$** (13 mg, 0.016 mmol, 48%, >99% f.f.) as a black powder.

**$^{13}$C NMR** (125 MHz, odcb-$d_4$) 143.192 (Kr@$C_{60}$), 142.802 ($C_{60}$, <1%).

**HRMS (APPI)** (*m/z*): Calculated for $[^{12}C_{60}Kr]^{+\bullet}$ 803.9119 found 803.9106.

**IR:** $V_{max}$ / $cm^{-1}$ 1427, 1180, 574.

**UV (toluene):** $\lambda_{max}$ 339.3 nm, ε 30000 $M^{-1}cm^{-1}$.

## 8.15.10 $N_2@C_{60}$

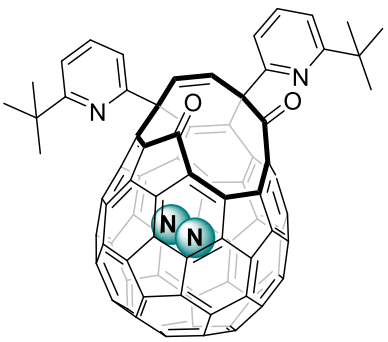


**$N_2$@DK**
$C_{82}H_{26}N_4O_2$ (1099.14)

A Jacketed Schlenk flask was charged with 70% filled **$N_2$@89** (40 mg, 0.033 mmol) and the apparatus placed under a $N_2$ atmosphere. Distilled MeCN (100 mL), AcOH (18 mL of a degassed 10% v/v aqueous solution) and toluene (70 mL) were added, and the resulting mixture was vigorously stirred under irradiation with a yellow LED lamp (100 W) for 17 h at 26 °C temperature controlled by water in the Jacket. Solvents were then removed *in vacuo*. Purification by rapid, repeat column chromatography ($SiO_2$ eluted with a 90:8:2 mixture of toluene:EtOAc:AcOH; then $SiO_2$ eluted with toluene → 5% AcOH in toluene) gave crude **$N_2$@46** as a black solid (15 mg, 25%, 58% f.f.) which was used directly in the next step. Filling was determined by comparison of integrals in the experimental $^1$H NMR and from HRMS spectrum.

**$^1$H NMR** (400 MHz, $CDCl_3$) δ 7.55 (t, *J* = 7.9 Hz, 1H, pyridyl), 7.49 (t, *J* = 7.8 Hz, 1H, pyridyl), 7.38 (dd, *J* = 7.8, 0.8 Hz, 1H, pyridyl), 7.21 – 7.05 (m, 4H pyridyl peaks overlapping with residual toluene), 7.00 (d, *J* = 10.1 Hz, 1H, alkenyl), 6.88 (d, *J* = 10.1 Hz, 1H, alkenyl), 5.86 (s, 1H, hydroxyl), 5.61 (s, 1H, hydroxyl), 1.15 (s, 9H, *t*-butyl), 1.10 (s, 9H, *t*-butyl).

**HRMS (ESI+)** (*m/z*): Calculated for $[C_{82}H_{29}N_4O_5]^+$ 1149.2132, found 1149.2110.

**$N_2$@46** obtained above (11 mg, 0.0096 mmol) was stirred with dry triphenylphosphine (41 mg, 0.15 mmol) in toluene (2 mL) at reflux for 17 h with exclusion of light. After cooling to room temperature, solvents were removed *in vacuo*. Purification by column chromatography ($SiO_2$ eluted with a gradient of 1:1 hexane:toluene → toluene) gave the title compound, **$N_2$@43**, as a brown/black solid (4 mg, 50% yield from **$N_2$@46**). >58% filling was determined by comparison of integrals in the experimental $^1$H NMR and from HRMS spectrum. $^{13}$C NMR of **$N_2$@43** has not been obtained due to small amounts of the sample.

**$^1$H NMR** (500 MHz, $CDCl_3$) δ 7.68 (t, *J* = 7.9 Hz, 1H, pyridyl), 7.66 (t, *J* = 7.9 Hz, 1H, pyridyl), 7.50 (dd, *J* = 7.8, 0.8 Hz, 1H, pyridyl), 7.39 (dd, *J* = 7.8, 0.8 Hz, 1H, pyridyl), 7.24 (dd, *J* = 1.9, 0.8 Hz, 1H, pyridyl), 7.22 (dd, *J* = 1.9, 0.8 Hz, 1H, pyridyl), 7.20 (d, *J* = 10.0 Hz, 1H, alkenyl), 7.16 (d, *J* = 10.0 Hz, 1H, alkenyl), 1.27 (s, 9H, *t*-butyl), 1.18 (s, 9H, *t*-butyl).

**HRMS (ESI+)** (*m/z*): Calculated for $[^{12}C_{82}\,^{1}H_{27}{}^{14}N_4{}^{16}O_2]^+$ 1099.2129, found 1099.2116.

**IR** $V_{max}$ / $cm^{-1}$ 2950, 1742, 1568, 1441, 791, 541.

Dry triisopropyl phosphite (0.03 mL, mol) was added to a solution of ~60% filled **$N_2$@43** (8 mg, mmol) in toluene (1 mL) and the resulting mixture was stirred at reflux for 17 h under $N_2$ atmosphere. After cooling to room temperature, the mixture was concentrated *in vacuo* and purified by column chromatography ($SiO_2$ eluted with toluene). The fractions containing material with $R_f$ = 0.95 were collected and evaporated to dryness to afford **$N_2$@42**. The compound was not completely dried due to its sensitivity to air.

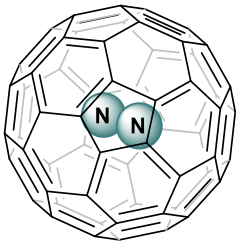


$N_2@C_{60}$
$C_{60}N_2$ (748.68)

The intermediate was dissolved in dry 1-chloronaphthalene (2 mL) and transferred to a Schlenk tube containing N-phenyl maleimide (3 mg, 0.02 mmol). The solution was degassed under dynamic vacuum for 15 min, put under $N_2$ atmosphere and sealed. The flask was immersed into a preheated metal heating block at 260 °C and stirred for 44 h. After cooling to room temperature, the solution was flushed through a $SiO_2$ column packed with toluene, collecting a purple band. The crude was directly injected into preparative HPLC where final compound was purified on a Cosmosil™ Buckyprep column (eluted with 100% toluene) and evaporated to dryness to give **$N_2@C_{60}$** (2.1 mg, 0.0028 mmol, 40%, 58% f.f.) as a black powder. Sample contained 22% of $H_2O@C_{60}$ and 20% of empty $C_{60}$.

**$^{13}$C NMR** (100 MHz, o-DCB-$d_4$) $N_2@C_{60}$ (143.151, 58%), $H_2O@C_{60}$ (142.914, 22%), $C_{60}$ (142.805, 20%).

**HRMS (APPI)** (*m/z*): Calculated for $[^{12}C_{60}N_2]^{+\bullet}$ 748.0056, found 748.0066.

**IR:** $V_{max}$ / $cm^{-1}$ 1428, 1181, 575.

## 8.16 Crystallography data

### 8.16.1 X-Ray structure determination of 92

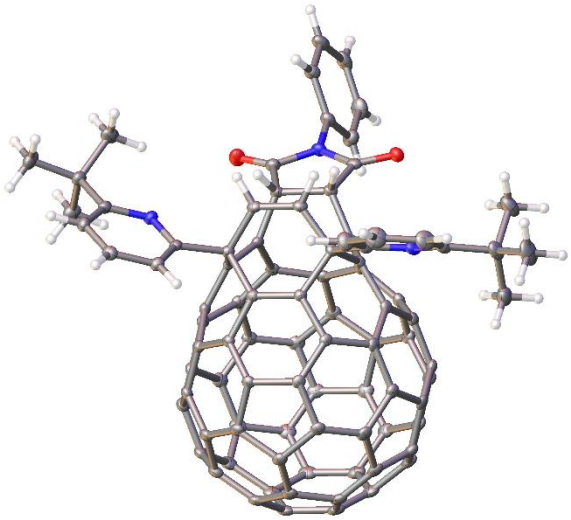

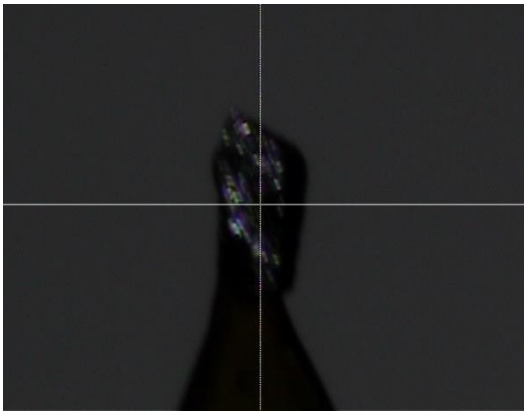

**Figure 43**. Thermal ellipsoids drawn at the 50% probability level. Solvent (0.7($C_6H_4Cl_2$), 1.8($CS_2$), $CH_4O$) omitted for clarity.

**Experimental.** Single dark orange block-shaped crystals of **2018sot0036_R1_100K** were recrystallised from methanol by slow evaporation. A suitable crystal 0.33×0.14×0.07 $mm^3$ was selected and mounted on a MITIGEN holder silicon oil on a Rigaku AFC12 FRE-VHF diffractometer. The crystal was kept at a steady $T$ = 100(2) K during data collection. The structure was solved with the **ShelXT** (Sheldrick, 2015) structure solution program using the Intrinsic Phasing solution method and by using **Olex2** (Dolomanov et al., 2009) as the graphical interface. The model was refined with version 2016/6 of **ShelXL** (Sheldrick, 2015) using Least Squares minimisation.

**Crystal Data.** $C_{99}H_{39.8}Cl_{1.4}N_3O_3S_{3.6}$, $M_r$ = 1484.18, monoclinic, $P2_1/n$ (No. 14), a = 13.5075(2) Å, b = 12.61709(19) Å, c = 38.5919(6) Å, $\beta$ = 94.8548(15)°, $\alpha = \gamma$ = 90°, $V$ = 6553.42(18) $Å^3$, $T$ = 100(2) K, $Z$ = 4, $Z'$ = 1, $\mu$(Mo$K_\alpha$) = 0.255, 146944 reflections measured, 16585 unique ($R_{int}$ = 0.0594) which were used in all calculations. The final $wR_2$ was 0.2157 (all data) and $R_1$ was 0.0747 (I > 2(I)).

## 8.16.2 X-Ray structure determination of 88

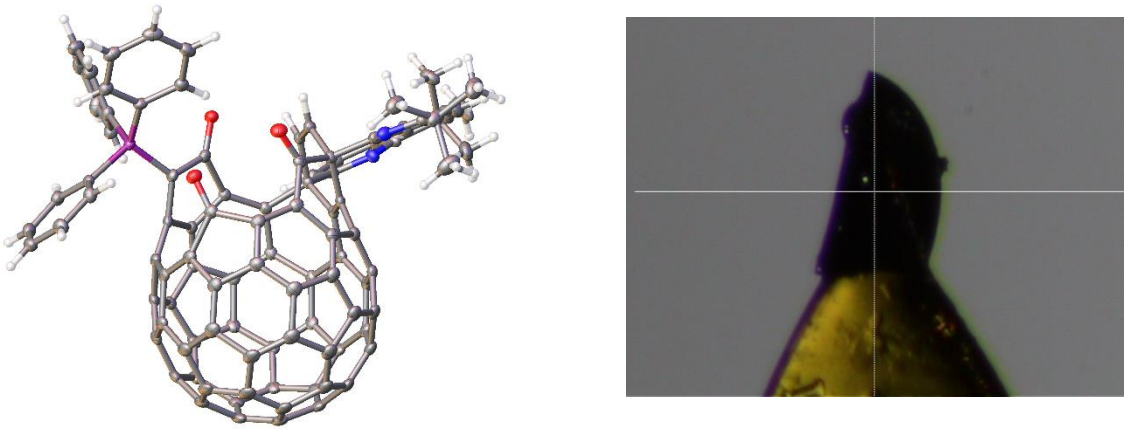

**Figure 44**: Thermal ellipsoids drawn at the 50% probability level. Solvent chloroform treated by solvent masking.

**Experimental.** Single orange plate-shaped crystals of **88** were recrystallised from chloroform by slow evaporation. A suitable crystal 0.43×0.19×0.06 $mm^3$ was selected and mounted on a MITIGEN holder with silicon oil on a Rigaku AFC12 FRE-VHF diffractometer. The crystal was kept at a steady $T$ = 100(2) K during data collection. The structure was solved with the **ShelXT** (Sheldrick, 2015) structure solution program using the Intrinsic Phasing solution method and by using **Olex2** (Dolomanov et al., 2009) as the graphical interface. The model was refined with version 2016/6 of **ShelXL** (Sheldrick, 2015) using Least Squares minimisation.

**Crystal Data.** $C_{101}Cl_3H_{42}N_2O_3P$, $M_r$ = 1468.68, monoclinic, $P2_1/c$ (No. 14), a = 23.5096(5) Å, b = 13.6771(2) Å, c = 19.8458(4) Å, $\beta$ = 95.8152(18)°, $\alpha = \gamma = 90°$, $V$ = 6348.4(2) $Å^3$, $T$ = 100(2) K, $Z$ = 4, $Z'$ = 1, $\mu(MoK_\alpha)$ = 0.237, 95342 reflections measured, 16105 unique ($R_{int}$ = 0.0573) which were used in all calculations. The final $wR_2$ was 0.1490 (all data) and $R_1$ was 0.0593 (I > 2(I)).

## 8.16.3 X-Ray structure determination of Ne@$C_{60}$

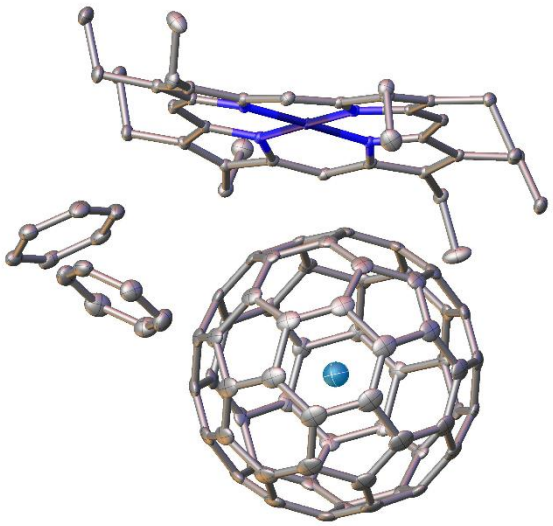

**Figure 45**: Thermal ellipsoids drawn at the 50% probability level.

**Experimental.** Single dark orange plate-shaped crystals of Ni porphyrin complex of **Ne@$C_{60}$** were recrystallised from benzene by slow evaporation. A suitable crystal 0.44×0.27×0.10 $mm^3$ was selected and mounted on a MITIGEN holder with silicon oil on an Rigaku AFC12 FRE-VHF diffractometer. The crystal was kept at a steady $T$ = 100(2) K during data collection. The structure was solved with the **ShelXT** (Sheldrick, 2015) structure solution program using the Intrinsic Phasing solution method and by using **Olex2** (Dolomanov et al., 2009) as the graphical interface. The model was refined with version 2016/6 of **ShelXL** (Sheldrick, 2015) using Least Squares minimisation.

**Crystal Data.** $C_{108}H_{56}N_4NeNi$, $M_r$ = 1488.45, triclinic, $P$-1 (No. 2), a = 14.09380(10) Å, b = 14.37270(10) Å, c = 17.1780(2) Å, $\alpha$ = 87.5290(10)°, $\beta$ = 75.7750(10)°, $\gamma$ = 75.6020(10)°, $V$ = 3266.45(5) $Å^3$, $T$ = 100(2) K, $Z$ = 2, $Z'$ = 1, $\mu$(MoK$\alpha$) = 0.368, 160930 reflections measured, 16553 unique ($R_{int}$ = 0.0388) which were used in all calculations. The final $wR_2$ was 0.0908 (all data) and $R_1$ was 0.0327 (I > 2(I)).

## 8.16.4 X-Ray structure determination of $CH_4$@99

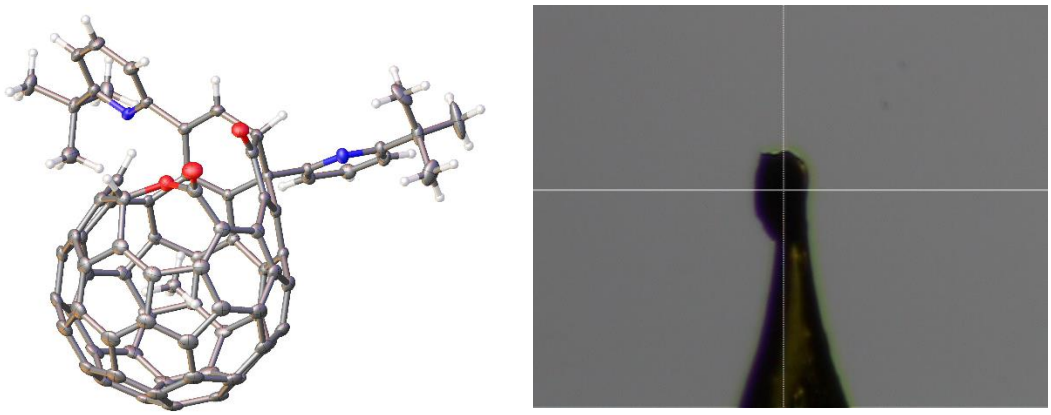

**Figure 46**: Thermal ellipsoids drawn at the 50% probability level, disordered hexane omitted for clarity.

**Experimental.** Single dark red (cut) plate-shaped crystals of **CH4@99** were recrystallised from hexane by slow evaporation. A suitable crystal 0.15×0.06×0.04 $mm^3$ was selected and mounted on a MITIGEN holder with silicon oil on an Rigaku AFC12 FRE-VHF diffractometer. The crystal was kept at a steady $T$ = 100(2) K during data collection. The structure was solved with the **ShelXT** (Sheldrick, 2015) structure solution program using the Intrinsic Phasing solution method and by using **Olex2** (Dolomanov et al., 2009) as the graphical interface. The model was refined with version 2016/6 of **ShelXL** (Sheldrick, 2015) using Least Squares minimisation.

**Crystal Data.** $C_{85}H_{39}N_2O_3$, $M_r$ = 1136.18, triclinic, $P$-1 (No. 2), a = 11.8888(2) Å, b = 13.9603(3) Å, c = 17.3569(3) Å, $\alpha$ = 107.822(2)°, $\beta$ = 99.732(2)°, $\gamma$ = 108.914(2)°, $V$ = 2476.67(9) $Å^3$, $T$ = 100(2) K, $Z$ = 2, $Z'$ = 1, $\mu(MoK_\alpha)$ = 0.092, 63739 reflections measured, 12559 unique ($R_{int}$ = 0.0440) which were used in all calculations. The final $wR_2$ was 0.1860 (all data) and $R_1$ was 0.0698 (I > 2(I)).

## 8.16.5 X-Ray structure determination of Kr@$C_{60}$

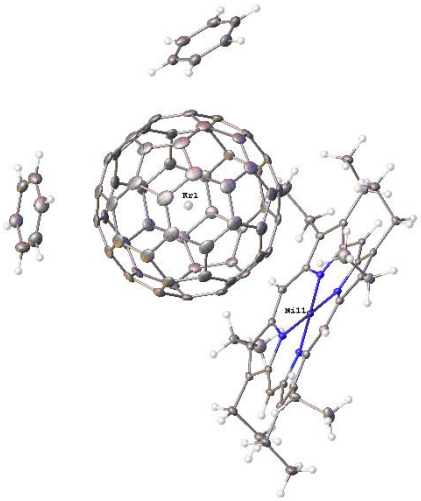


**Figure 47**: Thermal ellipsoids drawn at the 50% probability level.

**Experimental.** Single dark red plate crystals of Ni porphyrin complex of **Kr@$C_{60}$** were recrystallised from benzene by slow evaporation. A suitable crystal with dimensions 0.25 × 0.15 × 0.03 $mm^3$ was selected and mounted on a MITIGEN holder in perfluoroether oil on a Rigaku FRE+ equipped with VHF Varimax confocal mirrors and an AFC12 goniometer and HyPix 6000 detector diffractometer. The crystal was kept at a steady $T$ = 100(2) K during data collection. The structure was solved with the **ShelXT** (Sheldrick, 2015) solution program using dual methods and by using **Olex2** (Dolomanov et al., 2009) as the graphical interface. The model was refined with **ShelXL** 2018/3 (Sheldrick, 2015) using full matrix least squares minimisation on $F^2$.

**Crystal Data.** $C_{108}H_{56}KrN_4Ni$, $M_r$ = 1552.07, triclinic, $P$-1 (No. 2), a = 14.1170(3) Å, b = 14.3635(4) Å, c = 17.2002(4) Å, $\alpha$ = 87.620(2)°, $\beta$ = 75.874(2)°, $\gamma$ = 75.664(2)°, $V$ = 3276.23(14) $Å^3$, $T$ = 100(2) K, $Z$ = 2, $Z'$ = 1, $\mu$(Mo $K_\alpha$) = 1.033, 88173 reflections measured, 20140 unique ($R_{int}$ = 0.0465) which were used in all calculations. The final $wR_2$ was 0.1014 (all data) and $R_1$ was 0.0517 (I≥2 $\sigma$(I)).

# 9 Literature


[1] L. Tisza, *Zeitschrift fur Phys.* **1933**, *82*, 48–72.

[2] A. D. J. Haymet, *Chem. Phys. Lett.* **1985**, *122*, 421–424.

[3] A. D. J. Haymet, *J. Am. Chem. Soc.* **1986**, *108*, 319–321.

[4] R. E. S. H. W. Kroto, J.R. Heath, S.C. O'Brien, R.F. Curl, *Nature* **1985**, *318*, 162–163.

[5] W. Kratschmer, L. D. Lamb, K. Fostiropoulos, D. R. Huffman, *Nature* **1990**, *347*, 354–357.

[6] W. Krätschmer, K. Fostiropoulos, D. R. Huffman, *Chem. Phys. Lett.* **1990**, *170*, 167–170.

[7] R. E. Haufler, J. Conceicao, L. P. F. Chibante, Y. Chai, *J. Phys. Chem.* **1990**, *94*, 8634–8636.

[8] C. S. Yannoni, P. P. Bernier, D. S. Bethune, G. Meijer, J. R. Salem, *J. Am. Chem. Soc.* **1991**, *113*, 3190–3192.

[9] M. Ozaki, A. Taahashi, *Chem. Phys. Lett.* **1986**, *127*, 242–244.

[10] A. Anctil, C. W. Babbitt, R. P. Raffaelle, B. J. Landi, *Environ. Sci. Technol.* **2011**, *45*, 2353–2359.

[11] M. Otsuka, F. Kemper, S. Hyung, B. A. Sargent, M. Meixner, A. Tajitsu, K. Yanagisawa, *Astrophys. J.* **2013**, *764*, DOI 10.1088/0004-637X/764/1/77.

[12] A. Evans, J. T. van Loon, C. E. Woodward, R. D. Gehrz, G. C. Clayton, L. A. Helton, M. T. Rushton, S. P. S. Eyres, J. Krautter, S. Starrfield, R. M. Wagner, *Mon. Not. R. Astron. Soc. Lett.* **2012**, *421*, 92–96.

[13] F. Salama, in *EDIBLES*, **2016**, p. 1.

[14] E. K. Campbell, M. Holz, D. Gerlich, J. P. Maier, *Nature* **2015**, *523*, 322–323.

[15] M. A. Cordiner, H. Linnartz, N. L. J. Cox, J. Cami, F. Najarro, C. R. Proffitt, R. Lallement, P. Ehrenfreund, B. H. Foing, T. R. Gull, P. J. Sarre, S. B. Charnley, *Astrophys. J.* **2019**, *875*, L28.

[16] L. Becker, R. J. Poreda, T. E. Bunch, *Proc. Natl. Acad. Sci. U. S. A.* **2000**, *97*, 2979–2983.

[17] E. K. Campbell, E. S. Reedy, J. Rademacher, R. J. Whitby, G. Hoffman, *Astrophys. J.* **2020**, *897*, 88.

[18] D. J. Klein, T. G. Schmalz, G. E. Hite, W. A. Seitz, *J. Am. Chem. Soc.* **1986**, *108*, 1301–1302.

[19] G. C. Vougioukalakis, M. M. Roubelakis, M. Orfanopoulos, *Chem. Soc. Rev.* **2010**, *39*, 817–844.

[20] R. Taylor, D. R. M. Walton, *Nature* **1993**, *363*, 685.

[21] M. Bühl, A. Hirsch, *Chem. Rev.* **2001**, *101*, 1153–1183.

[22] R. E. Haufler, J. Conceicao, L. P. F. Chibante, Y. Chai, N. E. Byrne, S. Flanagan, M. M. Haley, S. C. O'Brien, C. Pan, Z. Xiao, W. E. Billups, M. A. Ciufolini, R. H. Hauge, J. L. Margrave, L. J. Wilson, R. F. Curl, R. E. Smalley, *J. Phys. Chem.* **1990**, *94*, 8634–8636.

[23] I. Dunlap, D. W. Brenner, W. Mmtmire, T. White, I. Final, *J. Phys. Chem.* **1991**, *95*, 5763–5768.

[24] M. Arndt, O. Nairz, J. Vos-Andreae, C. Keller, A. Zeilinger, G. Van der Zouw, *Nature* **1999**, *401*, 680–682.

[25] C. N. R. Rao, R. Seshadri, A. Govindaraj, R. Sen, *Mater. Sci. Eng. R* **1995**, *15*, 209–262.

[26] H. Shinohara, *Rep. Prog. Phys.* **1996**, *59*, 1665–1735.

[27] A. A. Popov, S. Yang, L. Dunsch, *Chem. Rev.* **2013**, *113*, 5989–6113.

[28] J. R. Heath, S. C. O'Brien, Q. Z. Y. Liu, R. F. Curl, F. K. Tittel, R. E. Smalley, H. W. Kroto, *J. Am. Chem. Soc.* **1985**, *107*, 7779–7780.

[29] D. M. Cox, D. J. Trevor, K. C. Reichmann, A. Kaldor, *J. Am. Chem. Soc.* **1986**, *108*, 2457–2458.

[30] D. M. Cox, K. C. Reichmann, A. Kaldor, *J. Chem. Phys.* **1988**, *88*, 1588–1597.

[31] F. D. Weiss, J. L. Elkind, S. C. O'Brien, R. F. Curl, R. E. Smalley, *J. Am. Chem. Soc.* **1988**, *110*, 4464–4465.

[32] L. M. Roth, Y. Huang, J. T. Schwedler, C. J. Cassady, D. Ben-Amotz, B. Kahr, B. S. Freiser, *J. Am. Chem. Soc.* **1991**, *113*, 6298–6299.

[33] Y. Chai, T. Guo, C. Jin, R. E. Haufler, L. P. F. Chibante, J. Fure, L. Wang, J. M. Alford, R. E. Smalley, *J. Phys. Chem.* **1991**, *95*, 7564–7568.

[34] H. Shinohara, H. Yamaguchi, N. Hayashi, H. Sato, M. Ohkohchi, Y. Ando, Y. Saito, *J. Phys. Chem.* **1993**, *97*, 4259–4261.

[35] S. Stevenson, H. C. Dorn, P. Burbank, K. Harich, J. Haynes, C. H. Klang, J. R. Salem, M. S. DeVries, P. H. M. van Loosdrecht, R. D. Johnson, C. S. Yannoni, D. S. Bethune, *Anal. Chem.* **1994**, *66*, 2675–2679.

[36] S. Stevenson, K. Harich, H. Yu, R. R. Stephen, D. Heaps, C. Coumbe, J. P. Phillips, *J. Am. Chem. Soc.* **2006**, *128*, 8829–8835.

[37] S. Stevenson, M. A. Mackey, C. E. Coumbe, J. P. Phillips, B. Elliott, L. Echegoyen, *J. Am. Chem. Soc.* **2007**, *129*, 6072–6073.

[38] S. Stevenson, M. A. Mackey, J. E. Pickens, M. A. Stuart, B. S. Confait, J. P. Phillips, *Inorg. Chem.* **2009**, *48*, 11685–11690.

[39] S. Aoyagi, E. Nishibori, H. Sawa, K. Sugimoto, M. Takata, Y. Miyata, R. Kitaura, H. Shinohara, H. Okada, T. Sakai, Y. Ono, K. Kawachi, K. Yokoo, S. Ono, K. Omote, Y. Kasama, S. Ishikawa, T. Komuro, H. Tobita, *Nat. Chem.* **2010**, *2*, 678–683.

[40] H. J. Chandler, M. Stefanou, E. E. B. Campbell, R. Schaub, *Nat. Commun.* **2019**, *10*, 1–8.

[41] C. Fuertes-Espinosa, C. García-Simón, E. Castro, M. Costas, L. Echegoyen, X. Ribas, *Chem. - A Eur. J.* **2017**, *23*, 3553–3557.

[42] C. Fuertes-Espinosa, J. Murillo, M. E. Soto, M. R. Ceron, R. Morales-Martínez, A. Rodríguez-Fortea, J. M. Poblet, L. Echegoyen, X. Ribas, *Nanoscale* **2019**, *11*, 23035–23041.

[43] C. Fuertes-Espinosa, A. Gómez-Torres, R. Morales-Martínez, A. Rodríguez-Fortea, C. García-Simón, F. Gándara, I. Imaz, J. Juanhuix, D. Maspoch, J. M. Poblet, L. Echegoyen, X. Ribas, *Angew. Chemie* **2018**, *130*, 11464–11469.

[44] S. Yang, T. Wei, F. Jin, *Chem. Soc. Rev.* **2017**, *46*, 5005–5058.

[45] Y. Iiduka, T. Wakahara, T. Nakahodo, T. Tsuchiya, A. Sakuraba, Y. Maeda, T. Akasaka, K. Yoza, E. Horn, T. Kato, M. T. H. Liu, N. Mizorogi, K. Kobayashi, S. Nagase, *J. Am. Chem. Soc.* **2005**, *127*, 12500–12501.

[46] S. Stevenson, G. Rice, T. Glass, K. Harlch, F. Cromer, M. R. Jordan, J. Craft, E. Hadju, R. Bible, M. M. Olmstead, K. Maltra, A. J. Fisher, A. L. Balch, H. C. Dorn, *Nature* **1999**, *401*, 55–57.

[47] W. Q. Shen, L. P. Bao, S. F. Hu, X. J. Gao, Y. P. Xie, X. F. Gao, W. H. Huang, X. Lu, *Chem. - A Eur. J.* **2018**, *24*, 16692–16698.

[48] Q. Tang, L. Abella, Y. Hao, X. Li, Y. Wan, A. Rodríguez-Fortea, J. M. Poblet, L. Feng, N. Chen, *Inorg. Chem.* **2016**, *55*, 1926–1933.

[49] Y. Hao, Q. Tang, X. Li, M. Zhang, Y. Wan, L. Feng, N. Chen, Z. Slanina, L. Adamowicz, F. Uhlík,

*Inorg. Chem.* **2016**, *55*, 11354–11361.

[50] N. Chen, C. M. Beavers, M. Mulet-Gas, A. Rodríguez-Fortea, E. J. Munoz, Y. Y. Li, M. M. Olmstead, A. L. Balch, J. M. Poblet, L. Echegoyen, *J. Am. Chem. Soc.* **2012**, *134*, 7851–7860.

[51] B. Q. Mercado, N. Chen, A. Rodríguez-Fortea, M. A. MacKey, S. Stevenson, L. Echegoyen, J. M. Poblet, M. M. Olmstead, A. L. Balch, *J. Am. Chem. Soc.* **2011**, *133*, 6752–6760.

[52] F. Liu, C. L. Gao, Q. Deng, X. Zhu, A. Kostanyan, R. Westerström, S. Wang, Y. Z. Tan, J. Tao, S. Y. Xie, A. A. Popov, T. Greber, S. Yang, *J. Am. Chem. Soc.* **2016**, *138*, 14764–14771.

[53] F. Liu, S. Wang, C. L. Gao, Q. Deng, X. Zhu, A. Kostanyan, R. Westerström, F. Jin, S. Y. Xie, A. A. Popov, T. Greber, S. Yang, *Angew. Chemie - Int. Ed.* **2017**, *56*, 1830–1834.

[54] M. Mikawa, H. Kato, M. Okumura, M. Narazaki, Y. Kanazawa, N. Miwa, H. Shinohara, *Bioconjug. Chem.* **2001**, *12*, 510–514.

[55] H. Kato, Y. Kanazawa, M. Okumura, A. Taninaka, T. Yokawa, H. Shinohara, *Physics (College. Park. Md).* **2003**, 4391–4397.

[56] M. Rohrer, H. Bauer, J. Mintorovitch, M. Requardt, H.-J. Weinmann, *Invest. Radiol.* **2005**, *40*, 715–724.

[57] T. Wang, C. Wang, *Small* **2019**, *15*, 1–13.

[58] R. B. Ross, C. M. Cardona, D. M. Guldi, S. G. Sankaranarayanan, M. O. Reese, N. Kopidakis, J. Peet, B. Walker, G. C. Bazan, E. Van Keuren, B. C. Holloway, M. Drees, *Nat. Mater.* **2009**, *8*, 208–212.

[59] F. Liu, G. Velkos, D. S. Krylov, L. Spree, M. Zalibera, R. Ray, N. A. Samoylova, C. H. Chen, M. Rosenkranz, S. Schiemenz, F. Ziegs, K. Nenkov, A. Kostanyan, T. Greber, A. U. B. Wolter, M. Richter, B. Büchner, S. M. Avdoshenko, A. A. Popov, *Nat. Commun.* **2019**, *10*, 1–11.

[60] W. Harneit, *Phys. Rev. A - At. Mol. Opt. Phys.* **2002**, *65*, 6.

[61] J. A. Larsson, J. C. Greer, W. Harneit, A. Weidinger, *J. Chem. Phys.* **2002**, *116*, 7849–7854.

[62] E. Almeida Murphy, T. Pawlik, A. Weidinger, M. Höhne, R. Alcala, J. M. Spaeth, *Phys. Rev. Lett.* **1996**, *77*, 1075–1078.

[63] J. H. Wesenberg, A. Ardavan, G. A. D. Briggs, J. J. L. Morton, R. J. Schoelkopf, D. I. Schuster, K. Mølmer, *Phys. Rev. Lett.* **2009**, *103*, 1–4.

[64] H. Itagaki, Y. Fujiwara, Y. Minowa, Y. Ikehara, T. Kaneko, T. Okazaki, Y. Iizumi, J. Kim, H. Sakakita, *AIP Adv.* **2019**, *9*, DOI 10.1063/1.5100980.

[65] M. Kanai, K. Porfyrakis, G. A. D. Briggs, T. J. S. Dennis, *Chem. Commun.* **2004**, *4*, 210–211.

[66] S. Zhou, K. Porfyrakis, in *Endohedral Fullerenes Electron Transf. Spin* (Ed.: A.A. Popov), Springer International Publishing, Cham, **2017**, pp. 265–295.

[67] S. C. Cho, T. Kaneko, H. Ishida, R. Hatakeyama, *J. Appl. Phys.* **2015**, *117*, 0–5.

[68] M. Scheloske, B. Naydenov, C. Meyer, W. Harneit, *Isr. J. Chem.* **2006**, *46*, 407–412.

[69] A. Hesselmann, T. Korona, *Phys. Chem. Chem. Phys.* **2011**, *13*, 732–743.

[70] V. V. Albert, R. J. Sabin, E. F. Harris, *Int. J. Quantum Chem.* **2011**, *111*, 4020–4029.

[71] M. Bühl, S. Patchkovskii, W. Thiel, *Chem. Phys. Lett.* **1997**, *275*, 14–18.

[72] S. K. Chaudhuri, R. K. Chaudhuri, P. K. Mukherjee, S. Chattopadhyay, *J. Chem. Phys.* **2017**, *147*, DOI 10.1063/1.4994569.

[73] F. Cimpoesu, S. Ito, H. Shimotani, H. Takagi, N. Dragoe, *Phys. Chem. Chem. Phys.* **2011**, *13*, 9609–9615.

[74] R. B. Darzynkiewicz, G. E. Scuseria, *J. Phys. Chem. A* **1997**, *101*, 7141–7144.

[75] A. You, M. A. Y. Be, I. In, **2014**, *5589*, 10–15.

[76] A. Koner, C. Kumar, N. Sathyamurthy, *Mol. Phys.* **2018**, *116*, 2728–2735.

[77] S. Osuna, M. Swart, M. Solà, *Chem. - A Eur. J.* **2009**, *15*, 13111–13123.

[78] M. S. Son, Y. Kiel Sung, *Chem. Phys. Lett.* **1995**, *245*, 113–118.

[79] R. Sure, R. Tonner, P. Schwerdtfeger, *J. Comput. Chem.* **2015**, *36*, 88–96.

[80] V. K. Dolmatov, M. Y. Amusia, L. V. Chernysheva, *Phys. Rev. A* **2017**, *95*, 1–10.

[81] M. Y. Amusia, L. V. Chernysheva, *JETP Lett.* **2016**, *103*, 260–264.

[82] A. J. Etindele, R. Maezono, R. L. Melingui Melono, O. Motapon, *Chem. Phys. Lett.* **2017**, *685*, 395–400.

[83] E. V. Gromov, S. Klaiman, L. S. Cederbaum, *Mol. Phys.* **2015**, *113*, 2964–2969.

[84] H. Yan, S. Yu, X. Wang, Y. He, W. Huang, M. Yang, *Chem. Phys. Lett.* **2008**, *456*, 223–226.

[85] Z. Y. Wang, K. H. Su, H. Q. Fan, Y. L. Li, Z. Y. Wen, *Mol. Phys.* **2008**, *106*, 703–716.

[86] A. L. R. Bug, A. Wilson, G. A. Voth, *J. Phys. Chem.* **1992**, *96*, 7864–7869.

[87] M. Saunders, H. Jiménez-Vázquez, B. W. Bangerter, R. J. James, S. Mroczkowski, D. I. Freedberg, F. A. L. Anet, *J. Am. Chem. Soc.* **1994**, *116*, 3621–3622.

[88] M. Saunders, H. A. Jiménez-Vázquez, R. J. Cross, S. Mroczkowski, D. I. Freedberg, F. A. L. Anet, *Nature* **1994**, *367*, 256–258.

[89] A. B. Smith, R. M. Strongin, L. Brard, W. J. Romanow, M. Saunders, H. A. Jiménez-Vázquez, J. R. Cross, *J. Am. Chem. Soc.* **1994**, *116*, 10831–10832.

[90] G. W. Wang, M. Saunders, R. J. Cross, *J. Am. Chem. Soc.* **2001**, *123*, 256–259.

[91] M. Riittimann, R. F. Haldimann, L. Isaacs, F. Diederich, A. Khong, H. Jimknez-vazquez, R. J. Cross, M. Saunders, *Chem. Eur. J.* **1997**, *3*, 1071–1076.

[92] H. G. Von Schnering, L. Walz, M. Schwarz, W. Becker, M. Hartweg, T. Popp, B. Hettich, P. M. G. Kpmpf, A. Chem, G. B. Ed, H. Der Prapururiven, *Angew. Chemie Int. Ed. English* **1991**, *7*, 884–886.

[93] A. K. Caldwell, D. E. Giblin, C. S. Hsu, D. Cox, M. L. Gross, *J. Am. Chem. Soc.* **1991**, *113*, 8519–8521.

[94] T. Weiske, T. Wong, W. Kratschmer, J. K. Terlouw, H. Schwarz, *Angew. Chemie Int. Ed. English* **1992**, *31*, 183–185.

[95] M. Saunders, H. A. Jiménez-Vázquez, R. J. Cross, R. J. Poreda, *Science.* **1993**, *259*, 1428–1430.

[96] M. Saunders, H. A. Jimenez-Vazquez, R. J. Cross, S. Mroczkowski, M. L. Gross, D. E. Giblin, R. J. Poreda, *J. Am. Chem. Soc.* **1994**, *116*, 2193–2194.

[97] M. Saunders, R. J. Cross, H. A. Jiménez-Vázquez, R. Shimshi, A. Khong, *Science.* **1996**, *271*, 1693–1697.

[98] R. J. Cross, A. Khong, M. Saunders, *J. Org. Chem.* **2003**, *68*, 8281–8283.

[99] R. Peng, S. Chu, Y. Huang, H. Yu, T. Wang, B. Jin, Y. Fu, C. Wang, **2009**, 3602–3605.

[100] M. Saunders, H. A. Jiménez-Vázquez, R. James Cross, S. Mroczkowski, M. Gross, D. E. Giblin, R.

J. Poreda, *J. Am. Chem. Soc.* **1994**, *116*, 2193–2194.

[101] A. Takeda, Y. Yokoyama, S. Ito, T. Miyazaki, H. Shimotani, K. Yakigaya, T. Kakiuchi, H. Sawa, H. Takagi, K. Kitazawa, N. Dragoe, *Chem. Commun.* **2006**, 912–914.

[102] K. Yamamoto, M. Saunders, A. Khong, R. J. Cross, M. Grayson, M. L. Gross, A. F. Benedetto, R. B. Weisman, *J. Am. Chem. Soc.* **1999**, *121*, 1591–1596.

[103] M. S. Syamala, R. J. Cross, M. Saunders, *J. Am. Chem. Soc.* **2002**, *124*, 6216–6219.

[104] J. I. Langford, D. Louer, *Rep. Prog. Phys.* **1996**, *59*, 131–234.

[105] Y. Rubin, T. Jarrosson, G. Wang, M. D. Bartberger, K. N. Houk, G. Schick, M. Saunders, R. J. Cross, *Angew. Chemie Int. Ed.* **2001**, 1543–1546.

[106] K. Komatsu, M. Murata, Y. Murata, *Science.* **2005**, *307*, 238–240.

[107] C. Thilgen, *Angew. Chemie - Int. Ed.* **2012**, *51*, 587–589.

[108] A. Krachmalnicoff, R. Bounds, S. Mamone, S. Alom, M. Concistrè, B. Meier, K. Kouřil, M. E. Light, M. R. Johnson, S. Rols, A. J. Horsewill, A. Shugai, U. Nagel, T. Rõõm, M. Carravetta, M. H. Levitt, R. J. Whitby, *Nat. Chem.* **2016**, *8*, 953–957.

[109] M. H. Levitt, *Philos. Trans. R. Soc. A Math. Phys. Eng. Sci.* **2013**, *371*, 20120429.

[110] C. Beduz, M. Carravetta, J. Y.-C. Chen, M. Concistre, M. Denning, M. Frunzi, A. J. Horsewill, O. G. Johannessen, R. Lawler, X. Lei, M. H. Levitt, Y. Li, S. Mamone, Y. Murata, U. Nagel, T. Nishida, J. Ollivier, S. Rols, T. Room, R. Sarkar, N. J. Turro, Y. Yang, *Proc. Natl. Acad. Sci.* **2012**, *109*, 12894–12898.

[111] J. C. Phys, M. H. Levitt, T. Rõõm, M. Carravetta, **2011**, *081103*, DOI 10.1063/1.3080163.

[112] S. Mamone, M. Jiménez-Ruiz, M. R. Johnson, S. Rols, A. J. Horsewill, *Phys. Chem. Chem. Phys.* **2016**, *18*, 29369–29380.

[113] R. Taylor, J. P. Parsons, A. G. Avent, S. P. Rannard, T. J. Dennis, J. P. Hare, H. W. Kroto, D. R. M. Walton, *Nature* **1991**, *351*, 277–277.

[114] T. Suzuki, Q. Li, K. C. Khemani, F. Wudl, *J. Am. Chem. Soc.* **1992**, *114*, 7301–7302.

[115] F. Wudl, *Acc. Chem. Res.* **1992**, *25*, 157–161.

[116] L. Isaacs, D. Philp, *Chem. Soc. Rev.* **1994**, 243–255.

[117] A. Skiebe, A. Hirsch, *J. Chem. Soc., Chem. Commun.* **1994**, 335–336.

[118] M. Prato, Q. C. Li, F. Wudl, V. Lucchini, *J. Am. Chem. Soc.* **1993**, *115*, 1148–1150.

[119] B. Nuber, F. Hampel, A. Hirsch, *Chem. Commun.* **1996**, 1799–1800.

[120] X. Zhang, A. Romero, C. S. Foote, *J. Am. Chem. Soc.* **1993**, *115*, 11024–11025.

[121] J. C. Hummeler, F. Wudl, M. Prato, *J. Am. Chem. Soc.* **1995**, *117*, 7003–7004.

[122] M.-J. Arce, A. L. Viado, Y.-Z. An, S. I. Khan, Y. Rubin, *J. Am. Chem. Soc.* **1996**, *118*, 3775–3776.

[123] Y. Z. An, G. A. Ellis, A. L. Viado, Y. Rubin, *J. Org. Chem.* **1995**, *60*, 6353–6361.

[124] J. Nishimura, J. A. C. Soc, T. Ishii, G. Schick, T. Jarrosson, Y. Rubin, *Angew. Chemie - Int. Ed.* **1999**, *38*, 2360–2363.

[125] Y. Murata, M. Murata, K. Komatsu, *J. Org. Chem.* **2001**, *66*, 8187–91.

[126] Y. Murata, M. Murata, K. Komatsu, *Chem. Eur. J.* **2003**, 1600–1609.

[127] M. Yamada, A. Ishitsuka, Y. Maeda, M. Suzuki, H. Sato, *Org. Lett.* **2020**, 4–7.

[128] Y. Murata, K. Komatsu, *Chem. Lett.* **2001**, *30*, 896–897.

[129] H. Inoue, H. Yamaguchi, S. I. Iwamatsu, T. Uozaki, T. Suzuki, T. Akasaka, S. Nagase, S. Murata, *Tet. Lett.* **2001**, *42*, 895–897.

[130] S. C. Chuang, Y. Murata, M. Murata, S. Mori, S. Maeda, F. Tanabe, K. Komatsu, *Chem. Commun.* **2007**, 1278–1280.

[131] S. Iwamatsu, F. Ono, S. Murata, *Chem. Lett.* **2003**, *32*, 614–615.

[132] S. Iwamatsu, F. Ono, S. Murata, *Chem. Commun. (Camb).* **2003**, 1268–9.

[133] Y. Yamamoto, A. Nagata, K. Itoh, *Tet. Lett.* **1999**, *40*, 5035–5038.

[134] A. Khong, H. A. Jiménez-Vázquez, M. Saunders, R. J. Cross, J. Laskin, T. Peres, C. Lifshitz, R. Strongin, A. B. Smith, *J. Am. Chem. Soc.* **1998**, *120*, 6380–6383.

[135] Y. Murata, S. Maeda, M. Murata, K. Komatsu, *J. Am. Chem. Soc.* **2008**, *130*, 6702–6703.

[136] K. Kurotobi, Y. Murata, *Science* **2011**, *333*, 613–616.

[137] Y. Hashikawa, M. Murata, A. Wakamiya, Y. Murata, *J. Am. Chem. Soc.* **2017**, *139*, 16350–16358.

[138] T. Futagoishi, M. Murata, A. Wakamiya, T. Sasamori, Y. Murata, *Org. Lett.* **2013**, *15*, 2750–2753.

[139] Y. Hashikawa, S. Okamoto, Y. Murata, *Commun. Chem.* **2020**, *3*, 1–7.

[140] H. Ajie, M. M. Alvarez, S. J. Anz, R. D. Beck, F. Diederich, K. Fostiropoulos, D. R. Huffman, W. Krätschmer, Y. Rubin, K. E. Schriver, D. Sensharma, R. L. Whetten, *J. Phys. Chem.* **1990**, *94*, 8630–8633.

[141] R. Zhang, T. Futagoishi, M. Murata, A. Wakamiya, Y. Murata, *J. Am. Chem. Soc.* **2014**, *136*, 8193–8196.

[142] S. I. Iwamatsu, T. Uozaki, K. Kobayashi, S. Re, S. Nagase, S. Murata, *J. Am. Chem. Soc.* **2004**, *126*, 2668–2669.

[143] C. S. Chen, T. S. Kuo, W. Y. Yeh, *Chem. - A Eur. J.* **2016**, *22*, 8773–8776.

[144] S. I. Iwamatsu, S. Murata, *Tet. Lett.* **2004**, *45*, 6391–6394.

[145] T. Tanaka, K. Morimoto, T. Ishida, T. Takahashi, N. Fukaya, J. C. Choi, Y. Kabe, *Chem. Lett.* **2018**, *47*, 503–506.

[146] L. Gan, S. Huang, X. Zhang, A. Zhang, B. Cheng, H. Cheng, X. Li, G. Shang, *J. Am. Chem. Soc.* **2002**, *124*, 13384–13385.

[147] S. Huang, F. Wang, L. Gan, G. Yuan, J. Zhou, S. Zhang, *Org. Lett.* **2006**, *8*, 277–279.

[148] S. Huang, Z. Xiao, F. Wang, L. Gan, X. Zhang, X. Hu, S. Zhang, M. Lu, Q. Pan, L. Xu, *J. Org. Chem.* **2004**, *69*, 2442–2453.

[149] Z. Xiao, J. Yao, D. Yang, F. Wang, S. Huang, L. Gan, Z. Jia, Z. Jiang, X. Yang, B. Zheng, G. Yuan, S. Zhang, Z. Wang, *J. Am. Chem. Soc.* **2007**, *129*, 16149–16162.

[150] B. L. Gan, D. Yang, Q. Zhang, H. Huang, **2010**, 1498–1507.

[151] Y. Murata, M. Murata, K. Komatsu, *J. Am. Chem. Soc.* **2003**, *125*, 7152–7153.

[152] C. M. Stanisky, R. J. Cross, M. Saunders, M. Murata, Y. Murata, K. Komatsu, *J. Am. Chem. Soc.* **2005**, *127*, 299–302.

[153] Y. Morinaka, F. Tanabe, M. Murata, Y. Murata, K. Komatsu, *Chem. Commun.* **2010**, *46*, 4532–4534.

[154] S. I. Iwamatsu, S. Murata, Y. Andoh, M. Minoura, K. Kobayashi, N. Mizorogi, S. Nagase, *J. Org.*

*Chem.* **2005**, *70*, 4820–4825.

[155] A. Krachmalnicoff, M. H. Levitt, R. J. Whitby, *Chem. Commun.* **2014**, *50*, 13037–13040.

[156] C. M. Stanisky, R. J. Cross, M. Saunders, *J. Am. Chem. Soc.* **2009**, *131*, 3392–3395.

[157] S. S. Zhukov, V. Balos, G. Hoffman, S. Alom, M. Belyanchikov, M. Nebioglu, S. Roh, A. Pronin, G. R. Bacanu, P. Abramov, M. Wolf, M. Dressel, M. H. Levitt, R. J. Whitby, B. Gorshunov, M. Sajadi, *arXiv:2006.02687* **n.d.**, DOI arXiv:2006.02687v1.

[158] Y. Yu, L. Shi, D. Yang, L. Gan, *Chem. Sci.* **2013**, *4*, 814–818.

[159] O. Hampe, T. Karpuschkin, M. Vonderach, P. Weis, Y. Yu, L. Gan, W. Klopper, M. M. Kappes, *Phys. Chem. Chem. Phys.* **2011**, *13*, 9818–9823.

[160] Y. Hashikawa, K. Kizaki, T. Hirose, Y. Murata, *RSC Adv.* **2020**, *10*, 40406–40410.

[161] A. Krachmalnicoff, R. Bounds, S. Mamone, M. H. Levitt, M. Carravetta, R. J. Whitby, *Chem. Commun.* **2015**, *51*, 4993–4996.

[162] L. Xu, H. Ren, S. Liang, J. Sun, Y. Liu, L. Gan, *Chem. - A Eur. J.* **2015**, *21*, 13539–13543.

[163] L. Shi, D. Yang, F. Colombo, Y. Yu, W. X. Zhang, L. Gan, *Chem. - A Eur. J.* **2013**, *19*, 16545–16549.

[164] H. Zhang, J. E. Barralet, *Adv. Drug Deliv. Rev.* **2017**, *122*, 84–104.

[165] B. Wang, W. Lin, Z. Mao, C. Gao, *J. Mater. Chem. B* **2018**, *6*, 3145–3155.

[166] R. R. Mallepally, C. C. Parrish, M. A. M. Mc Hugh, K. R. Ward, *Int. J. Pharm.* **2014**, *475*, 130–137.

[167] P. A. Troshin, A. G. Avent, A. D. Darwish, **2005**, 278–281.

[168] J. C. Hummelen, B. Knight, J. Pavlovich, R. González, F. Wudl, *Science* **1995**, *269*, 1554–1556.

[169] B. Nuber, A. Hirsch, *Chem. Commun.* **1996**, 1421–1422.

[170] G. Zhang, S. Huang, Z. Xiao, Q. Chen, L. Gan, Z. Wang, *J. Am. Chem. Soc.* **2008**, *130*, 12614–12615.

[171] Y. Li, N. Lou, D. Xu, C. Pan, X. Lu, L. Gan, *Angew. Chemie - Int. Ed.* **2018**, *57*, 14144–14148.

[172] S. I. Iwamatsu, C. M. Stanisky, R. J. Cross, M. Saunders, N. Mizorogi, S. Nagase, S. Murata, *Angew. Chemie - Int. Ed.* **2006**, *45*, 5337–5340.

[173] K. E. Whitener, M. Frunze, S. I. Iwamatsu, S. Murata, R. J. Cross, M. Saunders, *J. Am. Chem. Soc.* **2008**, *130*, 13996–13999.

[174] K. E. Whitener, R. J. Cross, M. Saunders, S. I. Iwamatsu, S. Murata, N. Mizorogi, S. Nagase, *J. Am. Chem. Soc.* **2009**, *131*, 6338–6339.

[175] S. C. Chuang, Y. Murata, M. Murata, K. Komatsu, *Chem. Commun.* **2007**, 1751–1753.

[176] Q. Zhang, T. Pankewitz, S. Liu, W. Klopper, L. Gan, *Angew. Chemie - Int. Ed.* **2010**, *49*, 9935–9938.

[177] T. Futagoishi, M. Murata, A. Wakamiya, Y. Murata, *Angew. Chemie - Int. Ed.* **2015**, *54*, 14791–14794.

[178] T. Futagoishi, M. Murata, A. Wakamiya, Y. Murata, *Angew. Chemie* **2017**, *129*, 2802–2806.

[179] S. Bloodworth, J. Gräsvik, S. Alom, K. Kouřil, S. J. Elliott, N. J. Wells, A. J. Horsewill, S. Mamone, M. Jiménez-Ruiz, S. Rols, U. Nagel, T. Rõõm, M. H. Levitt, R. J. Whitby, *ChemPhysChem* **2018**, *19*, 266–276.

[180] A. S. Bloodworth, G. Sitinova, S. Alom, G. R. Bacanu, S. J. Elliott, M. E. Light, M. Herniman, G. J. Langley, M. H. Levitt, *Angew. Chemie Int. Ed.* **2019**, DOI 10.1002/anie.201900983.

[181] T. Futagoishi, T. Aharen, T. Kato, A. Kato, T. Ihara, T. Tada, M. Murata, A. Wakamiya, H. Kageyama, Y. Kanemitsu, Y. Murata, *Angew. Chemie Int. Ed.* **2017**, *56*, 4261–4265.

[182] F. Hajjaj, K. Tashiro, H. Nikawa, N. Mizorogi, T. Akasaka, S. Nagase, K. Furukawa, T. Kato, T. Aida, **2011**, 9290–9292.

[183] S. Hasegawa, Y. Hashikawa, T. Kato, Y. Murata, *Angew. Chemie Int. Ed.* **2018**, *57*, 12804–12808.

[184] S. Bloodworth, G. Hoffman, M. C. Walkey, G. R. Bacanu, J. M. Herniman, M. H. Levitt, R. J. Whitby, *Chem. Commun.* **2020**, *56*, 10521–10524.

[185] M. Murata, Y. Murata, K. Komatsu, *J. Am. Chem. Soc.* **2006**, *128*, 8024–8033.

[186] Y. Morinaka, F. Tanabe, M. Murata, Y. Murata, K. Komatsu, *Chem. Commun.* **2010**, *46*, 4532.

[187] T. Futagoishi, M. Murata, A. Wakamiya, Y. Murata, *Chem. Commun.* **2017**, *53*, 1712–1714.

[188] S. Vidal, M. Izquierdo, S. Alom, M. Garcia-Borràs, S. Filippone, S. Osuna, M. Solà, R. J. Whitby, N. Martín, *Chem. Commun.* **2017**, *53*, 10993–10996.

[189] A. Krachmalnicoff, *Synthesis of Small Molecule Endohedral Fullerenes UNIVERSITY OF SOUTHAMPTON*, **2015**.

[190] G. Hoffman, M. C. Walkey, J. Gräsvik, R. Bacanu, S. Alom, S. Bloodworth, M. E. Light, M. H. Levitt, R. J. Whitby, *Angew. Chemie - Int. Ed.* **2021**, DOI 10.1002/anie.202100817.

[191] K. S. K. Goh, M. Jimenez-Ruiz, M. R. Johnson, S. Rols, J. Ollivier, M. S. Denning, S. Mamone, M. H. Levitt, X. G. Lei, Y. J. Li, N. J. Turro, Y. Murata, A. J. Horsewill, *Phys. Chem. Chem. Phys.* **2014**, *16*, 21330–21339.

[192] G. R. Bacanu, J. Rantaharju, G. Ho, M. C. Walkey, S. Bloodworth, M. Concistre, R. J. Whitby, M. H. Levitt, *J. Am. Chem. Soc.* **2020**, *142*, 16926–16929.

[193] A. J. Horsewill, K. S. Panesar, S. Rols, J. Ollivier, M. R. Johnson, M. Carravetta, S. Mamone, M. H. Levitt, Y. Murata, K. Komatsu, J. Y. Chen, J. A. Johnson, X. Lei, N. J. Turro, **2012**, *205440*, 1–12.

[194] M. Xu, S. Ye, R. Lawler, N. J. Turro, Z. Bačić, *Philos. Trans. R. Soc. A Math. Phys. Eng. Sci.* **2013**, *371*, DOI 10.1098/rsta.2011.0630.

[195] Y. Murata, S. C. Chuang, F. Tanabe, M. Murata, K. Komatsu, *Philos. Trans. R. Soc. A Math. Phys. Eng. Sci.* **2013**, *371*, 1–6.

[196] G. R. Bacanu, G. Hoffman, M. Amponsah, M. Concistrè, R. J. Whitby, M. H. Levitt, *Phys. Chem. Chem. Phys.* **2020**, *22*, 11850–11860.

[197] M. Saunders, H. A. Jimenez-vazquez, R. J. Cross, R. J. Poreda, *Science* **1993**, *259*, 1428–1431.

[198] M. M. Olmstead, D. A. Costa, K. Maitra, B. C. Noll, S. L. Phillips, P. M. Van Calcar, A. L. Balch, *J. Am. Chem. Soc.* **1999**, *121*, 7090–7097.

[199] Y. L. Chow, J. N. S. Tam, J. E. Blier, H. H. Szmant, *J. Chem. Soc. D Chem. Commun.* **1970**, 1604–1605.

[200] C. Karunakaran, M. Balamurugan, *Electron Paramagnetic Resonance Spectroscopy*, Elsevier Inc., **2018**.

[201] S. J. Elliott, S. Bloodworth, S. Alom, K. Kour, N. J. Wells, A. J. Horsewill, S. Mamone, R. J. Whitby, *Chem. Phys. Chem*., **2018**, 266–276.

[202] A. Weidinger, M. Waiblinger, B. Pietzak, T. Almeida Murphy, *Appl. Phys. A Mater. Sci. Process.*

**1998**, *66*, 287–292.

[203] B. Cao, T. Peres, R. J. Cross, M. Saunders, C. Lifshitz, *J. Phys. Chem. A* **2001**, *105*, 2142–2146.

[204] Tomohiro Suetsuna, Nita Dragoe, W. Harneit, A. Weidinger, H. Shimotani, S. Ito, H. Takagi, K. Kitazawa, *Chem. Eur. J.* **2002**, 5079–5083.

[205] S. Ito, H. Shimotani, H. Takagi, N. Dragoe, *Fullerenes Nanotub. Carbon Nanostructures* **2008**, *16*, 206–213.

[206] W. Adam, J. Bialas, L. Hadjiarapoglou, *Chem. Ber.* **1991**, *124*, 2377–2377.

[207] M. Mahesh, J. A. Murphy, F. Lestrat, H. P. Wessel, *Beilstein J. Org. Chem.* **2009**, *5*, 1–12.